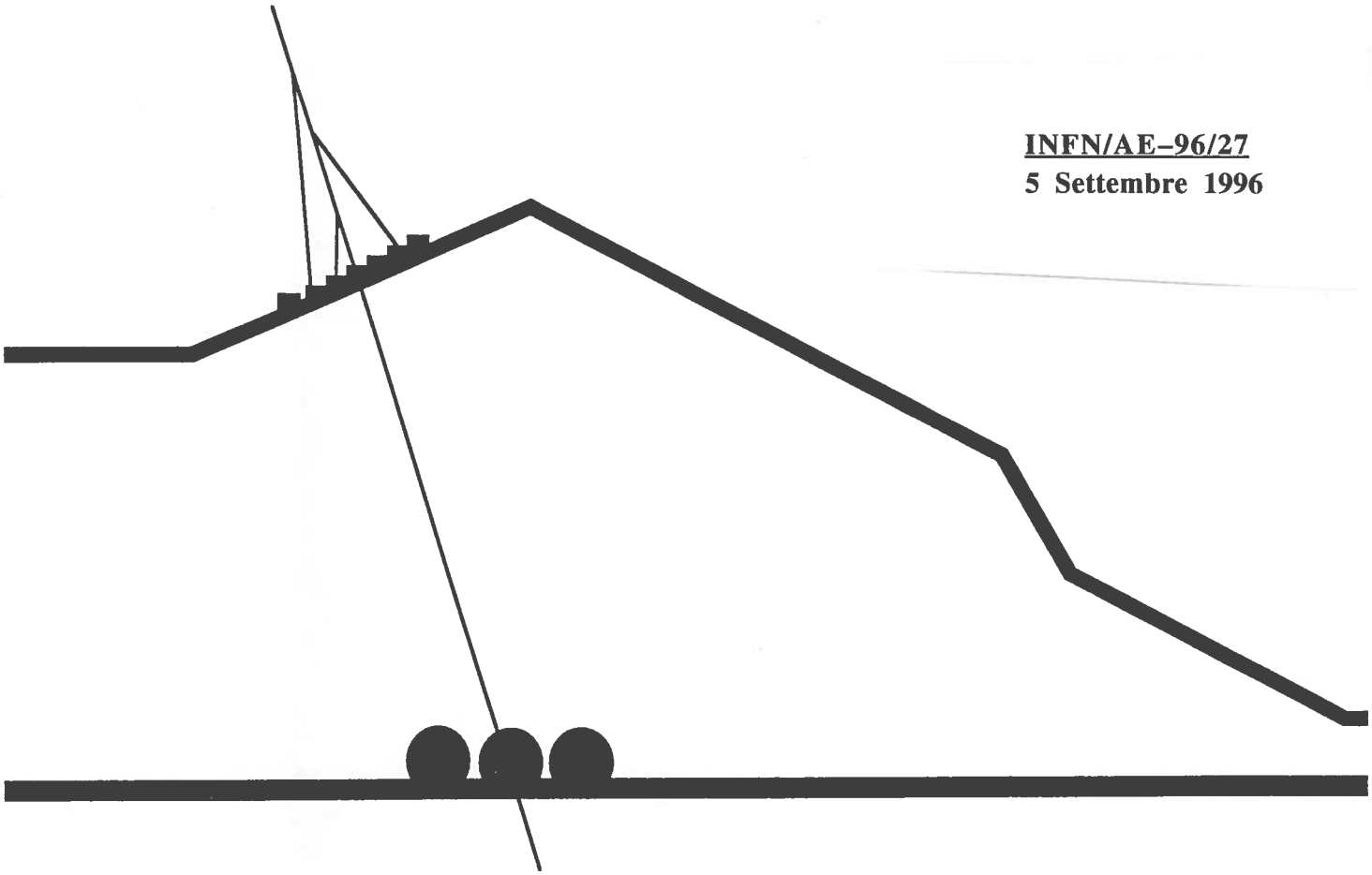

INFN/AE–96/27
5 Settembre 1996

L.N.G.S. Annual Report 1995

INFN - Laboratori Nazionali del Gran Sasso

Published by **SIS–Pubblicazioni**
dei Laboratori Nazionali di Frascati

INFN – Istituto Nazionale di Fisica Nucelare
Laboratori Nazionali del Gran Sasso

INFN/AE-96/27
5 Settembre 1996

L.N.G.S. Annual Report 1995

Published by **SIS-Pubblicazioni**
dei Laboratori Nazionali di Frascati

Contents

	page
Introduction	i
EAS-TOP Experiment	1
TRIS Experiment	17
GALLEX Experiment (and GNO Proposal)	21
LVD Experiment	85
MACRO Experiment	105
Counting Test Facility (Borexino)	123
ICARUS Experiment	131
A Cryogenic Experiment on ββ decay and Search for Rare Events	145
HEIDELBERG-MOSCOW ^{76}Ge ββ decay Experiment	151
ββ decay into excited states Experiment (DBGS)	189
Dark Matter Search with Very Low Activity Scintillators (BPRS and DAMA)	193
CRESST Dark Matter Search	199
Laboratory for Underground Nuclear Astrophysics (LUNA)	207
The Interferometric Station (INTER)	211
Theoretical Activity	217
MINUTES OF THE GRAN SASSO SCIENTIFIC COMMITTEE MEETING IN 1995	221

INTRODUCTION

This report summarizes the main experimental research activities carried out at the Gran Sasso National Laboratories (LNGS) during 1995.

EAS-TOP, the extensive air shower array located above the underground laboratory at 2000 m. a.s.l. has recorded data in the fields of UHE γ ray astronomy, primary cosmic ray spectrum and composition, also in off line coincidence with underground detectors MACRO and LVD.

TRIS is an experiment looking for spectral distortion of the Cosmic Background Radiation in the radio frequency range.

Among the big Collaborations running underground detectors:

GALLEX has continued taking data of low energy solar neutrinos. At the end of 1995, a second exposure to the artificial neutrino source was carried out. The results of the first exposure, published in 1995, already showed that the experiment is well under control.

LVD is taking data with the first two towers (2/5 of the final detector). The construction of the third tower has been delayed due to severe problems in the delivery of the liquid scintillator.

MACRO is taking data with the full apparatus (lower part + attico). The final trigger and electronic configuration have been completed in 1995. Transition Radiation Detectors have been added in order to measure the energy of the muons crossing the detector.

The Counting Test Facility (**CTF**) of Borexino has been completely equipped and filled with water and scintillator at the end of 1994; during 1995 several measurements have been done in order to prove that the background which can be foreseen for the final experiment is low enough to allow the measurement of Be-neutrinos from the sun.

During 1995 the **ICARUS** Collaboration proposed to build a 600-ton liquid Argon module, within a time scale of three years. The description of the proposed detector is included in this report.

Double beta decay searches are brought forward by several groups at Gran Sasso; in particular the **Milano** group, using thermal detectors, has published new limits on neutrinoless double beta decay of ^{130}Te.

The **HEIDELBERG-MOSCOW** group has measured the two neutrino $\beta\beta$ decay half life of ^{76}Ge and has published improved limits on the corresponding zero neutrino decay mode, and on the Majorana neutrino mass. Double beta decay to excited states is studied by the **DBGS** Collaboration.
A new experiment (**DBA**) on double beta decay using a liquid Argon ionization chamber is being installed in the underground laboratory.

Dark matter searches are performed by both the **BPRS** Collaboration and the **DAMA** groups looking for nuclear recoils in scintillators. Results have been obtained using NaI(Te) and CaF_2(Eu) and liquid Xenon .
A new experiment looking for dark matter candidates using criogenic detectors (**CRESST**) is being installed in Hall B.

The **LUNA** experiment has been installed underground for the measurement of very low energy fusion cross sections of astrophysical interest. The 50 KeV accelerator, built and tested at Bochum University, is currently working and the $^3He + ^3He$ reaction cross section is being measured at very low energy.

Beyond the experiments in the fields of astroparticle physics or elementary particle and nuclear physics, several geophysical experiments are being carried out in the underground laboratories.

The Scientific Committee of LNGS met once during 1995 at Gran Sasso on March 23-25 in connection with the Workshop on "Future Experiments at Gran Sasso". The minutes of the Scientific Committee meeting are reported in the appendix.

Several workshops, Conferences and Summer Institutes were held at Gran Sasso last year, in particular:

- Workshop on: "Beryllium Neutrinos: Problem and Detection" (March 22);
- Workshop on: "Future Experiments at Gran Sasso" (March 23-24);
- Workshop on: "Physics with e^+e^- Linear Colliders" (May 29-June 3);
- Summer Institute: "Signals of Unified Theories" (September 2-8);
- Workshop on: "Long Baseline Neutrino Oscillation Experiments" (November 9-10).

The new buildings for the external laboratories, partly funded by ASMEZ (Agenzia per lo Sviluppo del Mezzogiorno), have been completed and are now used by the laboratory and the external groups.

The Director of LNGS
Piero Monacelli

EAS-TOP
ACTIVITY REPORT 1995

G. Navarra
for the EAS-TOP Collaboration

1 Introduction

In 1995 the EAS-TOP array has been operating with :

- the e.m. detector (35 modules of scintillators, 10 m^2 each);
- the muon-hadron detector (140 m^2 calorimeter with 9 layers of 13 cm iron absorbers and streamer tubes active elements) + 130 m^2 scintillator muon detectors distributed in the field;
- the Cherenkov light detector (4 telescopes with tracking capabilities equipped with imaging photomultipliers);
- two radio antennas for EAS radio emission measurements.

The main activity in 1995 has been devoted to the maintenance and the running of the detectors, checking and improving the stability, with particular attention to the Cherenkov array.

Four e.m. modules have been equipped with vertical scintillators in order to improve the response to Horizontal Air Showers.

A run has been performed at CERN on a 10-50 GeV positron beam, to measure the response of the scintillators and stramer tubes to known energy and geometry electromagnetic primaries.

The data analysis has been pursued, and results (13 papers, one of which in collaboration with MACRO) have been presented to the 24th I.C.R.C. in Rome. Main results are summarized in the following.

2 The EAS size spectrum

The measured differential size spectrum, at depth $x_0 = 810\ gcm^{-2}$ is shown in fig. 1; we can clearly see the break in the spectrum (the "knee": notice its sharpness!).

The data are fitted, for $10^{5.2} < Ne < 10^7$, to a power-law with two different indexes:

$$S(Ne) = I_k \left(\frac{Ne}{Ne_k} \right)^{-\gamma_i} \tag{1}$$

with $\gamma_i = \gamma_1$ for $Ne < Ne_k$ and $\gamma_i = \gamma_2$ for $Ne > Ne_k$. The obtained results are $\gamma_1 = 2.706 \pm 0.004$, $\gamma_2 = 3.15 \pm 0.04$, $I_k = (1.18 \pm 0.18) \times 10^{-13} m^{-2} s^{-1} sr^{-1} Ne^{-1}$, $Ne_k = (1.38 \pm 0.06) \times 10^6$. Ne_k represents the best value of the knee of the size spectrum at 810 $g\ cm^{-2}$ and I_k the corresponding intensity.

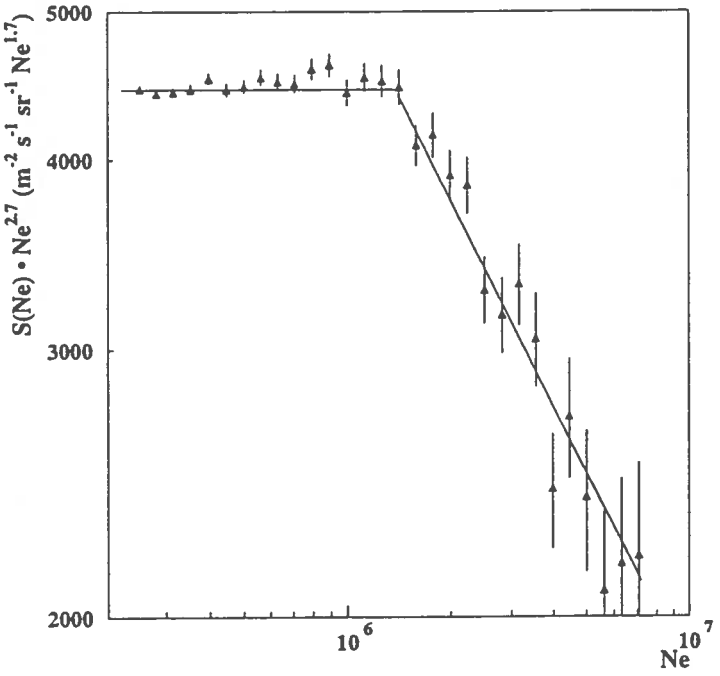

Figure 1: *Differential shower size spectrum measured at* $x_0 = 810 g cm^{-2}$

The same technique has been applied to the spectra measured at different zenith angles. This allows to study the dependence of Ne_k on the atmospheric depth. The results of the fit are reported in table 1 and in fig. 2: the intensity at the "knee", within the experimental errors, is independent from the atmospheric depth. This is expected in case that the change of slope of the primary spectrum occurs at a fixed primary energy, but had never been measured by a single array. The same result

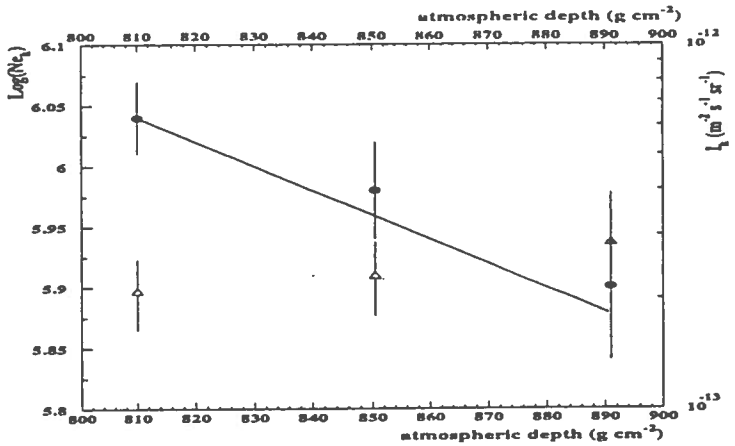

Figure 2: *Size value (•) and primary intensity (△) at the knee of the differential size spectrum as a function of atmospheric depth. The solid line shows the measured attenuation of EAS.*

can be deduced from the dependence of Ne_k on the atmospheric depth; from the same fig. 2 we see that the measured behaviour is consistent with the attenuation of the showers obtained at EAS-TOP (shown by a solid line):

$$Ne(\theta) = Ne(0°)e^{-\frac{x-x_0}{\Lambda_e}} = Ne(0°)e^{-\frac{x_0}{\Lambda_e}(1-\sec\theta)} \qquad (2)$$

with $\Lambda_e = 215.9 \pm 6.4\ g\ cm^{-2}$.

x ($g\ cm^{-2}$)	γ_1	γ_2	$I_k \times 10^{-13}$ ($m^{-2}s^{-1}sr^{-1}Ne^{-1}$)	Ne_k
$810 - 850$	2.69 ± 0.01	3.25 ± 0.07	2.1 ± 0.4	6.04 ± 0.03
$850 - 890$	2.67 ± 0.01	3.24 ± 0.09	2.3 ± 0.6	5.98 ± 0.04
$890 - 930$	2.66 ± 0.02	3.06 ± 0.09	2.8 ± 0.8	5.90 ± 0.06

Table 1: *Results of the power law fits to the differential size spectra measured in different intervals of zenith angles*

A comparison with the expectations from the extrapolation of the direct measured primary spectra and the interaction and cascade model implemented in HEMAS has been reported in the 1994 Report.

3 The Cosmic Ray primary composition

The study of the primary composition from the $Ne - N_\mu$ data recorded at the EAS-TOP level (muon energy threshold for vertical incidence $E_\mu^{th} = 1GeV$) has been performed by comparing the shower sizes measured by the e.m. array and the muon numbers recorded by the calorimeter with the expectations from the CORSIKA code (by including the detectors' responses).

N_μ is calculated from the measured muon densities ρ_μ through the relationship :

$$N_\mu = \frac{{R_0}^{1.25}}{0.269 R^{0.75}(1+\frac{R}{R_0})^{2.5}}\rho_\mu$$

with $R_0 = 455$ m obtained from the experimental data.

Results on the measured and simulated data are shown in fig. 3 concerning the muon lateral distributions, and in fig. 4 concerning the muon numbers (N_μ) vs. the shower sizes (Ne). A mixed primary composition as resulting from the extrapolations of the low energy measurements provides a good fit of the experimental data. Preliminarly it seems that a slightly heavier primary composition as predicted by the Peters-Zatsepin model gives a better fit above the "knee" of the primary spectrum than a constant mass composition.

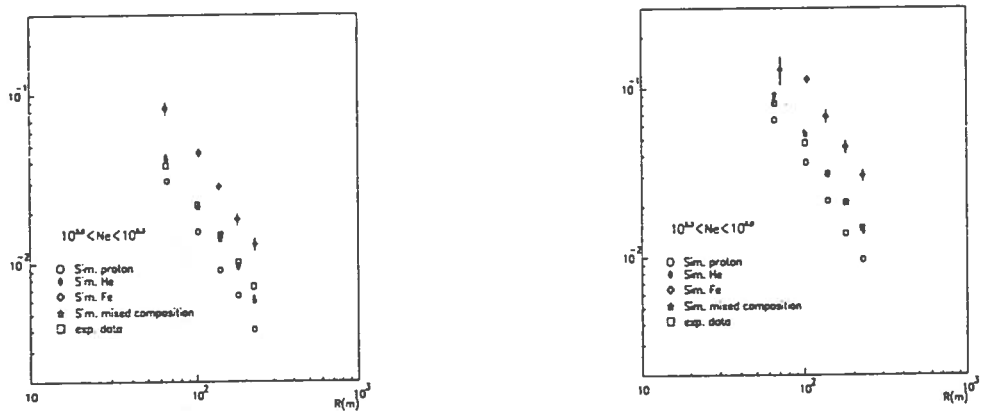

Figure 3: *Lateral distribution of muons measured at EAS-TOP compared with those expected from the MonteCarlo simulation CORSIKA for different primary chemical compositions and different size intervals:* $10^5 < Ne < 10^{5.3}$, *and* $10^{5.3} < Ne < 10^6$

On the same subject the statistics of the coincident EAS-TOP and MACRO data has been improved. As analysis tool the HEMAS code is used. The relation $Ne - N_\mu$, and the N_μ distributions in fixed bins of shower size Ne are shown in figs. 5 and 6.

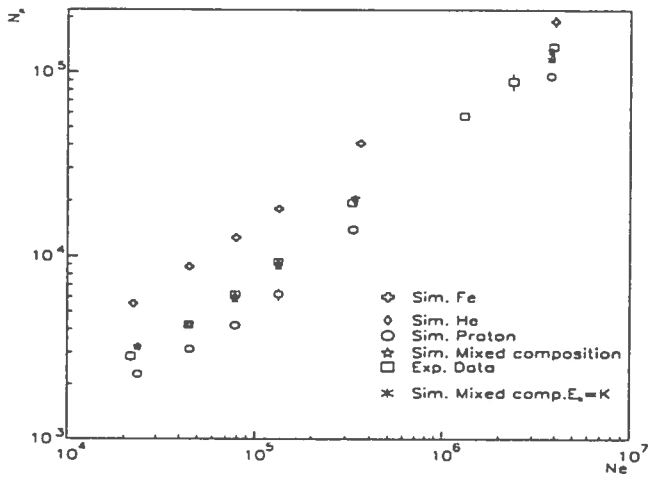

Figure 4: *N_μ vs Ne relation for GeV muons recorded at EAS-TOP (experimental data and calculations)*

The data are consistent with a mixed composition both below and above the "knee". In particular concerning the multiplicity distributions: i) the extrapolation of the direct low energy measurements gives a good account of observations within the extrapolation uncertainties (~20%), but seems to predict a flux of high multiplicity events lower than that of experimental data; ii) in the region above the knee of the size spectrum, a steepening of the energy spectra that preserves the mixed composition is consistent with the experimental data.

4 Cosmic Ray Anisotropies

Four years of data taking (1990-1994) have been analyzed, for a total of 1.3 10^9 EAS events at $E_0 \approx 10^{14}$ eV. A selection in primary energy and declination angle has been performed by selecting EAS with different arrival zenith angles: vertical ($\theta < 20^0$), and inclined ($20^0 < \theta < 60^0$) in different directions: E ($45^0 < \varphi < 135^0$), S ($135^0 < \varphi < 225^0$), W ($225^0 < \varphi < 315^0$), N ($315^0 < \varphi < 45^0$). The counting rates are corrected for the barometric coefficients measured at the appropriate zenith angles: $\beta = \mathrm{dn/dx} \approx$ - $0.77 sec\theta$ %mb^{-1}.

A summary of the results follows:

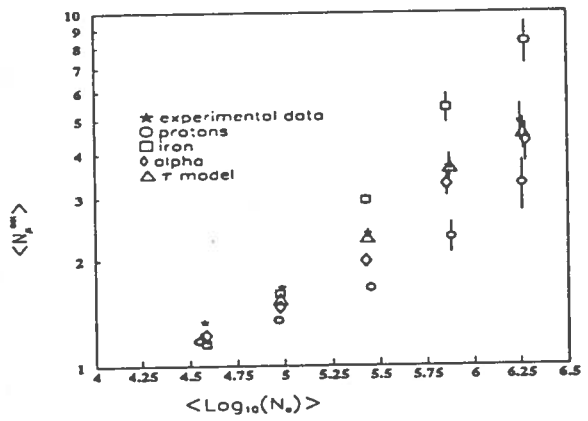

Figure 5: *Correlation between* $< N_\mu^{det} >$ *and* $<Log_{10}N_e>$ *for TeV muons recorded by MACRO.*

- for vertical events, i.e. mean primary energy $E_0 = 1.5\ 10^{14}$ eV, the amplitude and phase of the first sidereal harmonic are:

  $A_{sid}\ (1.5\ 10^{14}\ \text{eV}) = (3.60 \pm 0.61)\ 10^{-4}$, and $\varphi_{sid} = 2.77 \pm 0.65$ h lst,

  with significance 5.9 s.d..

  The counting rate vs. the local sidereal time in 20' time intervals is shown in fig. 7, from which the first harmonic over the fluctuations in the individual channels is clearly seen. The amplitude converted to the equatorial plane with the cosδ law gives:

  $A_{sid,\delta=0^0}\ (1.5\ 10^{14}\ \text{eV}) = (4.83 \pm 0.82)\ 10^{-4}$.

- for events with zenith angle $\theta > 20^0$, i.e. $E_m = 2.5\ 10^{14}$ eV, by using the measured cosδ dependence of the amplitude, we obtain (at the equatorial plane):

  $A_{sid,\delta=0^0}\ (2.5\ 10^{14}\ \text{eV}) = (3.22 \pm 0.67)\cdot 10^{-4}$ and $\varphi_{sid} = 0.95 \pm 0.68$ h lst,

  with significance 4.8 s.d..

  The cosδ dependence of the amplitude of the anisotropy on the declination (expected if it has a vectorial character), is shown in fig. 8.

- these data exclude a sharp increase of the c.r. anisotropy around 10^{14} eV, and (combined with lower energy experiments) show that the first harmonic of the

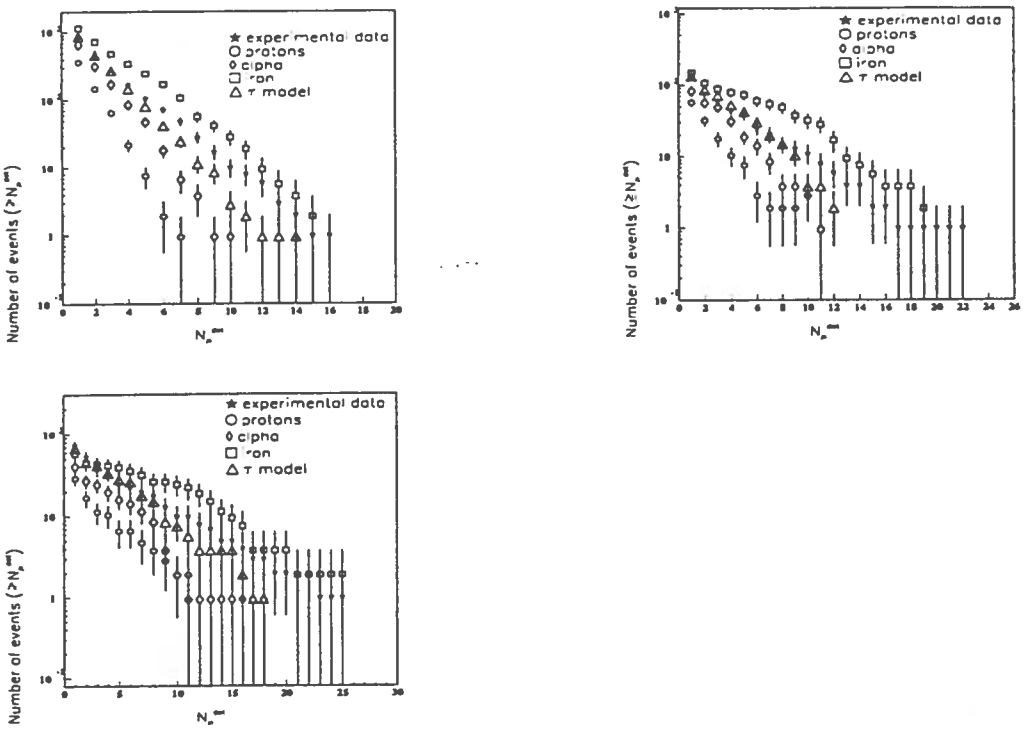

Figure 6: *Measured and expected integral distributions of detected muon multiplicities in MACRO, for 5.25≤ $Log_{10}N_e$ ≤ 5.75 (up left), 5.75≤ $Log_{10}N_e$ ≤ 6.05 (up right), and $Log_{10}N_e$ > 6.05 (below). 'tau model' represents the extrapolation of the direct data.*

cosmic ray anisotropy is nearly constant in amplitude and phase from $E_0 \approx 10^{12}$ to $E_0 \approx 10^{14}$ eV.

- by using the vertical and inclined data together, as belonging to the same sample, we obtain at primary energy $E_0 \approx 10^{14}$ eV, at the equatorial plane:

  $A_{sid,\delta=0^0}(E_0 \approx 10^{14}\ \text{eV}) = (3.73 \pm 0.57) \cdot 10^{-4}$, $\varphi_{sid} = 1.82 \pm 0.49$ h lst,

  with significance 6.5 s.d..

- a signal compatible with the Compton-Getting effect due to the motion of revolution of the Earth is seen. The measured amplitude and phase of the first harmonic in solar time are (at the equatorial plane):

  $A_{sol,\delta=0^0} = (4.06 \pm 0.55) \cdot 10^{-4}$, and $\varphi_{sol} = 4.92 \pm 0.5$ h

(with significance 7.4 s.d.), the expected values, due to the Compton-Getting effect, being $4.7 \cdot 10^{-4}$ and 6.0 h.

The consistency of the data is proved by:

i) the absence of significant anisotropies in antisidereal time;

ii) the consistency of the phases of the solar and sidereal anisotropies observed in the East and West directions;

iii) the correct rotation of the solar vector during the year, as expected from the combination of the measured solar and sidereal anisotropies;

iv) the quoted observation of the expected anisotropy in solar time due to the motion of revolution of the Earth around the Sun.

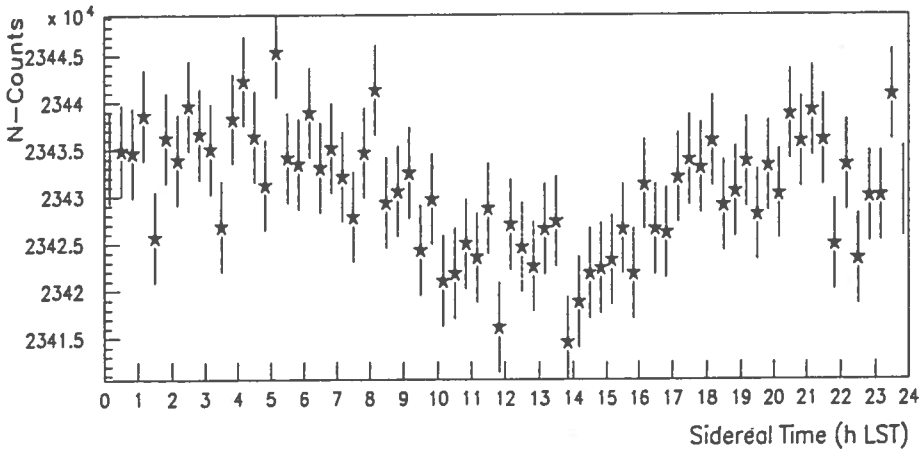

Figure 7: *Vertical events counting rate (in 20' bins) vs. the local sidereal time.*

5 UHE Gamma Ray Astronomy

The analysis of the candidate gamma-ray sources at UHE energies has been extended to about 5000-7000 hours/source. The obtained upper limits are (as an example) for the Crab Nebula (d.c.; 90% c.l.): $\Phi\ (> 25\ TeV) < 3.3 \cdot 10^{-13}\ cm^{-2}\ s^{-1}$,

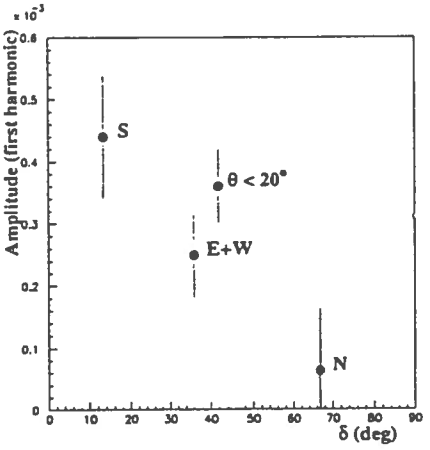

Figure 8: *Amplitude of the first harmonic of the c.r. anisotropy in sidereal time vs. the mean declination of observation in the different sectors (the East and West data, refering to the same declination, are averaged).*

$\Phi\ (> 105\ TeV) < 6.9 \cdot 10^{-14}\ cm^{-2}\ s^{-1}$, $\Phi\ (> 280\ TeV) < 1.4 \cdot 10^{-14}\ cm^{-2}\ s^{-1}$.

By selecting Extensive Air Showers with low muon contents, upper limit have been set to the rate of transient emissions:

$\Phi\ (> 250 \approx 300\ TeV) < (2 \approx 3) \cdot 10^{-13}\ cm^{-2}\ s^{-1}$,

depending on the source declination, i.e. a factor $\approx$ 10 lower than the flux observed from the Crab Nebula during the burst of February 23rd, 1989, observed by the KGF, Baksan and EAS-TOP arrays.

The same μ-poor technique has been used to obtain an upper limit to the rate of diffuse UHE gamma-ray primaries in the energy range $E_\gamma = 10^{14} - 10^{15}$ eV. In particular, for EAS electron sizes $N_e > 10^{5.8}$, no showers with no muons recorded in the 140 m^2 muon detector are observed within the fiducial area, during 8400 h live time. The 90% c.l. upper limit to the relative intensity of γ-rays with respect to primary cosmic rays is $I_\gamma / I_{c.r.} < 7.3 \cdot 10^{-5}$, at primary energy $E_0 \geq 1. \cdot 10^{15}$ eV.

6 Search for Gamma Ray Bursts

Gamma Ray Bursts are studied at primary energies $E_1 \geq 10$ GeV and $E_2 \geq 80$ TeV by searching for short transients in the cosmic ray intensity in the single particle (E_1) and Extensive Air Shower (E_2) counting rates, both in a sky survey and in correlation with BATSE events.

In the search in correlation with BATSE events, no evidence for gamma ray emission is observed in both energy ranges, either in coincidence with $\sim$ 50 BATSE bursts, nor in the 2 hour intervals around the BATSE recording times. The ranges of upper limits to the energy fluence during the time intervals in which BATSE detected 90% of the flux are drawn in fig. 9, for the energy intervals 10-100 GeV and 100-1000 TeV. The fluence limits span over large ranges due to the different time durations and zenith angles of observation of the events. As a comparison, in the same figure the fluences measured by BATSE (line *c*) and EGRET (line *d*) at lower energies during the powerful GRB940217 are reported, together with the fluence associated to the 18 GeV photon detected by EGRET 1.5 hours after the onset of the burst.

In the sky survey, during $\sim$ 800 days live time, the distributions of the numbers of events recorded in different time intervals follow the expectations from the background fluctuations in both energy ranges, showing the stability of the experiment at a poissonian level over long running times.

In the energy range $E_1 \geq 10$ GeV a statistically significant excess (10.6 and 20.1 standard deviations in 2 different measurement channels) was observed during a time interval of 2 s on 1992 July 15 at 13:22:26 UT. Assuming this candidate to be due to gamma rays, the corresponding energy fluence is $F = 1.7 \times 10^{-4} / (\cos\theta)^{10.5}$ erg cm^{-2} for $10 < E < 100$ GeV. This value, together with the other data reported in fig. 9 shows that EAS-TOP, in the 10-100 GeV energy range, for this search, has a sensitivity comparable to the EGRET one.

In the energy range E $\geq$ 100 TeV, the 90% C.L. upper limit to the rate of GRBs of time duration Δt = 1 s (10 s) and energy fluence F $> 8.4(9.8) \times 10^{-6}$ erg cm^{-2} ($100 < E < 1000$ TeV), is R < 1.14 y^{-1} sr^{-1}.

7 Study of the EAS cores

As an example of the study of the EAS cores with the calorimeter, a multi-core event is shown in fig. 10. The core position resulting from a fit of the l.d.f. that excludes the pads inside 1 meter from the two local maxima, is closer to the core indicated by the arrow in fig. 10, that we will therefore assume to be the main one.

This result is confirmed by the different characteristics of absorption inside the detector (shown in fig. 11) of the two cores. The secondary one presents an absorption compatible with an electromagnetic cascade.

If we interpret the main maximum as the shower core generated by the primary and the subcore as a large p_T shower produced by the primary interaction in the atmosphere (possibly a jet), we can evaluate the energies and the p_T involved.

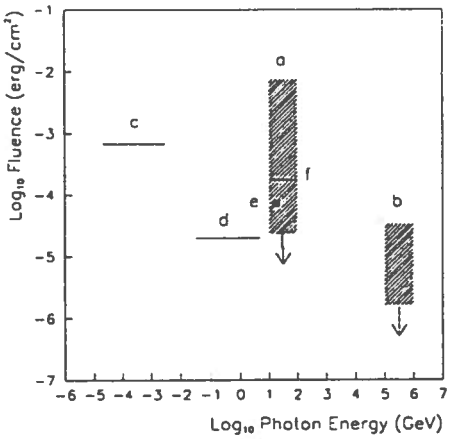

Figure 9: *a) Range of upper limits to the energy fluence obtained by EAS-TOP in the energy range 10-100 GeV during 45 BATSE bursts, b) range of upper limits to the fluence in the energy range 100-1000 TeV during 56 BATSE bursts, c) and d) fluences respectively measured by BATSE and EGRET during GRB940217, e) fluence associated to the 18 GeV photon observed by EGRET 1.5 hours after GRB940217, f) fluence associated to the EAS-TOP candidate of July 15, 1992, assuming* $\theta = 0$.

First, by means of a fit to the l.d.f. made by excluding the subcore region, we obtain $N_e \sim 1.6 \cdot 10^5$ that corresponds to a primary energy (for a proton) of approximately 450 TeV. It is then possible to subtract the contribution of the main shower in the subcore region and we obtain for the secondary $N_e \sim 2.4 \cdot 10^4$. Assuming the secondary shower to be an electromagnetic one at the maximum of its development (which minimizes the p_T evaluation and is justified by the observed absorption curve), we obtain $E_S \sim 24$ TeV and $h \sim 6700$ m, production height. From

$$p_T \sim E_S \cdot \frac{r}{h}$$

being $r = 2.5$ m the distance between subcore and core, we obtain $p_T \sim 10$ GeV/c.

By comparing the phenomenology of these events with the data recorded high in the atmosphere in emulsion chamber experiments (see e.g. the 'binocular' structures observed in Chacaltaya, 5200 m a.s.l.) it is shown that they very likely represent the same physical processes. These are related to the high p_T jet production observed at colliders except that the EAS data refer to a different (very forward) kinematic region.

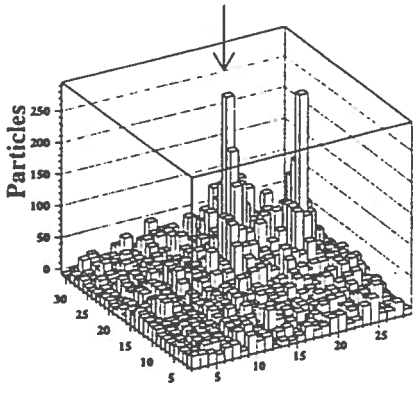

Figure 10: *A multi-core event as seen by the EAS-TOP calorimeter. The arrow points to the "main" core (see text).*

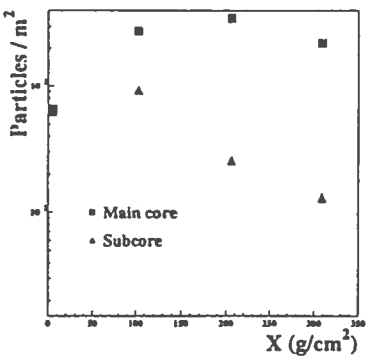

Figure 11: *Absorption characteristics in the upper levels of the two subcores shown in Fig. 10.*

8 The Cherenkov array

The shape of the images and their relations with the detection geometry have been studied (a discussion can be found in the 1994 Report). The symultaneous operation of four detectors allows now the stereoscopic observation of the showers. First images have been reported and an example is shown in fig. 12, showing that their general features follow the expectations from the detection geometry as derived from the e.m. component (i.e. the images are oriented towards the shower axis).

From the point of view of TeV gamma-ray astronomy, a campaign of observation of the Crab Nebula has been undertaken, and the data are under analysis.

9 Future Programs

The 1996 programm, besides the operation of the experiment and the data analysis, includes:

- starting operation of the last four Cherenkov telescopes (some delay being due to the telescope deliverers);

-installation of vertical scintillators in four further modules for a better definition of the Horizontal Air Showers;

- installation of two layers of vertical streamer tube cameras on two sides of the calorimeter, to trigger on horizontal muon groups, and for a better definition of

muon tracks recorded al large zenith angles.

More significant completions of the detectors (inside the existing main structure) foreseen in the future consist of:

- the increasing of the area of the muon detector by a simple module made of three layers of iron absorber of 12x12 m^2 interleaved with six layers of streamer tubes (that will allow a better definition of μ-poor showers and a reduction of the energy threshold of operation of the μ-poor selection in gamma-ray astronomy, and a measurement of the N_μ/Ne ratio in individual events);

- the coverage of the calorimeter with a lead absorber 15 cm thick to allow hadron calorimetry at the highest primary energies. and with a detector of the e.m. component of the EAS core made of a layer of streamer tubes operating in proportional mode. and read with the same resolution as inside the calorimeter.

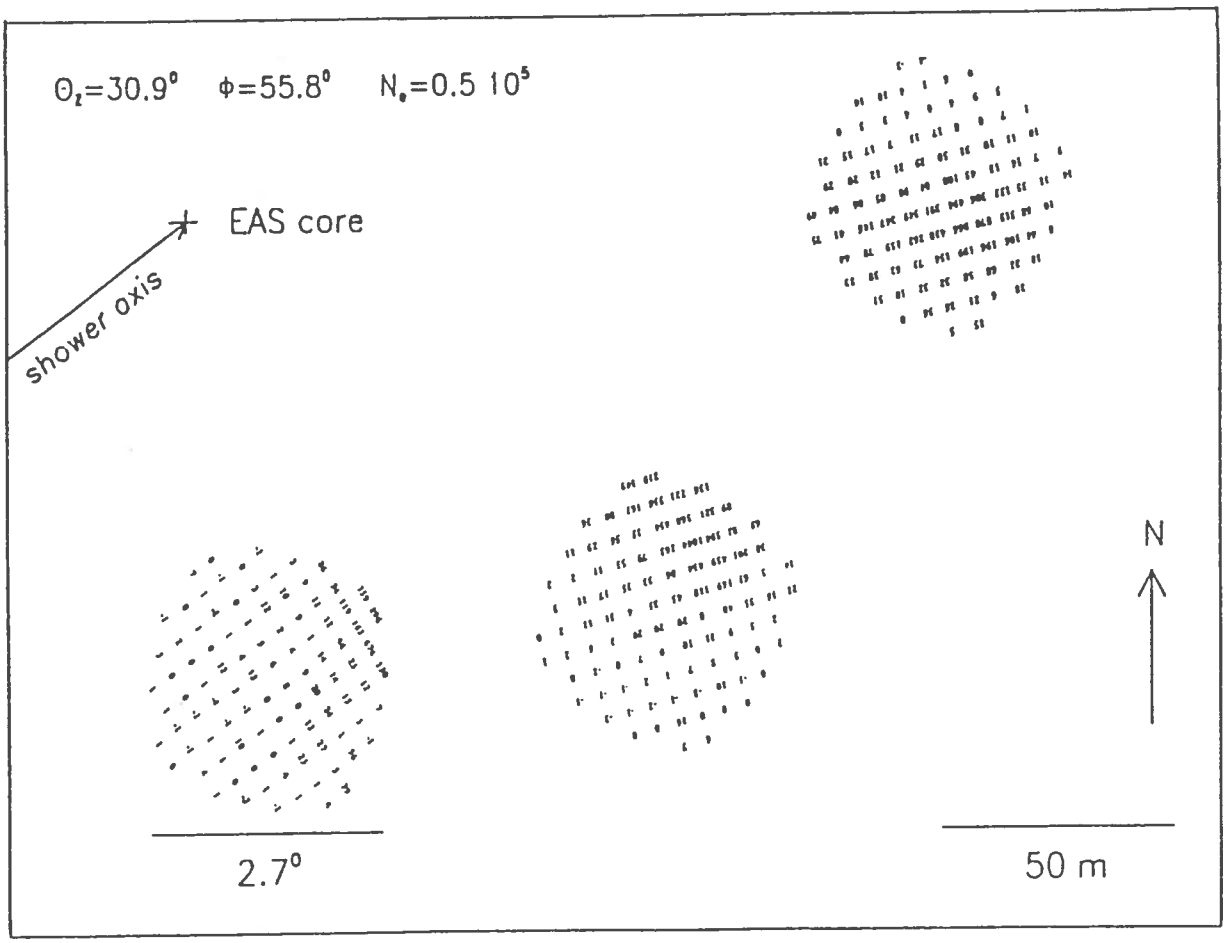

Figure 12: *Image of a three-fold Cherenkov event in coincidence with the particle detector together with the core position and the arrival direction*

EAS-TOP COLLABORATORS and INSTITUTIONS

M. Aglietta, B. Alessandro, V.V. Alexeenko, P. Antonioli, F. Arneodo, J. Bellandi, V.S. Berezinsky, L. Bergamasco, M. Bertaina, A. Bosio, A. Campos Fauth, A. Castellina, C. Castagnoli, A. Chiavassa, G. Cini Castagnoli, B. D'Ettorre Piazzoli, G. Di Sciascio, W. Fulgione, P. Galeotti, A. Gazizov, P. L. Ghia, R. Granella, M. Iacovacci, A. Lima de Godoi, G. Mannocchi, C. Melagrana, N. Mengotti Silva, C. Morello, G. Navarra, H. Nogima, L. Periale, P. Picchi, L. Riccati, O. Saavedra, M. Serio, G. C. Trinchero, A. Turtelli, P. Vallania, S. Vernetto, C.Vigorito

Technical staff: C. Barattia, R. Bertoni, M. Canonico, G. Giuliani, A. Giuliano, G. Pirali

Istituto Nazionale di Fisica Nucleare, Sezione di Torino, Torino, Italy
Istituto di Cosmo-Geofisica del CNR, Torino, Italy
Dipartimento di Fisica Generale dell' Università di Torino, Torino, Italy
Dipartimento di Fisica dell' Università dell'Aquila, L'Aquila, Italy
INFN, Laboratori Nazionali del Gran Sasso, Assergi (AQ), Italy
Dipartimento di Scienze Fisiche dell' Università and INFN, Napoli, Italy
Istituto Nazionale di Fisica Nucleare, Sezione di Bologna, Bologna, Italy
Instituto di Fisica, Universidade Estadual, de Campinas, Campinas (SP), Brazil

EAS-TOP PUBLICATIONS 1995

"Search for gamma ray bursts of energy $E_\gamma \geq 10$ GeV and $E_\gamma \geq 100$ TeV in correlation with BATSE events", *Astrophysics and Space Science,* 231 (1995) 351

"Study of the EAS cores from the EAS-TOP calorimeter and observation of multi-core events", *Proc. 24th International Cosmic Ray Conference*, Roma, 1 (1995) 2.3

"The shape of the atmospheric Cherenkov light images of extensive air showers", *Proc. 24th I.C.R.C.*, Roma, 1 (1995) 430

"Stereoscopic observation of atmospheric Cherenkov extensive air showers", *Proc. 24th I.C.R.C.*, Roma, 1 (1995) 434

"The HE muon and neutrino fluxes from measurements of Horizontal Air Showers at EAS-TOP", *Proc. 24th I.C.R.C.*, Roma, 1 (1995) 638

"Search for Gamma Rays Bursts of energy $E_\gamma \geq 10GeV$ and $E_\gamma \geq 100TeV$", *Proc. 24th I.C.R.C.*, Roma, 2 (1995) 132

"VHE observations of the Crab Nebula from the Cherenkov array of EAS-TOP", *Proc. 24th I.C.R.C.*, Roma, 2 (1995) 342

"UHE γ-ray astronomy with EAS-TOP", *Proc. 24th I.C.R.C.*, Roma, 2 (1995) 421

"On the rate of UHE γ-ray primaries", *Proc. 24th I.C.R.C.*, Roma, 2 (1995) 459

"Study of the primary composition from the $N_e - N_\mu$ data at EAS-TOP", *Proc. 24th I.C.R.C.*, Roma, 2 (1995) 664

"Study of the Primary Cosmic Ray Composition in the PeV region with EAS-TOP and MACRO", (In collaboration with the MACRO group), *Proc. 24th I.C.R.C.*, Roma, 2 (1995) 710

"A measurement of the EAS differential size spectrum for $10^5 < N_e < 10^7$ and of the absorption of EAS in the atmosphere", *Proc. 24th I.C.R.C.*, Roma, 2 (1995) 732

"Study of the cosmic ray anisotropy at $E_0 \sim 100$ TeV from EAS-TOP: 1992-1994", *Proc. 24th I.C.R.C.*, Roma, 2 (1995) 800

"Fractal Analysis of Cosmic Ray Signals Detected in the EAS-TOP Experiment", *Proc. 24th I.C.R.C.*, Roma, 4 (1995) 964

"New Astronomies with Extensive Air Showers", *Il Nuovo Cimento 18C* (1995) 183

"Large-P_T Physics with Cosmic Ray events", *Il Nuovo Cimento 18C* (1995) 663

TRIS Status Report

March 1996

G.Sironi, M. Gervasi, M. Zannoni, F. Cavaliere, A. Passerini
Dipartimento di Fisica dell'Universitá di Milano

G. Bonelli
Istituto di Fisica Cosmica del CNR - Milano

Introduction

Aim of TRIS is the detection of spectral distortions in the frequency distribution of the Cosmic Background Radiation near 1 GHz. Various theoretical arguments suggest in fact that a dip in the frequency distribution of the measured values of the CBR temperature can be expected in this frequency region. The expected deviation from the undistorted spectrum is less than few hundreds mK. The detection of the dip is of great cosmological interest ; the frequency at which the minimum occurs can be used in fact to evaluate the Universe Barion Density Ω. Unfortunately the data available in literature are insufficient to confirm or reject the existence of the dip.
Below 1 GHz, in fact, the accuracy of the measured values of the temperature is ~ 30% or worse, while the deviation suggested by existing models is less than 10% (a complete discussion and appropriate list of references can be found in the 1993 and 1994 TRIS Status Reports).

The TRIS experiment

TRIS is a system of three radiometers measuring the absolute temperature of the sky at three frequencies: 0.6, 0.82 and 2.5 GHz. The radiometers, composed by pyramidal E-plane corrugated horns and total power super-etherodyne receivers, are installed at Campo Imperatore to minimise any influence from the atmospheric emission/absorption. The radiometers can be operated in two different configurations :

a) drift scan configuration
b) calibration configuration

In configuration a) we let the sky transit through the antennas beam pointed at a given declination δ thus measuring the sky signal as a function of right ascension. Drift scans at different declinations are foreseen in order to map an extended region of the sky. In this configuration the system sensitivity (mV/mK) is the only instrumental parameter needed because we measure just the relative amplitude of the sky signal. To measure the system sensitivity a noise source periodically (i.e. once every 15 minutes) inject a known signal into the receivers.
In order to avoid frequency bands polluted by man made radio-frequency interference the receivers can be tuned into carefully selected 300 KHz wide channels.

In configuration b) we measure the absolute sky temperature by comparing the signal from the sky to the signal from a calibration source maintained at the liquid helium temperature. The calibration source is a matched load injecting its noise power into a coaxial to waveguide transition ; the matched load and the transition are immersed in liquid helium. We use a GaAs switch to periodically (i.e. once every few minutes) feed the receiver input with the signal from either the horn aimed at the sky or the load. For a complete description of our calibrator see Gervasi et al., Rev. of Scientific Instruments, 66 (10), October 95.

The status of the TRIS experiment

During 1995 we completed our program of observation in both configuration a) and b) for the 600 Mhz radiometer at declination +41 (i.e. with the radiometer pointed at the zenith) : we made drift scan during winter and fall and an absolute calibration run in June. In Fig. 1 is shown the absolute sky temperature profile at 606.2 MHz at δ=+41. The peak around RA=7 h is the sun contribution ; also shown is the expected (solid line) signal obtained by extrapolating and convolving with our beam the all sky map of Haslam (Haslam C.G.T. et al., Astr. & Astroph. Supp 47,1,1982). Altough the extrapolated data are known to a $\pm$ 3 K + 10% accuracy level, it is clear that our profile is higher than expected by about 1 K ; we think that problem is due to an unexpected contribution from the GaAs switch ; we are trying to better understand this issue by accurately measuring the noise contribution of the GaAs switch in the laboratory in Milan.

During 1995 we completed also our observation program in configuration a) for the 820 MHz radiometer and we made a calibration run in configuration b) in October. Due to both adverse weather conditions and malfunctioning of the GaAs switch, the calibration data are not as satisfactory as the 600 Mhz one.

We acquired also drift scans with both 600 and 820 Mhz radiometers at declinations other than δ=+41. Unfortunately, the level of radio frequency interference is a lot higher than with the horn pointed at the zenith and this prevents us to have clean profiles of the sky signal at these declinations.

At the end of October we prepared the radiometers to survive the winter and we brougth the receivers in Milan to refurbish them. Therefore, no data have been taken during the winter.

Programs for 1996

As soon as Campo Imperatore will be free from snow we will restart the observation in particular with the 2.5 GHz radiometer. The program for 1996 is as follows :

1. Perform observations in configuration a) with the 2.5 GHz radiometer
2. Perform a calibration run in configuration b) with the 2.5 GHz radiometer
3. Perform ancillary measurements to estimate possible systematic effects such as the contribution from the ground emission

In the meantime we will complete the analysis of the data so far acquired.

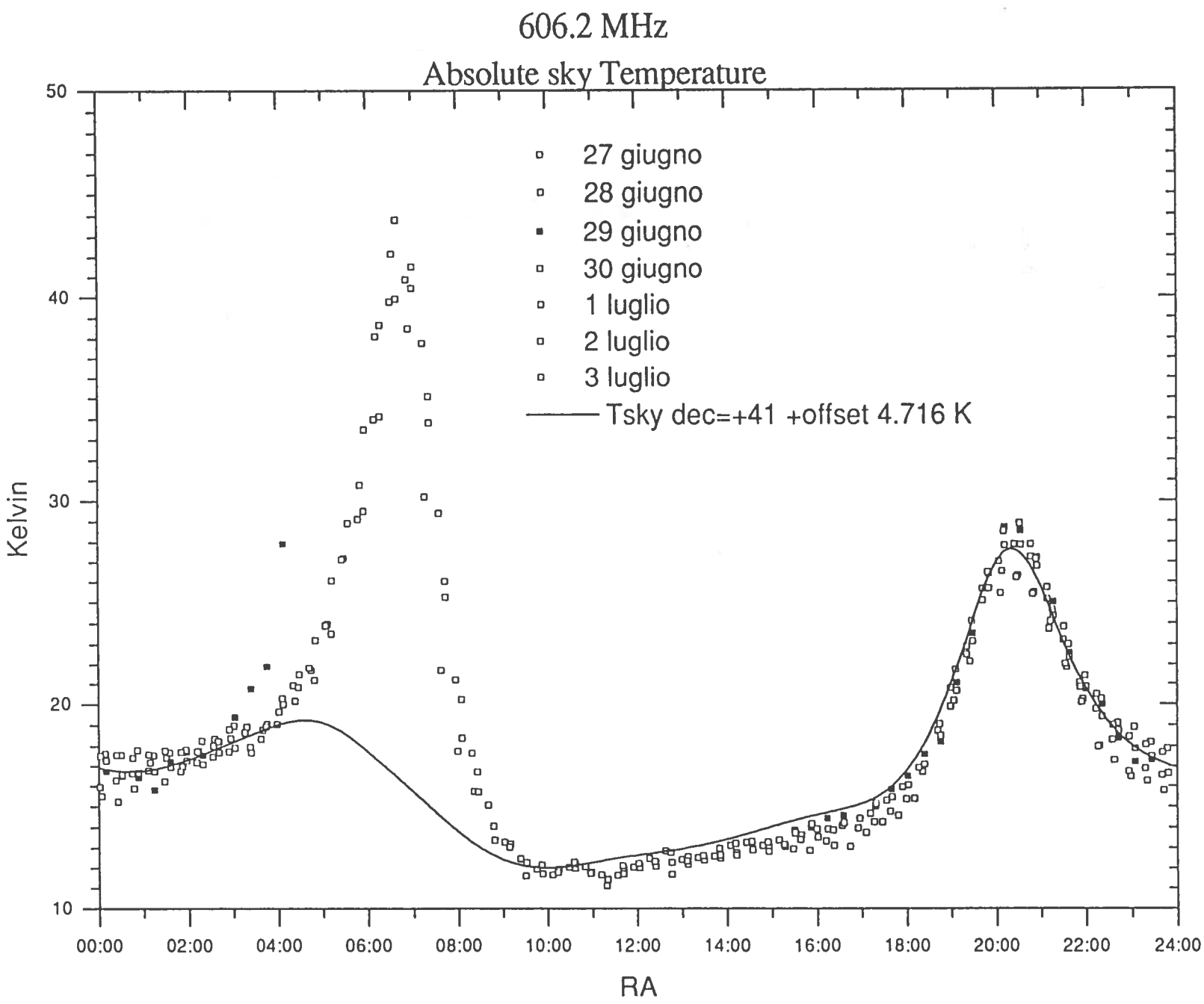
606.2 MHz
Absolute sky Temperature
27 giugno
28 giugno
29 giugno
30 giugno
1 luglio
2 luglio
3 luglio
Tsky dec=+41 +offset 4.716 K
Kelvin
RA
50
40
30
20
10
00:00
02:00
04:00
06:00
08:00
10:00
12:00
14:00
16:00
18:00
20:00
22:00
24:00

PROGRESS REPORT

for the year 1995

GALLEX PROJECT

performed largely at

LABORATORI NAZIONALI del GRAN SASSO

ABSTRACT

GALLEX has continued to register solar neutrinos (12 runs) and performs a second ^{51}Cr neutrino source experiment. The further error reduction in our newly published data and the exclusion of major systematical errors in GALLEX from the results of the first Cr source experiment have further increased the significance of the ^{7}Be neutrino problem.

GALLEX will operate till end of 1996. Beyond that date, new organizational and financial structures would have to be found to permanently operate a gallium solar neutrino observatory (GNO) at Gran Sasso.

CONTEXT TO PREVIOUS GALLEX REPORTS:

Earlier *Status Reports* have been given in May *1993,* March *1994 and April 1995.* In addition, a Progress Report on the *Chromium Neutrino Source* preparation was given in May 1994. The present *Annual Report* connects to these earlier reports. However, for readability we do repeat the general cover information, appropriately updated. The updated GALLEX membership list reflects the status on 31 December 1995. The earlier Reference list (Ref. 1-50) is continued starting with Ref. 51 through 64. In addition, we continue the list of GALLEX internal reports which are not fully published but made available to all parties interested (GX69,GX74,GX76-78,GX80).
As an appendix we add to this report the proposal:
„Proposal for a permanent Gallium Neutrino Observatory (GNO) at Laboratori Nazionali del Gran Sasso"

BRIEF DESCRIPTION OF GALLEX

PURPOSE

Measurement of solar neutrinos including pp-neutrinos from the primary solar fusion reaction: $p + p \rightarrow d + e^+ + \nu_e$ and ^{7}Be - neutrinos.

TYPE OF DETECTOR

Radiochemical

DETECTION METHOD

low-level counting of ^{71}Ge, monthly extracted from 100 tons of galliumchloride target solution. The production reaction is ^{71}Ga (ν_e, e^-) ^{71}Ge . Expected rates are of order 1 capture per day.

COLLABORATION

W.Hampel, G.Heusser, J.Kiko, **T.Kirsten** (spokesperson), M.Laubenstein, E.Pernicka, W.Rau, U.Rönn, M.Sann, C.Schlosser, M.Wójcik[1]: Max-Planck-Institut für Kernphysik (MPIK), Postfach 103980, D-69029 **Heidelberg**, Germany

R.v.Ammon, K.Ebert, T.Fritsch, D.Heidt, E.Henrich, L.Stieglitz, F.Weirich: Institut für Technische Chemie, Kernforschungszentrum Karlsruhe (KFK), Postfach 3640, D-76021 **Karlsruhe**, Germany

M.Balata, F.X.Hartmann: INFN - Laboratori Nazionali del Gran Sasso (LNGS), S.S. 17/bis Km 18+910, I67010 **L'Aquila**, Italy

E.Bellotti, C.Cattadori, O.Cremonesi, N.Ferrari, E.Fiorini, L.Zanotti: Dipartimento di Fisica, Università di Milano e INFN, Via Celoria 16, I-20133 **Milano**, Italy

M.Altmann, F.v.Feilitzsch, R.Mößbauer: Physik Department E15, Technische Universität **München** (TUM), James-Franck Straße, D-8046 Garching b.München, Germany

G.Berthomieu, E.Schatzman: Observatoire de la Cote d'Azur, Departement Cassini, B.P. 229, 06004 Nice Cedex 4, France

I.Carmi, I.Dostrovsky: Department of Environmental and Energy Research, The Weizmann Institute of Science (WI), P.O.Box 26, 76100 **Rehovot**, Israel

C.Bacci, P.Belli, R.Bernabei, S.D'Angelo, L.Paoluzi: Dipartimento di Fisica II Università di Roma 'Tor Vergata' e INFN, Sezione di Roma2, Via della Ricerca Scientifica, I-00133 **Roma**, Italy

A.Bevilacqua, M.Cribier, L.Gosset, J.Rich, M.Spiro, C.Tao, D.Vignaud: CEA,DAPNIA, CE **Saclay**, F 91191 Gif-sur-Yvette Cedex, France

J.Boger, R.L.Hahn, J.K.Rowley, R.W.Stoenner, J.Weneser: Department of Chemistry, Brookhaven National Laboratory (BNL), **Upton**, NY 11973, USA

[1] present address: Max-Planck-Institut für Physik, D-8000 München 40,Germany

[2] permanent address: Instytut Fizyki, Uniwersytet Jagiellonski, ul. Reymonta 4, PL-30-059 Kraków, Poland

SPOKESMAN

T.Kirsten (MPIK Heidelberg)

UNDERGROUND FACILITIES

'Main building' and 'Counting building' in the Eastern wing of hall A of LNGS, occupying ca. 40% of hall A.

DESCRIPTION OF THE EXPERIMENTAL SET-UP

For detailed and illustrated descriptions of GALLEX we refer to [1,4].

Here we only list major hardware components:

- Two exchangeable polyester target tanks (70 m^3 volume each)
- 54 m^3 (101 tons) of 8.2 molar gallium chloride solution, serving as the target
- Germanium desorption system consisting of liquid nitrogen reservoirs, evaporators, and Teflon like (PVDF) purging pipes within the target tank.
- 3 large Ge-absorber columns (3.1 m height)
- Two GeH_4 preparation lines to convert $GeCl_4$ into GeH_4
- Gas chromatography and 2 purification systems for counting gas preparation
- 2 counter filling lines
- Atomic absorption spectrophotometer for Ge-yield determinations
- More than 30 top quality miniaturized low background HD2-gas proportional counters with counter backgrounds below 1 count in two weeks within the acceptance windows for ^{71}Ge decays
- Multiple shielding devices (onion shell- philosophy): individual shield tank (radon protected); Faraday cage; Gran Sasso rocks
- Fast electronics (CAMAC bases) for registration of pulses, pulse shapes, and signals from peripheral detectors (e.g. anti coincidences, radon monitoring)
- MicroVax and periphery

PAST TIME TABLE

1986 - 1988	Preparation of underground facilities
1987 - 1990	Experiment installation and gallium accumulation
1990 - 1991	Test extractions and experiments
30 Nov 1990	GALLEX inauguration ceremony at LNGS
14 May 1991	Start of solar neutrino recording, phase 'GALLEX I'
29 April 1992	End of exposure period 'GALLEX I' (15 extractions)
30 April 1992	Transfer of target solution from 'B'-tank to 'A'-tank
- 19 Aug 1992	Technical conditioning of target in A-tank
19 Aug 1992	Restart of solar neutrino recording, phase 'GALLEX II';
since then	GALLEX II, monthly extractions routinely followed by a blank extraction
2 Nov 1992	End of counting of GALLEX I - samples
27 May -20 June 1994	Cr neutrino source irradiation at Grenoble
22 June 1994	GALLEX II series of runs completed after 24 GALLEX II Solar runs (SR16-SR39) and 19 Blank runs (BL6-24) had been successfully performed
23 June - 10 Oct 1994	11 Cr-source exposure runs (Cr1-Cr11) successfully performed
11 October 1994	Start of GALLEX III series of runs
31 Dec 1994	-2 GALLEX III Solar runs (SR40-SR41) successfully performed -Counting completed for GALLEX II

MAJOR ACTIVITIES IN 1995

1 January 1995 onwards	GALLEX III solar exposure period ongoing
2 May 1995	Counting completed for Cr- Source I
5 Sept - 1 Oct 1995	Cr- Source II irradiation at Grenoble
4 Oct 1995	GALLEX III series of runs completed after 14 solar runs (SR 40 - 53) and 4 Blank runs (BL 28 - 31), bringing solar observations to 53 runs in toto
5 Oct 1995	Start of 2nd Cr-Source exposure runs
31 Dec 1995	5 Source II runs (S138-S142) successfully performed. Source II-runs and counting of GALLEX III ongoing. Therefore, these data can only be released in 1996.

EXPERIMENT PERFORMANCE

GALLEX continues to operate as planned. All major and minor experimental processes perform properly. We list the most important items:

- Target purity far better than specified for required reduction of side reactions
- Extraction yield of ^{71}Ge from target solution >99%, with duration of nitrogen sweep reduced to 12 hours in the A-tank
- The achieved counter backgrounds (for both, K- and L-peak of the Ge-electron capture decay) are even lower than required, such that the errors are determined by the (very low) production rate rather than by background
- Side reactions contribute little to the signal
- Very high duty cycle (>95%). Neutrino recording is virtually uninterrupted.

These statements are documented e.g. in Ref. [2,5,6,14,15,22,24,43,46,51]

- First ever test of a solar neutrino detector with a calibrated manmade neutrino source.

COLLABORATION PERFORMANCE

GALLEX continued to operate smoothly. Two regular collaboration meetings were held in 1995: GALLEX 21 in Brookhaven (3 - 4 April) and GALLEX 22 at Tor Vergata, Roma (10 October). A Cr-source data evaluation and planning meeting took place in Paris (CdF), 12 - 13 July.

RESULTS

1. SUN

Table 1 and Figure compile the GALLEX solar data updated up to solar run SR39. We have published these data in August 1995 [51].

Table 1: Results from GALLEX solar exposure periods. Errors quoted are 1σ.

	GALLEX I [2]	GALLEX II [51]	combined [51]
time period	14.5.91-29.4.92	19.8.92-22.6.94	14.5.91-22.6.94 exc. 30.4.-18.8.92
exposure days	324	649	973
runs	15	24	39
L-result, [SNU]	105 ± 28	67.6 ± 14.4	77.6 ± 13.1
K-result,[SNU]	64 ± 21	81.0 ± 13.1	76.7 ± 11.1
(L + K) main result [SNU]	$81 \pm 17 \pm 9$	$75.2 \pm 9.7 \pm {}^{4.1}_{4.6}$	$77.1 \pm 8.5 \pm {}^{4.4}_{5.4}$

The result for the 24 GALLEX II runs is 75.2 ± 9.7[stat] ± $^{4.1}_{4.6}$[syst.] SNU. It confirms the result of GALLEX I of 81±17[stat]±9[syst.] SNU. The combined result for GALLEX-I and GALLEX-II is 77± 10 SNU (1σ) which is 59 ± 8% of the Standard Solar Model (SSM) of Bahcall and Pinsonneault*) or 63 ± 9 % of the SSM expectation value according to Turck-Chieze**) , respectively. The "minimal model" allowed value without neutrino disappearance is 79 SNU, but the Standard Solar Model predicts ~ 128 SNU. The reduced error of this improved result (±10.6 SNU (1σ) or 13.8% of the measured value) lends further support to the absence of ^{7}Be neutrinos, possibly due to MSW neutrino oscillations (see below and discussion in [49], [51]).

*)Bahcall, J.N. and Pinsonneault, M.H., Rev. Mod. Phys. 64 (1992) 885.

**)Turck-Chièze, S. and Lopes I., Ap. J. 408 (1993) 347.

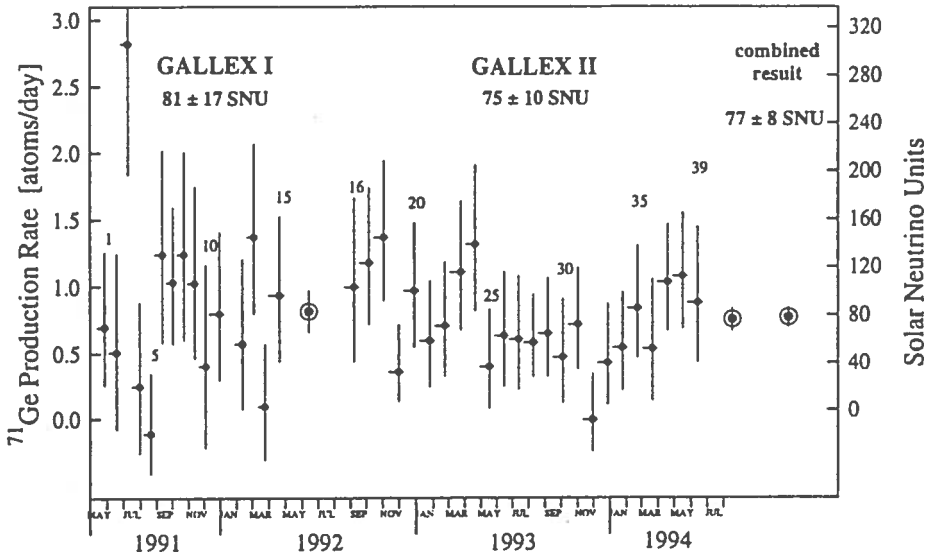

Fig.1: Results for the 24 solar neutrino runs of GALLEX II (labels 16-39) together with the 15 GALLEX I solar runs (labels 1-15). The left hand scale is the measured ^{71}Ge production rate, the right hand scale , the net solar neutrino production rate (SNU) after subtraction of side reaction contributions. Error bars are ± 1σ, statistical only. The point labeled 'combined' applies to the mean global value for the total of all 39 runs. Horizontal bars represent run duration, their asymmetry reflects the 'mean age' of the ^{71}Ge produced.

Possible Time Variations in the GALLEX Signal

We have investigated the complete GALLEX I+II data (39 runs) for possible time variations [51]. In the first of these tests, a periodic variation in time of the production rate about a constant value was assumed and the equation

$$P(t) = a + b \cdot \sin\left(\frac{2\pi}{T}(t - t_0)\right)$$

was solved without any restrictions on the amplitude, period and phase. The best fit to the data gave the values a = 77.0 ± 9.0 SNU, b = 10.8 ± 12.0 SNU, T = 312 ± 79 days, t_0 = 2.2 ± 2.6 days (zero time is May 1, 1991). The goodness-of-fit confidence level for this model using the likelihood ratio test is 82% which has to be compared to 88% resulting from the standard analysis (assuming a production rate constant in time).

In the second analysis, we checked for a possible correlation of the production rate P(t) with the variation of the sunspot number $N_S(t)$ relative to the mean $\langle N_S \rangle$ for the GALLEX data-taking periods:

$$P(t) = a + b \cdot \left(\frac{N_s(t) - \langle N_s \rangle}{\langle N_s \rangle} \right)$$

The same model has previously been applied to the data of the Homestake detector*). Our result for the GALLEX data is a = 78.5 ± 9.1 SNU for the constant part and b = 6.5 ± 17.6 SNU for the variable amplitude, with a goodness-of-fit confidence level of 86%. The results from both of these calculations are consistent with no time variation of the GALLEX production since (1) the calculated time-independent production rate a agrees with the present measured GALLEX mean value, (2) the time-dependent amplitude b is consistent, within the errors, with a value of zero, and (3) the goodness-of-fit does not improve by invoking a time dependence.

2. CHROMIUM NEUTRINO SOURCE

In 1995, the ^{51}Cr neutrino source which had been used in 1994 was reactivated for a second target exposure. This exposure started on October 5, 1995. Five ^{71}Ge extractions were done until the end of the reporting period. Counting will continue till summer 1996.

Counting for the runs of the first Cr source experiment (see previous Progress Report and [46]) has been completed in May 1995 and the published preliminary value (104 ± 12 % of the ^{71}Ge activity expected from the calibration of the Cr source) [46] has been updated (97 ± 11 %) and released through Ref. [52]. Fig.2 displays the results of all 11 individual ^{51}Cr neutrino source runs in comparison with the expectation from the source calibration.

This is a very satisfactory result. It excludes experimental artifacts or unknown errors that are comparable to the 40% deficit in the observed solar neutrino signal [51].

*) Filippone B.W., and Vogel P., Phys. Lett. B246 (1990) 546-550.

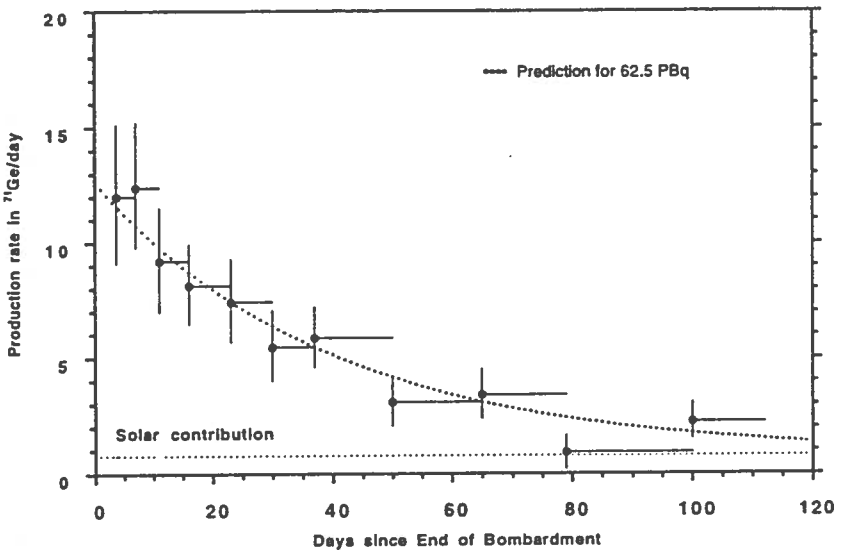

Fig.2: Results of all 11 GALLEX ^{51}Cr neutrino source runs in comparison with the expectation from the source strength determination (dotted line). The contribution from solar neutrinos is also indicated.

The ^{51}Cr Source Experiment as Neutrino Oscillation Experiment

It has long been known that an experiment with an artificial ^{51}Cr neutrino source is in principle also a short range neutrino oscillation experiment (Hampel*) . Since ^{51}Cr emits electron neutrinos and since the GALLEX detector is sensitive to these neutrinos only, the GALLEX Cr source experiment is of the disappearance type. Any deficit in the measured signal of the Cr experiment as compared to the expectation could then in principle be ascribed to neutrino oscillations into the muon or tau neutrino types. On the other hand, if the signal observed corresponds to the expected value, as it is the case, this limits the parameters of possible neutrino oscillations. The dark region in Fig. 3 shows the parameter space in the Δm^2-$\sin^2 2\theta$ plane which is excluded at the 90% confidence level by the outcome of the GALLEX Cr source experiment. A similar analysis has been done by Bahcall et al.**)

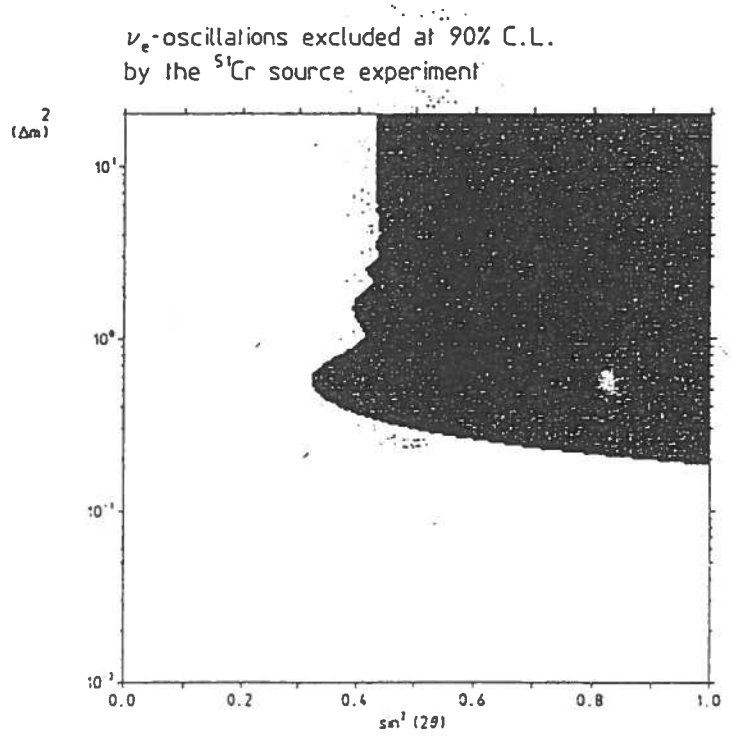

Fig. 3: Parameter space (dark region) in the Δm^2-$\sin^2 2\theta$ plane which is excluded by the GALLEX Cr source experiment at 90% confidence level

*) Hampel W., Proc. Neutrino 1981, University of Hawaii, Honolulu, Vol. 1 (1981) 6-18.
**) Bahcall, J.N., Krastev P.I. and Lisi E., Phys. Lett. B 348,

3. COUNTER CONSTRUCTION

GALLEX proportional counters with a shaped silicon cathode have been successfully applied in GALLEX runs in order to reduce the counter end effects and thus to increase the counting efficiency . In order to combine the advantage of this increased counting efficiency with the very high reliability and robustness of the GALLEX counters with iron cathode, a prototype counter with a shaped iron cathode has been built which revealed no difficulties and problems in the course of counter construction and handling. Three such counters are presently counting background at Gran Sasso. The count rates obtained so far are (within statistical errors) comparable with those of other GALLEX counters. In addition to these Fe counters, a series of 6 counters with silicon cathodes has been completed (4 with an unshaped *cathode (Si), 2 with a shaped cathode (SC)). Three of them passed the initial tests and control measurements in Heidelberg and the background measurements at Gran Sasso Underground Laboratory. Since the rates obtained for all three are sufficiently low, they can be used without restriction in future GALLEX runs [106].*

IMPLICATIONS

Concerning the prevalent judgements in the international neutrino physics community, 1995 was marked by a general acceptance of the view that the ^{7}Be neutrino deficit is at the core of the solar neutrino problem. Many recent phenomenological analyses have pointed out that, relative to solar model predictions, the flux of ^{7}Be neutrinos derived from the different solar neutrino detectors appears to be strikingly low, especially when compared to the measured Kamiokande flux of ^{8}B neutrinos. This conclusion appears to argue against an "astrophysical solution" to the solar neutrino problem (see for instance [44]): even those (non-standard) solar models that are able to reduce the neutrino fluxes from both ^{7}Be and ^{8}B still cannot come close to reproducing the experimentally derived ^{7}Be and ^{8}B fluxes. The evidence for the ^{7}Be problem has strengthened over time as GALLEX data have accumulated. The early GALLEX results with their larger error ranges hinted at but could not precisely define the scope of the deficit of ^{7}Be neutrinos. Now, little room remains for the contributions from ^{7}Be and CNO neutrinos. It is obvious that the evidence for a small

value of the ^{7}Be flux and thus for the ^{7}Be solar neutrino problem has only gradually evolved as the errors have shrunk in the continuing GALLEX measurements.

GALLEX observes solar neutrinos in sufficient quantity to account for the solar luminosity, reflected in the flux of low-energy pp-neutrinos from the primary hydrogen fusion, yet the other neutrino fluxes also expected from solar models, in particular ^{7}Be neutrinos, turn out to be depressed or even totally absent. If this is interpreted as evidence for neutrino mass mediated neutrino flavor oscillations, the far-reaching consequences of such a conclusion call for the utmost achievable statistical and systematical significance of the data, keeping in mind that all solar neutrino data are low-rate by any usual standard. This is why solar observations as well as neutrino source irradiations should continue for quite some time, even if this were the only motivation, which it is not.

FUTURE TIME TABLE

Jan - 12 Febr 1996	Completion of Cr-source II exposure period
13 Feb - Dec 1996	GALLEX IV solar neutrino runs, interrupted by doping experiments (^{71}As, fast neutrons, ..) from September 1996 onwards
	Completion of Cr-Source II counting and data release
	Completion of GALLEX III counting and data release
	This will bring the integral exposure time to 4 years. As originally proposed and planned for, this is the time required to reduce the statistical error to 6 SNU.
Jan - July 1997	Counting of GALLEX IV runs
Jan - Dec 1997	Internal counter calibrations using active ^{71}Ge , prohibited during all previous times because of the contamination risk

REQUESTED SUPPORT

GALLEX appreciates again the generous support it enjoys at LNGS. We are grateful that INFN has granted general support and use of the site in hall A by GALLEX and gave high level administrative support concerning licenses and handling permits also for the chromium source as well as financial help to assure continued use of the gallium target until end of 1996 .

Concerning the future of the gallium solar observations we refer to the GNO-proposal attached as 'Appendix' . The relationship between GALLEX and GNO was already described in last years Progress Report, as follows:

'Conceptions beyond 1996':

The GALLEX collaboration with its present structures and responsibilities plans to definitely cease solar target exposures end of 1996 in fulfillment and successful completion of the scientific goals for which the experiment was proposed. Afterwards, the collaboration will continue to exist for whatever period is required to complete counting, to work up the acquired data and their interpretation, eventually to perform peripheral experiments, but not to continue to register the solar neutrino flux.

This applies only for the GALLEX collaboration in its present structure. It does not exclude the possibility that another group of scientists (including present members of GALLEX) favors a new proposal for continued operation of a Gallium Neutrino Observatory (GNO) at Gran Sasso with newly defined objectives in context with the time constancy of the solar neutrino flux and with the upcoming second generation of solar neutrino experiments, which observe other parts of the neutrino spectrum. Depending on whether or not such an initiative will find the necessary support to take over the gallium target, GALLEX would either help to transfer the experimental equipment to this new GNO collaboration in good spirit, or otherwise to disassemble the GALLEX main equipment. Disassembling of the counting facilities (GFL,FFL) is not planned in view of their potential for low level counting beyond ^{71}Ge- detection.
For the arguments which would make continued operation of a gallium detector at Gran Sasso desirable we refer to the proposal (Appendix 1).

GALLEX LIST OF PUBLICATIONS AND REPORTS

Note: The GX-## refers to the GALLEX collection of papers, internal reports, preprints ect. All GX-items are made available to any interested party on request.

A PUBLICATIONS and THESES

(i) Fully completed references for entries already listed in preliminary form in previous Annual GS Status Reports

34	GX29	T.Stolarczyk	GALLEX:Results, status, and future. ed. J.Tran Thanh Van Proc. XIII Moriond Workshop: Perspectives in neutrino physics, atomic physics and gravitation (1993) 77
38	GX41	G. Heusser	Background in ionizing radiation-by Ge-spectrometry (Proc. 3rd International Summer School on Low-Level Measurements of Radioactivity in the Environment, La Huelva, Spain, 1993, ed. M.Garcia-Leon, World Scientific, Singapore (1993) 69.
40	GX50	G.Heusser	Characteristics of the GALLEX spectrometer Proc. of the 2nd Int. Conf. on Trends In Astroparticle Physics, Aachen, Germany) ed. P.Bosetti, B.G.Verlags-gesellschaft, Leipzig, (1994), 33
41	GX52	T.Kirsten	GALLEX solar neutrino results and their implications Proc.Int.Conf.Non-Accelerator Physics, Bangalore 1994, ed. R.Cowsik, World Scientific, Singapore (1995) 158-166
44	GX62	W.Hampel	Recent Results of the GALLEX Solar Neutrino Detector and its Implications AIP Conf.Proc. 327 (1995) 59-62

48	GX71	T.Kirsten	Analysis of Ultra-Low Activities to detect Solar Neutrinos with the Radiochemical GALLEX detector ed.H.J.Kluge, AIP Conf.Proc. 329 (1995) 15-21
49	GX72	T.Kirsten	Solar Neutrino Problems. (Texas Conf.) Ann. NY Acad.Sci. 759 (1995)1-20

(ii) *New entries*

51	GX 75	P.Anselmann et al GALLEX collaboration	GALLEX solar neutrino observations: complete results for GALLEX II. Phys.Lett.B357(1995)237-247
52	GX79		
53	GX81	D.Vignaud	The solar neutrino problem after the GALLEX artificial neutrino source experiment. ed. B.Guiderdoni Proc. XV Moriond Workshop: Dark matter in cosmology, clocks and tests of fundamental laws (1995) 237
54	GX82	D.Vignaud	The 62 PBq Cr-51 artificial neutrino source experiment, Moriond Workshop, Jan 1995
55	GX83	D.Vignaud	GALLEX: Update of the solar neutrino results and of the Cr-source experiment. EPS Conference, Brussels, July 1995
56	GX84	M.Cribier et al	Radiochemical measurement of fast neutrons using a $Ca(NO_3)_2$ aqueous solution. NIM A265 (1995) 533
57	GX85	M.Cribier et al	The neutron induced background in GALLEX. Astroparticle J. 4 (1995)

58	GX86	H.Lalla	Status of the GALLEX solar neutrino project. XXVII ICHEP, Glasgow, (1994) 969
59	GX87	D.Vignaud	GALLEX: Update of the solar neutrino results and of the Cr-source experiment. Proc. II Renc.du Vietnam, Ho Chi Minh City 1995
60	GX88	R.Bernabei	Implications of the GALLEX results after the Chromium source experiment. Proc.TAUP 95, Toledo, Sept.1995
61	GX90	T.Kirsten	GALLEX and the Solar Neutrino Problem. ed. H.Ejiri, Yamada Conf.XL IV, World Scientific, Singapore (1995) 135-143
62	GX91	T.Kirsten	Solar Neutrino Data. ed.M.Greco, Results and Perspectives in Particle Physics'. (La Thuile).Edition Frontieres, Gif s.Yvette (1994)3-20
63	GX105	S.Pezzoni	Non-solar neutrino production of ^{71}Ge in GALLEX. PhD.Thesis, Heidelberg University, 1995
64	GX106	W.Rau	Bau von Zählrohren mit geformter Eisenkathode. Master Thesis, Heidelberg University, 1995

B INTERNAL REPORTS

GX69	03.95	M.Altmann	Pulse Shape Analysis by Fitting the TDF-Pulse
GX74	03.95	T.Kirsten	GALLEX Project at LNGS. Progress Report for the year1994. LNGS 95/07 (1995) 17-48

GX76	05/95	M.Altmann	GALLEX after the source experiment: Status and implications. Proc.'Ringberg Workshop on Astroparticle Physics' Schloß Ringberg, March 1995
GX77	05/95	F.X.Hartmann	Energy weighted result from GALLEX I and GALLEX II
GX78	11/95	J.Boger, R.L.Hahn, Y.Y.Chu	Determination of the ^{51}Cr Source Strength at BNL
GX80	11/95	R.v.Ammon, P.Dressler	Dissolution of Chromium samples and their gamma spectrometry

PROPOSAL

FOR A PERMANENT

GALLIUM NEUTRINO OBSERVATORY (GNO)

AT LABORATORI NAZIONALI DEL GRAN SASSO

E.Bellotti [1], C.Cattadori, N.Ferrari, L.Zanotti
Dipartimento di Fisica dell'Universitá e INFN,
Via Celoria 16; I 20133 Milano (Italy)

P.Belli, R.Bernabei, S.d'Angelo
Dipartimento di Fisica, II Universitá di Roma "Tor Vergata" e INFN
Sezione di Roma 2, Via della Ricerca Scientifica, I 00133 Roma (Italy)

M.Balata, M.Sann
Laboratori Nazionali del Gran Sasso (LNGS),
SS 17/bis Km 18+910, I 67010 L'Aquila (Italy)

W.Hampel, G.Heusser, J.Kiko, T.Kirsten, E.Pernicka
Max-Planck-Institut für Kernphysik (MPIK),
Postfach 103980, D-69029 Heidelberg (Germany)

K.Ebert, E.Henrich
Institut für Technische Chemie, Forschungszentrum Karlsruhe (FZK),
Postfach 3640, D-76021 Karlsruhe (Germany)

M.Altmann, F.von Feilitzsch
Physik Department E15, Technische Universität München (TUM),
James Franck Straβe D-8748 Garching (Germany)

It is anticipated that other institutes may join this collaboration

February 1996

[1] Principal investigator

INDEX

SUMMARY 43

1. INTRODUCTION 44

2. SOLAR NEUTRINOS 47

2.1 Solar neutrino fluxes 47

2.2 Measuring the solar neutrino flux 47

3. SOLAR NEUTRINOS: PERSPECTIVES FOR THE FUTURE .. 49

3.1 Proposed solutions of the solar neutrino problem 49

3.2 Future solar neutrino experiments 50

3.3 Future prospects of neutrino physics 52

4. GALLEX 58

4.1 Outline 58

4.2 GALLEX history and results 59

4.3 The ^{51}Cr neutrino source experiment 61

4.4 Implications of the GALLEX results 62

5. THE GNO PROJECT (Gallium Neutrino Observatory) 63

5.1 Outline 63

5.2 Objectives for GNO 63

5.2.1 Importance of monitoring the pp neutrino flux 63

5.2.2 Refinements of the measurement of the solar neutrino capture rate . 64

5.2.3 Reducing the systematic error in GNO 64

5.2.4 Searches for time variations of the signal 65

5.2.5 The production background in GNO100 66

5.2.6 Statistical significance of a single GNO100 run 67

5.3 Technical aspects and operations 73

5.3.1 LNGS facilities 73

5.3.2 Galliumchloride versus Gallium metal target 74

5.4 Financial aspects and funding request 76

APPENDIX : Time variations of the solar neutrino flux ? 78

REFERENCES 81

SUMMARY

We propose a radiochemical experiment to monitor the solar neutrino flux over many years (more then one solar cycle) using 100 tons of gallium as target.

This Gallium Neutrino Observatory (GNO) :

- would provide the mean flux of solar neutrinos above 233 keV with an accuracy of $\sim 5\%$, or 4 Solar Neutrino Units (SNU) if the total production rate is 80 SNU.
- will be sensitive to time variations at the level of 5 - 10 %

This explores neutrino properties (mass, mixing, magnetic moment) as well as stellar structure.

The entire experimental set-up (gallium target, extraction system, chemical laboratory, counting system) can be housed in the southern wing of Hall A in the Laboratori Nazionali del Gran Sasso, without requiring major civil works.

The experiment has practically no technical uncertainties. This is based on the fruitful experience of the GALLEX experiment, which would be succeeded by GNO.

1 INTRODUCTION

Solar neutrino physics is one of the most exciting fields of research both in astrophysics and in elementary particle physics.

The observation of solar neutrinos, and especially of low energy solar neutrinos, demonstrated that the Sun is producing energy via the so-called Hydrogen cycle.

However, for all 4 experiments which have provided data up to now, the measured rates are short of expectation. The magnitude of the deficit differs, as does the spectral response of the experiments.

The initial approach is to interpret the results in terms of 'astrophysical' solutions. Somewhat arbitrarily, this term is defined to include:

- modifications of the Standard Solar Model (SSM);
- modification of input parameters such as initial solar conditions (solar elemental abundances, age of the Sun), cross-sections (S-factors) for stellar reactions, opacities for the solar plasma;
- questioning the results of the experiments or the rate predicted for them.

No consistent explanation of the experimental results arises from such treatment. Therefore these results are considered to be evidence (although not yet unquestionable) of non standard neutrino physics. The favoured interpretation of solar neutrino data is in terms of neutrino oscillations, which require violation of lepton flavour conservation and non zero mass of at least one neutrino. In terms of 2 flavour-mixing there are three sets of allowed mixing parameters which are compatible with the data:

- Oscillations in matter, large mixing angle	$\Delta m^2 \sim 2 \cdot 10^{-5}\, eV^2$	$; sin^2 2\theta \sim 0.7$
- Oscillations in matter, small mixing angle	$\Delta m^2 \sim 6 \cdot 10^{-6}\, eV^2$	$; sin^2 2\theta \sim 0.006$
- Oscillations in vacuum	$\Delta m^2 \sim 10^{-10}\, eV^2$	$; sin^2 2\theta \sim 0.85$

where θ is the flavour mixing angle and Δm^2 is the squared mass difference between the two mass eigenstates. Therefore solar neutrino data indicate oscillation parameter values which are presently unaccessible to laboratory experiments (sec. 3.3).

Solar neutrino data collected by R.Davis have been also analyzed in terms of time variations. More specifically, an anticorrelation of the neutrino flux with solar activity, indicated by the sunspot number, has been suggested. Such an effect, if confirmed, would proof the existence of a neutrino magnetic moment of $\sim 10^{-11}\, \mu_B$ and a large magnetic field in the Sun. In fact present data can also be explained with the so called Resonance Spin Flavour Precession mechanism; in this case typical values of the flavour mixing parameters are $\Delta m^2 \sim 10^{-8} - 10^{-7}\, eV^2$; $sin^2 2\theta \sim 0.2 - 0.3$ for a neutrino magnetic moment of $\sim 10^{-11}\, \mu_B$ and a time dependent magnetic field in the convective zone variing during the solar cycle from 15 to 45 kGauss.

Solar neutrino detection is a very difficult task for many reasons:

- The interaction rates are very low, much less than 1 event per day per ton also in the most favourable cases for realistic targets;
- The energy of the events is in the MeV range where, at least in principle, many other sources than solar neutrinos can simulate the true solar events; moreover it is impossible to have real 'beam-off' blanks;
- It is extremely difficult to expose the target to artificial neutrino sources with the same energy spectrum as solar neutrinos have.

Due to the above mentioned difficulties, we believe that many years are required to fully use all the potential of such an experiment. As an illustration, the HOMESTAKE Chlorine experiment has operated now for more than 25 years, but methodological questions are still being discussed.

In the near future two new experiments (SUPERKAMIOKANDE and SNO) will start data taking; both are exclusively sensitive to ^{8}B neutrinos. A third experiment, BOREXINO, is under way at Laboratori Nazionali del Gran Sasso: it will be most sensitive to ^{7}Be neutrinos. A real time detector for the very low energy pp-neutrinos (by far the most luminous neutrino type) is far off in the future.

The radiochemical Gallium experiments GALLEX (Laboratori Nazionali del Gran Sasso) and SAGE (Baksan, Caucasus), are the only experiments presently measuring the pp neutrino flux, which is fixed by the solar luminosity constraint. GALLEX has been measuring the solar neutrino flux since 1991, and according to the present plans is supposed to stop data taking at the end of 1996. Since the future of SAGE is very uncertain, there is a high risk that no experiment will measure the pp neutrino flux in the next years.

Therefore we propose a radiochemical experiment with 100 tons of Gallium as a target, GNO100, using $\sim$ 65 tons of gallium in form of $GaCl_3$ in HCl solution (like in GALLEX), and the remaining part either in metallic form or also as chloride. The target can be accomodated in the South wing of the Hall A of the Laboratori Nazionali del Gran Sasso without major infrastructural works.

The procedure for the extraction of germanium from the chloride solution will be unchanged with respect to GALLEX, while some research and development would be necessary for the metallic target.

The use of Ga in two different forms will allow a cross check of the background due to side reactions (radioactive impurities in the sample, neutrons and cosmic muons entering the target), and increases the confidence in the evaluation of systematic effects.

The experience acquired with GALLEX allows us to state that a significant reduction of the systematic error is possible; uniformization of the counters, improved electronics, and data analysis could lower the systematic errors on counter efficiencies from 4% to $\sim$ 2%. Overall a total systematic error of $\sim$ 4% is feasible, corresponding to a total error of $\sim$ 5% after a live time of 4 years. Therefore such an experiment would provide a solar neutrino measurement with an accuracy of $\sim$ 5 SNU.

Assuming that the present capture rate measured by GALLEX is confirmed, *GNO*100 by itself would then be able to exclude all standard and many non-standard models at more than 3 sigma level. Furthermore it could restrict the incident pp and ^{7}Be-neutrino fluxes much more stringent then presently possible. Moreover the entire set of data available in a few years will significantly reduce the allowed region in the mixing parameter space.

The possible observation of time variations in excess of the geometrical effect would be a model independent proof of non-standard physics in the elementary particle sector.

Disposition:
Section 2.1 presents the solar model predictions for the solar neutrino fluxes; section 2.2 summarizes the results of the 4 experiments which have detected solar neutrinos up to now. In section 3 we discuss of the perspectives of solar neutrino physics, from the theoretical (3.1) and from the experimental (3.2) point of view. The strong connections to neutrino physics in terrestrial experiments are mentioned in section 3.3.
In section 4 we give a description of the GALLEX experiment and of the ^{51}Cr neutrino source experiment performed with the GALLEX detector. Section 5 is devoted to a

detailed discussion of the GNO project, which foresees a gradual extension from 30 to 100 tons of gallium (5.1). This includes detector performance and physical motivations (5.2), as well as some technical (5.3) and financial (5.4) aspects.

2 SOLAR NEUTRINOS

2.1 Solar neutrino fluxes

It is well known that the present Sun operates as a thermonuclear power station which converts hydrogen into ^{4}He by means of the thermonuclear fusion reactions of the pp-chain and of the CNO cycle [BAH89].

Electron neutrinos are produced during these processes, with principal energies ranging from 0 up to $\sim$ 14 MeV. It is useful to distinguish solar neutrinos according to the reaction by which they are produced, as shown in Tab. 2.1 .

Neutrino type (*)	Reaction	Energy Range (keV)	Mean energy (keV)	SSM flux (Earth) $s^{-1}cm^{-2}$
pp	$p(p,e^+\nu)d$	$0 \rightarrow 420$	260	$(6.00 \pm 0.04) \cdot 10^{10}$
^7Be	$^7Be(e^-,\nu)^7Li$	380 , 860	380 , 860	$(4.89 \pm 0.29) \cdot 10^9$
^8B	$^8B(,e^+\nu)^8Be$	$0 \rightarrow 14060$	7300	$(5.69 \pm 0.81) \cdot 10^6$
pep	$p(pe^-,\nu)d$	1440	1440	$(1.43 \pm 0.02) \cdot 10^8$
^{13}N	$^{13}N(,e^+\nu)^{13}C$	$0 \rightarrow 1200$	710	$(4.92 \pm 0.51) \cdot 10^8$
^{15}O	$^{15}O(,e^+\nu)^{15}N$	$0 \rightarrow 1400$	996	$(4.26 \pm 0.83) \cdot 10^8$
^{17}F	$^{17}F(,e^+\nu)^{17}O$	$0 \rightarrow 1730$	1000	$(5.39 \pm 0.86) \cdot 10^6$
hep	$^3He(p,e^+\nu)^4He$	$.. \rightarrow 18770$	9620	$1.23 \cdot 10^3$

(*) ^7Be is produced via $^3He(^4He,\gamma)^7Be$; ^8B is produced via $^7Be(p,\gamma)^8B$

Table 2.1 Neutrinos produced in the Sun according to the Standard Solar Model [BAH92]

The production rate of different types of solar neutrinos is obviously determined by the rates of the respective reactions. Solar models predict these reaction rates, and so the solar neutrino spectrum (Fig. 2.1); for a recent review see for example [TUR93a] and the references quoted therein.

If neutrinos have standard properties, that is if they do not decay or oscillate, then solar neutrinos will freely escape from the solar core and reach the Earth with unchanged energy spectrum and undepressed fluxes, as predicted from the solar model (Fig. 2.1). The experimental determination of the solar neutrino spectrum reaching the Earth is therefore a crucial test for solar (and stellar) astrophysics.

On the other hand, non-standard neutrino properties (e.g. non zero rest mass, non-zero magnetic moment) can lead to spectral and flux distortions on the way from the solar core to the detector on Earth. Then, character and magnitude of these distortions become diagnostic for these neutrino properties.

2.2 Measuring the solar neutrino flux

Due to the very low neutrino-matter cross-sections it is very difficult to detect solar neutrinos; at present 4 experiments have been performed, analyzing different parts of the spectrum; Tab. 2.2 summarizes the main features of them and the recent results. Also shown for each experiment is the ratio between the observed neutrino interaction rate and the theoretical interaction rate expected from the SSM.

The neutrino detection threshold is different in the 4 experiments, so that each of them is sensitive to different neutrino types, as shown in Tab. 2.3.

We notice that all 4 experiments measure a deficit in the solar neutrino flux as predicted by the SSM; this discrepancy between theory and observation is generally known as Solar Neutrino Problem (SNP) [HAT94a] [BAH92].

Experiment	Target	Detection Reaction	E_{th} (keV)	Observed Rate (SNU)	Expected Rate (SNU) [BAH92]	Ratio (obs/exp)
HOMESTAKE (radiochem)	615 t C_2Cl_4	$^{37}Cl(\nu_e,e^-)^{37}Ar$	813	2.55 ± 0.23 [CLE95]	7.9 ± 2.5	0.32 ± 0.10
KAMIOKANDE (real-time)	3000 t H_2O	$e^-(\nu_x,\nu_x)e^-$	7000	0.31 ± 0.04 ev/d [SUZ95]	0.62 ± 0.22 ev/d	0.50 ± 0.18
GALLEX (radiochem)	101 t $GaCl_3$	$^{71}Ga(\nu_e,e^-)^{71}Ge$	233	77 ± 10 [ANS95b]	132 ± 17	0.58 ± 0.11
SAGE (radiochem)	55 t Ga metal	$^{71}Ga(\nu_e,e^-)^{71}Ge$	233	69 ±13 [NIC94]	132 ± 17	0.52 ± 0.12

Table 2.2 Solar neutrino experiments and their results

Experiment	pp	^7Be	^8B	pep	^{15}O	^{13}N
HOMESTAKE	–	15.0%	77.5%	2.5%	3.8%	1.2%
KAMIOKANDE	–	–	100%	–	–	–
GALLEX-SAGE	53.9%	27.3%	10.5%	2.3%	3.7%	2.3%

Table 2.3 Composition of the neutrino signal (%) expected in solar neutrino experiments according to the SSM

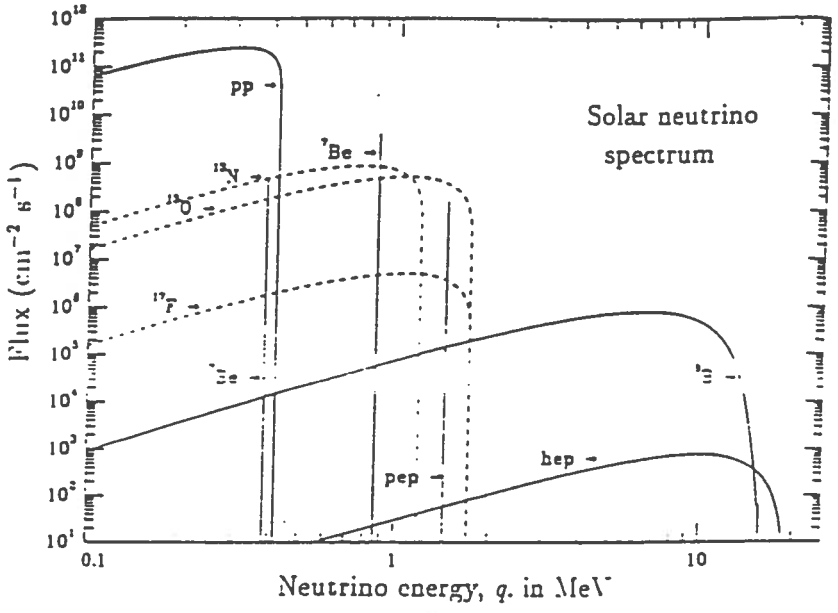

Figure 2.1 The solar neutrino spectrum as predicted by the Standard Solar Model [BAH92]

3 SOLAR NEUTRINOS : PERSPECTIVES FOR THE FUTURE

3.1 Proposed solutions of the Solar Neutrino Problem

Three different types of solutions have been proposed for the SNP :

Experimental problems with solar neutrino detection

One possible explanation of the observed deficit could in principle be some unknown inefficiency problem connected with the experiments; this is however rather unlikely since deficits are observed in 4 independent experiments based on widely different procedures and systematics. It is then most unlikely to have this problem in all the experiments. Furthermore for GALLEX and SAGE the experimental procedure has been verified with strong man-made ^{51}Cr sources, yielding the expected results.

Astrophysical solutions

This solution assumes that the solar neutrino fluxes calculated from the SSM are not applicable:

- either since certain physical processes are misjudged or ignored
- or because certain input parameters are in error (e.g, cross-sections, abundances, opacities)
- or because the SSM is too simplistic and does not fully describe the state of the solar interior.

Many ad-hoc non-standard solar models have been proposed, but none of them can simultaneously explain the flux deficits as observed in the 4 experiments and the helioseismological observations. In fact, logical conflicts occur if the results of all 4 experiments are to be explained simultaneously.

Non-standard neutrino properties

This hypothesis assumes that the SSM prediction of the neutrino spectrum is correct, but flux and spectrum of electron neutrinos undergo changes on the way from the solar core to the detector.

The most popular class of solutions implies that neutrinos have a (small) mass, which allows them to experience flavour oscillations: electron neutrinos produced in the Sun may oscillate to another flavour ($\nu_\mu, \nu_\tau, \nu_{sterile}, \ldots$) before reaching the Earth, therefore becoming undetectable in present experiments. Considering the simplified case of two neutrinos of different flavours ($\nu_e, \nu_x, (x = \mu, \tau)$), two parameters have to be considered: $sin^2 2\theta$, θ being the mixing angle between the two mass eigenstates, and the squared mass difference Δm^2.

Three solutions are consistent with presently available experimental data:

a Vacuum oscillations (VO)

As suggested by Pontecorvo [PON68], for mixing parameters $\Delta m^2 \sim 10^{-11} eV^2$, $\sin^2 2\theta \sim 0.8$, the neutrino oscillation length is of the order of the Sun-Earth distance, so that the neutrino survival probability at Earth depends heavily on its energy. Seasonal modulation of the ^{7}Be flux is expected in this context (see Appendix) . Fig. 3.1 shows the parameter region allowed by a fit of the present data of the 4 experiments measuring the solar neutrino flux. For a recent analysis see for example [KRA92][BER95][CAL95].

b MSW solution

Flavour oscillations can become resonantly enhanced by the so-called matter effect, or Mikheyev-Smirnov-Wolfenstein effect [WOL78] [MIK86]. Even if the vacuum mixing angle is small, very effective (even complete) flavour conversion can occur through coherent neutrino electron scattering at the very high electron density prevailing in the solar interior. The magnitude of the reduction factor in the various experiments differs with the energy threshold and, consequently, with the different spectral response of the neutrino detectors (see Tab. 3.2).
The set of MSW parameters which can account for the neutrino fluxes measured by the present experiments is shown in Fig.3.2:
$\Delta m^2 \sim 6 \cdot 10^{-6} eV^2$, $\sin^2 2\theta \sim 0.006$ is the so called 'small angle solution', and
$\Delta m^2 \sim 2 \cdot 10^{-6} eV^2$, $\sin^2 2\theta \sim 0.7$ is the 'large angle solution'.
For a recent analysis see for example [HAT94b] [FIO94].

c Resonance Spin Flavour Precession

Another suggested 'non-standard-physics' solution to the SNP is Resonance Spin Flavour Precession (RSFP) [AKH88][LIM88]. Supposing that neutrinos have a magnetic moment of $\sim 10^{-11}\mu_B$, a resonant flavour transition (or a flip into a right handed sterile state) is possible while the neutrinos are crossing the magnetic field in the Sun, giving rise to oscillations $\nu_{eL} \leftrightarrow \nu_{\mu,\tau R}$ (Dirac neutrinos), $\nu_{eL} \leftrightarrow \overline{\nu}_{\mu,\tau R}$ (Majorana neutrinos).

One expects two effects:

- a global reduction of the ν_e flux
- an anticorrelation of the registered neutrino fluxes with the solar activity is feasible. It could depend on the changing intensity and direction of the solar magnetic field (Appendix).

However this depends on the intensity of the solar magnetic field, the structure of which is unknown. For recent analyses see for example [AKH88][LIM95][MAS95]. The effect of a combination of RSFP and MSW has also been studied [NUN93].

3.2 Future solar neutrino experiments

A number of new experiments are under construction or in preparation. In the following we give a brief description of those future experiments which are most progressed; for a more complete review see for example [BEL94a].

SUPERKAMIOKANDE [SUZ95]

The SUPERKAMIOKANDE experiment is an extension of KAMIOKANDE. It consists of 50,000 tons of water (18,000 tons fiducial mass), looking for the elastic scattering reaction

$$\nu_x + e^- \rightarrow \nu_x + e^-$$

It is mainly sensitive to the electron flavour ($x = e$). Improved photomultiplier timing resolution, higher light collection efficiency and lower level of natural radioactivity should allow to lower the threshold for scattered electrons to 5-6 MeV. This still confines the experiment to detect exclusively the rare ^{8}B neutrinos. Moreover, a very high counting rate is expected, $\sim$ 25 per day for the ^8B neutrino flux measured by KAMIOKANDE. ($\Phi_{^8B} \sim 2.9 \cdot 10^6\, cm^{-2} s^{-1}$) Therefore, SUPERKAMIOKANDE will be very sensitive to time variations, thanks to the high statistics. Moreover data will allow a study of the energy spectrum of the recoil electrons.
This is very important to test the neutrino oscillation hypothesis: if the MSW effect

applies a deformation of the ^{8}B β decay neutrino spectrum should become evident after about 3 years of measurements. The deformation is most relevant in the low energy part of the spectrum, where the signal to noise ratio is less favourable.
SUPERKAMIOKANDE is going to start data taking in 1996.

SNO – Sudbury Neutrino Observatory [MAK94]

This experiment consists of a 1,000 ton heavy water Čerenkov detector in the "INCO Creighton Mine", near Sudbury (Canada). The experiment is in an advanced construction state and plans are to start data taking end of 1997. Solar neutrinos will be detected both by elastic scattering and by semileptonic interactions.

ES elastic scattering	$\nu_x + e^- \rightarrow \nu_x + e^-$	
CC charged current	$\nu_e + d \rightarrow p + p + e^-$	$Q = 1.44\,MeV$
NC neutral current	$\nu_x + d \rightarrow p + n + \nu_x$	$Q = 2.2\,MeV$

The ES reaction is predominantly sensitive to electron neutrinos, while the NC reaction is flavour independent. The expected count rate is $\sim$ 0.3 events per day for ES. The CC reaction has a relatively large cross section; the detected event rate should be $\sim$ 15 events per day, for a ^{8}B neutrino flux $\Phi \sim 2.9 \cdot 10^6 cm^{-2} s^{-1}$, for an assumed threshold of 6.5 MeV on the scattered electron. With such a rate it will be possible to measure the spectral shape of ^8B neutrinos with good statistics. This is a powerful method for testing the MSW hypothesis [HAT94] (see Tab. 3.1) which implies a suppression in the low energy part of the spectrum.
The NC reaction is sensitive to all neutrino flavours; an event rate of $\sim$ 4 events per day is expected, independent of neutrino oscillation effects. The signature of the reaction is given by the detection of a neutron. Two possibilities are now under study for the neutron detection:

- adding NaCl to the solution, with detection of the 8.5 MeV gamma from the n capture on Chlorine $^{35}Cl(n,\gamma)^{36}Cl$;
- inserting ^{3}He gas proportional counters inside the tank.

The detection of NC is important but difficult. Success will depend on the final radiopurity of the whole apparatus. It measures the neutrino flux leaving the Sun irrespective of eventual flavour conversions. The rate ratio NC/CC is an important test for neutrino flavour oscillations, the expected rate ratio being 0.2-0.6 in case of the MSW effect and $\sim$ 0.13 in case of no oscillations (astrophysical solution).

BOREXINO[BOR91]

BOREXINO is a liquid scintillation detector based on $\nu - e^-$ scattering. It will be installed at Laboratori Nazionali del Gran Sasso. The detector will consist of $\sim$ 300 tons of liquid scintillator inside a transparent spherical plastic vessel viewed by 1,700 PMTs.

The expected threshold will probably be $\sim$ 250 keV for the scattered electrons with a 100 tons fiducial volume. The low threshold will allow to detect the monochromatic ^7Be neutrinos, E = 860 keV. The expected counting rate according to the SSM prediction is $\sim$ 50 events per day, but the actual solar neutrino experiments suggest a suppression of the ^7Be flux: a high sensitivity is therefore required for such an experiment. A prototype (Counting Test Facility [BEL94b]), is in operation at Gran Sasso to check the purification procedure of the liquid scintillator and other experimental aspects on the experimental apparatus. If the required radiopurity is achieved, BOREXINO will

provide very important informations about the ^7Be component of the solar neutrino flux, such as day-night effects, seasonal modulations and solar cycle correlations. Tab.3.1 shows the main characteristics of the experiments discussed above.

Experiment	Target	Detection Reaction	E_{th} (MeV)	Dominant signal	Expected Rate events/day	Start of data taking
SUPER KAMIOKANDE (Japan)	50000 t H_2O	$\nu_e + e^- \rightarrow \nu_e + e^-$	6.0 on e^-	^{8}B	25	1996
SNO (Canada)	1000 t D_2O	$\nu_e + e^- \rightarrow \nu_e + e^-$ $\nu_e + d \rightarrow p + p + e^-$ $\nu_x + d \rightarrow p + n + \nu_x$	7.0 on e^- 6.5 on e^- 2.2	^{8}B	0.3 15 4.0	1997
BOREXINO (Italy)	300 t liq. scint.	$\nu_e + e^- \rightarrow \nu_e + e^-$	0.25 on e^-	^{7}Be line	50	1998

Table 3.1 Main characteristics for upcoming solar neutrino projects. The expected rates are given assuming the ^{8}B flux measured by KAMIOKANDE, and the SSM ^{7}Be flux

Apart from the projects ready for immediate implementation, two more projects are in an advanced state:

- ICARUS [ICA89][REV93] is a liquid argon TPC (3 modules, 5 Kton each) to be installed at Laboratori Nazionali del Gran Sasso; apart from its other objectives, the experiment could allow the study of ^{8}B neutrinos by measuring CC and NC events separately.

- An Iodine radiochemical experiment has been proposed by the University of Pennsylvania [CLE93]; neutrinos are captured on ^{127}I producing ^{127}Xe (halflife 36 days, energy threshold 789 keV).

3.3 Future prospects of neutrino physics

To summarize the possible evolution of the SNP in the next years, it is useful to refer to Tab.3.2, which lists the sensitivity of the previously considered experiments to the different solutions of the SNP.

The MSW large angle solution implies only a moderate ^{7}Be neutrino suppression and no detectable deformation of the ^{8}B energy spectrum. In this case, SNO would measure an anomalous NC/CC ratio; BOREXINO should detect a ^{7}Be neutrino flux of $\sim \frac{2}{3}$ of the SSM value.

The MSW small angle solution requires an almost complete suppression of the ^{7}Be neutrino flux (only very small signal in BOREXINO) and a deformation of the ^{8}B neutrino spectrum which would probably be detectable by SUPERKAMIOKANDE and SNO [HAT94].

The main characteristic of the VO solution is the presence of a seasonal modulation of the ^{7}Be flux (which has to be detected by BOREXINO) together with a deformation of the ^{8}B energy spectrum [BER95].

The RSFP hypothesis suggests that the ^{7}Be and ^{8}B fluxes are anticorrelated with the solar activity (see Appendix) so that the signal of the experiments should be modulated with a period of about 11 years, [AKH95],[LIM95].

In all the above considered cases, the pp-neutrino flux remains practically unaffected; the ^{7}Be flux, on the contrary, is heavily suppressed.

For the future development of the SNP, it is important to consider the possible implications of the terrestrial neutrino oscillation experiments (for a recent review see for example [GEL95]:

- Oscillations of $\overline{\nu}_e$ to other flavours are looked for by nuclear reactor experiments. These $\overline{\nu}_e$ are detected by the inverse β reaction on protons. Since these are disappearance experiments, the resulting bounds apply to oscillations into any type of neutrinos, and they actually represent the best experimental constraint on $\nu_e \leftrightarrow \nu_\tau$ oscillations.
- $\nu_\mu \leftrightarrow \nu_e$ oscillations are searched for by accelerator esperiments looking for ν_e appearence from a ν_μ beam; such experiments have achieved sensitivities to $\sin^2 2\theta$ much smaller than those reached at reactors (Fig.3.3 (a)(b)), but for higher values of Δm^2.
- Regarding $\nu_\mu \leftrightarrow \nu_\tau$ oscillations, the searches are performed looking for ν_τ appearance from a ν_μ beam (Fig.3.3 (c)(d)).

So far, apart from solar neutrino experiments, the only possible evidence for neutrino oscillations seems to come from experiments looking for atmospheric neutrinos [GA194], that is high energy neutrinos produced by the interactions of cosmic rays in the atmosphere. A number of experiments have measured the ν_e and the ν_μ flux but find a ratio $\phi(\nu_\mu)/\phi(\nu_e)$ lower than the expected value. This discrepancy can be interpreted as due to $\nu_\mu \leftrightarrow \nu_e$ oscillations and/or $\nu_\mu \leftrightarrow \nu_\tau$ oscillations.

The mixing parameter ranges which can explain the present data and which are compatible with the accelerator and reactor limits discussed above are

$\Delta m^2 > 5 \cdot 10^{-3} eV^2$, $\sin^2 2\theta \sim 0.4 - 0.7$ for $\nu_\mu \leftrightarrow \nu_e$ oscillations, and

$\Delta m^2 > 10^{-3} - 10^{-1} eV^2$, $\sin^2 2\theta > 0.5$ for $\nu_\mu \leftrightarrow \nu_\tau$ oscillations (Tab. 3.4).

As can be seen in the figures, all these experiments provide data in a parameters region quite far from the preferred solutions compatible with solar neutrino data.

A joint consideration of all experiments sensitive to neutrino oscillations leads to the following scenario:

- Solar neutrino experiments should be explained by $\nu_e \leftrightarrow \nu_\mu$ oscillations.
- Atmospheric neutrino experiments should be explained by $\nu_\mu \leftrightarrow \nu_\tau$ oscillations.

If we assume $m_{\nu_e} \ll m_{\nu_\mu} \ll m_{\nu_\tau}$, we obtain from solar neutrino data $m_{\nu_\mu} \sim 2 \cdot 10^{-3} eV$, and from atmospheric neutrino data $m_{\nu_\tau} > 3 \cdot 10^{-2} eV$.

Within the seesaw mechanism, this suggests the following pattern for the neutrino masses:

$m_{\nu_e} \sim 10^{-8}\, eV$

$m_{\nu_\mu} \sim 10^{-3}\, eV$

$m_{\nu_\tau} \sim 10^{-1} - 20\, eV$

where the mass range for the ν_τ comes from scaling either with leptons or with quark masses. Therefore putting together some theoretical speculations with the present experimental situation, one might expect that possibly future terrestrial neutrino oscillation experiments could find oscillations between μ and τ flavours. Besides , if the above scheme is correct, solar neutrinos will remain the only way to study $\nu_e \leftrightarrow \nu_\mu$ mixing.

In conclusion the problem of neutrino masses and oscillations is open. In the next years all results from solar, atmospheric, and terrestrial neutrino experiments should

be compared and their combination will probably give us some important answers on the so far unknown physical properties of neutrinos.

	MSW large ϑ	MSW small ϑ	VO	RSFP
ϕ(pp)	~ 0.6	1	0.5 - 0.6	1
$\phi(^7Be)$	0.4 - 0.6	~ 0	0.2 - 0.9	0 - 0.2
$\phi(^8B)$	0.25 - 0.35	0.35 - 0.45	0.25 - 0.45	0.5
Gallium Rate	0.4 - 0.5	0.5 - 0.7	0.5 - 0.7	0.6 - 0.7
KAMIOKA Rate (active) Rate (sterile)	0.4 - 0.5 0.25 - 0.35	0.45 - 0.55 0.35 - 0.45	0.4 - 0.55 0.25 - 0.45	0.5
HOMESTAKE Rate	0.3 - 0.4	0.3 - 0.4	0.3 - 0.5	0.3 - 0.4
SUPERKAMIOKANDE Rate (active) Rate (sterile) e^- spectrum	0.4 - 0.5 0.25 - 0.35 ~ stand.	0.45 - 0.55 0.35 - 0.45 deform.	0.4 - 0.55 0.25 - 0.45 deform.	0.5 deform.
SNO Rate CC (act) Rate CC (st) CC e^- spectrum rate NC/rate CC	0.4 - 0.5 0.25 - 0.35 ~ stand. 0.2 - 0.3	0.45 - 0.55 0.35 - 0.45 deform. 0.2 - 0.6	0.4 - 0.55 0.25 - 0.45 deform.	0.5 deform.
BOREXINO Rate (^7Be)	0.5 - 0.7	~ 0.2	0.4 - 0.9	0.2 - 0.3

Table 3.2 Expectations for the solar neutrino fluxes and for the solar neutrino experiments. Each column contains a different "solution" to the SNP:
SSM = Standard Solar Model; MSW = Mikheyev-Smirnov-Wolfenstein effect
VO = Vacuum Oscillations; RSFP = Resonance Spin Flavour Precession
For the experiments the expectations on the main observables are given.

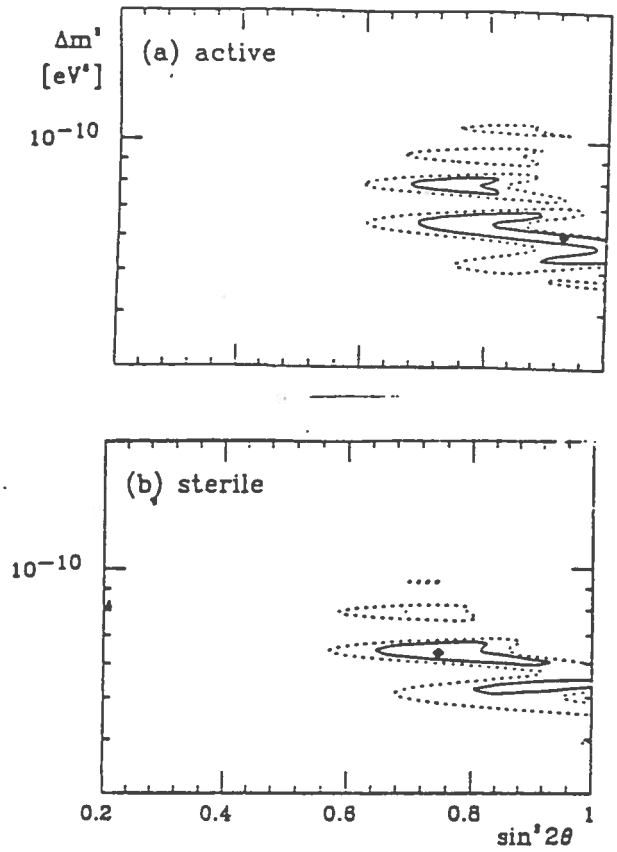

Figure 3.1 Diagram Δm^2 versus $\sin^2(2\theta)$ for vacuum neutrino oscillations. The allowed region, at 95 % C.L., for the results of GALLEX, SAGE, HOMESTAKE and KAMIOKANDE is represented by the dotted area, [CAL95].

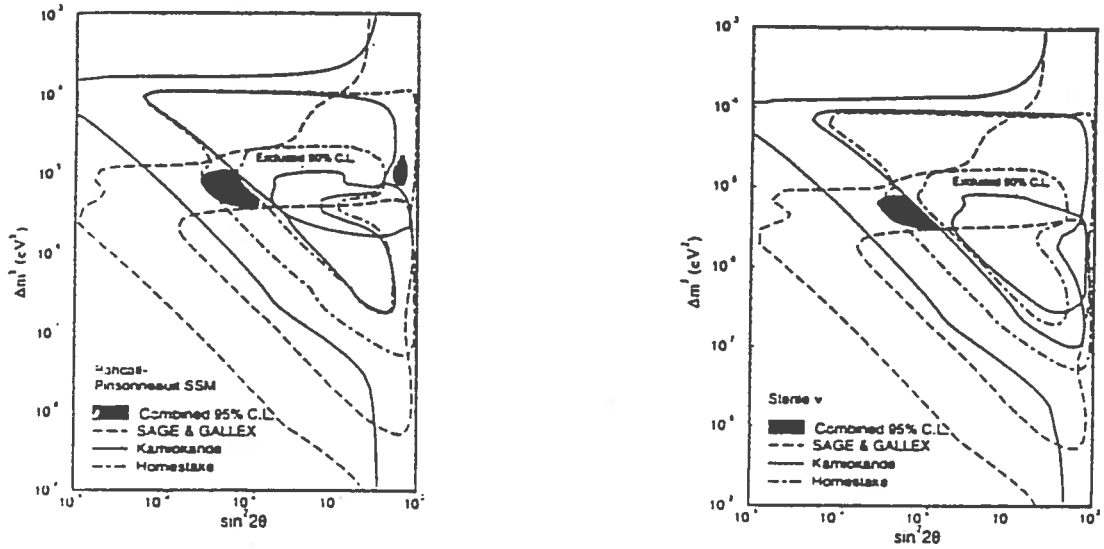

Figure 3.2 Δm^2 versus $\sin^2(2\theta)$ for neutrino oscillations. MSW effect. The allowed region, at 95 % C.L. for the results of GALLEX and SAGE, HOMESTAKE and KAMIOKANDE is represented by the black area [HAT94a].

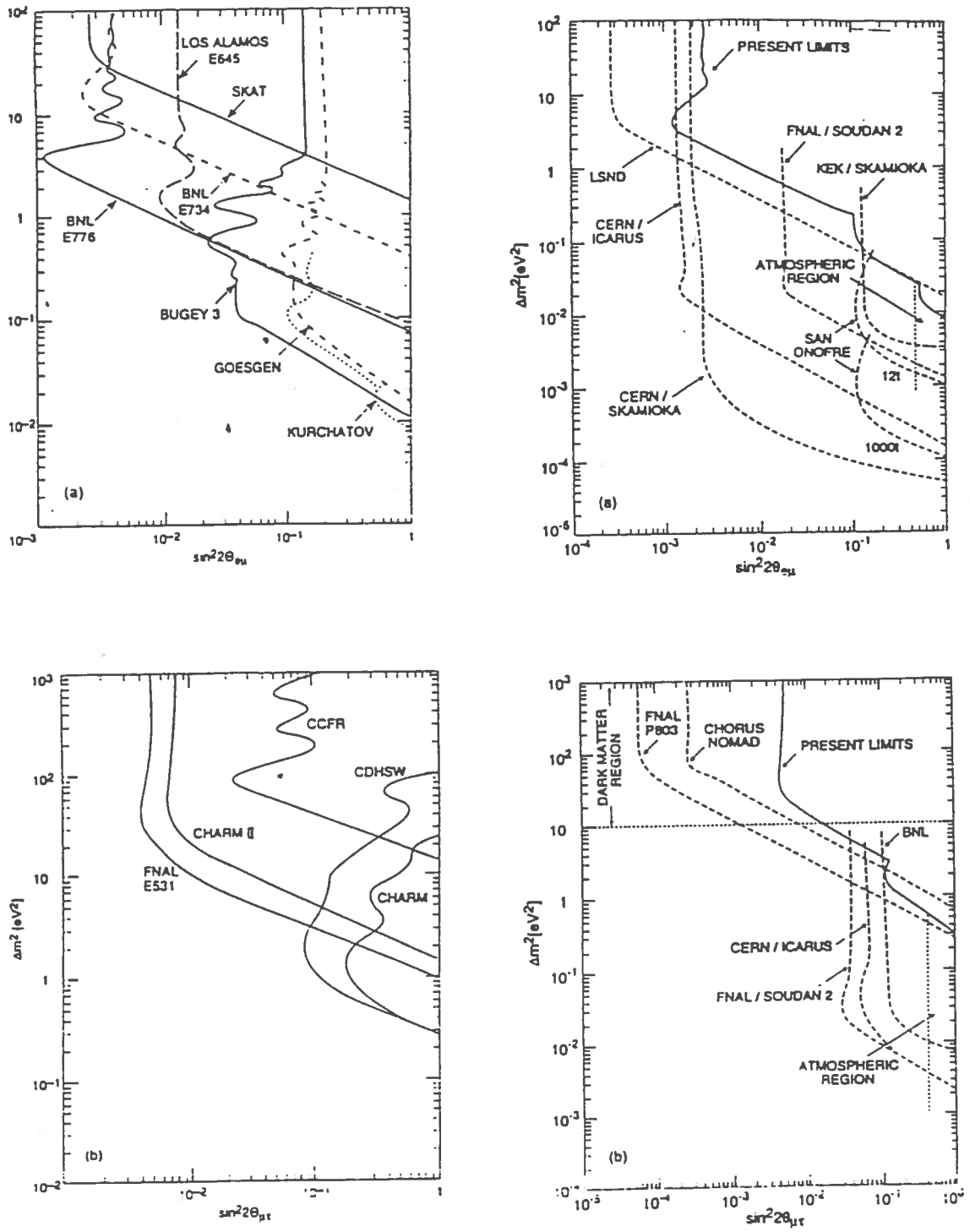

Figure 3.3 Δm^2 versus $\sin^2(2\theta)$ for present and future terrestrial oscillation experiments. The areas represent exclusion plots on the parameter space.
(a) Present limits for $\nu_e \leftrightarrow \nu_\mu$
(b) Expected limits for $\nu_e \leftrightarrow \nu_\mu$ from future experiments
(c) Present limits for $\nu_\mu \leftrightarrow \nu_\tau$
(d) Expected limits for $\nu_\mu \leftrightarrow \nu_\tau$ from future experiments

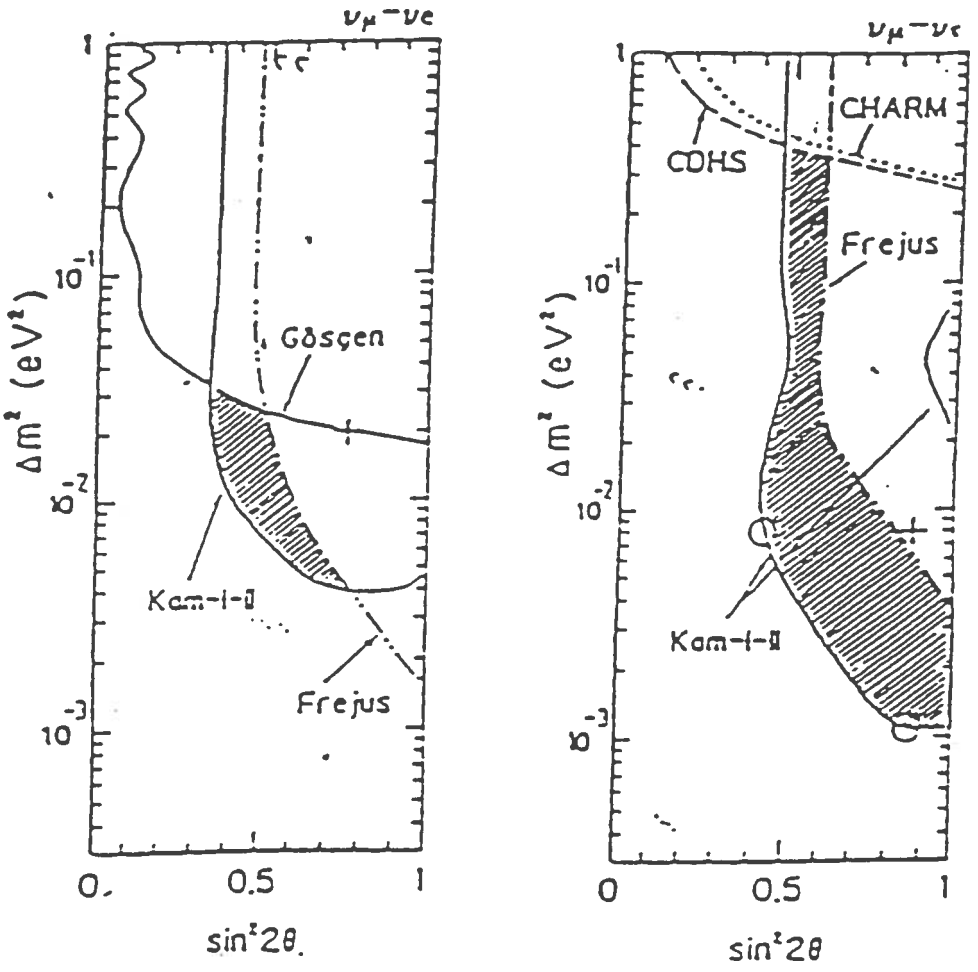

Figure 3.4 Δm^2 versus $\sin^2(2\theta)$ for atmospheric neutrino data: the shaded area represents the 90 % C.L. allowed mixing parameters taking into account the limits given by present reactor and accelerator experiments.

4 GALLEX

4.1 Outline

The GALLEX solar neutrino detector is installed at "Laboratori Nazionali del Gran Sasso" in Abruzzo, Italy. GALLEX looks for solar neutrinos via the reaction

$$^{71}Ga\,(\nu_e, e)^{71}Ge$$

which has a threshold of 233 keV and is sensitive mainly to the pp-neutrinos .
The target is 101 tons solution of $GaCl_3$ in water and HCl, containing 30.3 tons of natural gallium; this corresponds to $\sim 10^{29}\,^{71}Ga$ nuclei.
The solar neutrino flux above threshold is deduced from the number of ^{71}Ge atoms produced. They are registered through their decay after chemical separation from the target.
In short the experimental procedure is the following [ANS92]:

1 The solution is exposed to solar neutrinos for about 4 weeks; at the end of this exposure about 16 ^{71}Ge nuclei should be present in the solution if the SSM model is correct and all neutrinos do reach the Earth.

2 The ^{71}Ge, present in the solution as volatile $GeCl_4$, is chemically extracted into water by pumping $\sim$ 2,000 m^3 of Nitrogen through the solution.

3 The extracted ^{71}Ge is converted into GeH_4, Germane gas, and introduced into miniaturized proportional counters [WIN93] mixed with Xenon as counting gas. At the end $\sim 95-98\%$ of the ^{71}Ge present in the solution at the time of the extraction is in the counter; extraction and conversion efficiencies are under constant control using non radioactive germanium isotopes as carriers [HEN92].

4 The ^{71}Ge e-capture (meanlife 16.5 days)

$$^{71}Ge\,(e^-, \nu_e)^{71}Ga$$

is observed for a period of 6 months, allowing all the ^{71}Ge to decay and permitting a good determination of the time constant counter background.

5 Data taken during the counting time are analyzed to obtain the most probable number of ^{71}Ge counted. Counter backgrounds are minimized by rigorous application of low-level technology in counter design and construction. The residual background is mostly rejected through application of amplitude and shape analysis of the pulses recorded. This reduces the mean background rate to less than 0.1 counts per day. The data are analyzed with a maximum likelihood method to obtain the most probable number of ^{71}Ge nuclei at the beginning of counting, which, after the correction for counting, extraction and filling efficiencies, gives the number of ^{71}Ge produced in the solution during the exposure and, therefore, the ^{71}Ge production rate.

6 A correction is made to account for contributions to the observed signal from sources other than solar neutrinos, mainly due to interactions in the solution generated by high energy muons from cosmic rays and by products due to natural radioactivity. Another contribution comes from background signals in the counter that can be confused with ^{71}Ge decays. Altogether 7 SNU [2] have to be subtracted from the measured ^{71}Ge production rate.

[2] 1 SNU (Solar Neutrino Unit) = 10^{-36} captures per second and per absorber nucleus

4.2 GALLEX history and results

In the following, we list the main phases of the GALLEX experiment. More detailed records are contained in the Progress Reports regularly submitted to L.N.G.S. and in the regular GALLEX publications in Physics Letters B [ANS92], [ANS93], [ANS94], [ANS95b].

* June 1990 - May 1991.
  28 test extractions are performed. It becomes evident that a small but nevertheless disturbing proportion of the cosmogenic ^{68}Ge produced in the Gallium target outside the underground laboratory was trapped in nonvolatile form in the solution and continously released at very low rate. This jeopardized the detection of the solar neutrino signal since the decay signature of ^{68}Ge is very similar to that of ^{71}Ge, only distinguished by its half-life, 288 days vs 11.4 days for ^{71}Ge. The ^{68}Ge problem was solved by heating the solution and allowing in this way the efficient release of the trapped ^{68}Ge, which was then extracted from the target solution.
* May 1991 - April 1992 **GALLEX I**
  21 extractions including 15 solar runs, SR1-SR15, and 5 short exposure runs, 1 day, BL1-BL5. Results are published in [ANS94]
* May 1992 - August 1992
  The target solution was transferred into a new tank which can accomodate a neutrino source for the overall test of the experiment. 8 extractions were performed for technical conditioning.
* August 1992 - June 1994 **GALLEX II**
  48 extractions performed including 24 solar runs, SR16-SR39, and 22 short exposure runs, BL6-BL27. Results are published in [ANS95b]
* June 1994 - October 1994
  First experiment with a high intensity manmade ^{51}Cr neutrino source (see next section). 11 extractions have been performed; results are published in [ANS95a] and updated in the internal note [GAL95].
* October 1994 - October 1995 **GALLEX III**
  18 extractions including 14 solar runs, SR40-SR53, and 4 short exposure runs, BL29-BL32. Due to the 6 month counting period for each sample, there is respective delay between the end of exposure and the availability of the counting results.
* October 1995 - February 1996.
  Second source experiment. 7 extractions have been performed.
* Late February 1996
  Beginning of **GALLEX IV** data taking. According to the originally defined plans, solar neutrino exposures must end in December 1996, since the gallium must then be removed from the laboratory for fiscal reasons (see sect. 5.4).
  At that time after a total live time of $\sim$ 4.5 years, the statistical error will be about 8.5 % (77 SNU signal).

The results obtained in GALLEX I and GALLEX II are summarized in Tab.4.1. The results of the individual runs are shown in Fig.4.1.

OBSERVATION	Measured capture rate
GALLEX I SR1 - SR15 [ANS93]	81 ± 17(stat) ± 9(sys) SNU
GALLEX II SR16 - SR39 [ANS95b]	75.5 ± 9.7(stat) ± 4.5(sys) SNU
GALLEX I + GALLEX II SR1 - SR39 [ANS95b]	77.1 ± 8.5(stat) ± 4.9(sys) SNU

Table 4.1 Results obtained in GALLEX I + GALLEX II

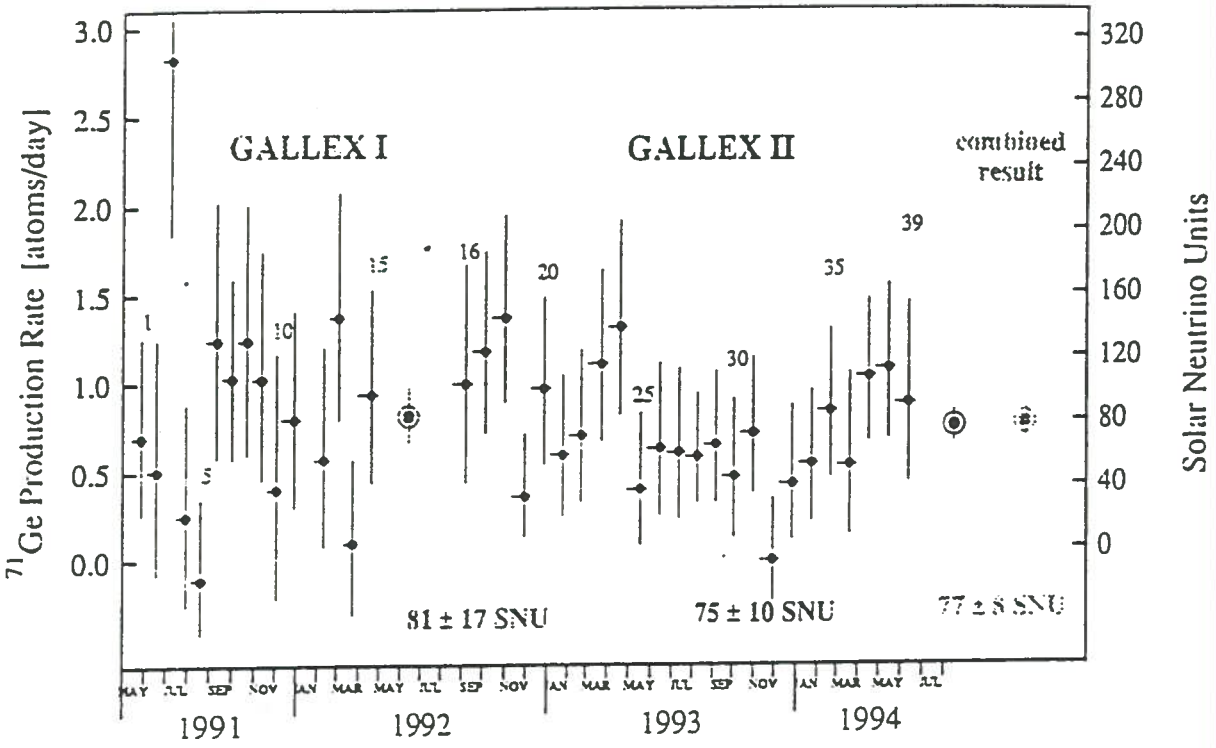

Figure 4.1 The single run results of GALLEX I and GALLEX II

4.3 The ^{51}Cr neutrino source experiment

GALLEX has been 'calibrated' with a man-made low energy ^{51}Cr neutrino source whose activity has been determined with 4 independent methods to be 1.69 ± 0.03 MCi [ANS95b]. The aim of this exposure was to perform an integral test of all major steps of the GALLEX experiment, in particular the ^{71}Ge extraction, the GeH_4 synthesis and the counting efficiency. At the same time, the neutrino capture cross section of 751 keV neutrinos on ^{71}Ga was to be checked.

^{51}Cr has a lifetime of 40.0 days and decays by electron capture to ^{51}V:

$$^{51}Cr\,(e^-, \nu_e)\,^{51}V$$

Neutrinos are produced with the discrete energy spectrum shown in Tab. 4.2 .

^{51}Cr has been produced by irradiating ~ 36 kg of Chromium, (isotopically enriched to 38.6 % in ^{50}Cr) by neutron capture on ^{50}Cr. The enriched Cr has been acquired from the "Kurchatov Institute" in Moscow. The irradiation has been performed at the "Centre d'études nucleaires de Grenoble" using the 35 MW reactor "Siloé".
The first irradiation ended on June 20, 1994. The source was then immediately transported to the Laboratori Nazionali del Gran Sasso, and on June 23 the first source exposure started. Knowing the activity, we expect a ^{71}Ge production rate of ~ 12 ^{71}Ge atoms per day at the beginning of the first exposure, decreasing with the meanlife of ^{51}Cr. 11 extractions were performed during 4 months of exposure.
The ratio R between the measured production rate from the source neutrinos and the expected production rate as deduced from the known source activity is [ANS95b][GAL95]:

$$R = 0.97 \pm 0.11$$

This is a very important result, indicating that in GALLEX any unknown systematic errors are at a level of less than 10 %.

A second source experiment employing the same experimental procedure has been performed from October 1995 to February 1996. The same enriched Chromium sample was reactivated in "Siloé", under similar conditions as the first source. 7 extractions have been performed and are now counting. The results of this second source experiment will be published in late summer 1996.

The source experiment is an overall performance test for GALLEX, excluding unknown systematic errors. It is not used for calibration since its error of ~ 11 % is appreciably larger than the systematic error of the GALLEX experiment with its intrinsic efficiency determinations.

e Capture	Energy (keV)	Relative Intensity
K	746	81
L	751	9
K	426	9
L	431	1

Table 4.2 Energy and intensity of neutrinos produced in the ^{51}Cr e-capture decay.

4.4 Implications of the GALLEX results

Theoretically, the SSM expectation value for gallium is $\sim$ 127 SNU (mean of [BAH92] and [TUR93b]), partitioned to the different neutrino sources, as shown in Tab. 2.3 . The pp-rate is dominant with 58 % of the total. Next a ^{7}Be contribution is rather sizable with 26 %. Contrary, ^{8}B-neutrino are of little importance for the gallium detector.

Experimentally, the GALLEX result of 77 $\pm$ 10 SNU(1σ) is 61 % of the SSM expectation value or 104 % of what is expected for pp (and pep) -neutrinos alone. In that quality, the result

- confirms the fundamentals of the theory of stellar structure and evolution through the first observation of hydrogen fusion in the solar interior [ANS92] [ANS95b]

and, at the same time

- confirms a solar neutrino problem through a deficit of higher energy neutrinos from ^{7}Be (and ^{8}B), adding evidence to what has been found earlier in the HOMESTAKE and KAMIOKANDE experiments.

The GALLEX data do not yet exhibit any statistically significant time variation and are consistent with a production rate constant in time. The error is dominated by the statistical one. Its continued reduction through the accumulation of more and more data has played a key role in their interpretational consequences.

The earlier GALLEX results [ANS92], with their large error ranges, hinted at, but could not precisely define the scope of the deficit of ^{7}Be neutrinos. Now [ANS95b] only little room remains for the contributions from ^{7}Be and CNO-neutrinos [KIR95a]. Further error reduction in GNO could prove even the complete absence of ^{7}Be neutrinos at a high ($> 3\sigma$) confidence level. Then, ^{7}Be neutrinos are more reduced than ^{8}B neutrinos (observed in KAMIOKANDE) in spite of the fact that ^{8}B is made from ^{7}Be ($^7Be + p \rightarrow ^8 B + \gamma$).

These findings have severe consequences. Contrary to PPIII (^{8}B), the 14% PPII (^{7}Be) branch of the fusion reaction chain is much more robust and there are not many possibilities to significantly affect it. Thus, with further shrinking error, it may at some point become even inescapable to conclude ν_e-disappearance for reasons other than those related to the Sun. For a more detailed recent discussion, see [KIR95b].

5 The GNO Project (Gallium Neutrino Observatory)

5.1 Outline

The GNO project is designed to monitor the pp neutrino flux for a long time (at least 10 years) with a gallium detector at Laboratori Nazionali del Gran Sasso. Therefore GNO is going to be a semipermanent neutrino observatory for the detection of low energy neutrinos coming from the Sun.

If approved and funded, GNO could start data taking just after the end of GALLEX (31 December 1996), with a target of 30 tons of gallium (the present GALLEX amount).

The scientific value of a gallium experiment for the next decade would be greatly improved if the mass of Gallium could be substantially increased. For this, we propose a gradual extension of the GNO target from 30 to $\sim$ 100 tons. The upgrade should consist of the following steps:

- For about two years GNO is going to continue with the same gallium mass as used in GALLEX (30 tons). To distinguish between the original GALLEX experiment and this prosecution, we will refer to it as GNO30.
- The first extension step is from 30 to 60 tons (GNO60), planned for 1999. For this extension no principal changes in the experimental technique and no major civil works are required.
- The second extension step is from 60 to $\sim$ 100 tons of gallium (GNO100), after the year 2000. It requires some enlargements, but still within the present experiment location, the southern wing of the Hall A (see sect. 5.3.1). As an option, it is conceivable to have the last 40 tons of gallium in metallic form (see sect. 5.3.2 for details); this could be desirable for methodological reasons. Also it would enable a superior check of the background from side reactions using two independent targets and extraction techniques.

5.2 Objectives for GNO

In this section we describe the scientific interest for continuing the solar neutrino flux measurements with a gallium detector in the next decade.

5.2.1 Importance of monitoring the pp neutrino flux

pp-neutrinos are the most fundamental and by far the most abundant solar neutrinos. Unfortunately, the radiochemical technique is still the only possibility to monitor them. The ultimate goal would obviously be a real-time pp-neutrino detector with good energy resolution, but this is far from being realized in the next decade. Meanwhile, this task must be covered by GNO, or else the data base for a whole decade of intense research at higher neutrino energy will be irrevocably lost. GNO would be a reliable "trait d'union" between the first and the second generation experiments. The latter are mainly $\nu - e$ scattering experiments (apart from SNO), that will not be calibrated, at least for several years.

To illustrate the importance of continuous monitoring, we may recall the ongoing debate about the comparison of the HOMESTAKE and the KAMIOKANDE results, namely whether the KAMIOKANDE results have to be compared to the global HOMESTAKE result or to the result restricted to the same years of data taking.

5.2.2 Refinement of the measured solar neutrino capture rate

Fig. 5.1 shows the statistical uncertainty on the signal obtained by GNO versus live time, assuming the same signal and background as in GALLEX. At the end of GALLEX, the total error on the measured rate is already heavily affected by the systematic component(Tab. 5.1). Consequently only a relatively small improvement on the global error is expected to come from GNO, unless the systematic error is reduced. Actually, a reduction of the systematic error to $\sim$ 4% is conceivable (see sect. 5.2.3) and a global improvement of the result should be possible. The GALLEX data alone have already provided evidence for a strong depression of the ^{7}Be-neutrino flux [ANS95b] (see sect. 4.4). If the rate could be measured to $\sim$ 5% (Tab. 5.1, last line) it could prove the total absence of ^{7}Be neutrinos and, together with the results from BOREXINO, investigate the possibility of a small depression of the pp-neutrino flux. This would be the most direct signature for ν_e disappearance.

In addition, lowering the errors will further restrict the possible oscillation parameters, in particular if combined with the results from SUPERKAMIOKANDE and SNO.

	Live Time years	Statistical Error %	Systematic Error %	Total Error %
GALLEX I	0.94	21	11	24
GALLEX I + II	2.72	11	6.5	12.5
GALLEX (1991-1997)	4.5	8.4	6.0	10.3
GNO30 (1997-1999)	6.3	7.0	5.5 ?	8.9
GNO60 (1999-2001)	8.1	5.2	5.0 ?	7.2
GNO100 (2001-2007)	13.5	2.9	4.0 ?	5.0

Table 5.1 Evolution of the statistical and systematic error in GALLEX and GNO (77 SNU signal)

5.2.3 Reducing the systematic error in GNO

As discussed, big efforts are justified to reduce the systematic error below 6 %, otherwise GNO would soon be dominated by it.

Tab. 5.2 lists the various components of the GALLEX II systematic error; the two main sources are:

- The uncertainty in counting efficiency
- The background in the counter due to the introduction of Rn and cosmogenic ^{68}Ge.

Concerning ^{68}Ge the contribution is going to become lower and lower because of decay and because this radioisotope is no more produced when the target is inside the underground laboratory. In fact ^{68}Ge is produced by cosmic rays only when the gallium is outside the laboratory (see sect. 4.2).

The contribution from Rn is reduced by increasing the target mass, because it is introduced in the counters during the germane synthesis. Assuming that the mean number of Rn atoms is the same in GALLEX and in GNO100 we can expect a reduction of the systematic error from Rn to about 1/3 of the present value. Further reductions are conceivable by improving the germane synthesis line.

An important potential for the reduction of the systematical error rests in the possibility of a full standardization of the counters. Presently 25 quarz low level background counters are available in GALLEX. They are the result of many years of development [WIN93][PLA91] and represent the present state of the art to meet the background level required to detect the decay of just a few atoms. Their background is $\sim$ 0.08 counts/day in the acceptance region for energy and rise time of ^{71}Ge pulses. The counters are individually glass-blown, hence none is exactly alike the other. Consequently, up to now, the detection efficiencies had to be determined individualy.

In GNO we see new technological possibilities to fully standardize the counters without compromising their background properties and thus to reduce the systematic error for the total efficiency.

Another improvement will come from a more precise definition of the energy and rise time cuts used to distinguish genuine ^{71}Ge pulses from background, and a better noise reduction through improvement of electronics.

The substantial technological progress in electronics (relative to the conceptual design of GALLEX which goes back to 1986) allows major gains. Examples are individual pulse shaping on each line (instead of the present multiplexing), preamplifiers with larger bandwidth, better uniformity of the response function, and improved front-end electronics.

Altogether, the systematical error from this source is expected to be cut in a half.

Source of Error	Error size (%)
Background from side reactions (μ,n,^{69}Ge,Actinides ..)	1.8
Background from ^{68}Ge	3.5
Background from Rn in the counters	1.5
Energy Window Cut	4.0
Rise Time Window Cut	2.0
Chemical Yield	1.7
Target size	0.8
Total	6.5

Table 5.2 Systematic error in GALLEX II

5.2.4 Searches for time variations of the signal

The prolongation of the measurement of the solar neutrino flux for a relatively long time, at least 10 years, would allow to look for time variations in the signal; in this case the systematic component of the error can in part be neglected. GNO100 will have a quite good capability to look for time variations in the signal.

Time variations in the solar neutrino fluxes are predicted in a number of scenarios suggested for the solution of the SNP. The different potential causes for time variations are described in the Appendix.

Their relevance for GNO is as follows:

Seasonal effects Suppose to divide the data in two bins corresponding to high and low flux: to detect the effect at 95 % C.L., we require that the 2 sigma error on each bin be less than the expected modulation.[3] Fig. 5.2 shows the sensitivity of GNO at a signal modulated over 1 year, assuming to sort the single run data in two bins as explained above. We can see that the modulation from the geometrical variation of the Earth-Sun distance (4%) is out of range for detection.
The modulation due to the VO (Vacuum oscillation) mechanism implies for GNO a reduction of the signal of $\sim$ 50-60% of the SSM prediction and a modulation ranging from 5 to 15 % (see Fig.A.1 in Appendix). Therefore GNO can explore at 95% C.L. a significant part of the VO parameter region.

Solar cycle correlation A 10 year gallium experiment could also investigate the eventual modulation of the signal correlated with the solar cycle, as suggested by the data from the Chlorine experiment [MAS95] (see Appendix), theoretically interpreted by the RSFP effect.
Let us first note that the present GALLEX data are not sufficient to do a good search for solar activity correlations because of the short period of data taking compared to the 11 year solar cycle (see Fig. 5.5).
We must mention however that the theoretical predictions on the magnitude of the RSFP effect for a gallium experiment are not certain, as the effect strongly depends on the shape of the solar magnetic field [LIM95], which is not well known.
Repeating the considerations made above for seasonal modulations we suppose to sort the data taken during 10 years in two bins with "high activity Sun" and with "low activity Sun". From Fig. 5.2 we can see that after 10 years of observations with GNO (1997-2007), one could investigate at 95 % C.L. a modulation of about 8%.
A modulation of the same order as the one claimed by HOMESTAKE, $\sim$ 20% [OAK94] [MAS95], would be clearly detectable by GNO. The improved statistics of GNO100 on shorter time bins is particularly well suited for the study of sporadic Sun activity correlations, with even better sensitivity as for periodic changes.

5.2.5 The production background in GNO100

The background production of ^{71}Ge from side-reactions relative to the neutrino signal is independent of the target mass, if one assumes the same concentration of impurities and the same neutrons and muons flux.
As mentioned before, in GNO100 it is conceivable to have the gallium target in two forms, e.g. 60 tons as $GaCl_3$ and 40 tons as metallic gallium. The extraction procedures and the background reactions for the two targets are rather distinct. A comparison between the extractions made from the two different targets will then provide more direct informations for the understanding of background and side reactions.

---

[3] In the following we suppose to have a mean signal of 77 SNU. The modulation, M, is defined here as the difference between the high rate bin, R_H, and the low rate bin, R_L, normalized to the mean rate, $< R >$, namely

$$M = \frac{R_H - R_L}{< R >} \sim \frac{1}{2}\frac{R_+ - R_-}{< R >}$$

where R_+ and R_- are respectively the maximum and the minimum observed rates.

5.2.6 Statistical significance of a single GNO100 run

In GNO100 the statistical significance of the single run would be heavily improved. GALLEX measures a solar neutrino capture rate of [ANS95b]:

$$77 \pm 8(stat) \pm 5(sys) \quad SNU$$

corresponding to an average excess count number, N, of ~ 5.3 decays per run, which becomes 4.8 after subtracting the estimated background. N obviously scales with the exposed mass so that, if we assume a Poisson statistics, we have

$$GALLEX \qquad N \sim 5.3 \qquad \frac{\Delta N}{N} \sim 43\%$$

$$GNO100 \qquad N \sim 17.5 \qquad \frac{\Delta N}{N} \sim 24\%$$

In Fig. 5.3 we compare the simulated distribution of the single run statistics of GALLEX/GNO30 and GNO100, assuming a capture rate of 77 SNU, the same background in GNO100 as in GALLEX (see sect. 5.2.5), and a duration of 28 days for each run.
The distribution for GNO100 is symmetric and well apart from zero: this means that the single run significance is strongly improved, and all the problems of the treatment of runs where the signal is 0 or below are avoided.
Fig. 5.4 shows a typical GALLEX run and a run during the ^{51}Cr exposure; the latter has been chosen to have a statistic representative of a 100 ton experiment. The events selected as ^{71}Ge decay are hatched: it is immediately evident that with the statistics of GNO100 one can directly recognize both the L- and K-capture peaks in single run data.
To be more quantitative, assuming that the counter background in GNO100 will be at the level of GALLEX ($\sim$ 0.08 counts per day), the Signal to Noise ratio would change from GALLEX/GNO30 to GNO100 as shown in Tab. 5.3 .

	L+K	L+K	K	K	L	L
Background	0.076 c/d	0.076 c/d	0.01 c/d	0.01 c/d	0.066 c/d	0.066 c/d
Counting duration	32 d	48 d	32 d	48 d	32 d	48 d
S/N GALLEX	2.46	1.64	9.4	6.25	1.4	0.94
S/N GNO100	8.2	5.5	31	21	4.7	3.1

Table 5.3 Signal to noise ratios in GALLEX and GNO100 assuming a capture rate of 77 SNU and the background quoted in the text. L and K are respectively the events coming from L and K shell ^{71}Ge electron capture.

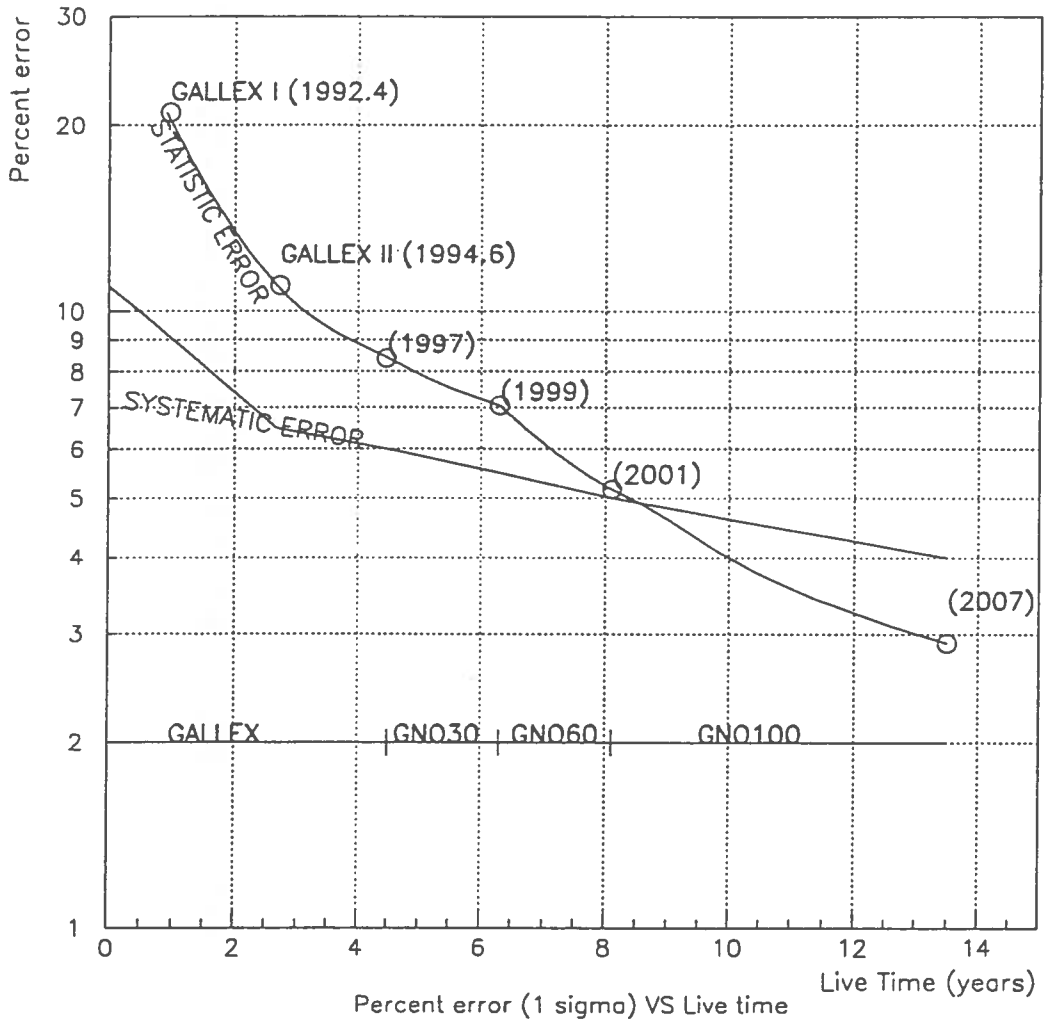

Figure 5.1 Time evolution of the statistical error in GNO (77 SNU signal). The time schedule described in the text is used for the extension of the target mass. To be conservative we have assumed a live time of 90% of the real time measurement.

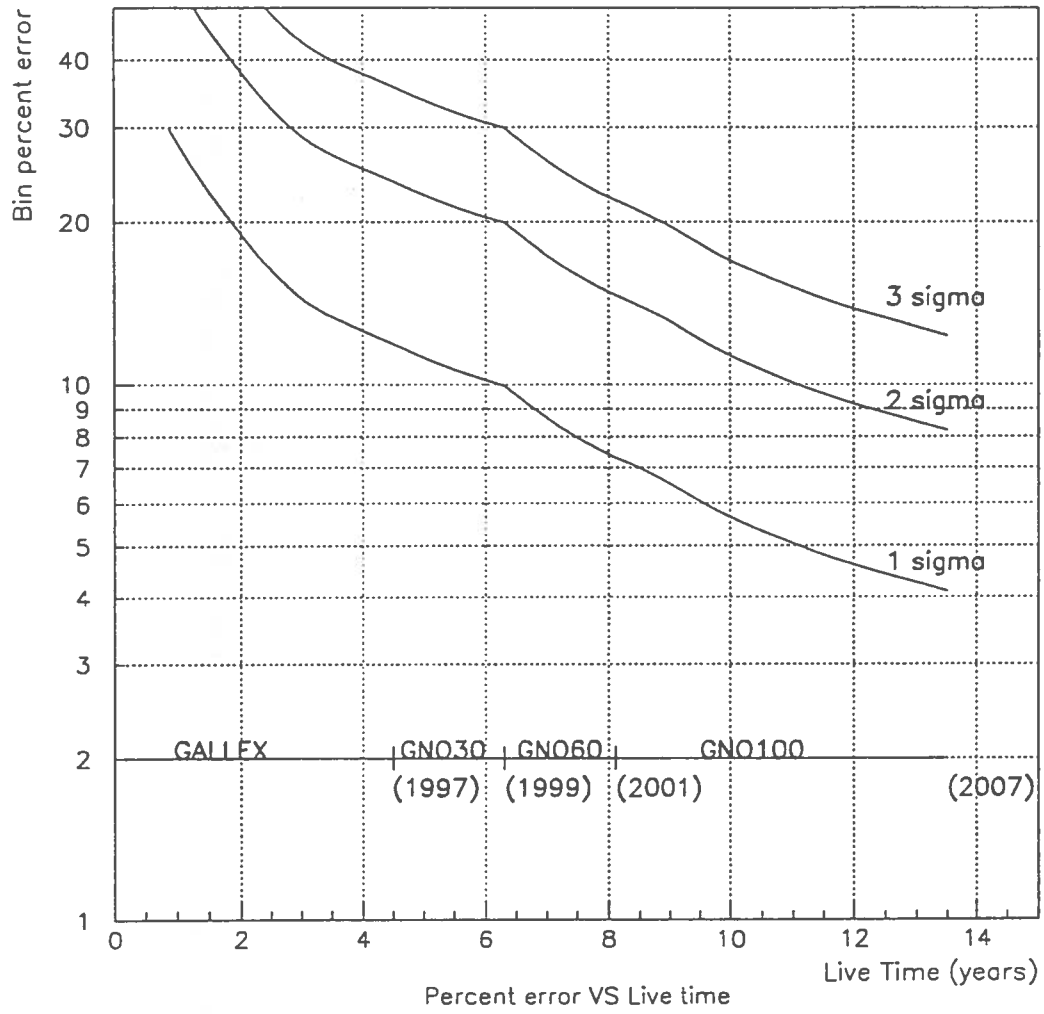

Figure 5.2 Time evolution of the statistical error in GNO after sorting data in two bins, high flux and low flux. The time schedule described in the text is used for the extension of the target mass. To be conservative we have assumed a live time of 90% of the real time measurement.

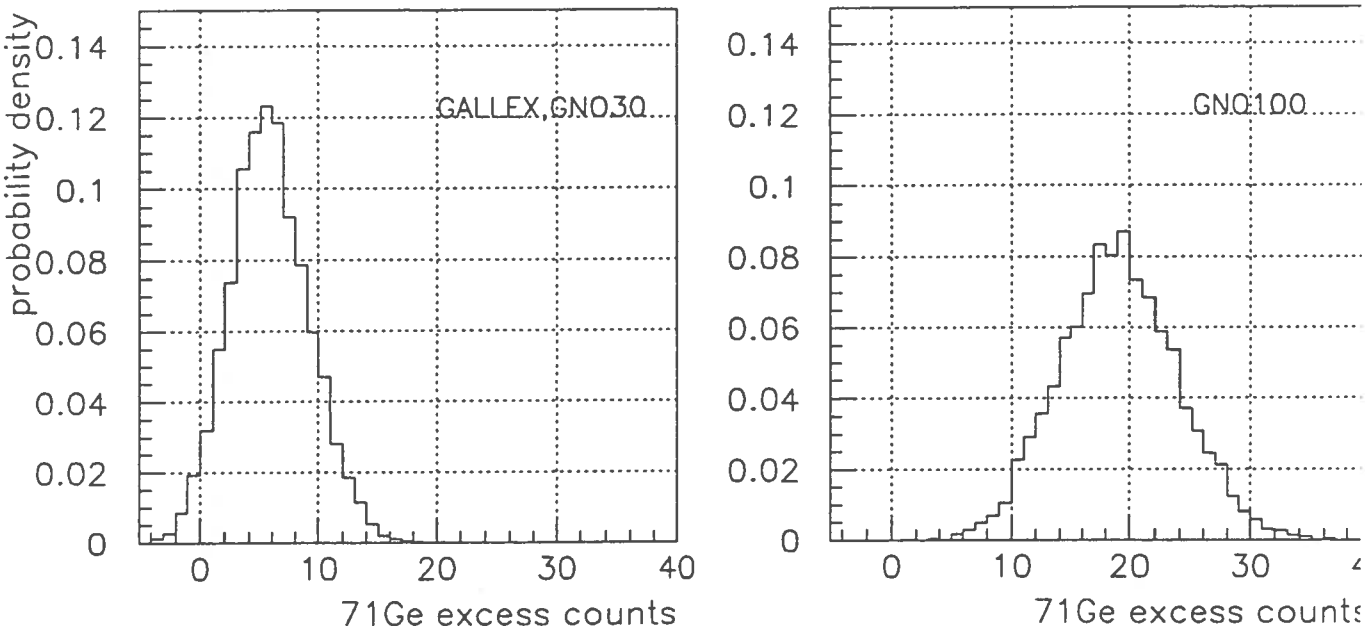

Figure 5.3 Excess counts in single runs for GALLEX and GNO100, 77 SNU signal + 8 SNU background.

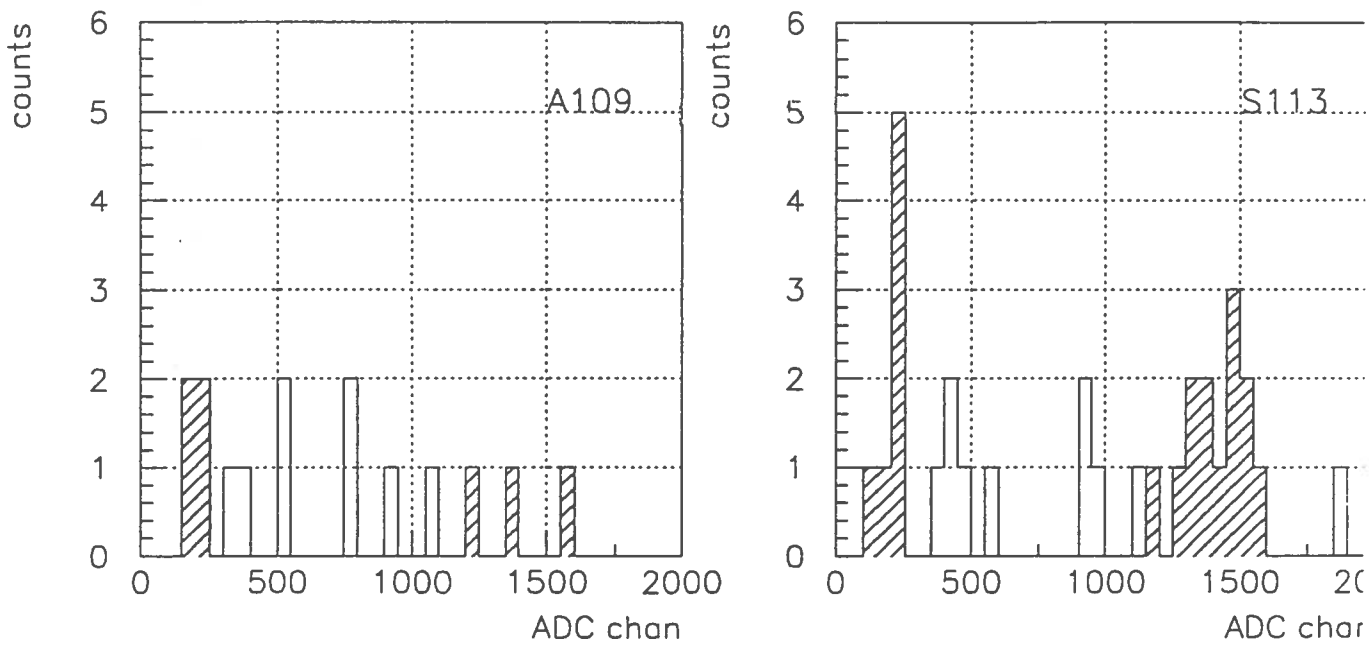

Figure 5.4 Energy spectra from solar run A109 and from the source run S113, which has about the same statistics as a GNO100 single run. Hatched bars mark counts in the L-peak (left) and K-peak (right) energy acceptance windows for ^{71}Ge-decay

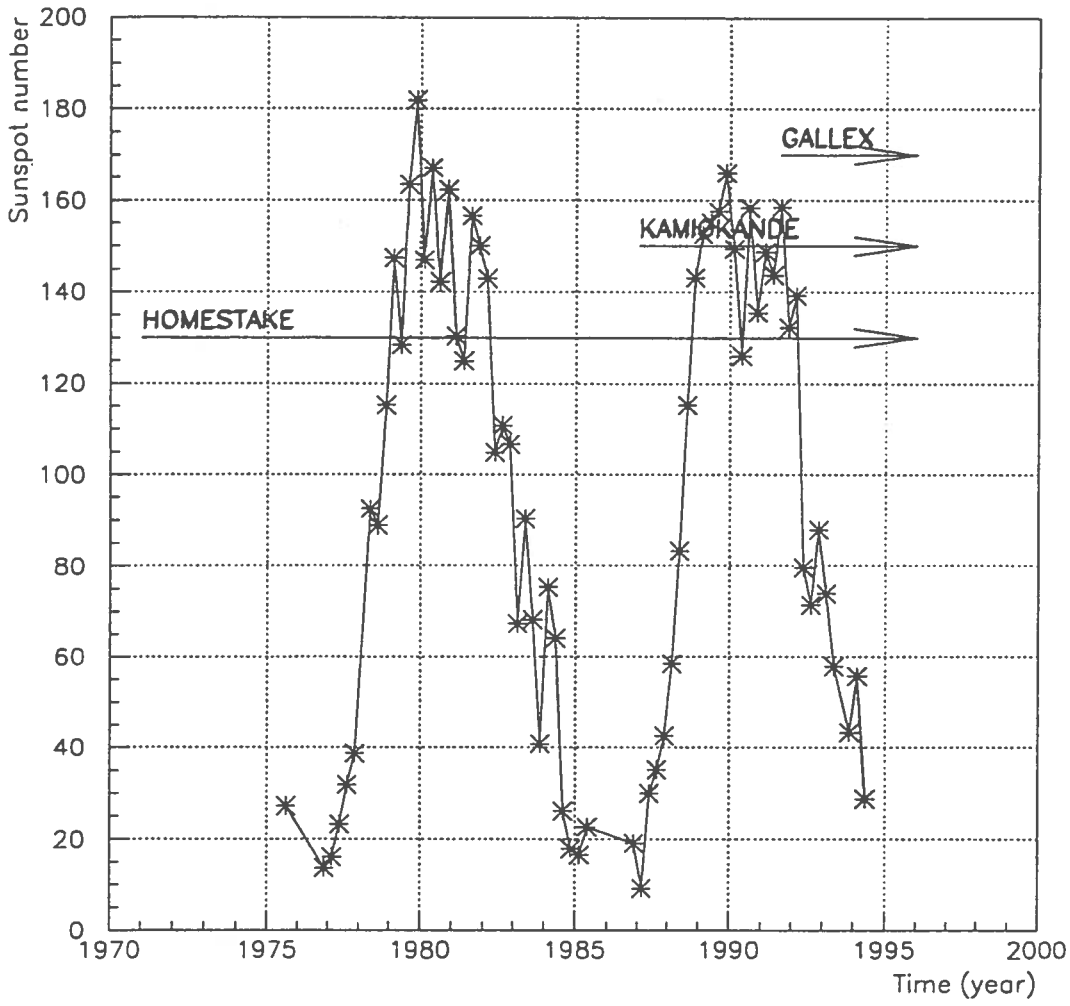

Figure 5.5 Sunspot number versus time for the last two solar cycles.
The HOMESTAKE, GALLEX and KAMIOKANDE data taking period is shown.

5.3 Technical aspects and operations

5.3.1 LNGS Facilities

The proposed GNO30 phase can be performed with the presently existing facilities in the southern wing of Hall A: the Main Building (containing two target tanks and the extraction facilities), and the Counting Building. The GALLEX owner of the tanks and the extraction equipment (FZK Karlsruhe) is ready to transfer this equipment to INFN at no cost. Similarly, the Counting facilities will be maintained by MPIK Heidelberg as necessary.

Data taking during the GNO30 phase is based on the operating experience of the GALLEX collaboration, which will be preserved by participation of members of this collaboration. Note, however, that the technical personnel performing the regular extraction runs in GALLEX will not be available for GNO and replacements are needed.

For the upgrading to GNO100 a stepwise and gradual extension is appropriate, simultaneous with the time required to accumulate the additional gallium.

The first extension step (from GNO30 to GNO60) would require about two years. An Italian crew of about 4 chemical engineers or technicians is needed, which would have two responsibilities: periodic operation of GNO30 extraction runs and planning the new facilities. To operate, maintain and improve the low level counting facilities, two electronic engineers or technicians would be required. These people should be permanently at LNGS under the supervision of an experienced scientist also stationed on site. Even though the present counting laboratory is fully operational, the new aspect of planning long time operations calls for considerable modernization of the counting system and electronics.

The existing spare tank B in the GALLEX building can be used as a second target tank in parallel with tank A. Simultaneous Ge-desorption from both tanks is possible by adjustment of the present piping system and by operation at a reduced but sufficient flow rate of 120 m^3 nitrogen per hour.

Further required installations are as follows

a) For safety, an additional spare tank similar to the target tanks must be installed in a ventilated side extension of the GALLEX building. This could be done in the space between the Main and the Counting buildings, where there is already a useful depression gap in the concrete bottom.

b) Also for safety, the existing spill tanks below the road for emergency use have to be enlarged from presently 100 m^3 to 140 m^3 in order to recover the liquor (and dilution water) in case of simultaneous catastrophic rupture of both tanks (earthquake).

c) The liquid nitrogen tanks (presently located between Hall A and B) must be moderately enlarged.

d) Tank B must be equipped with a new PVDF sparging system, as now in tank A.

The second extension step (from GNO60 to GNO100) requires major changes and a redesign of the installations inside the southern wing of Hall A. A further target tank of the same size as the present tanks would have to be installed in front of the present main building (direction toward the main road). Note that the presently used 70 m^3 tank size (suitable to take up to 35 tons of gallium as 115 tons of $GaCl_3$ solution) is the largest size which can be transported in one piece on the highway access. Any larger size would require mounting on site, impossible for these special resin tanks.

Alternatively, if it is decided to use the additional 40 tons in form of gallium metal, a chemical reactor could be put in place of the additional gallium chloride tank.

Upscaling to even larger target sizes in the future is still possible in principle and still within the confinements of the southern wing of Hall A. Among other options, this would involve the consideration of using a metal target rather than a $GaCl_3$ target. For this purpose a new technology with a huge metal tank has to be considered, quite different not only from the Chloride technique but also from the SAGE technique of using metal in many small containers.

5.3.2 Gallium Chloride versus Gallium metal target

Chloride target

The composition of an optimum $GaCl_3$-target solution is $\sim 8\ mol\,dm^{-3}$ $GaCl_3$ and $\sim 2\ mol\,dm^{-3}$ free HCl acid (by weight $\sim$ 75 % $GaCl_3$, 21 % H_2O and 4% HCl). Germanium is desorbed as a volatile Tetrachloride, $GeCl_4$, by sparging with any non-reactive gas (air, nitrogen). The solution resembles a molten salt more than an aqueous solution and is highly corrosive; it must be kept in the optimum composition range by occasional addition of HCl-gas.

Metal target

The Ga metal target is kept liquid at a temperature slightly above the melting point of 30° C. Ge is extracted by fast and heavy mixing with a slightly acidic H_2O_2-solution in a complex time-dependent process and extraction is usually not complete. In every extraction, several permille of Ga-metal are unwillingly also dissolved. The subsequent Ge-isolation from the extract is similar to the GALLEX procedure.

Major advantages and disadvantages of both targets are briefly summarized as follows:

Volume For a given amount of Gallium, a metal target is $\sim$ 10 times smaller than a $GaCl_3$-target. However, lower space requirements for the metal target are partly compensated by the space needed for additional equipment for the recovery of large volumes of process chemicals.

Ge-separation The metal-process requires more process steps and much more personnel is needed in the very elaborated extraction procedure. In every run, the target amount decreases by several permille. Ge-separation from a $GaCl_3$-solution is technically less complex and there is no target loss.

Sensitivity to trace impurities Conventional and radioactive trace impurities can - at least in principle - be removed from the metal-target on-site in the underground laboratory by using a wide spectrum of different extraction chemicals. However, the need to add large amounts of chemicals in each extraction increases the risk of contaminating the target from outside. Removal of nonvolatile impurities from the corrosive $GaCl_3$-solutions can hardly be done on-site; the $GaCl_3$-solution must be produced in sufficient purity and kept in that state for a long time.

Sensitivity to side reactions The presence of hydrogen and chlorine in the $GaCl_3$-target enhances the sensitivity especially to fast neutrons. The GALLEX data show that the contribution of side reactions in LNGS is known and low enough.

Artificial neutrino source Neutrino activation is far more efficient for a metal target, (compared to a $GaCl_3$ solution), especially if a single target is used and not a modular design as in SAGE. For the GNO100 phase, the development of a large single metal target is an interesting alternative to using Chloride. However, considerable efforts are needed to make this feasible (large pilot plant).

Safety The large volume of highly corrosive and HCl containing target solution must stay confined even if equipment fails, to prevent the release of HCl-vapor into the atmosphere of the underground laboratory.

Ventilated buildings, spare tanks, spill trays, emergency tanks plus additional personal protection measures are an inevitable necessity to cover the unlikely event of a sudden target tank failure (earthquake).

Though a metal target is much safer in this respect, larger amounts of HCl-gas and liquids must be handled and recycled routinely during normal operation (smaller incidents might be expected more frequently).

Technical equipment Both options are technically feasible. Space requirements for the larger $GaCl_3$-target are higher, especially in view of higher safety requirements: spare tank, emergency tanks.

Conclusion: Both processes are feasible, but all practical advantages are on the side of Gallium Chloride, at least for GNO30 and GNO60. In the long run (GNO100 or larger), the metal version gains some attraction.

was indicated that a decision would require a long time.

Materials, Investments and Operational Costs

At this stage it would be premature to file a detailed financial plan, but a few orienting figures for items other than gallium may be in order.

A crude estimate for the technical extensions, adjustments and improvements described in sect. 5.3.1 is $\sim$ 2 GLira. The largest items included in this figure are the additional tanks, the building extension and the emergency tank extension.

The operational costs (apart from personnel) are relatively moderate, mainly for nitrogen at a level similar as the operations of GALLEX.

APPENDIX

Time variations of the solar neutrino flux ?

In this Appendix we give a short summary of the possible causes which could produce a time modulation in the solar neutrino flux :

Geometrical effect

The Earth is farther to the Sun in summer (July 4^{th} aphelion, $R_+ = 1.51 \cdot 10^{11}$ m) than in winter (January 4^{th} perihelion, $R_- = 1.47 \cdot 10^{11}$ m). Therefore the neutrino flux during the summer semester is $\sim 4.2\%$ lower than during the winter semester. This is the only modulation effect that is definitely present.

VO variations

The vacuum oscillation hypothesis entails that the ^{7}Be neutrinos flux varies with time, with a period of 1 year, [CAL95],[BER95].
This is due to the fact that for the actual best fit parameters, the oscillation length at the energy of ~ 860 keV, the energy of ^{7}Be neutrinos, is of the order of the difference between the Earth position at aphelion and at perihelion. The amplitude of the effect depends on the specific choice of flavour mixing angle parameters: Fig. A.1 shows the suppression and maximal variation of the GALLEX rate, as predicted for some points inside the best fit region; Fig. A.2 shows the expected signal for the best fit parameters.

Solar cycle anticorrelation

In the case that the RSFP (Resonance Spin Flavour Precession) effect is present, an anticorrelation of the neutrino flux with respect to the solar activity cycle of ~ 11 years is expected. In fact, the variation of the external magnetic solar field is directly connected to the solar activity: when the solar activity and the external magnetic field are high, the RSFP effect is strenghtened and a lower neutrino flux is expected; the opposite effect applies when the solar activity is low.
There are some indications that the mentioned anticorrelation has been observed in the HOMESTAKE experiment [OAK94][MAS95], but this evidence has not been confirmed by the KAMIOKANDE data [SUZ95], see Fig. A.2 .
Moreover there is no definite agreement on the significance of the effect: the situation in this respect is not clear up to now.

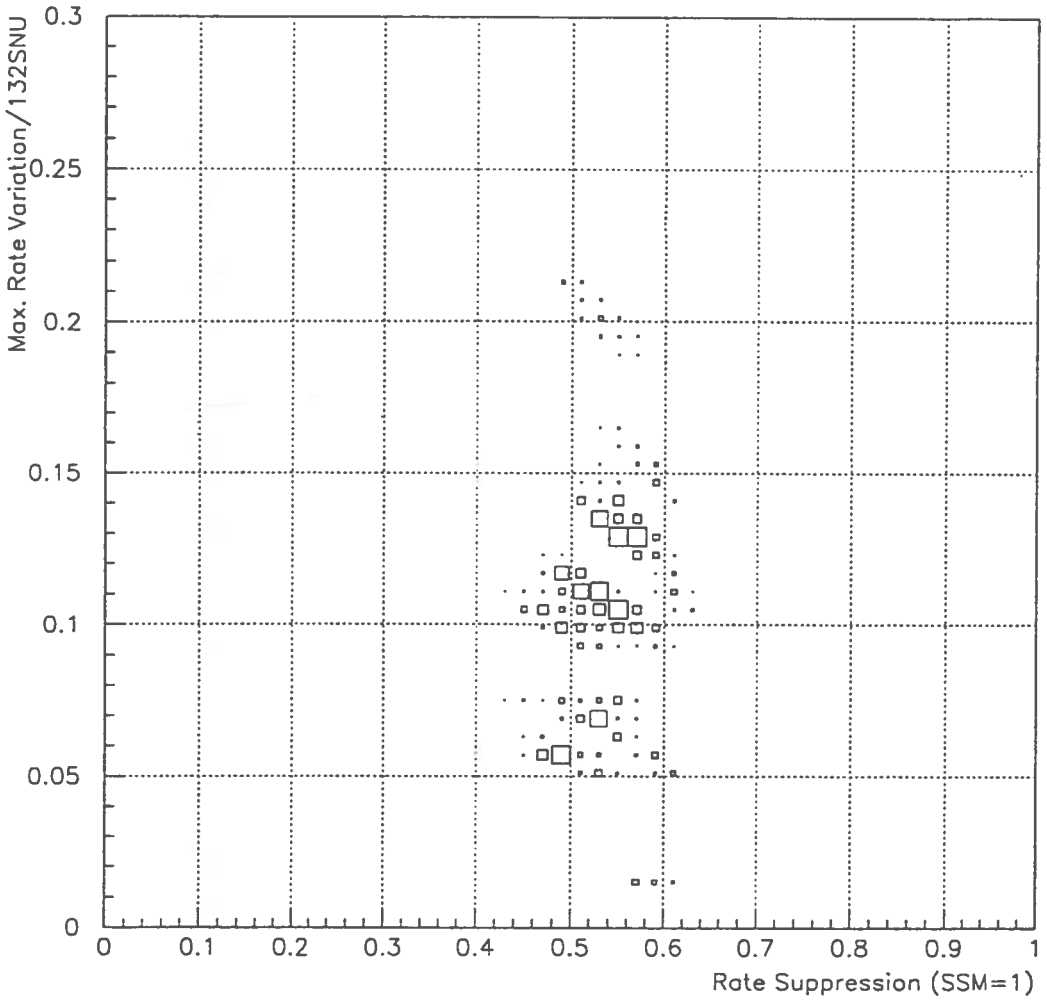

Figure A.1 Scatter plot of the maximal variation versus the suppression of the GALLEX signal within the vacuum oscillations hypothesis. The points are representative of the 90% C.L. allowed mixing parameters, see Fig. 3.1. All numbers are normalized to a standard solar model prediction for the GALLEX rate.

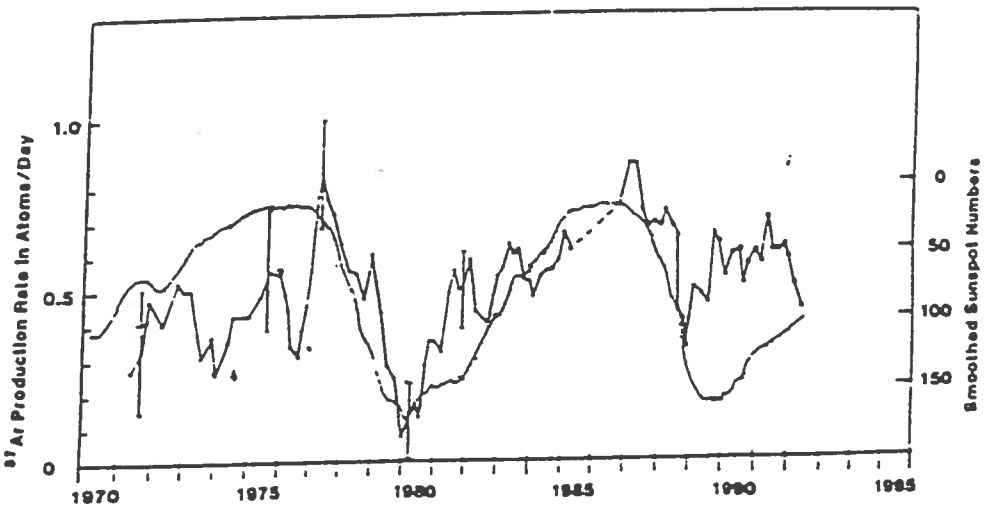

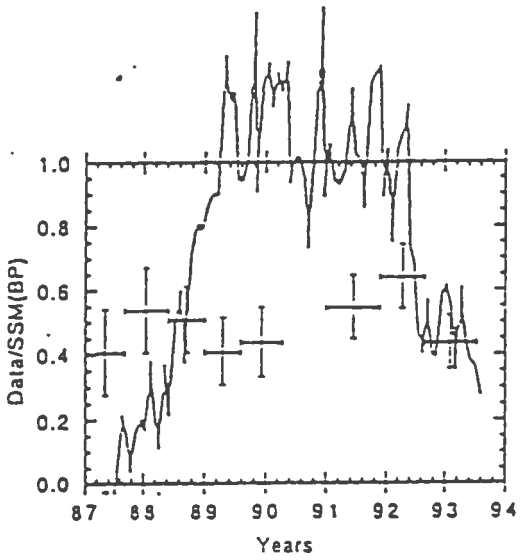

Figure A.2 a) 'Anticorrelation' of the HOMESTAKE data with the sunspot number. The apparent relationship deteriorated during the last 5 years
b) Corresponding plot for the KAMIOKANDE experiment.

REFERENCES

[AKH88] E.K.Akhmedov
Resonant amplification of neutrino spin rotation in matter and the solar neutrino problem
Phys. Lett. B 213,64 (1988)

[AKH95] E.K.Akhmedov, A.Lanza, S.T.Petcov
Solar neutrino data, neutrino magnetic moments and flavour mixing
Phys. Lett. B 348, 124 (1995)

[ANS92] P.Anselmann et al.
Solar neutrinos observed by GALLEX at Gran Sasso
Phys. Lett. B 285,376 (1992)

[ANS93] P.Anselmann et al.
GALLEX solar neutrino observations: the results from GALLEX I and early results from GALLEX II
Phys. Lett. B 314,445 (1993)

[ANS94] P.Anselmann et al.
GALLEX results from the first 30 solar neutrino runs
Phys. Lett. B 327.377 (1994)

[ANS95a] P.Anselmann et al.
First results from the ^{51}Cr neutrino source experiment with the GALLEX detector
Phys. Lett. B342,440 (1995)

[ANS95b] P.Anselmann et al.
GALLEX solar neutrino observations: complete results for GALLEX II
Phys. Lett. B 357,237 (1995)

[BAH89] J.N.Bahcall
Neutrino astrophysics
Cambridge Univ. Press (1989)

[BAH92] J.N.Bahcall, M.H.Pinsonneault
Standard solar models, with and without diffusion, and the solar neutrino problem
Rev. Mod. Physics 64,885 (1992)

[BAR94] I.R.Barabanov et al.
Fluorine scintillator neutrino detector
Nucl.Phys. B (Proc.Suppl.) 35,461 (1994)

[BEL94a] E.Bellotti
Non-accelerator experiments, neutrino masses and oscillations
Proc. XXVII Int. Conf. on HIGH ENERGY PHYSICS - Glasgow(Scotland) (1994)

[BEL94b] G.P.Bellini et al.
The counting test facility of the BOREXINO experiment
Proc. XXVII Int. Conf. on HIGH ENERGY PHYSICS - Glasgow(Scotland) (1994)

[BER95] Z.Berezhiani, A.Rossi
Vacuum oscillation solution to the solar neutrino problem in standard and non standard pictures
Phys.Rev. D 51,5229 (1995)

[BON94] G.Bonvicini
A solar neutrino experiment with neutrino energy resolution
Nucl.Phys. B (Proc.Supp.) 35,438 (1994)

[BOR91] BOREXINO coll.
Proposal for a real time detector for low energy solar neutrino
(1991)

[CAL95] E.Calabresu et al.
Just so ? Vacuum oscillations and MSW : an update
Astropart.Phys. 4,159 (1995)

[CLE93] B.T.Cleveland et al.
Proc. of XXIII I.C.R.C.- Calgary (Canada) (1993)

[CLE93] B.T.Cleveland
Update of the measurements of the solar neutrino flux with the HOMESTAKE Chlorine detector
Nucl.Phys. B (Proc.Supp.) 38,47 (1995)

[FIO94] G.Fiorentini, M.Lissia
Solar neutrino experiments and determination of the neutrino oscillation paramenters
Phys.Rev. D 49,6298 (1994)

[GAI94] T.K.Gaisser
Fluxes of ν_μ and ν_e in the atmosphere: Is there an anomaly?
Nucl. Phys. B (Proc. Supp.) 35,209 (1994)

[GAL95] GALLEX collaboration
Update of the major results from the GALLEX Cr-neutrino source experiment
Internal note GX79 (1995)

[GEL95] G.Gelmini,E.Roulet
Neutrino Masses
Rep. Prog. Phys. 58,1207 (1995)

[HAT94a] N.Hata, S.Bludman, P.Langacker
Astrophysical solutions are incompatible with the solar neutrino data
Phys. Rev. D 49,3622 (1994)

[HAT94b] N.Hata, P. Langacker
Solar model uncertainties, MSW analysis, and future solar neutrino experiments
Phys.Rev. D 50,632 (1994)

[HAT95] N.Hata, P.Langacker
Model-independent determination of the solar neutrino spectrum with and without the MSW effect
Phys.Rev. D 62,1 (1995)

[HEN92] E.Henrich, K.Ebert
The chemistry of GALLEX
Angew. Chem. Int. Ed. Engl. 31,1283 (1992)

[ICA89] Icarus Coll.
Preprint LNF-89/005(R) (1989)

[KRA82] P.I.Kratsev, S.T.Petcov
Neutrino oscillations in vacuum as a possible solution of the solar neutrino problem
Phys.Lett. B 285,85 (1992)

[KIR95a] T.Kirsten
GALLEX and the ^{7}Be solar neutrino problem
Proc. WEIN95, Osaka, World Scientific (H.Ejiri ed.) 135 (1995)

[KIR95b] T.Kirsten
Results from solar neutrino experiments
Invited talk at XXIV ICRC Rome(Italy) 1995, to appear in Nuovo Cimento 1996.

[LAU93] G.Laurenti et al.
A study of a high rate solar neutrino detector with neutrino energy determination
Prep. CERN/LAA/PC/93-10

[LIM88] C.S.Lim, W.J.Marciano
Phys. Rev. D 37, 1368 (1988)

[LIM95] C.S.Lim, H.Nunokawa
A natural explanation of all solar neutrino data by the resonant spin flavour precession scenario
Astropart. Phys. 4,63 (1995)

[MAK94] N.B.Mak
Search for solar neutrinos: progress and future ideas
Proc. VI works. on NEUTRINO TELESCOPES - Venezia(Italy) 120 (1994)

[MAS95] S.Massetti et al
Summary of correlative analysis between Homestake neutrino data and parameters related to solar activity
Proc. XXIV ICRC Rome(Italy), Vol. 4 (1995)

[MIK86] S.P.Mikheyev, A.Smirnov
Resonant amplification of neutrino oscillations in matter and solar neutrino spectroscopy
Nuovo Cim. C 19,17 (1986)

[NIC94] J.Nico
Results from SAGE II
Proc. XXVII Int. Conf. on HIGH ENERGY PHYSICS - Glasgow(Scotland) (1994)

[NUN93] H.Nunokawa, H.Minakata
Phys. Lett. B 314,371 (1993)

[OAK94] D.S.Oakley et al.
On the correlation of solar surface magnetic flux with solar neutrino capture rate
Astrophys. Jour. 437,L63 (1994)

[PLA91] R.Plaga, T.Kirsten
Reduction of degraded events in miniaturized proportional counters
Nucl.Instr.Meth. A 309,560 (1991)

[PON68] B.Pontecorvo
Neutrino experiments and the problem of the conservation of the leptonic charge
Sov.Phys. JETP 29,984 (1969)

[REV93] J.P. Revol
Preprint CERN-PPE/93-01

[SUZ95] Y.Suzuki
KAMIOKANDE solar neutrino results
Nucl.Phys. B (Proc.Supp.) 38,54 (1995)

[TUR93a] S.Turck-Chièze et al.
The solar interior
Phys. Rep. 230,57 (1993)

[TUR93b] S.Turck-Chièze, I.Lopes
Toward a unified classical model of the Sun
Astrophys. Jour. 408,347 (1993)

[WIN93] R.Wink et al.
Miniatturized proportional counters HD-2(Fe)/(Si) for the GALLEX solar neutrino experiment
Nucl.Instr.Meth. A 329,541 (1993)

[WOL78] B.Wolfenstein
Neutrino oscillations in matter
Phys.Rev. D 17,2369 (1978)

LVD

STATUS REPORT 1995

M.Aglietta[19], B.Alpat[16], E.D.Aleya[10], P.Antonioli[19], G.Badino[19], Y.Ban[5], G.Bari[1], M.Basile[1], V.S.Berezinsky[13], R.Bertoni[19], A.Bizzetti[6], A.Bosco[8], G.Bruni[1], Y.Cao[5], G.Cara Romeo[1], C.Castagnoli[19], A.Castellina[19], K.Chen[5], R.Chen[5], A.Chiavassa[19], J.A.Chinellato[3], L.Cifarelli[1], F.Cindolo[1], G.Conforto[20], S.Cong[5], A.Contin[1], V.L.Dadikin[13], P.Desiati[6], S.DePasquale[7], A.DeSilva[2], M.Deutsch[11], L.G. Dos Santos[3], R.I.Enikeev[13], F.L.Fabbri[7], W.Fulgione[19], P.Galeotti[19], P.Ghia[19], P.Giusti[1], R.Granella[19], F.Grianti[20], S.Gu[5], G.Guidi[20], Y.Guo[11], E.S.Hafen[11], P.Haridas[11], G.Iacobucci[1], N.Inoue[17], E.Kemp[3], F.F.Khalchukov[13], E.V.Korolkova[13], P.V.Kortchaguin[13], V.B.Kortchaguin[13], V.A.Kudryavtsev[13], G.Landi[6], K.Lau[9], X.Lin[5], L.Lu[5], M.Luvisetto[1], J.Ma[5], Z.Ma[5], G.Maccarone[1], A.S.Malguin[13], R.Mantovani[20], Z.Mao[5], M.A.Markov[13], T.Massam[1], B.Mayes[9], C.Melagrana[19], N.Mengotti Silva[3], A.Misaki[17], G.H.Mo[9], B.Monteleoni[6], C.Morello[19], J.Moromisato[12], R.Nania[1], G.Navarra[19], L.Panaro[19], D.Parks[9], P.G.Pelfer[6], L.Periale[19], A.Pesci[1], P.Picchi[19], P.Pinna[6], L.Pinsky[9], I.A.Pless[11], M.Pu[5], J.Pyrlyk[9], J.Qiu[5], V.G.Ryasny[13], O.G.Ryazhskaya[13], O.Saavedra[19], K.Saitoh[18], D.Sanders[9], S.Santini[20], G.Sartorelli[1], D.Shen[5], N.Taborgna[8], V.P.Talochkin[13], H.Tang[6], J.Tang[11], W.Tian[5], G.C.Trinchero[19], A.Turtelli[3], I.Uman[16], P.Vallania[19], S.Vernetto[19], F.Vetrano[20], C.Vigorito[19], E.von Goeler[12], L.Votano[7], T.Wada[14], F.Wang[5], H.Wang[5], S.Wang[5], R.Weinstein[9], M.Widgoff[2], L.Xu[11], Z.Xu[5], V.F.Yakushev[13], I.Yamamoto[15], G.T.Zatsepin[13], X.Zhou[5], Q.Zhu[5], X.Zhu[5], B.Zhuang[5], A.Zichichi[4]

1 *University of Bologna and INFN-Bologna, Italy*
2 *Brown University, Providence, USA*
3 *University of Campinas, Campinas, Brazil*
4 *CERN, Geneve, Switzerland*
5 *Chinese Academy of Sciences, Beijing, China and I.C.S.C. World Laboratory*
6 *University of Firenze and INFN-Firenze, Italy*
7 *INFN-LNF, Frascati, Italy*
8 *INFN-LNGS, Assergi, Italy*
9 *University of Houston, Houston, USA*
10 *Indiana University, Bloomington, USA*
11 *Massachusetts Institute of Technology, Cambridge, USA*
12 *Northeastern University , Boston, USA*
13 *INR, Russian Academy of Sciences, Moscow, Russia*
14 *Okayama University, Okayama, Japan*
15 *Okayama University of Science, Okayama, Japan*
16 *University of Perugia and INFN-Perugia, Italy*
17 *Saitama University, Saitama, Japan*
18 *Ashikaga Institute of Technology, Ashikaga, Japan*
19 *Institute of Cosmo-Geophysics, CNR, Torino, Italy, and University of Torino and INFN-Torino, Italy*
20 *University of Urbino and INFN-Firenze, Italy*

1. Introduction

The LVD experiment is a multipurpose detector consisting of a large volume of liquid scintillator interleaved with limited streamer tubes in a compact geometry. The major purpose of the LVD is to search for neutrino bursts from gravitational stellar collapses in all our Galaxy. However, the LVD is also very well suited to study cosmic ray muons: spectrum, interactions and muon-produced particles and cascades, muon bundles and mass composition of primary cosmic rays. Since the very beginning, our experimental results have confirmed that a thick, large volume detector, sectioned in identical scintillation counters, located deep underground and carefully shielded against the local radioactivity, is extremely sensitive to detect neutrinos from collapsing stars in our Galaxy. This is because it has a very low background and allows detection of both products of $\bar{\nu}_e$ interactions with protons, which give the main signal of supernovae neutrinos, with a very good signature. Moreover, the detector's core (consisting of the inner counters) is very well shielded against the low-energy radioactive background by the passive anticoincidence with the surface counters. As a consequence the total noise of the detector's core is so low that its sensitivity to detect neutrinos from gravitational collapses easily covers all our Galaxy. The LVD experiment can detect ν_e through the elastic scattering reaction with electrons, which adds further information on the study of gravitational stellar collapses from the neutronization peak at the initial stages of the collapse, where only ν_e are produced. Neutrinos of all flavours can also be detected in LVD through neutral and charged currents interactions with the carbon nuclei of the scintillator, giving information on the emission of neutrinos of different flavours from the collapsing core.

One of the unique features of the Gran Sasso Laboratory is the rich mountain structure: below $\cos\theta = 0.5$ there is a wide range of slant depths

at each zenith angle, and a wide range of zenith angles at each slant depth. This will enable separating angle dependent effects from energy dependent effects in a way not possible in other laboratories. Our muon data extend to a nearly horizontal zenith angle, so we can measure the zenith angle distribution of the π and K components, extract the prompt muon flux, and observe the neutrinos interacting in the rock.

The LVD data underground, correlated with the extensive air shower data collected by the EAS-TOP array on the surface of the mountain, provide a unique telescope for detailed multicomponent study of EAS. The surface array (consisting of an electromagnetic detector, a muon-hadron detector, and a Cerenkov light system) measures the electromagnetic, muonic and hadronic components of the shower; the deep underground detector measure high energy muons, their interactions, and the possible neutral penetrating component. The correlated data from the two experiments allow us to operate at primary energies above 10^{15} eV.

The joint information on the number of hits observed in the tracking system and the energy loss measured in the scintillator give us a unique possibility to separate showering and non-showering particles. This is a very important experimental feature to reduce systematics errors in the study of atmospheric neutrino oscillations, a very interesting field where controversary results have been obtained by presently running detectors, where different experimental techniques are used.

2. The LVD experiment

The LVD experiment is installed in Hall A of the underground Gran Sasso Laboratory at the minimal depth of 3,300 hg/cm^2. The mean muon energy at the LVD site is 320 GeV, taking into account the real depth distribution. The detector has a modular structure made of 190 identical modules arranged in five towers. Each module contains 8 scintillation

counters, with about 9.6 tons of liquid scintillator and 9.5 tons of steel, surrounded by an L-shaped tracking system. The final total mass is 1840 tons of liquid scintillator and the dimensions are 40m x 13m x 12m. The complete first tower is taking data since June 1992, and the second one since June 1994 with the full tracking system and 20 of the 38 scintillation modules. The single LVD tower has a surface area of 660 m^2 and a geometric acceptance of 1768 m^2sr for an isotropic flux. Table I summarizes the main characteristics of one tower. The total scintillator mass in data taking at present (562 tons) makes LVD one of the largest supernovae neutrino observatories in the world.

Characteristics	Value
surface area	660 m^2 sr
acceptance for isotropic flux	1768 m^2 sr
length x width x height	7m x 13m x 12m
scintillator mass	368 tons
iron mass (scintillator containers and carriers)	360 tons
streamer tubes	2828
tracking channels	17408
tracking spatial resolution	~ 1 cm
angular resolution	$\lesssim$4 mrad
energy resolution	~ 15% at 10 MeV

Table I - Main characteristics of 1 LVD tower

Each scintillation counter has an active volume of 1m x 1.5m x 1m and contains 1.2 tons of liquid scintillator. The internal walls of the counter are lined with aluminized mylar foils for light reflection. The scintillator is viewed by 3 photomultipliers (15 cm diameter) placed on the top of each counter. The scintillator density is 0.8 gcm^{-3}, the attenuation length is >15 m (at λ = 420 nm), the light output produces about 15 photoelectrons per MeV from the 3-fold coincidence of the

photomultipliers of one counter. The energy resolution is about 40%, 15% and better than 10% at 2 MeV, 10 MeV and 100 MeV respectively.

Each scintillation counter is self-triggered by the 3-fold coincidence of the signals from the 3 photomultipliers after discrimination. This high-energy threshold (HET), which allows the detection of single interactions occuring in the scintillation counter, can be set in the range from 2 to 10 MeV. The sum of the charges from the 3 photomultipliers is measured and recorded by the ADC, which has a dynamic range of 12 bits, a conversion time of 800 ns and an accuracy of about 100 keV/channel at 5-10 MeV. The ADC allows to measure the energy release in the counter from 0.5 MeV to 500 MeV. For measurements of high energy releases (up to several TeV) the intermediate dinode output of the photomultipliers and another ADC will be used. During 1 ms period after the HET trigger a low-energy threshold (LET) is enable in the range 0.5 - 2 MeV. Both the amplitude and the relative time (with an accuracy of 12.5 ns) of all pulses are measured. This allows us to detect both products of the inverse β decay, furnishing the signature of $\bar{\nu}_e$ interactions with the protons of the scintillator. The present values of the 2 energy thresholds are HET = 5 MeV, and LET = 0.8 MeV respectively. Photons emitted by n-capture are detected with an average efficiency of about 60%.

The rate of cosmic ray muons, at the LVD depth underground, is about 1 muon per m^2 per hour. Muons are easily recognized by the combined observation of their high energy release in the scintillator, the time coincidence between counters, and the reconstructed tracks from the tracking system. Natural radioactivity, essentially due to gammas and neutrons, gives an event rate of $8 \cdot 10^{-2}$ Hz in one tower for a HET of ~ 7 MeV. In the LVD, particular attention was paid to reduce the background due to natural radioactivity. This was achieved by minimizing the total surface exposed to the rock, by choosing materials with low radioactive contamination and by covering the floor with iron and borax paraffin. The average counting rate per counter, for energy release greater than 1.5

MeV, is about $2 \cdot 10^2$ Hz when averaged over all the 304 counters of one tower, and only 40 Hz when averaged over the 88 counters at the core of the tower.

Each element of an L-shaped tracking detector contains two staggered layers of 6.3 m long limited streamer tubes. The tube has 8 cells with 9x9 mm^2 active cross sectional area for each cell. Below and parallel to, and above and perpendicular to, the streamer tubes wires, are 4 cm wide pickup strips (x and y strips) to provide bidimensional information about an ionizing particle's impact point. The staggered double layer of streamer tubes and their orthogonal readout strips yield an effective strip width of 2 cm with no dead space, high overall tracking efficiency, and an angular resolution better than 4 milliradians.

The acceptance of the LVD detector as a function of zenith ($\cos\theta$) and azimuth (ϕ) angles depends on the trigger strategy, detector efficiencies, and the operational fraction of the detector. All of these effects were included in a simple straight-line Monte Carlo generated on a sphere containing the full LVD (5 towers), only one tower of which was active. These Monte Carlo data were then analyzed with the same event selection criteria as the experimental data.

3. Neutrinos from collapsing stars

For a burst of $3 \cdot 10^{53}$ erg emitted in neutrinos of all flavours at the galactic center (8.5 kpc), the expected number of interactions in LVD has been estimated for an high energy threshold HET = 7 MeV (see table II). These estimates assume equipartition of energy, Fermi-Dirac neutrino energy spectra, opacity of the star outer layers, and temperatures of the ν_e, $\bar{\nu}_e$ and $\nu_{\mu\tau}$, $\bar{\nu}_{\mu\tau}$ neutrinospheres to be in the ranges 3 to 5 MeV and 6 to 10 MeV, respectively. For the full experiment (5 towers), the expected

number of interactions ranges from 500 to 1000, being the difference due to the different theoretical predictions on the emission from the source.

	Reaction	Number of events
[1]	$\bar{\nu}_e + p \rightarrow n + e^+$ $n + p \rightarrow d + \gamma$	100 - 200
[2]	$\nu_e + e^- \rightarrow \nu_e + e^-$	3 - 5
[3]	$\nu_{e,\mu,\tau} (\bar{\nu}_{e,\mu,\tau}) + {}^{12}C \rightarrow \nu_{e,\mu,\tau} (\bar{\nu}_{e,\mu,\tau}) + {}^{12}C^*$ ${}^{12}C^* \rightarrow {}^{12}C + \gamma$	5 - 16
[4]	$\nu_e + {}^{12}C \rightarrow {}^{12}N + e^-$ ${}^{12}N \rightarrow {}^{12}C + e^+ + \nu_e$.	0 - 3
[5]	$\bar{\nu}_e + {}^{12}C \rightarrow {}^{12}B + e^+$ ${}^{12}B \rightarrow {}^{12}C + e^- + \bar{\nu}_e$	1 - 3

Table II - Predicted number of neutrino interactions in 1 LVD tower, from a stellar collapse at the distance of the galactic center (E_{th} = 7 MeV)

The neutrino reactions detectable in LVD are the following:

1) <u>inverse β decay</u>: $\bar{\nu}_e + p \rightarrow n + e^+$. Both products of this interaction are detected, namely a prompt pulse from the positron above the high energy threshold, followed by a delayed pulse from neutron capture $n + p \rightarrow d + \gamma$. The γ is emitted with an average delay of about 200 μs at the energy of 2.2 MeV. These photons are detected with an average efficiency of about 60%, in a 1 ms time window (gate), during which the low energy threshold is enabled by the main trigger. This reaction, which produces the largest number of events in a neutrino experiment, has a very clear signature in LVD, given by 2 pulses in a delayed coincidence in the same scintillation counter.

2) neutrino-electron scattering: $\nu_e + e^- \rightarrow \nu_e + e^-$. This reaction produces a single pulse in one scintillation counter above the high energy threshold.

3) neutral currents interactions: $\nu_{e,\mu,\tau}$ ($\bar{\nu}_{e,\mu,\tau}$) + $^{12}C \rightarrow \nu_{e,\mu,\tau}$ ($\bar{\nu}_{e,\mu,\tau}$) + $^{12}C^*$, followed by the de-excitation process: $^{12}C^* \rightarrow {}^{12}C + \gamma$, being the γ emitted at the energy of 15.1 MeV. Also this interaction has a very clear signature because the γ from carbon de-excitation is monoenergetic, observable in a scintillator counter in a well defined energy range.

4) charged currents interactions: $\nu_e + {}^{12}C \rightarrow {}^{12}N + e^-$ (energy threshold 17.3 MeV), followed after a time delay τ = 15.9 ms by $^{12}N \rightarrow {}^{12}C + e^+ + \nu_e$.

5) charged currents interactions: $\bar{\nu}_e + {}^{12}C \rightarrow {}^{12}B + e^+$ (energy threshold 14.4 MeV), followed after a time delay τ = 29.4 ms by $^{12}B \rightarrow {}^{12}C + e^- + \bar{\nu}_e$. The signature of reactions 4) and 5) is given by two pulses recorded in the same scintillation counter, both above the high energy threshold and in time coincidence within 3τ.

We wish to recall that the number of interactions reported in Table II are computed assuming equipartition of energy among the neutrino flavours. However, if the more energetic muon and tau neutrinos oscillate into electron neutrinos during their flight from the supernova to the detector, then these numbers cange, and in particular reactions [4] and [5] produce many more events in LVD because of the higher cross section these high energy electron neutrinos have with carbon. This is an indirect possibility to estimate neutrino oscillations from a stellar collapse.

The neutrino burst emitted by a collapsing core is expected to occur several hours or days earlier than the increase of the optical emission. The fast recognition of the burst by an international neutrino detector network could alert astronomical observatories and permit a detailed study of the first stages of the supernova evolution. In the LVD experiment the liquid scintillator counting rate, after muon subtraction, is continuously monitored by the Supernova On-line Monitor (SOM), a high priority task which examines all the events. This on-line burst selection is

based on pure statistical analysis of all signals: the SOM analyzes the clustering characteristics of the time sequence of single pulses; time coincidences ($\Delta t \leq 250$ ns) between contiguous counters are assumed to be muons and are rejected. A cluster of multiplicity m and duration Δt is defined as a sequence of m events within a time interval $\Delta t \leq 200$ seconds. Each such cluster is compared with the corresponding Poisson probability computed on the basis of the current trigger rate. If the probability of observing such a cluster is lower than a preset value, (e.g. 0.1 year^{-1}) the cluster is flagged and the corresponding data copied into the Burst Candidate Data File.

After the candidate selection has been made on a purely statistical basis, a complete analysis of the cluster selected by the SOM will test its consistency with a neutrino burst. This will be done on the basis of:

1. topological distribution of pulses. A real burst should have pulses almost uniformely distributed over the entire detector, while background pulses are more frequent in the surface than in the core counters.
2. energy distribution. A real burst should have a Fermi-Dirac spectrum, while the background spectrum drops exponentially with energy.
3. presence of delayed low energy pulses in the gate, i.e. the signature of $\bar{\nu}_e$ interactions in the scintillator.

Since June 1991 the LVD experiment has been sensitive to neutrino bursts from stellar collapses in our Galaxy. The active mass of liquid scintillator has increased from 20 tons in June 1991 to 368 tons (one full LVD tower) in June 1992, and to 562 tons in June 1994. The results of the off-line analysis of the data from the first LVD tower, for the period from 11 June 1992 to 31 May 1993, during which 2,208,574 single events (after muons rejection) were detected in 285.1 days of running time (average running time efficiency = 79%), have shown no burst candidate. The average rate of single pulses in the full tower for energy release

greater than 7 MeV was 0.09 Hz (324 events/hr). The total exposure in this period was about 244 tons·year.

In June - July 1993, the high energy threshold of the scintillation counters was reduced and settled between 4 and 6 MeV on the different counters, depending on their exposure to the local background. No burst candidate has been selected also from the off-line analysis of the data collected in this second period of data taking, from 4 August 1993 to 11 March 1995, during which 11,430,669 single events (after muons rejection) were detected in 397 uptime days, with an average rate of single pulses of 0.33 Hz, and 0.06 Hz above the energy threshold of 7 MeV. The total exposure in this period was 369 tons·year, including the data from the active part of the second tower.

As we have discussed, the search for neutrino bursts is performed in two steps, the first one based only on the statistical analysis of signal clusters above 7 MeV. The result of this analysis shows that the background imitation rate (i.e. the rate of background clusters with a duration Δt ranging from 1 to 200 s) never occours more frequently than 1 event every 10 years. In addition, we wish to remark that the lower is the HET level, the fainter is the detectable burst, but for a standard burst a software energy cut in the event selection increases the signal to noise ratio. For example, a cut at the threshold E = 10 MeV, reduces the tower counting rate of a factor of 6 while the expected number of interactions remains almost unchanged. Notice that in our reports the analysis is made taking into account all the raw data, i.e. all pulses with energy release above the HET hardware threshold, and no software cut is made.

In conclusion, the LVD experiment is monitoring our Galaxy since June 1992 with a large mass of liquid scintillator, and no evidence for a neutrino burst from a supernova explosion has been observed. We have also shown that the burst identification in LVD has an high statistical significance and that can be confirmed by several independent tests.

Information on the physics of the collapse easily follows from the observed energy spectrum.

4. Neutrinos associated with γ-ray bursts

The emission of neutrinos and γ rays is often associated in many astrophysical sources and processes. For this reason, we believe that the detection of both neutrinos and γ-ray burst (GRBs) in time coincidence would be an important step toward the understanding of the nature of the astrophysical source and its production mechanisms. This correlation analysis has been performed by using the LVD data to search for correlations with the GRBs data obtained by the BATSE experiment aboard the Compton Observatory. The 41 GRBs considered in the analysis, have been selected from the BATSE observations in a period extending from June 1993 to March 1995. The time duration of a burst (Δt_{90}) is defined as the time during which BATSE saw 90% of the γ-ray flux. The total duration of the 41 GRBs is 1488.42 seconds. For each GRB, the LVD data (mostly background pulses) have been analyzed in a time window of ± 5 hours centered on the time of the GRB, for a total analyzed time of 403.57 hours. Only LVD data recorded by counters in the detctor's core, very well shielded by the surface ones against the low-energy local radioactive background, have been considered in this analysis. The total scintillator mass of these counters is 162 tons, containing a target of 1.51 10^{31} protons and 8.24 10^{30} ^{12}C nuclei. Obviously, the neutrino reactions detectable in LVD are the same quoted in the previous section. For this correlation analysis we have used the following ones:

1. <u>inverse β decay</u>: We have searched for trigger pulses in the energy range from 7 to 55 MeV (produced by $\bar{\nu}_e$ signal with energy from 9 to 50 MeV), followed in the same scintillation counter by a low energy

pulse in the gate. The rate of such double pulses, averaged over the coincidence time with the 41 GRBs considered in this analysis, is 5.66 events per hour.

2. neutral currents interactions: We have searched for single pulses in the energy range from 12 to 18 MeV; the measured average rate of such pulses is 15.2 events per hour, and the γ detection efficiency is ~ 35%.
3. charged currents ν_e interactions: We have searched for double pulses recorded in the same scintillation counter in the energy range between 7 and 55 MeV (produced by ν_e signals with energy ranging from 25 to 50 MeV), and in time coincidence within 48 ms (~3τ). The rate of such double pulses, 5 10^{-5} events per hour, is estimated assuming Poisson distribution of the background.

This correlation analysis has been done in two steps. Firstly we have searched for on-source candidates, namely neutrino events in time correlation with GRBs during their time duration Δt_{90}; secondly we have searched for an excess of coincidences in several time windows, centered on the start time of the GRB and with duration from 1 to 1,000 seconds.

The results of this analysis, obtained by adding together the LVD data over the 41 GRBs, show that no statistically significant excess of events has been observed in the LVD experiment, neither in time coincidence with the BATSE γ-ray bursts during their duration Δt_{90}, nor in any of the time windows considered in the analysis.

From this comparison between expected and observed events, we were able to derive the 90% c.l. upper limits to the flux of neutrinos associated with each GRB. Table 3 gives the minimum and maximum values of these limits, integrated over the time duration Δt_{90} of the corresponding γ-ray burst. These upper limits have been conservatively calculated using cross-section values corresponding to the lower limit of the neutrino energy range considered in the analysis, and taking into

account the energy resolution of the detector and the detection efficiency for the different products of the neutrino interaction.

	Energy range	minimum	maximum
$F(\bar{\nu}_e + p)$	$9 \leq E \leq 50$ MeV	$\leq 4.7\ 10^{10}$ cm^{-2}	$\leq 9.8\ 10^{10}$ cm^{-2}
$F(\nu_e,\nu_\mu,\nu_\tau)$ n.c.	$20 \leq E \leq 50$ MeV	$\leq 2.9\ 10^{12}$ cm^{-2}	$\leq 6.1\ 10^{12}$ cm^{-2}
$F(\bar{\nu}_e, \bar{\nu}_\mu, \bar{\nu}_\tau)$ n.c.	$20 \leq E \leq 50$ MeV	$\leq 3.2\ 10^{12}$ cm^{-2}	$\leq 6.6\ 10^{12}$ cm^{-2}
$F(\nu_e)$ c.c.	$25 \leq E \leq 50$ MeV	$\leq 1.8\ 10^{11}$ cm^{-2}	$\leq 1.8\ 10^{11}$ cm^{-2}

Table 3 - Minimum and maximum upper limit flux of neutrinos associated to a GRB, integrated over its time duration Δt_{90}.

5. Cosmic ray muons and muon bundles

The muons reaching LVD are of three types:

1. muons that are the decay products of pions and kaons produced by the interaction of cosmic rays with the Earth's atmosphere,
2. muons that are the decay products of short lived particles such as charm mesons, also produced by interactions of cosmic rays with the Earth's atmosphere,
3. muons that are produced by the charged currents interactions of muon neutrinos that interact in the rock near the LVD detector. The ν_μ are the products of particles that decay in the Earth's atmosphere.

At slant depths less than about 14,000 hg/cm^2 of standard rock, the major contribution to the muon intensity is muons of type 1 cited above. Muons of type 2 above, so called prompt muons, certainly contribute to the muon intensity at slant depths less than 12,000 hg/cm^2 of standard rock, but they constitute a much less frequent source of muons than the pions and kaons. The muons of type 3 are dominant at slant depth greater

than about 14,000 hg/cm^2 of standard rock. In this report, we will discuss the results obtained by LVD in studying muons of type 1 and 3; the study of muons of type 2 with LVD is in progress. In particular, we will present here our measurements of the flux of muons produced by neutrinos in the rock close to LVD at a zenith angle close to 90° and energy above 1 GeV.

The selection of the data sample required that at least one scintillation counter was triggered in the event, and there was a minimum of three space points available for track reconstruction. In total, 978,074 single muon events were selected during 11,566 hours of live time. Note that our study is an exclusive one, namely the data include only events containing single muons, and that they have been acceptance corrected.

The LVD acceptance corrected single muon angular distributions show, as expected from the shape of the Gran Sasso mountain, that most of the muons arrive at the LVD through the plateau near $\cos\theta = 0.9$, and pointing toward Campo Imperatore. However, the flux of nearly horizonthal muons is not negligible, because the LVD acceptance (1 tower) extends to $\cos\theta = 0$ and is zero on only 8% of the Monte Carlo sphere. Thus, these very interesting horizonthal events can be studied with LVD with a good statistics.

The thickness of rock crossed by muons was determined from the mountain map of Gran Sasso. The muon vertical intensity in a given depth interval ($h \pm \Delta h/2$) was obtained from the number of events at the corresponding slant depth, by using the following formula:

$$I(h) = \frac{1}{\Delta T \Omega(h)} \sum_i^n \frac{N_i \cos(\vartheta_i)}{A_i(\vartheta_i, \varphi_i)}$$

where ΔT is the live time, $\Omega(h)$ is the solid angle corresponding to the slant depth interval, n is the number of (θ,ϕ) bins contributing to the slant

depth interval, N_i is the number of events in bin i of slant depth h, A_i is the acceptance, θ_i and ϕ_i are the zenith and azimuth angles.

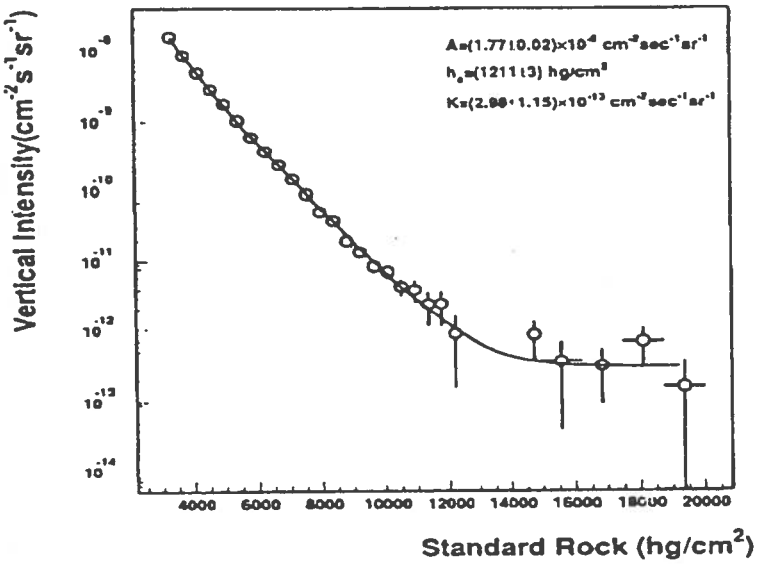

Figure 1 - Muon vertical intensity vs. slant depth in standard rock.

Fig.1 displays the vertical muon intensity as a function of slant depth. The main features of this plot are roughly the exponential shape up to a slant depth of about 14,000 hg/cm^2 of standard rock and the roughly constant behaviour beyond that point. These data, which cover over five decades of vertical intensity, can be fit with three parameters over the full range, from 3,000 hg/cm^2 to 20,000 hg/cm^2. The function we fit is:

$$I_v(h) = A \cdot e^{\frac{h}{h_0}\left(\frac{h_0}{h}\right)^2} + K$$

Our best fit to these 3 parameters are: A = (1.77 $\pm$ 0.02) 10^{-6} cm^{-2}s^{-1}sr^{-1}, h_0 = (1211 $\pm$ 3) hg/cm^2 of s.r., K = (2.98 $\pm$ 1.15) 10^{-13} cm^{-2}s^{-1}sr^{-1} (all quoted errors are statistical).

The vertical intensity of the data from our experiment between 3,000 hg/cm^2 and 9,000 hg/cm^2 have been compared with the results of Nusex,

Frejus and Macro. All experiments are in reasonable agreement, taking into account that our work is an exclusive study (only single muons are included in our data set with appropriate corrections), while the other are inclusive ones (muons from all multiplicities are included in their data sets). Our points in the intensity plot should therefore be ~10% lower than the other three experiments.

A direct way to establish the existence of atmospheric muon neutrinos interacting in the rock near an underground detector is to show that for a fixed zenith angle close to 90° the muon flux is independent of slant depth for depths greater than about 14,000 hg/cm^2 of standard rock. The unique topology of the Gran Sasso Laboratory allows us to explore slant depths from 14,000 to 20,000 hg/cm^2 of standard rock at a fixed zenith angle close to 90°. In our data sample there are 17 single muon events beyond a slant depth of 14,000 hg/cm^2 of standard rock, of which 14 have a zenith angle greater than 82.5°. Hence, we have establish that for the fixed zenith angle of about 90° and for slant depths greater than 14,000 hg/cm^2 the muon flux is independent of slant depth. We measure the value of this flux near 90° to be:

$$I(90^{\circ}) = (8.3 \pm 2.6) \times 10^{-13}\ \mathrm{cm^{-2}s^{-1}sr^{-1}}$$

As stated above, this is direct evidence of the existence of a muon flux induced by neutrinos in the rock surrounding LVD.

The data in fig. 1 have been used also to calculate the power index $\gamma_{\pi K}$ of the differential energy spectrum of pions and kaons in the atmosphere, using the muon survival probabilities for Gran Sasso rock obtained by Monte Carlo simulation. The muon spectrum at sea level was taken in the most general form modified to take into account the rise of the cross section of hadron-nucleon interactions at high energies. This muon spectrum at sea level is a function of two parameters: a normalization

parameter and the power index. We fit the data using this two free parameters, and our best fit was $\gamma_{\pi K} = 2.75 + 0.03$ (the error includes the systematic uncertainties).

6. Correlations with EAS-TOP

Finally, the underground LVD experiment and the surface EAS-TOP array provide a telescope for detailed multicomponent study of extensive air showers (EAS). The surface array (consisting of an electromagnetic detector, a muon-hadron detector, and a Cerenkov light system) measure the electromagnetic, muonic and hadronic components of the shower; the deep underground detector measure the high energy (TeV) muons, their interactions, and the possible neutral penetrating component. The two experiments are separated by ~ 1000 m in altitude and ~ 500 m on the horizontal projection, the relative zenith angle being 25 degrees; the combined geometric acceptance is G ~ 10^5 cm^2sr. The correlated data from the two experimental apparata allow us to operate at primary energies above 10^{15} eV.

The combined measurements are in operation since June 1992 with the first LVD tower, and since June 1994 with the two LVD towers running at present. About 27,000 coincident events have been recorded in a livetime period of 444 days, giving a coincidence frequency of 2.4 events per hour with one LVD tower in data taking. The analysis of the largest multiplicity muon bundle ($N_\mu = 32$ muons) detected in LVD in time coincidence with an EAS-TOP air shower with a size of $N_e = 5\ 10^7$ particles, corresponds to a primary energy of 10^{17} eV.

The analysis of events like this is very important to study primary cosmic ray composition, and proton and nuclei interactions at the quoted primary energies. In addition, the thickness and modular structure of LVD also allows to study the penetrating neutral component produced by high

energy cosmic rays in the atmosphere, using as an anticoincidence those LVD modules facing towards the direction of EAS-TOP. No muon-like track originated inside the detector, in temporal coincidence with an EAS-TOP event, has been found in this first analysis, thus showing the feasability of this kind of experiment.

7. Conclusions

In this report we have discussed some results on cosmic neutrinos and cosmic ray muons obtained with the first of the five towers of LVD (operational since June 1992) and part of the second tower (operational since June 1994). The results of the search for supernovae neutrinos show that LVD is a neutrino observatory able to detect neutrinos of different flavours from gravitational stellar collapses in all our Galaxy, with a very high discriminating power over the background (given by different and complementary techniques) and covering a wide range of burst durations. No evidence for burst candidates has been found in the data recorded from June 1992 to March 1995, for a total live-time of 682 days and a total exposure of 613 tons·year.

The results of a time-coincidence analysis between low energy events recorded in LVD and γ ray bursts detected by the BATSE experiment have been used to obtain upper limits on the flux of neutrino of different flavours associated to γ rays sources.

The muon intensity as a function of slant depth is presented over five decades of intensity. An interesting result is that this flux is independent of slant depth beyond a depth of about 14,000 hg/cm^2 of standard rock, and corresponds to near horizonthal muons. This is direct evidence that this flux is due to atmospheric neutrinos interacting in the rock surrounding LVD.

LVD papers published in 1995

1 - Neutrino induced and atmospheric single-muon flux measured by LVD at Gran Sasso
Astroparticle Physics, 3, 311, 1995

2 - The LVD experiment at Gran Sasso
Nuovo Cimento, 18C, 629, 1995

Papers presented by the LVD collaboration to the XXIV ICRC (Roma)
- Description and operational characteristics of the LVD experiment
- Search for neutrinos from collapsing stars with the LVD experiment
- Analysis of underground events recorded in LVD correlated with γ-bursts
- Experimental limit on the solar antineutrino flux
- Atmospheric single muon flux measured by LVD at Gran Sasso
- Power index of pion and kaon spectrum in the atmosphere obtained by LVD
- Neutrino-induced single muon flux measured by LVD at Gran Sasso
- Comparison of LVD single muon angular distribution with simulated data
- A study of single muon intensity structure observed in the LVD experiment
- Landau energy loss in liquid scintillator and the search for wifs with LVD

Status Report of the MACRO experiment

March, 1996

The MACRO Collaboration

M. Ambrosio[12], R. Antolini[7], G. Auriemma[14,a], R. Baker[11], A. Baldini[13], G. C. Barbarino[12], B. C. Barish[4], G. Battistoni[6,b], R. Bellotti[1], C. Bemporad[13], P. Bernardini[10], H. Bilokon[6], V. Bisi[16], C. Bloise[6], T. Bosio[7], C. Bower[8], S. Bussino[14], F. Cafagna[1], M. Calicchio[1], D. Campana[12], M. Carboni[6], M. Castellano[1], S. Cecchini[2,c], F. Cei[13,d], V. Chiarella[6], A. Corona[14], S. Coutu[11], G. De Cataldo[1], H. Dekhissi[2,e], C. De Marzo[1], I. De Mitri[9], M. De Vincenzi[14,f], A. Di Credico[7], O. Erriquez[1], R. Fantini[2], C. Favuzzi[1], C. Forti[6], P. Fusco[1], G. Giacomelli[2], G. Giannini[13,g], N. Giglietto[1], M. Goretti[14], M. Grassi[13], P. Green[m], A. Grillo[7], F. Guarino[12], P. Guarnaccia[1], C. Gustavino[7], A. Habig[8], K. Hanson[11], A. Hawthorne[8], R. Heinz[8], J. T. Hong[3], E. Iarocci[6,h], E. Katsavounidis[4], E. Kearns[3], S. Kyriazopoulou[4], E. Lamanna[14], C. Lane[5], D. S. Levin[11], P. Lipari[14], G. Liu[4], R. Liu[4], N. P. Longley[n], M. J. Longo[11], G. Ludlam[3], G. Mancarella[10], G. Mandrioli[2], A. Margiotta-Neri[2], A. Marini[6], D. Martello[10], A. Marzari-Chiesa[16], M. N. Mazziotta[1], D. G. Michael[4], S. Mikheyev[7,i], L. Miller[8], P. Monacelli[9], T. Montaruli[1], M. Monteno[16], S. Mufson[8], J. Musser[8], D. Nicoló[13,d], R. Nolty[4], C. Okada[3], C. Orth[3], G. Osteria[12], O. Palamara[10], S. Parlati[7], V. Patera[6,h], L. Patrizii[2], R. Pazzi[13], C. W. Peck[4], S. Petrera[10], N. D. Pignatano[4], P. Pistilli[10], V. Popa[2,l], A. Rainó[1], J. Reynoldson[7], F. Ronga[6], U. Rubizzo[2,c], A. Sanzgiri[15], F. Sartogo[14], C. Satriano[14,a], L. Satta[6,h], E. Scapparone[7], K. Scholberg[4], A. Sciubba[6,h], P. Serra-Lugaresi[2], M. Severi[14], M. Sitta[16], P.F. Spada[2], P. Spinelli[1], M. Spinetti[6], M. Spurio[2], R. Steinberg[5], J. L. Stone[3], L.R. Sulak[3], A. Surdo[10], G. Tarlé[11], V. Togo[2], V. Valente[6], C. W. Walter[4] and R. Webb[15]

1. Dipartimento di Fisica dell'Università di Bari and INFN, 70126 Bari, Italy
2. Dipartimento di Fisica dell'Università di Bologna and INFN, 40126 Bologna, Italy
3. Physics Department, Boston University, Boston, MA 02215, USA
4. California Institute of Technology, Pasadena, CA 91125, USA
5. Department of Physics, Drexel University, Philadelphia, PA 19104, USA
6. Laboratori Nazionali di Frascati dell'INFN, 00044 Frascati (Roma), Italy
7. Laboratori Nazionali del Gran Sasso dell'INFN, 67010 Assergi (L'Aquila), Italy
8. Depts. of Physics and of Astronomy, Indiana University, Bloomington, IN 47405, USA
9. Dipartimento di Fisica dell'Università dell'Aquila and INFN, 67100 L'Aquila, Italy
10. Dipartimento di Fisica dell'Università di Lecce and INFN, 73100 Lecce, Italy
11. Department of Physics, University of Michigan, Ann Arbor, MI 48109, USA
12. Dipartimento di Fisica dell'Università di Napoli and INFN, 80125 Napoli, Italy
13. Dipartimento di Fisica dell'Università di Pisa and INFN, 56010 Pisa, Italy
14. Dipartimento di Fisica dell'Università di Roma "La Sapienza" and INFN, 00185 Roma, Italy
15. Physics Department, Texas A&M University, College Station, TX 77843, USA

16. Dipartimento di Fisica Sperimentale dell'Università di Torino and INFN, 10125 Torino, Italy
a Also Università della Basilicata, 85100 Potenza, Italy
b Also INFN Milano, 20133 Milano, Italy
c Also Istituto TESRE/CNR, 40129 Bologna, Italy
d Also Scuola Normale Superiore di Pisa, 56010 Pisa, Italy
e Also Faculty of Sciences, University Mohamed I, B.P. 424 Oujda, Morocco
f Also Dipartimento di Fisica, Università di Roma Tre, Roma, Italy
g Also Università di Trieste and INFN, 34100 Trieste, Italy
h Also Dipartimento di Energetica, Università di Roma, 00185 Roma, Italy
i Also Institute for Nuclear Research, Russian Academy of Science, 117312 Moscow, Russia
l Also Institute for Atomic Physics, 76900 Bucharest, Romania
m Sandia National Laboratory, Albuquerque, NM 87185, USA
n Swarthmore College, Swarthmore, PA 19081, USA

1 Introduction

The MACRO (Monopole, Astrophysics, and Cosmic Ray Observatory) collaboration operates a large area underground detector optimized to search for the supermassive magnetic monopoles predicted by Grand Unified Theories (GUTs). The detector allows to perform observations relevant to particle physics, astrophysics, and cosmic ray physics. These include different studies of the high energy underground muon flux relevant to primary cosmic ray composition and origin, search for low energy gravitational collapse neutrinos, high energy neutrino astronomy and study of atmospheric neutrinos. Other research topics include a study of the underground muon residual energy spectrum with transition radiation detectors and a search for lightly ionizing particles using the new waveform digitization system.

In order to provide redundant and complementary particle identification, MACRO employs three different detector types: liquid scintillation counters, gas filled limited streamer tubes, and Lexan/CR39 nuclear track detectors. The active components (the scintillators and the streamer tubes) measure particle tracks with resolutions of approximately 0.2° in angle, 1 cm in position, 700 ps in time of flight, and 1 MeV in energy loss (for muons). The passive nuclear track detector can provide additional information for monopole candidates, for which the detector is sensitive in the range of $10^{-4} < \beta < 1$, or for other interesting events.

The MACRO detector has been completed in august 1995 and since then it is running in its final configuration.

2 The Detector

The MACRO detector is composed of six adjacent supermodules, each of which is 12.6 × 12 m^2 with a height of 9.6 m (Fig. 1). Including the enclosed steel support structure, the full detector measures 76.5 × 12 m^2 and 9.6 m high, with a total acceptance for isotropic flux of $\sim 10^4$ m^2 sr. A cross sectional view is shown in Fig. 2.

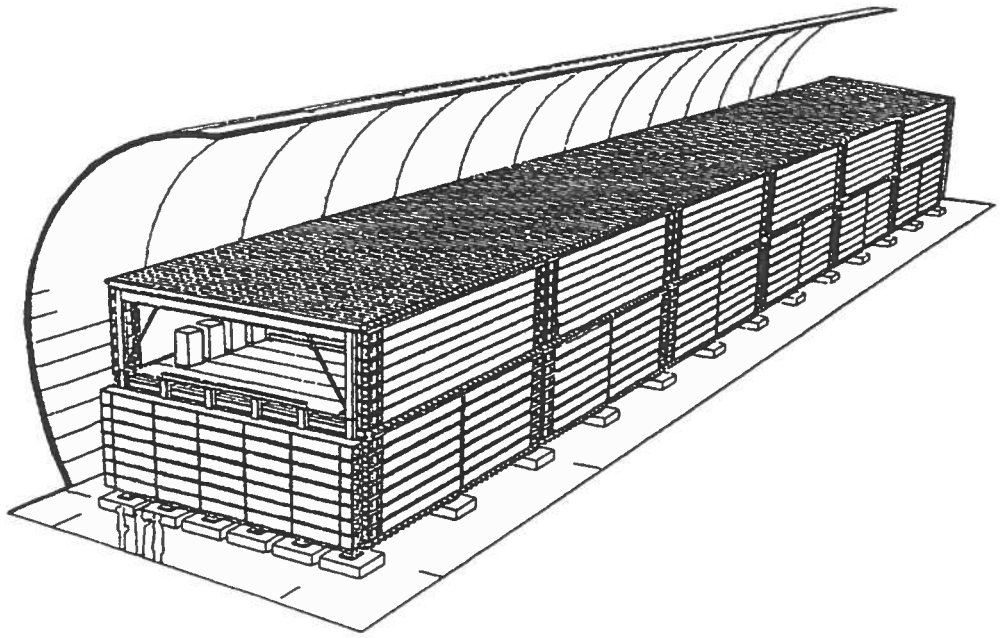

Figure 1: The complete MACRO detector in perspective view. It is 76.5 m long, 12 m wide, and 9.6 m high. The upper part (attico) houses the electronics.

Each supermodule contains seventy-seven scintillator tanks, divided into three horizontal (bottom, center, and top) and two vertical (east and west) planes. The bottom and center horizontal planes, along with the lower seven tanks of the east and west planes, occupy the lower section of the supermodule, while the top and upper seven tanks of the east and west planes occupy the upper section (attico). The north and south planes cover only the lower sections of the extreme ends of the detector, while the attico, where the readout electronics are located, is left open. Horizontal tanks measure 11.9 × 0.75 m^2 and 0.25 m tall and hold two phototubes at each end, while vertical tanks measure 12.0 × 0.25 m^2 and 0.50 m tall, with one phototube per end. All are filled with a scintillating mixture of 96.4% mineral oil and 3.6% pseudocumene, with an additional 1.44 g/l of PPO

and 1.44 mg/l of bis-MSB which act as wavelength shifters. In all there are 476 scintillator boxes (294 horizontal and 182 vertical), with a total active mass of approximately 600 tons, observed by 1540 individual photomultiplier tubes.

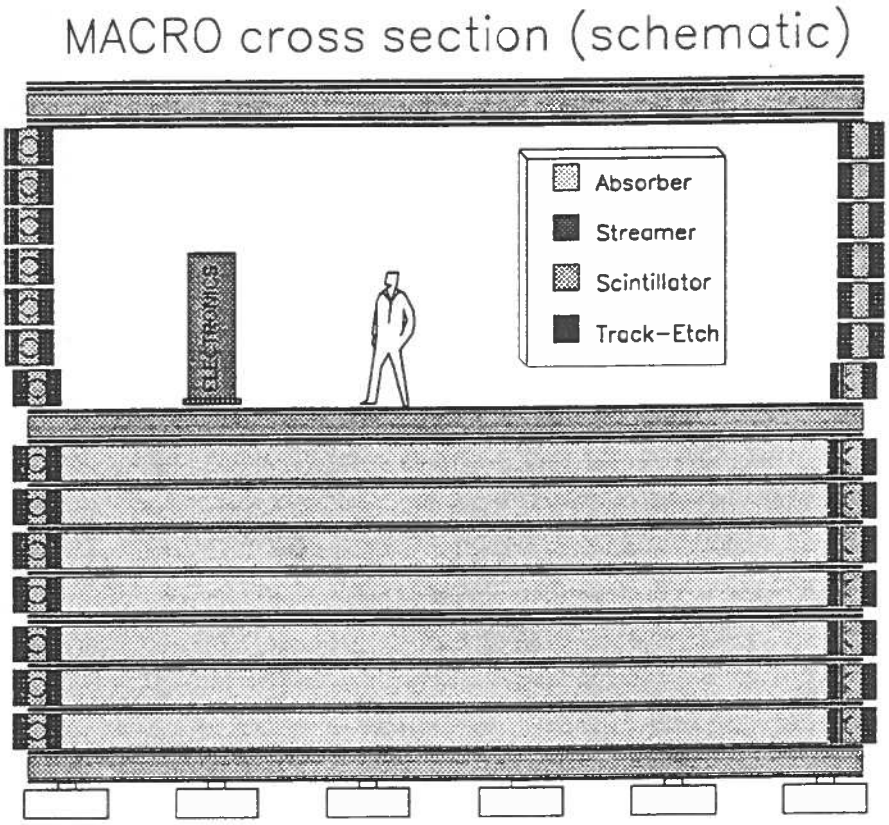

Figure 2: A cross sectional view of MACRO

The lower section of each supermodule contains ten horizontal planes of limited streamer tubes, the middle eight of which are separated by seven layers of passive rock absorber with a total thickness of 420 g/cm^2. The attico contains an additional four layers of horizontal tubes, two on either side of the top scintillator layer, but no rock absorber. There are also twelve vertical streamer tube planes, arranged in four groups of three, which sandwich the east and west vertical scintillators. A similar arrangement covers the north and south scintillator planes. There are a total of 55,200 individual streamer tubes, each 3×3 cm^2 and 12 m long and filled with a gas mixture of 73% He and 27% n-pentane. All horizontal planes and the attico vertical planes are additionally equipped with stereo pickup strips running across the wires at an angle of 26.5°.

The track etch detector is deployed in three planes: one horizontally in the center of the lower section of the apparatus (just above the fifth streamer tube

plane), one covering the east face, and the last plane covering the lower part of the north face. Each of the 14,100 individual track etch modules is composed of three layers of CR39, three layers of Lexan, and one layer of aluminum absorber, and measures 24.5×24.5 cm^2 and 0.14 cm thick. The track etch system is operated in triggered mode, in which interesting events identified by the active components of the detector are traced to individual track etch modules, which can then be removed for analysis.

Construction of the MACRO detector was completed on March 1994. The new WaveForm Digitizer (WFD), Lightly Ionizing Particle (LIP) trigger, and attico scintillator slow monopole (Time-Over-Half-Maximum or TOHM) trigger became operational in august 1995. The detector is now completely operational.

MACRO has so far recorded approximately 26 million muons. This total increases at the rate of $\simeq 6.6 \times 10^6$ muons per live year, or $\simeq 18,000$ each day. The muon threshold and mean residual energies are $\simeq 1.4$ TeV and $\simeq 240$ GeV, respectively. Neutrino interactions in the rock surrounding MACRO can also produce muon tracks; those muons that travel in the upward rather than the downward direction are easily recognized as ν-induced (the are approximately one per day).

The new WFD was designed to enhance scintillator signal resolution. Hardware zero suppression and individual signal discrimination allow it to record signals from individual scintillation counters for times of the order of milliseconds. The scintillator slow monopole trigger (TOHM) employs surface mount and Field Programmable Gate Array (FPGA) technology to reduce the size and cost of the system.

The scintillator and streamer tube systems allow monopole detection over the interval $10^{-4} < \beta < 1$.

The Lighthly Ionizing Particle Trigger, LIP, employs FPGA technology similar to that in TOHM, which at moderate cost allows a search for lightly ionizing (including fractionally charged) particles based on their WFD signals. Unlike previous LIP searches, MACRO will also be able to examine candidate tracks within high multiplicity muon showers, making it sensitive to any particle which might be produced in ultra high energy cosmic ray interactions.

In addition three transition radiation detector (TRD) modules are now in operation. Each TRD module measures 2×6 m^2 and 2 m high, and is composed of ten horizontal planes of thirty-two polystyrene proportional counters. The individual counters measure 6×6 cm^2 and 6 m long and are filled with 90%/10% Ar/CO_2 gas. The proportional counter planes are separated by 10 cm thick polyethylene foam radiators with typical cell diameter 1 mm and wall thickness 30 μm. As relativistic muons cross the numerous air/polyethylene boundaries inside the radiator, they produce X rays (of 11 keV peak energy) in proportion to their total energy. These X rays are detected by the polystyrene proportional counters, allowing the TRD to measure muon residual energies in the range of 100 GeV$< E_\mu <$1 TeV.

The first MACRO TRD module, installed in the attico in March 1994, has recorded approximately 20,000 muon tracks. The other two modules are located alongside the first prototype in the southern end of the attico. The three modules yield a total TRD muon event rate of about 300 per day.

3 Selected Physics Results

The year 1995 saw a great deal of progress in MACRO physics. Papers were published on the performance of the streamer tube system on the search for magnetic monopoles [1], on the vertical muon intensity [2] and on atmospheric neutrino flux measurements [3]. Several interesting results have appeared in preliminary form in conference proceedings and LNGS reports [4-11] on magnetic monopoles and nuclearites searches, on muon astronomy and seasonal variations, on the study of primary cosmic interactions and composition, on upward going muons, on the performance of the transition radiation detectors, etc.

3.1 Magnetic monopoles

One of the main objectives of MACRO is the search for supermassive magnetic monopoles predicted by most GUT theories. The use of three different detectors implies that a single candidate event may provide distinctive and multiple signatures in the three system.

While GUT monopoles are normally expected to have relatively low velocities ($\beta \sim 10^{-4}$ if gravitationally bound to the solar system and $\sim 10^{-3}$ if bound to the galaxy), it might also be possible for them to be accelerated in neutron stars or extragalactic sources; in any case light Dirac monopoles could easily have relativistic velocity. Therefore the MACRO experiment has been designed to identify magnetic monopole candidates in the range of $\beta \sim 10^{-4}$ to $\beta = 1$. Furthermore, because the survival of the galactic magnetic field implies that the monopole flux not exceed the Parker bound of $10^{-15}\mathrm{cm}^{-2}\mathrm{sr}^{-1}\mathrm{s}^{-1}$, we plan a search to a level well below this value.

In addition to increasing the monopole exposure, we also continued improving the detection techniques, as described in reference [1] for the streamer tube system, in [7-10] for the scintillator and track-etch systems and in § 2 for the new WFD for the scintillators.

New preliminary interesting limits have been presented at the 1995 conferences for the whole β-range, $10^{-4} < \beta < 1$, as shown in Fig. 3 [7-10]. The new improved limits were obtained: (i) with the streamer tube system at low β-values, (ii) with the scintillator system in the whole β-range, using the ERP and PHRASE electronics and a new method employing wavelets technique for waveform classification, and (iii) with the track-etch system. The limits apply to

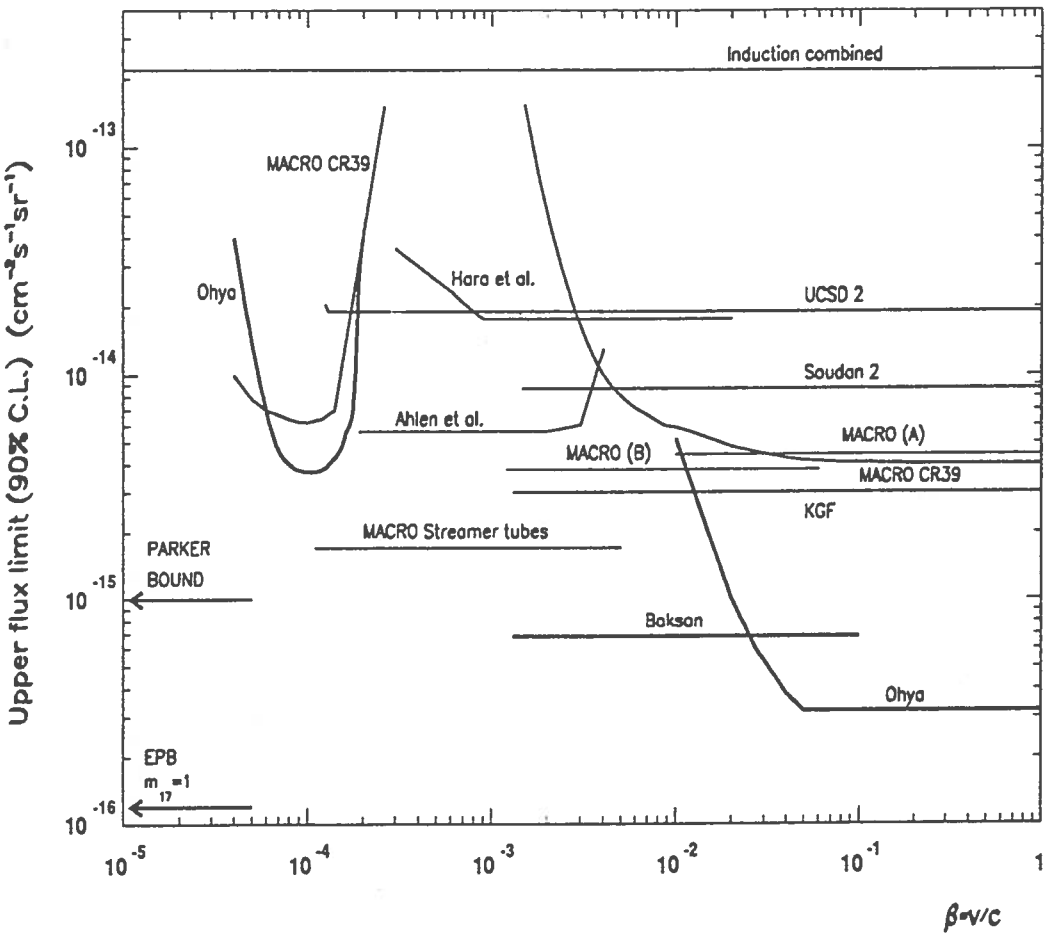

Figure 3: MACRO upper limits on the flux of superheavy magnetic monopoles with $g = g_D$ versus monopole velocity, compared to other published limits.

an isotropic flux of unit bare magnetic charges, ($g = g_D$), and for catalysis cross sections smaller than 10 mb.

3.2 Cosmic Ray Muons

Muon intensity, decoherence (the lateral distribution within multiple muon events), decorrelation (the relationship between muon angular and spatial separation), and muon arrival time distributions are relevant to primary interaction models. As with other aspects of underground cosmic ray physics, the large size and versatility of the MACRO detector allow it to pursue these studies with great acceptance and resolution.

Intensity. The underground muon intensity provides information on the high energy atmospheric muon flux ($E > 1$ TeV) and on the all-particle cosmic ray primary spectrum. These, in turn, place constraints on cosmic ray interaction models and provide important systematic checks for cosmic ray Monte Carlo

studies. MACRO results acquired with the streamer tube system of the lower sections of the full six supermodules are shown in Fig. 4.

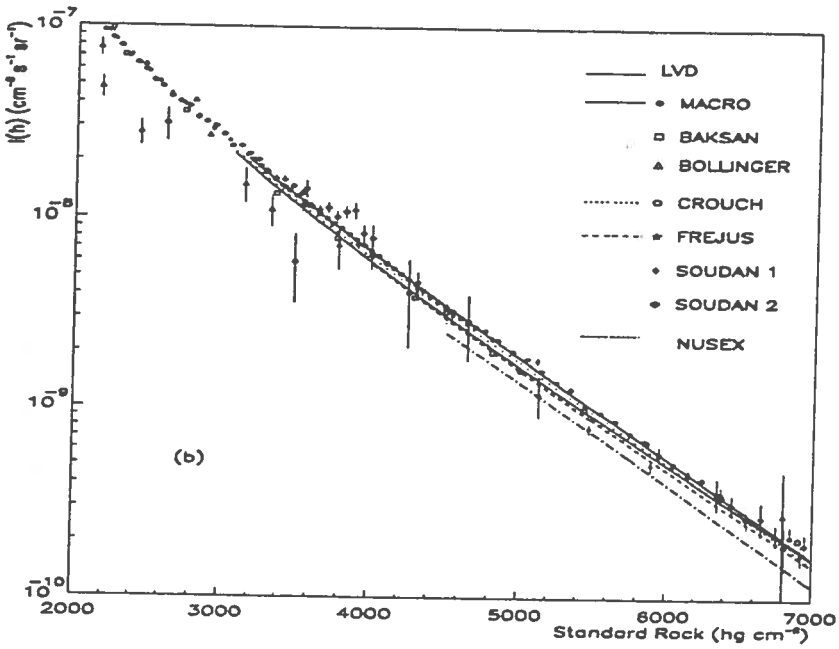

Figure 4: The vertical muon intensity versus depth in standard rock, compared with other results.

Decoherence. The data sample analyzed so far consists of approximately 1.5×10^5 muon pairs, whose separations extend to greater than 70 m. Experimental data have been compared to a full HEMAS Monte Carlo model of the underground muon flux, which examines the possible systematic effects due to uncertainties in the primary interaction cross section, the question of superposition versus fragmentation in the nuclear interaction models, energy losses in the rock overburden, and the effect of the geomagnetic field. The results demonstrate that the Monte Carlo is robust with respect to these considerations, an important result for any cosmic ray study which depends upon such simulations. There is, however, a tendency for the data to exhibit more events than are predicted in the high separation tail of the muon decoherence distribution. This effect is observed at varying levels for all composition models, indicating that additional study of the theoretical transverse momentum distribution may be warranted.

Decorrelation. The muon decorrelation function describes the relationship between the angular and spatial separations of underground muons. Like the decoherence function, it is sensitive to the details of high energy cosmic ray interaction models. Unlike the decoherence, however, the decorrelation function is largely independent of the primary composition. The so far preliminary analysis indi-

cates that there is some disagreement between the Monte Carlo and the data at low muon pair separations, and that further study of energy losses in the rock overburden might be in order:

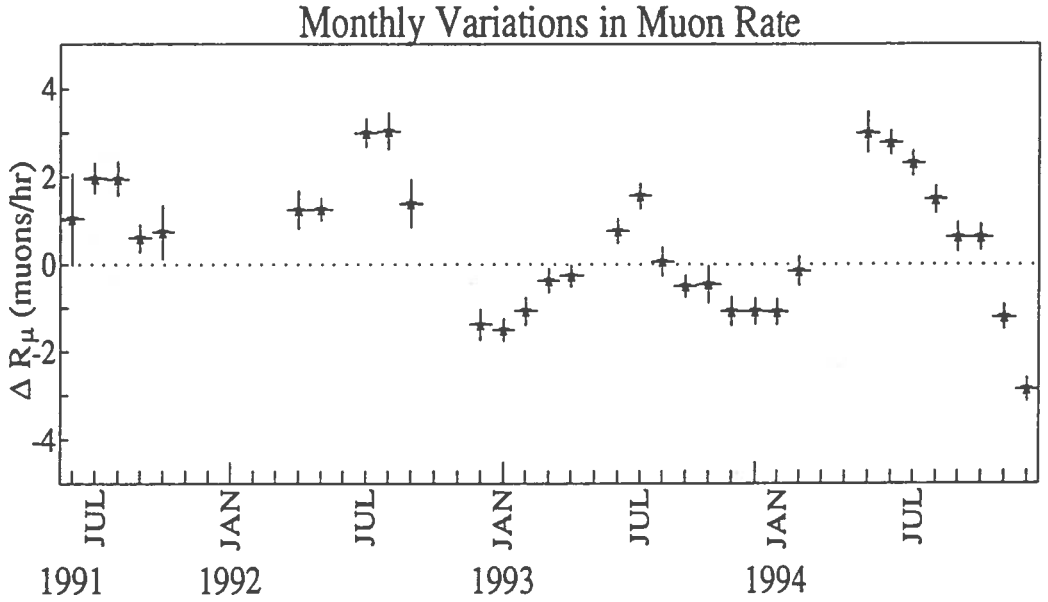

Figure 5: Percent deviation of the monthly muon intensity from average, plotted versus month (numbered consecutively from January 1991). The data extend from June 1991 to December 1994.

Muon Arrival Times. Analysis of the muon arrival time distribution is focused on the search for delayed muon tracks, which could be produced by relatively long-lived heavy particles created in high energy cosmic ray interactions in the upper atmosphere. If such particles were to be heavy enough and long-lived enough, their decay products (muons) could arrive appreciably later than those generated in normal shower processes. While some previous searches in this area have been made at relatively low energies, the MACRO detector depth makes it sensitive to only the highest energy muons, eliminating a great part of the low energy background in which new particle production is less likely. A total of 51,236 muon bundles have been examined, containing 109,039 muons. So far results have been negative, and work is underway in order to convert these measurements into a limit on the long-lived massive particle production cross section.

Muon Astronomy. There have been contradictory reports in the literature regarding the possible existence of localized sources of underground muons. So far, a total of eight million muons have been reconstructed in order to investigate the possibility of statistically significant muon excesses. In an all-sky search, careful statistical analysis does not indicate any such excess, nor are any seen in

the direction of any of several astronomical objects which have been proposed as candidate sources. While it is possible that there exist sources with energy spectra that make them visible in detectors located at different depths, or that have exhibited time-dependent flux increases for periods in which MACRO was not active, there nevertheless does not at this time appear to be any indication in our data for the existence of localized deep underground muon sources.

Seasonal Variation. Because high energy muons are produced by meson decay in the upper atmosphere, their flux depends on the ratio of decay and mean interaction pathlengths. Essentially, the flux is expected to decrease in the winter when the upper atmosphere is colder and slightly more dense, making it less likely for the parent mesons to decay into muons before they interact. Although expected flux variations are not large (the maximum is of the order of 2-3%), our extensive data sample makes the effect quite obvious (Fig. 5).

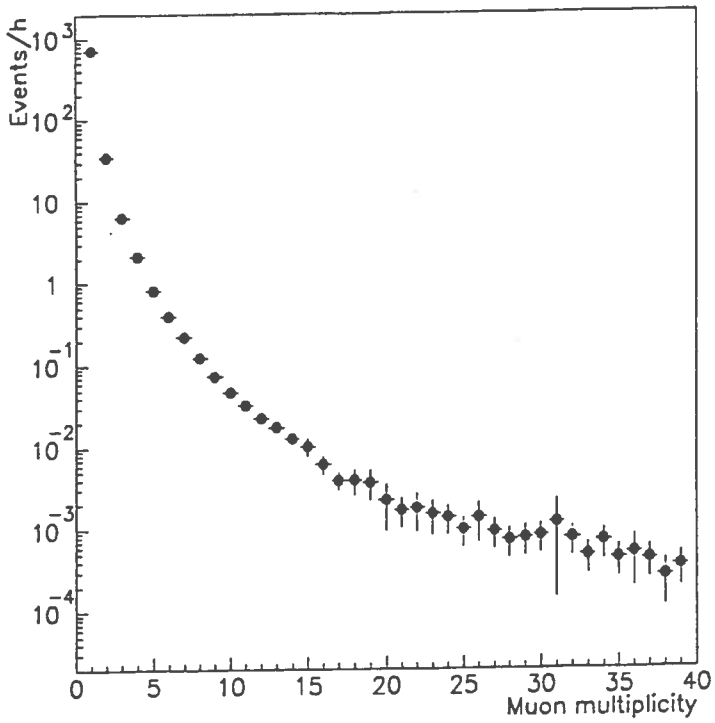

Figure 6: MACRO muon multiplicity distribution.

3.3 Cosmic Ray Composition

An understanding of the primary cosmic ray composition near the knee of the spectrum, where there is a change in the spectral index between 10^3 and 10^4 TeV, could shed some light on the fundamental problem of the origin of high energy

cosmic rays.

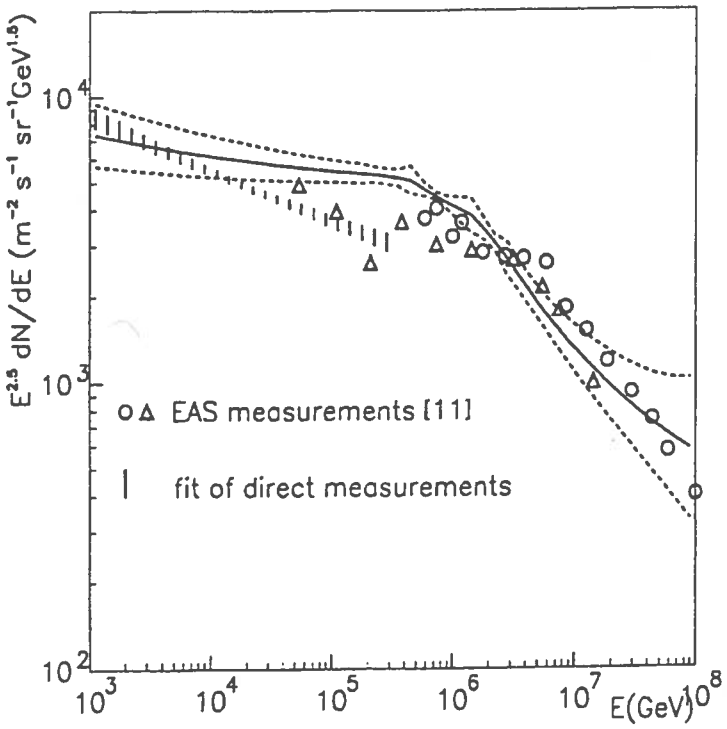

Figure 7: All-particle spectrum derived from the fit to MACRO muon multiplicity data.

The essential idea behind using muons for cosmic ray composition studies is that at high energy ($E \gg 10^2$ TeV), heavy nuclei should produce more underground muons than lighter nuclei of the same total energy. Past composition studies used this feature to make comparisons of data to Monte Carlo models of various *ad hoc* compositions. While these studies have produced consistent results, indicating that the composition through the knee region remains predominantly light, we have improved the phenomelogical approach used. This has resulted in our current "best-fit" approach , whereby the contributions of several different nuclear mass groups can be fit to the available muon multiplicity data. In this approach, we allow each of several nuclear mass groups to have two possible spectral indices around a central break-point. In order to provide some reasonable constraint to the fitting procedure, the mass dependent break-point energy is determined according to the relationship $E_{cut}(Z) = E_{cut}(Fe) \times Z/27$. The indices and fractional abundance for each element are determined by minimizing a χ^2 based on both the muon multiplicity data and direct measurement data at lower energies. The relative weight of the constraint coming from the direct measurement data is allowed to vary in order to check the consistency of

the result. Figure 6 shows the distribution of muon multiplicities in MACRO based on 4.4×10^6 muon events (of which 2.6×10^5 are multi-muons) coming from a total live-time of 5850 hours using the full length of MACRO. Figure 7 shows the all-particle spectrum calculated from the MACRO fit along with a compilation of results from extensive air shower measurements. It is interesting to note that the MACRO measurements are in good agreement with the EAS measurements which have not been included in the fitting procedure employed here. The resulting composition requires two spectral indices for each element and an increase in the average mass at higher energies (see Fig. 8).

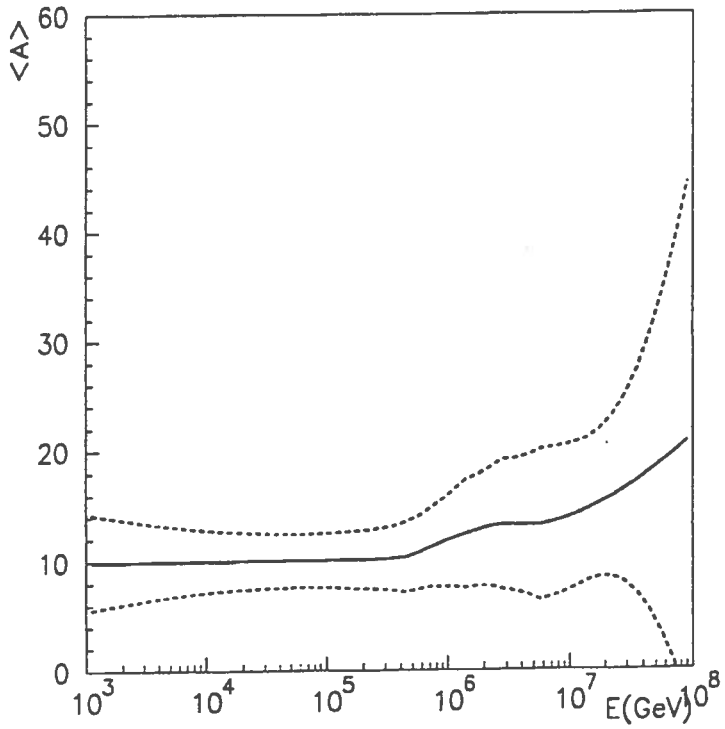

Figure 8: Average mass number from fit to muon multiplicity.

3.3.1 MACRO/EAS-TOP correlations

The combination of MACRO's good muon acceptance with the powerful EAS-TOP surface array can further refine composition studies based on underground muon data alone. In particular, EAS-TOP shower size measurements can be used to estimate the total shower energy, allowing the detailed study of energy dependences in the MACRO underground muon data.

The most recent MACRO/EAS-TOP analysis includes 4813 coincident events, including 200 events with primary energies above the knee in the spectrum.

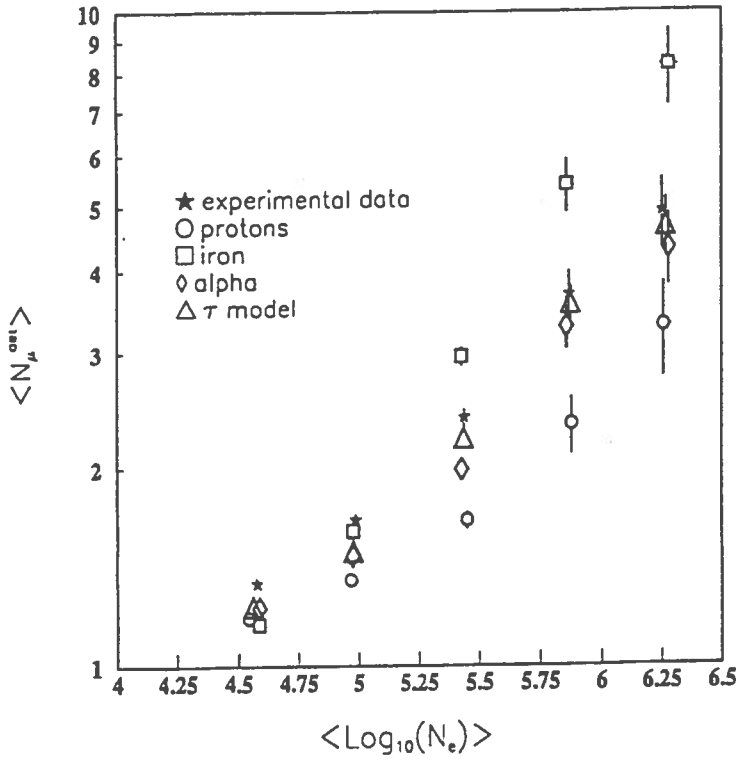

Figure 9: Correlation between the average observed muon multiplicity $\langle N_\mu^{det} \rangle$ in MACRO and the average logarithm of the shower size $\langle log_{10} N_e \rangle$ in EASTOP.

Figure 9 shows the multiplicity of muons observed in MACRO relative to the size of the air shower observed by EASTOP. Also shown are the predicted results using the HEMAS Monte Carlo code for an all proton, iron or helium composition and for a mixed composition based on an extension of direct measurements of the composition at lower energies (the τ model). For the highest energy measurements, the data clearly favor mixed-composition models or a model based on helium. The data exclude a pure iron or pure proton composition at a level of 3.5 σ for energies above the knee. A pure helium composition fails to produce the high-multiplicity tail observed in the highest energy data. A mixed composition (the τ model) does a better job at reproducing this tail.

3.4 Neutrino-induced upgoing muons

The search for upgoing muons is done using tracking and the time-of-flight method. A rejection factor of at least 10^5 is necessary to separate the upgoing muons from the downgoing muons from ordinary cosmic rays. The muon trajectory is established by the streamer tubes, while the muon versus is determined by the time-of-flight between 2 or 3 layers of scintillators. Fig. 10 shows

the $1/\beta$ distribution for throughgoing up-muons when using 2 or 3 layers of horizontal scintillators: the improvement brought about by the addition of the third layer of liquid scintillators is evident.

Throughgoing up-muon flux. The apparent anomaly in the ratio of contained muon neutrino to electron neutrino interactions in the Kamiokande and IMB detectors has raised considerable interest in precise measurements in the flux of atmospheric neutrinos even if other lower statistics experiments did not see any apparent anomaly. A precise analysis of the upgoing muon flux was perfomed using limited statistics from three running periods with the lower part of the detector. Although the small observed deficit could be consistent with neutrino oscillation hypotheses, it is also consistent with a no-oscillation hypothesis at the 90% confidence level [6].

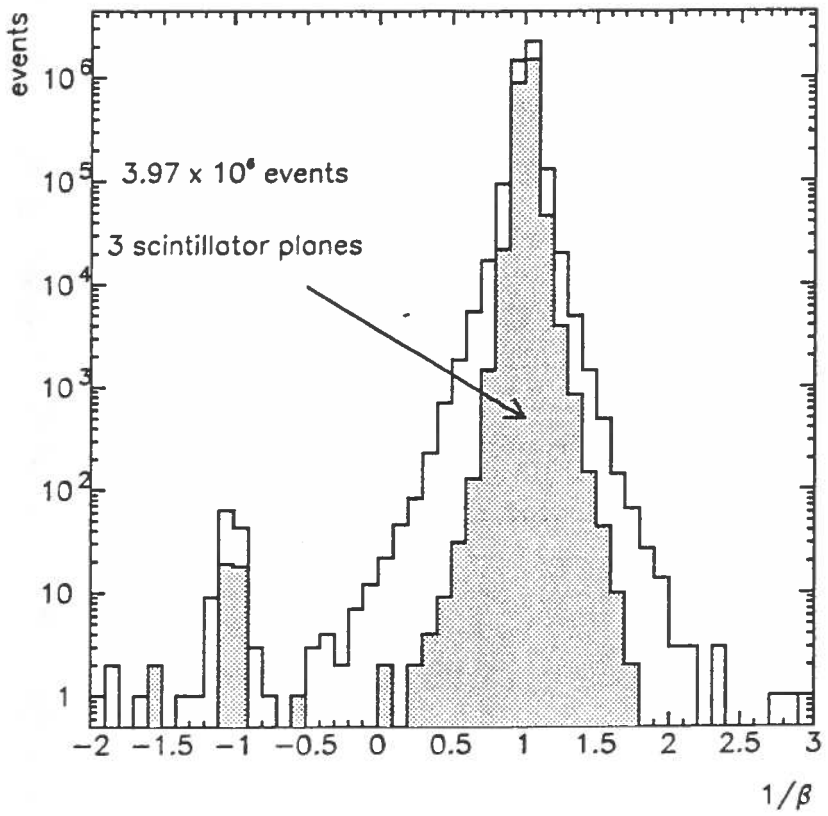

Figure 10: Distribution in $1/\beta$ of upgoing muons after analysis cuts for runs with the two lower scintillator planes and with the three scintillator plane (shadowed hystogram).

Search for astrophysical point sources. A search has been made for upgoing muons produced by neutrinos coming from celestial sources, using about 100

events from the first running periods. The good angular resolution (0.5°) allows to use tight angular bins around possible sources: hence the background from atmospheric neutrinos is small, resulting in better flux limits than using an equal exposure with a detector with worse resolution. For neutrino-induced muons the resolution smearing, resulting from the combination of multiple scattering in the rock and the production angle of the muon with respect to the neutrino direction, depends on the spectral index of the neutrino energy distribution. For a spectral index of 2.0-2.2 the choice of an angular acceptance of 3° (half width) around the source direction includes 90% of the observed muons. The search yielded 90% CL upper limits which range from 2.4 10^{-14} cm $^{-2}$ s^{-1} for LMCX-4 to 6.0 10^{-13} for Cyg X-3.

UHE neutrinos. A number of models predict large accelerations of protons in Active Galactic Nuclei (AGN) leading to neutrinos with energies larger than hundreds of TeV [6].

Between the horizontal planes of the limited streamer tubes of the lower part of the MACRO detector there are seven layers of rock absorbers, each of 60 g cm^{-2} thickness. Very high energy muons would shower in these absorbers; an estimate of the muon energy is given by the combined information of the number of hit wires (N_w) in the streamer tubes and the energy released in the scintillators. Monte Carlo studies show that the variable $Q = a\ E_{sc} + b\ N_w$, with $a = 0.0389$ MeV^{-1} and $b = 0.816$, yields the best estimate of the muon energy.

A search was made trying to extract from the data a sample enriched with high energy upgoing muons, making a cut on the Q-variable. The candidate events were visually scanned and one event remained . This has to be compared with the simulation which predicts 1.4 events from the standard atmospheric neutrino flux and 2.9 events for a neutrino flux including also the component from AGN. We estimate that at the present data taking rate it would take 2-3 years of data to exclude these AGN models.

Searches for upgoing muons from the earth and the sun. WIMPs trapped inside celestial bodies would concentrate on their cores and would annihilate into products which could decay into neutrinos of GeV or of TeV energy. These neutrinos may be detected as upward going muons.

The absolute neutrino flux yields immediately a limit on WIMPs trapped inside the earth, by evaluating the number of neutrinos coming vertically from the core of the earth, say within a cone of 10° around the vertical. The extra neutrino flux limit for neutrinos with energies larger than 1 GeV is at the level of 4 10^{-14} cm^{-2} s^{-1}.

The present flux limit for neutrinos with energies larger than 2 GeV coming from the sun is at the level of about 10^{-13} cm^{-2} s^{-1}.

In some models the WIMPs can be identified with the smallest mass neutralinos. In order to see if these data can constrain the stable neutralino mass the limits have been compared with the predictions of a specific model. The limits start to constrain phenomenological WIMPs models.

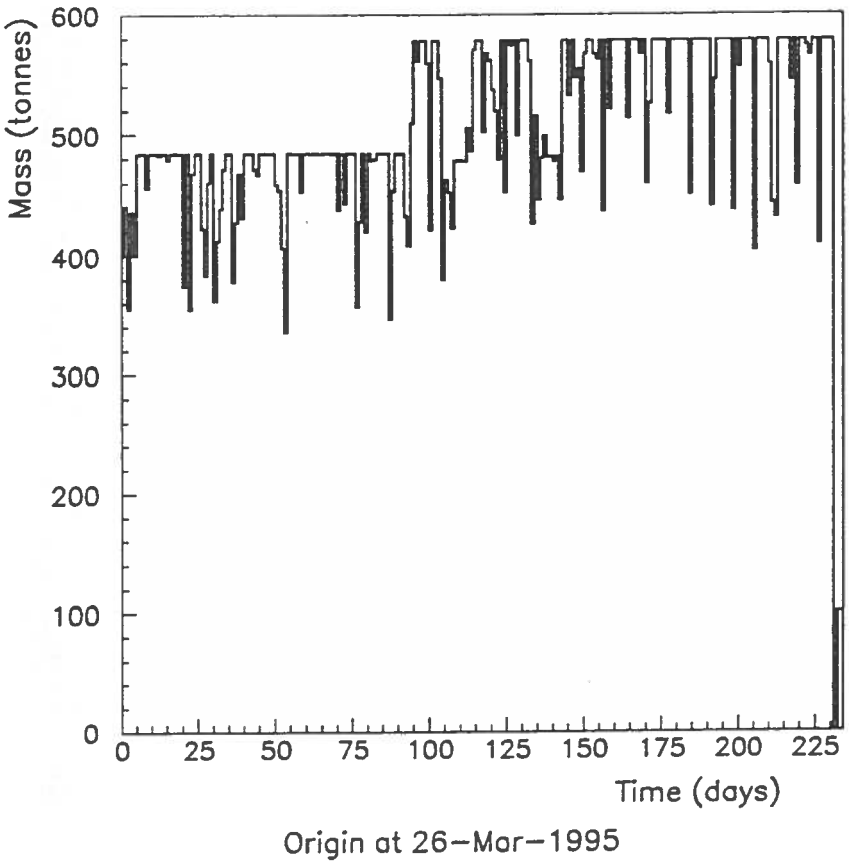

Figure 11: Active scintillator mass versus time.

3.5 Search for neutrinos from stellar collapses

A stellar gravitational collapse should result in the emission of a large number of 10-15 MeV electron antineutrinos in a burst of about 10 s duration. The antineutrinos may be observed in MACRO via their dominant reaction $\bar{\nu}_e + p \rightarrow n + e^+$ in the approximately 600 t of liquid scintillator. The trigger threshold is at about 7 MeV; if a trigger occurs, the threshold is lowered to 1 MeV for a duration of about 1 ms in order to be able to observe the gamma rays coming from the neutron capture (with an efficiency of about 25%). A supernova collapse at the center of our galaxy should yield about 110 antineutrino interactions with a positron with an energy larger than 10 MeV.

A redundant supernova alarm system is in operation alerting immediately MACRO physicists in different parts of the world. A procedure for alerting the physics and astrophysics community is under study.

Fig. 11 shows the liquid scintillator active mass for the study of neutrinos from stellar gravitational collapses during 1995; the live-time is larger than 95%.

No stellar collapse has occurred in our galaxy in the last few years.

4 Conclusions

The MACRO detector is now running in its final configuration. The collaboration continues to push monopole flux limits, has performed studies of interesting topics in cosmic ray physics, like the seasonal variations, the high energy composition and others. It has begun to study high energy neutrino physics and astrophysics and continued to search for neutrinos from stellar collapses. The completed detector should allow the achievements of all the MACRO goals.

MACRO publications and Conference Proceedings in 1995

1. MACRO Collaboration, M. Ambrosio et al. (Performance of the MACRO streamer tube system in the search for magnetic monopoles), LNGS 95/11 (1995), Astroparticle Physics 4 (1995) 33.
2. MACRO Collaboration, M. Ambrosio et al. (Vertical muon intensity measured with MACRO at the Gran Sasso Laboratory), Phys. Rev. D52 (1995) 3793.
3. MACRO Collaboration, M. Ambrosio et al. (Atmospheric neutrino flux measurements using upgoing muons), Phys. Lett. B357 (1995) 481.
4. MACRO Collaboration, M. Ambrosio et al., Paper presented at the January 1995 Tucson Monterey meeting:
   - Search for nuclearites with MACRO.
5. MACRO Collaboration, M. Ambrosio et al., Paper presented at the Rencontres de Physique de La Thuile:
   - Astrophysics with MACRO.
6. MACRO Collaboration, M. Ambrosio et al., Papers presented at the XXIV Int. Cosmic Ray Conf., Roma:
   - MACRO absolute muon flux measurement: comparison with Monte Carlo predictions, LNGS 95/41.
   - Muon astronomy and seasonal variations of the underground muon flux with MACRO, LNGS 95/42.
   - Sensitivity of MACRO to U.H.E. neutrinos, LNGS 95/43.
   - Study of the primary interactions with multiple muon events in MACRO, LNGS 95/44.
   - Search for fast magnetic monopoles with the MACRO scintillator system, LNGS 95/45.
   - Estimate of the primary cosmic ray composition from a multi-parametric fit of MACRO multimuon events, LNGS 95/46.
   - Upward-going muons in MACRO, LNGS 95/47.
   - Search for GUT monopoles with the MACRO streamer tube and track etch systems, LNGS 95/48.
   - Performance of the transition radiation detector in MACRO, LNGS 95/49.
7. EASTOP and MACRO Collaborations, Paper presented at the XXIV Int. Cosmic Ray Conf., Roma:

- Study of the primary cosmic ray composition in the PeV region with EASTOP and MACRO, LNGS 95/40.

8. MACRO Collaboration, M. Ambrosio et al., Papers presented at the European High En. Conf., Brussels:
   - Search for GUT monopoles with the MACRO detector;
   - Upward-going muons in the MACRO experiment.
9. MACRO Collaboration, M. Ambrosio et al., Papers presented at the TAUP-95 Workshop, Toledo:
   - Results from the EASTOP-MACRO Collaboration,
   - Multimuons;
   - H.E. Cosmic Ray composition;
   - Neutrino astronomy;
   - Search for magnetic monopoles with the MACRO detector.
10. MACRO Collaboration, M. Ambrosio et al., Dark matter Conf., Roma:
    - Search for magnetic monopoles with the MACRO detector.
11. MACRO Collaboration, M. Ambrosio et al., IV Convegno di Cosmologia, Frascati:
    - The MACRO experiment at Gran Sasso.
12. MACRO Collaboration, M. Ambrosio et al., LXXXI Meeting of the Italian Physical Society, Perugia.

STATUS OF THE BOREXINO PROJECT

R. Wordel
I.R.M.M. - EURATOM - Geel, BELGIUM

F. von Feilitzsch, T. Goldbrunner, T. Hagner, T. Hertrich, E. Kellner, G. Korschinek, L. Oberauer, J. Jochum, S. Schoenert
Technical Univ. of Munich, Garching, GERMANY

W. Hampel, G. Heusser, J. Kiko, T. Kirsteen, (E. Pernika), Y. Zakharov
Max-Plank-Institute f. Kernphysik, Heidelberg, GERMANY

L. Cser, D. Kiss, I. Manno, G. Marx, L. Tanko
Research Inst. for Particle & Nuclear Physics, Budapest, HUNGARY

C. Arpesella, M. Balata, M. Laubenstein, R. Tartaglia
Laboratori Nazionali del Gran Sasso, Assergi, ITALY

F. Gatti, G. Manuzio, G. Testera, S. Vitale
University and I.N.F.N. of Genova, ITALY

G. Alimonti, G. Bellini, S. Bonetti, L. Cadonati, C. Galbiati, M.G. Giammarchi, D. Giugni, A. Golubchikov, A. Goretti, F. Hartmann, A. Ianni, S. Magni, S. Malvezzi, I. Manno, E. Meroni, G. Ranucci, R. Scardaoni
University and I.N.F.N. of Milano, ITALY

G. Cecchet, A. De Bari, A. Perotti
University and I.N.F.N. of Pavia, ITALY

F. Elisei, F. Masetti, U. Mazzuccato
University and I.N.F.N. of Perugia, ITALY

O. Smirnov, O. Zaimidoroga
Joint Institute for Nuclear Research, Dubna, RUSSIA

P. Raghavan, R.S. Raghavan
AT&T Bell Laboratories, Murray Hill, NJ, U.S.A.

M. Deutsch, P. Fischer
Massachusetts Institute of Technology, Cambridge, U.S.A.

J. Benziger, F. Calaprice, M. Chen, N. Darnton, R. Eisenstein, M. Johnson, F. Loeser, R.B. Vogelaar, R. Parsells, R. Walls
Princeton University, U.S.A.

S. Pakvasa
University of Hawaii, Honolulu, U.S.A.

The Borexino experiment is a real time detector for low energy solar neutrinos. Its goal is to study the solar neutrinos from Be with high statistics. In order to study technical solutions and backgrounds a test is running in Gran Sasso since about one year. We discuss here the results obtained until now.

1. INTRODUCTION

The Borexino design consists of a transparent and spherical Inner Vessel, 8.5 m of diameter, filled with 300 tons of liquid scintillator, viewed by about 2000 PMT. The PMT's supporting structure is a stainless steel sealed sphere, 12.5 m of diameter, plonged in a water tank, 18 m of diameter, 18 m high. The scintillator is, most likely, Pseudocumene with PPO as fluor (with perhaps bis-MSB as shifter). The Buffer Liquid between the Inner Vessel and the phototube will be most likely pure PC and the water tank will be filled with purified water. An additional shiedling is provided by the definition of a fiducial volume of 100 tons, with a shielding scintillator thickness of 1.25 m.

Following this scheme the radiopurity levels needed for Borexino are listed in Table 1:

Table 1

Radiopurity levels needed for Borexino	
Stainless steel	~ 10^{-9} g/g
External water	~ 10^{-10} g/g
PMT	~ 10^{-10} g/g
Buffer liquid	~ 10^{-14} g/g
Inner Vessel	~ 10^{-12} g/g
Scintillator	~ 10^{-16} g/g

The expected background in the fiducial volume is ~11 counts/day, which has to be compared with a signal running from ~15 to ~60 events/day following various physics hypotheses (see G. Fiorentini, this Conference).

Taking into account the shielding design of Borexino we are concerned especially with the intrinsic background of the scintillator (the so called "Internal Background") because the other sources of background (constructing materials, surface contaminations, rocks: the so called "External Background") are shielded in order to depress the background to a negligible level. As a consequence the Borexino Collaboration has installed, in the Hall C of the Gran Sasso, a test (called Counting Test Facility - CTF) with the following goals:

- to serve as a bench mark for Borexino construction;
- to measure ^{14}C;
- to measure scintillator radiopurity;
- to check our background estimation.

2. THE COUNTING TEST FACILITY

It is a semplified Borexino detector with reduced sizes. It consists of a transparent vessel, 2 m of diameter, containing 4 tons of scintillator, viewed by 100 PMT. The PMT are supported by an open tubular structure, 6 m of diameter, plonged in an external water tank of 11 m of diameter, 10 m high.

The phototube are 8" THORN EMI 9351, developed by the Company in collaboration with us. The main characteristics are a transit time spread limited to σ=1 ns (important for a good spatial resolution) and a low after pulsing probability (2.5% - important for the α / β discrimination)

The PMT are coupled to light concentrators constructed with acrylic substrate, reflective silver layer, copper shield and acrylic paint, to resist against ultrapure water. The concentrator shape is a "truncated string cone", which has a good acceptance for the light within a solid angle corresponding to the Inner Vessel projection cone and a good probability to reflect back the light, if arriving from other directions. The coverage assured by the PMT's plus concentrators is ~20%.

The read out electronics consists of two parallel detection channels per each phototube, measuring the charge and time of firing of each of them, and correlated events within a window of 8 ms after the first event. The event pulse shapes are recorded through fast transient digitizers.

The Inner Vessel is a sphere of 500 μm thick nylon film, which has to resist to a buoyant force of 500 Kg, (due to the different densities of the internal scintillator and of the external water). The full constructing process, from the pellets and the extrusion phase up to the fabrication and installation, was done in clean rooms of various classes to avoid contaminated dust. But we did not succeeded to have a Rn free air and then to exclude possible surface contamination from implanted Rn daughters.

The scintillator used is a mixture of PC + 1.5 g/l of PPO. The measured photoelectron yield in CTF is 260 p.e./MeV and the attentuation lenght larger than 5 m. The photoelectron yield is larger than the expected design characteristics and this is probably due to the effect of absorption-reemission of the light by the fluor at very short range (10-20 cm). This effect can be studied properly only in a light collection having a spherical geometry as in CTF and it can be a potential source of a worsening of the spatial resolution.

The auxiliary plants of CTF are: the water purification and the scintillator purification systems.

The water purification system consists of a production line, to fill the water tank (1000 tons), and of a circulation loop to continuously maintain the good purification level of the water in the tank. The water plant consists of: reverse osmosis, deionization unit, ion exchange, ultrafilters, N stripping. The input water is the Gran Sasso water. In Table 2 the water contamination levels after and before the cleaning processes are shown.

Table 2
The purification levels of the water plant

	Gran Sasso water	from the Purif. Plant
U, Th	10^{-10} g/g	7×10^{-15} g/g
Knat	10^{-7} g/g	10^{-11} g/g
Rn	10 Bq/l	<8 μBq/l

The scintillator purification plants include: N stripping, water extraction and distillation. The purification plants run in the following way: the scintillator is taken out from the top of the Inner Vessel and is put again to the Inner Vessel from the bottom. Because the scintillator already purified through the plant with a continuous process is put back into the Inner Vessel, it is mixed with the scintillator not yet purified. This means that, when 4 tons are processed through one of the purification plant (1 cycle), the maximum purification factor which can be achieved is e=2.72.

The program followed during 1995 by CTF was the following:

- January 1995: filling of the water tank;
- January 1995: data taking run with only water, without scintillator;
- February 1995: filling of the Inner Vessel with 1 m^3 of scintillator;
- April 1995: filling of the I.V. with 4.5 m^3 (4 tons) of scintillator;
- June 1995: N sparging of the scintillator;
- July-August 1995: water extraction (3 cycles):
- October-November 1995: distillation (2 cycles);
- December 1995: increase of the Rn level of the external water of a factor 60 to study the penetration of the decay gamma's of the external Rn and daugthers in the scintillator;
- January-February 1996: calibration with Rn sources.

During this running time we found two serious obstacles.

The first was connected to a wrong operation which caused that 70 l of PC falled in the water of the external tank. The sealing of the PMT was studied to resist against the aggressive ultrapure water, but not to the chemical effects of the PC. As a consequence since July 1995 we had a sequence of PMT's failures. Now we are running with only 60 phototubes, but, due to the high photon yield of the scintillator, the resolution is still good.

The second problem was the relatively high Rn level in Nytrogen. The N is used for the purifications of the water and of the scintillator. For the water the N purity level cannot exceed ~1 mBq/m^3 of Rn; for the scintillator this contamination has to be lowered to ~1 μBq.

While for the water the Rn level fits our requirements, for the scintillator the N contamination is too high, even if we use a boil off system, which maintains the temperature of the N cryostat at ~-170 ^{o}C (the boiling points of N and Rn are -196 ^{o}C and -62 ^{o}C, respectively).

This contamination level is probably introduced into the N already in gaseous phase by the walls of the cryostat, which is a commercial vessel, not prepared following special cleanliness procedures.

3. BACKGROUND FROM THE WATER

The background due to the Chere ıkov light produced in the water by incident muons and gammas have been studied using the data of the run with only water.

The Cherenkov light produced by gammas are characterized by a very low energy detected in the scintillator and by a detection time spectrum of the first photoelectrons ranging within a very short interval.

The muon events, on the other hand, show a photoelectron time distribution characterized by a photoelectron bunch arriving about 30 ns later with respect to the main bunch. Infact the muon arriving from the top of the tank produces a light cone which is detected first by the phototubes installed at the bottom emisphere, but part of the light is reflected by the concentrators toward the upper emisphere, where it is detected by the PMT with ~30 ns of delay. By exploiting this time distribution and the asymmetry in the light detection between the upper and the lower PMT's emispheres, cuts are defined to reject the Cherenkov events of the water (the so called "standard cuts").

The events produced by gammas are fully rejected by the standard cuts, while ~100 muons/day survive. They produce pulses, which fall in the energy range 250-800 KeV (the so called "neutrino window": it is the detection energy range of Borexino). The efficiency in cutting the external muons has been evaluated by means a set of MWPC, installed at the top of the water tank and running in coincidence with the scintillator signals.

We have studied also the neutrons generated by interactions induced in the water by the muons. The neutrons, after a delay time of ~240 μsec, are captured by the hydrogen nuclei, generating 2.2 MeV gammas. A measurement done in CTF through 130 days shows that 1.2 delayed coincidences produced by neutrons are detected per day. All these events correspond to primary muon events rejected by the standard cuts.

4. RESOLUTIONS

The energy resolution in CTF has been checked using the α peaks of the ^{222}Rn and its daugthers (^{218}Po, ^{214}Po) and the ^{212}Po (daugther of ^{220}Rn). This was possible because few liters of air were injected into the scintillator by mistake during the filling phase and Rn was present in the scintillator during the purification periods due to the contamination level of the N (see paragraph 2)

The energy resolutions are summarized in Table 3:

Table 3
Energy resolution in CTF

E (KeV)	$\Delta E / E (1\sigma)$
200	18%
400	13%
600	10.5%
800	9%
1000	8%

The spatial reconstruction is complicated by three problems:

1- the probability density function (PDF), included in the reconstruction code, needs calibrations with sources. The PDF is the probability distribution of the time of the photoelectrons at the output of the constant fraction discriminators. It includes the effects of the scintillator decay time, of the trans't time jitter of the PMT's, of the discriminator. The calibration with sources is now in progress and presently we can quote only preliminar results on the spatial reconstruction. The decision to delay the calibration with sources was caused by the fear that the sources could contaminate the scintillator and the Inner Vessel.
2- Absorption and reemission of the photons by the scintillator. This effect, as explained in paragraph 2, can affect the spatial resolution.
3- Reflections of the light by the Inner Vessel walls, due to the different refraction indeces between the scintillator (n=1.505), and the water (n=1.33).

Preliminary results on the spatial resolution have been already obtained with a source placed on the center of the Inner Vessel. They are quoted in Table 4, but, of course, they do not include possible effects of reflection on the walls. If we compare the numbers of Table 4 with the expected design resolutions we have to conclude that the effects of the absorption and reemission by the scintillator are not very important.

Table 4

E(KeV)	x[σ-cm]	y	z
250-550	17	16	19
550-850	14	13	15
850-1500	12	11	13
1500 --->	12	10	13
825	13	12	15

5. RESULTS

The results obtained from the CTF data concern the contamination of the scintillator due to the ^{14}C, Th, U and contaminations introduced in the scintillator after the production synthesis by its handling (transport and store vessels, filling of the Inner Vessel, etc..).

5.1. ^{14}C

The contamination level due to the ^{14}C has been studied in the energy range 20-200 KeV. We measure the ^{14}C decay to ^{14}N via a β emission (Q=156 KeV; $T_{1/2}$=5730 y).

The β energy spectrum fits very well the simulated distribution in the range 50-200 KeV; below 50 Kev there is an additional contribution due to the Cherenkov light produced in the water by gammas. We have normalized the simulation spectra on the data in the energy interval 50-100 KeV and we have calculated the area below the curve. The results is:

$^{14}C/^{12}C=(1.2\pm0.01)\times10^{-18}$

This contamination level meets the Borexino design goal; on this basis we can evaluate that the contribution of ^{14}C to the background in Borexino is ~0.1 counts/day (threshold at 250 KeV).

5.2. Th

The contamination of Th in the scintillator has been measured by means of a delayed coincidence measuring the correlated events ^{212}Bi-^{212}Po. ^{212}Bi is a $\beta+\gamma$ emitter with an end point at 2.25 MeV; ^{212}Po is an α emitter with 8.785 MeV of energy, which taking into account the quenching factor in our scintillator, is reduced to 1060 KeV. The delay time of these correlated events is = 432.8 ns.

The Th contamination was measured during three periods: June 1995 (40 days)[1], September 1995 (20 days)[2], December 1995 (20 days)[3]. The results are shown in Table 5:

Table 5

Period	Th contamination
[1]	$2.5^{+1.3}_{-1.0}\times10^{-16}$ g/g
[2]	$2.3^{+1.9}_{-1.5}\times10^{-16}$ g/g
[3]	$2.7^{+2.2}_{-1.5}\times10^{-16}$ g/g

5.3. U

Before to quote the results of the U contamination I would like to recall that in the lower part of the U radioactive chain there is the ^{222}Rn (τ=5.48 days). Among its daugthers two short time correlated events: ^{214}Bi-^{214}Po (τ=236 μs) are present. ^{214}Bi is a $\beta+\gamma$ emitter (end point=3.2 MeV) and ^{214}Po is an α emitter (E=7.69 MeV quenched to 825 KeV).

This delayed coincidence is used to establish the U contamination level in the scintillator but it is produced also by the Rn introduced from outside, independently from the U chain. Because of the Rn contamination level of the N used for the scintillator sparging and for the other purification steps, we had to restrict the determination of the U contamination level to the periods when the presence of Rn in the scintillator was negligible. This was a period of 31 days.

We carried out one measurement during the full period and another one during the last 16 days of the same period. The results are shown in Table 6:

Table 6
U contamination level (g/g)

31 d	$4.8\pm3.5\times10^{-16}$
last 16 d	$4.2\pm4.0\times10^{-16}$

5.4. Further background

The sequence of the counting rates in the 250-800 KeV range of energy, (V window) can be summarized in the following way:

1-before any purification: 2200 counts/day;

2-after the N sparging and three cycles of water extraction this rate dropped down of ~800 counts/day. This decreasing can be attributed totally to the internal background, because the external water was not involved in any operation. About 250 counts/day concerned ^{85}Kr, which is present in the air and accompanied the Rn, when at the beginning few liters of air were injected in the scintillator.

The presence of ^{85}Kr has been measured through two correlated events: ^{85}Kr decays to a metastable state of ^{85}Rb with a β emission having an end point at 173 KeV; the metastable ^{85}Rb decays to the ground state emitting a 514 KeV γ with $\tau_{1/2}$=1 μs. This decay sequence through the metastable ^{85}Rb represents the 0.43% of the ^{85}Kr-^{85}Rb decay.

Before the N sparging we measured 1.3 ±0.3 delayed coincidence per day corresponding to ~300±70 counts/day for ^{85}Kr. After the stripping we measured 0.2±0.15 delayed coincidences per day corresponding to ~50±35 counts/day. This means that the N sparging reduced the Kr presence to a negligible level.

3-After the phase 2 we started up the water loop. This decision was triggered by the presence of PC in the water and by the growing up of the bacteria in the water. The start up of the water loop caused an increase of the total rate of ~700 counts/day. This increase has to be attributed totally to the external background because in the meantime no actions have been taken on the scintillator. The reason of this increase of the counting rate can be attributed to the following mechanism:

- the coating of the internal walls of the water tank is done with Permatex which, as measured in our laboratories, emits ~10 Bq of Rn in total;
- when the water is maintained quiet the emitted Rn remain close to the tank walls because the simple diffusion is quite slow;
- the water loop induces convective motions of the water which bring the water from regions near to the walls directly to regions close to the Inner Vessel.

As a consequence of this mechanism the Rn is distributed in different way in the external tank by the water loop increasing its density near to the Inner Vessel and then producing an increase of the total rate due to the external Rn gammas penetrating the Inner Vessel.

4-After two cycles of distillations the total rate was reduced of further ~300 counts/day. This decreasing is attributed to the internal background.

Presently the total rate is ~1800 counts/day.

In order to understand the sources of this background we can analyze the energy spectra and the radial distributions of the events.

The energy spectrum of the external background, dominated by the Rn in the water, was very well measure during the Rn test (see paragraph 2). This test was carried out by increasing of a factor 60 the Rn level in the external water: in this way the total counting rate was totally dominated by the external Rn.

By comparing this spectrum with the analogous one of the background we can extract the contribution of events which can be attributed to the internal background. To perform this comparison the two curves (external Rn and total background) have been normalized on the high energy tail (>1.2 MeV) which is typical of the events induced by the external background.

The difference between the two spectra leads to 350±60 events/d, 100 of them being due to muons surviving after the stardard cuts. These events are possible candidates to the internal background. The energy spectrum of these 250 events/d (once subtracted the muon contribution) shows a peak centered around the energy value of the ^{210}Po alpha's.

To find the ^{210}Po location we compare:

- the radial distribution of the external background (from the Rn test);
- the radial distribution of events omogeneously distributed in the Inner Vessel: this distribution was obtained by ^{214}Po, measured with the second electronic chain as second events of the delay coincidence ^{214}Bi-^{214}Po in the runs with an important Rn presence in the scintillator;
- radial distribution of the 1800 counts/d of our residual background

By this comparison we can conclude that the 250±60 events/d have a radial distribution very similar to the external background: then these events are most likely due to the contamination of the internal walls of the Inner Vessel. This contamination is probably due to the Rn daugthers implanted on the surface during the Inner Vessel fabrication.

This conclusion is still very preliminar. We plan to proceed with this analysis after a proper calibration with sources installed also near to the walls and in various space points within the Inner Vessel. In addition we want to increase the statistics in order to decrease the errors.

6. CONCLUSIONS

From the data collected in CTF during one year of running we can conclude that:

1- the radiopurity of the Borexino design goals for the materials and the external water has been achieved. Nevertheless a solution as carbon steel coated with Permatex is not ideal for the external tank; this tank will be constructed in Borexino with stainless steel.
2- The Th and U design contamination levels are essentially achieved.
3- The residual internal background due to the scintillator handling seems strongly depressed by the purification steps. The presence of external or surface backgrounds are not worrying because the shieldings in Borexino are definitely higher than in the CTF design (see Table 7):

Table 7
Comparison of the shielding sizes between CTF and Borexino
(1/2 m of shielding water corresponds to more than 1.2 order of magnitude in the reduction of the background)

	CTF (m)	Borexino (m)
scintillator buffer*	0	1.25
buffer liquid	2	2
water	8	10

* (due to the definition of a fiducial volume in Borexino)

The CTF schedule for the next few months include:

- optimization of the calibrations with Rn and ^{32}P sources;
- test with a scintillator mixture with a shifter as bis-MSB to study the absorption-reemission effect;
- test of a further purification method via a column containing silica or alumina gel;
- test with a new scintillator solvent: PXE. The main interest for this solvent is its density (~0.9901 g/cc) very close to the water. This will allow to use simple water as buffer liquid with reduced buoyant forces on the Inner Vessel. The PXE option could be an interesting possibility, but the use of pure PC as buffer liquid remains our first and most likely option.

ICARUS: a first 600-ton module at Gran Sasso Laboratory

The ICARUS Collaboration[1]

Abstract

As a first part of the experimental programme proposed by the ICARUS Collaboration, we aim to build a first 600-ton detector at Gran Sasso Laboratory within a time-scale of three years. This choice allows the fulfilment of two main goals: (1) the realization of an intermediate technical step between the 3-ton detector, operational at CERN for R&D purposes, and the final 5000-ton experiment, originally proposed in the ICARUS project, and (2) the beginning of a second-generation phase in neutrino physics and proton decay search.

1 Introduction

Since the initial ICARUS proposal and the subsequent update[2], intense activity in research and development has firmly established the technology of using ultrapure argon and the readout technique of ionization data (LAr-TPC) for very large sensitive mass detector.

Traditional bubble chambers have played a fundamental role in particle physics because they provide non-biased images in three dimensions and with high resolution. The ICARUS experiment represents a new generation of bubble chambers, with the advantage of being a fully electronic device operated over a very large sensitive volume, continuously sensitive, self-triggering, able to provide three-dimensional views of ionizing events with particle identification from $\mathrm{d}E/\mathrm{d}x$ and range measurements. At the same time, the detector acts as a good homogeneus calorimeter of very fine granularity and high accuracy. Therefore, this type of detector can be considered as an ideal device for rare event searches, such as proton decays and neutrino interactions.

The physics programme of the ICARUS project, requiring a sensitive mass of liquid argon of 5000 tons as described in Volume I of the ICARUS proposal [1], was submitted to the Gran Sasso Scientific Committee in early 1994.

We now consider that the best way to reach this sensitive mass needed to fulfil our scientific goals is to pass through an intermediate stage between the 3-ton detector, currently operating at CERN for R&D purposes, and the major engineering design described in Volume II of the ICARUS proposal [1]. This step-by-step strategy should allow us to develop progressively at the Gran Sasso Laboratory (1) the infrastructure needed to build and operate a large detector, (2) the in situ experience needed in terms of safety but with a still modest liquid argon volume, and (3) a definitive and practical evaluation of the engineering choice for the final phase. The most efficient and economical way to have a module of intermediate size in operation is to

[1]Aquila, Beijing, CERN, Dallas (UT), Frascati (INFN), Legnaro (INFN), Padova, Pavia, Pisa (INFN), Torino (ICGF-CNR), UCLA

[2] For more information on the ICARUS physics programme and detector characteristics, see the URL page: *http://www.aquila.infn.it/icarus*

build and test it outside the Laboratory and after move it inside the underground laboratory for the final assembly. This implies that the module has to be transportable. The size of the module is therefore limited by this requirement (about 600 tons). It also happened that an intermediate detector of this size would, at the same time, allow an important first step in the ICARUS scientific programme. In fact, this detector has a mass close to the Kamiokande detector mass, but the higher efficiency and the much more detailed information which can be collected for each event should rapidly allow us to reach definite conclusions about the phenomena to be studied. In particular, the ICARUS technique can provide a background-free detection of proton decay and neutrino events. While, as in the case of the final 5000-ton ICARUS detector, a sensitive mass in excess of a few thousand tons of liquid argon is suitable to achieve, in a number of proton decay channels, the 10^{34} years range in proton decay lifetime, many exotic channels have so far been poorly investigated (lifetime limits in the 10^{31} years range) or not investigated at all, and would easily be covered in this first phase with a 600 tons detector. Moreover, we could establish whether the anomalies observed by various experiments in the field of atmospheric and solar neutrinos are due to instrumental effects or are indeed genuine. Finally, this intermediate step opens, in addition, the possibility of exploring a new route towards larger detector volumes: the construction of a number of identical 600-ton detectors installed next to one another.

A proposal for a first 600-ton module [2] was submitted for funding in 1995 and has recently been approved.

A brief description of the detector and the physics programme which can be achieved with the first 600-ton module at Gran Sasso is given below.

2 The ICARUS 600-ton module

The operating principle of the ICARUS liquid argon TPC is rather simple [3]: any ionizing event (from particle decay or interaction) taking place in a volume of liquid argon, where a uniform electric field is applied, produces ion–electron pairs. A fraction of them, depending on the field intensity and on the density of ion pairs, will not recombine and will immediately start to drift parallel to the field in opposite directions. Only the motion of the much faster electrons induces a current on a number of parallel wire planes (the readout chambers) located at the end of the sensitive volume.

The choice of the liquid was driven by the following considerations: (a) it must be an excellent insulator and available at an extremely high purity level, so that free electrons produced by ionization can drift in the liquid over long distances; (b) it must have a high electron–ion pair yield with respect to the energy deposited in the liquid; (c) it must be easily available in large quantities, which is the case for argon, a natural component of the Earth's atmosphere ($\sim 1\%$).

The readout chamber scheme [4] consists of a focusing grid placed in front of the readout planes to allow both a squeezing of the electric field lines and a shielding of the readout part of the chamber from the sensitive-volume part. Information is read both by electric charge induction on the first readout plane encountered by drifting electrons and by electric charge collection on the second readout plane, whose wires are orthogonally placed with respect to

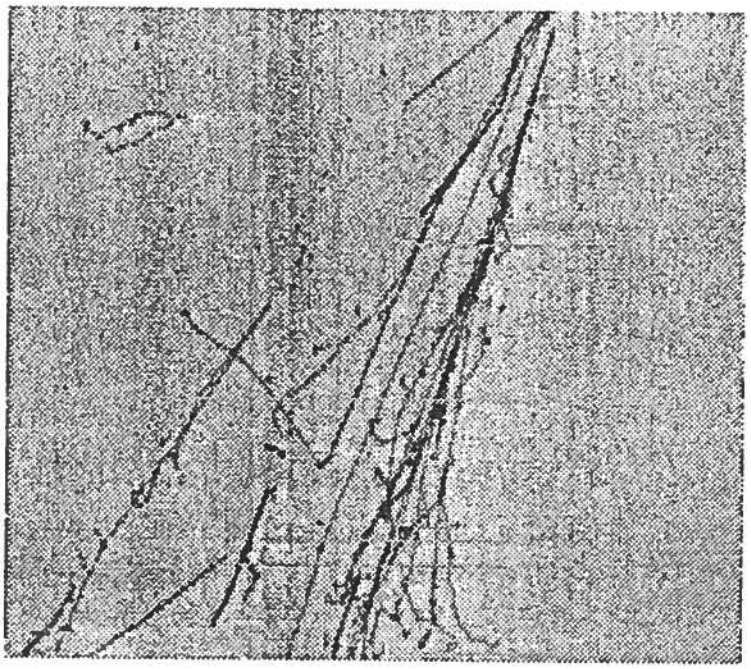

Figure 1: *Cosmic ray shower observed in the ICARUS 3-ton prototype at CERN. Each electron in the conversion pair visible at the upper left corner of the picture has about 5 MeV of energy and corresponds to the typical energy range of ^8B solar neutrinos in ICARUS. Also clearly visible near the centre of the figure is a $\pi^+ \rightarrow \mu^+(\nu_\mu) \rightarrow e^+(\nu_e\bar{\nu}_\mu)$ candidate as well as a clear electromagnetic shower.*

those of the induction plane. The signals from the two wire planes, together with measurement of the drift time, provide a full 3-D image reconstruction of the event. A typical cosmic ray event recorded by the 3-ton detector at CERN [4] is shown in Fig. 1.

The main feature of this type of chamber is that there is no charge amplification in the chamber so that the drifting electrons may induce signals on different wire planes. This requires high-quality electronics to maintain a good signal-over-noise ratio.

For the 600-ton detector [2], the liquid argon cryogenic container has been conceived in two stainless-steel, C-shaped semi-independent and symmetric halves giving a rectangular cross-section, whose individual dimensions of 3.9×4.2 m^2 and a length of 19 m, corresponding to a total internal volume of 465 m^3 and a total mass of 600 ton of liquid argon, are limited by the transportability on the highway network and inside the Gran Sasso Underground Laboratory. The two opposed C-halves will be connected, with walls in tight cool contact, in the final assembly at Gran Sasso underground site. A sketch of the ICARUS 600-ton module is shown in Fig. 2.

The readout chambers (two for each half-vessel) can be mounted on the internal walls with the cathode at the centre, to maximize the LAr sensitive volume (corresponding to about 540 ton in mass), see Fig. 2. The maximum drift length of the electrons produced by ionizing events is 1640 mm, equivalent to a maximum drift time of about 1 ms for standard electric

field conditions (at E $\simeq$ 300 V/cm the drift velocity is $v_d \simeq 1.6$ mm/μs). This requires ultrahigh-purity liquid argon to reduce electron capture by electronegative molecules diluted in the liquid, during the drift time. A contamination kept to around 0.1 ppb, corresponding to free-electron lifetimes in the range of several milliseconds, is routinely obtained by the purification system developed during the ICARUS R&D phase on the 3-ton prototype at CERN [5]. The same purification technique will be applied on an adequate scale with the 600-ton module. In order to improve the linearity of the detector response (correlation between collected charge and deposited energy) and to further reduce the charge lost by electron-ion recombination, the liquid argon will be doped with tetra-methyl-germanium (TMG), a photosensitive hydrocarbon able to convert part of the scintillation light from electron-ion recombination into additional free electron-ion pairs. This is particularly important for the particle identification capability of the detector. Feasibility and advantages of this doping technique have been established during the ICARUS R&D phase on the 3-ton prototype at CERN [6]

The wire pitch, in the readout chamber planes, is reduced to 3 mm, instead of the 5 mm foreseen for the 5000-ton module, in order to allow for higher precision measurements. The total number of electronic readout channels is 55 000. Alternatives to the wire planes in the readout chamber are under investigation: a multilayer printed board with orthogonal strips has been succesfully tested at CERN [7] and a hybrid with a printed board equipped with a wire plane in front, to add a third coordinate for redundancy, is also under test.

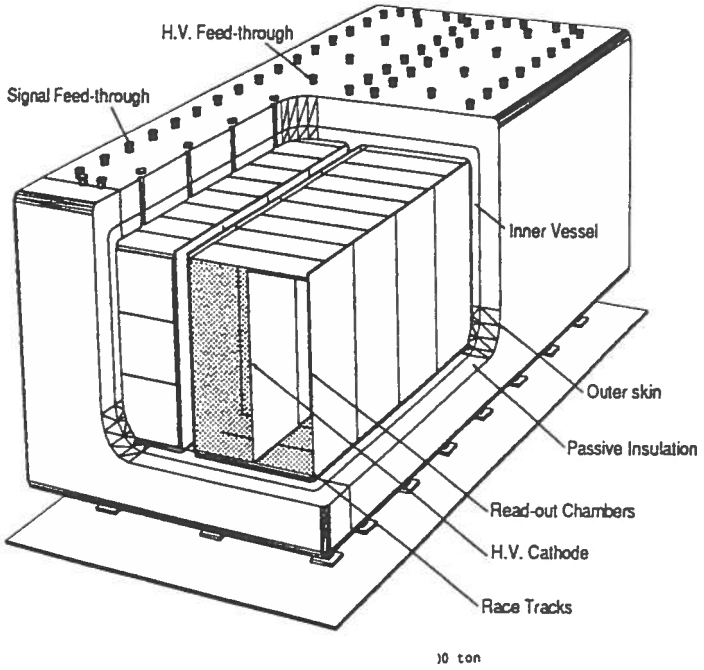

Figure 2: *The ICARUS 600-ton detector.*

We opted for a passive insulation of the dewar instead of the vacuum insulation that was

foreseen for the 5000-ton detector. Passive insulation has two main advantages over vacuum insulation: (1) it eliminates completely the risks coming from a vacuum breakdown, and (2) it allows for the internal cold vessel to be transported alone with an increase, for equal external dimensions, of the internal volume. The proposed solution for the external insulation foresees the use of modules of honeycomb structures flushed with nitrogen gas, see Fig. 2. These modules are transportable and easily assembled or disassembled.

A suitable neutron shield is foreseen around the entire volume, in order to reduce as much as possible the radioactive background. It should be made of a neutron-moderating medium (water or other hydrogenated material) and a thermal neutron absorber, or of a combination of both (polythene, borate polyurethane, etc.). The choice of the neutron shield characteristics will be defined after a dedicated test at the Gran Sasso Laboratory.

The final assembly of the external insulation and the construction of the neutron shield will be the only major work that will be performed inside the underground laboratory.

3 Atmospheric neutrinos

The atmospheric neutrino issue is currently considered one of the most burning questions in high-energy physics. Of the various studies performed by different experiments, the Kamiokande results are at present the most significant.

The overall analysis of the Kamiokande data [8] strengthens the neutrino oscillation hypothesis and yields allowed regions of the oscillation parameters for both the $\nu_\mu \leftrightarrow \nu_e$ and $\nu_\mu \rightarrow \nu_\tau$ channels, see Fig. 3. On the other hand, a recent study [9] of a possible underestimated neutron background from muon interactions in the surrounding rocks showed that the electron sample from Kamiokande and IMB experiments could be contaminated by π^0's from isolated neutrons faking the electron signature ($n + \mathrm{A} \rightarrow \pi^0 + \mathrm{X}$). Taking into account this extra background, the authors of Ref. [9] concluded that the atmospheric neutrino anomaly vanishes completely.

The size of the ICARUS module (600 ton) is comparable to the size of Kamiokande but the detector performance and the background level are substantially better. Therefore the ICARUS experiment at the Gran Sasso Laboratory (under a thick rock cover of 4200 metres of water equivalent) is ideally suited for performing the atmospheric neutrino study in a short time scale and with sufficient sensitivity to cover the present Kamiokande allowed regions in the neutrino oscillation parameter space.

Neutrino oscillation studies are usually performed by looking for possible deviations from the expected value in the observed neutrino interaction rate. The charged-current event rate, expected without oscillations, in one year, for a sensitive mass of 540 tons, is about 140 events, 80 from ν_μ and 60 from ν_e interactions. These rates correspond to the number of events with a vertex within this sensitive mass, regardless of whether the outgoing particles are contained or not.

Atmospheric neutrino interactions, with a mean neutrino energy of the order of a few hundred MeV, produce low-multiplicity events with a lepton (μ or e) accompanied by a nucleon (p or n) and possibly by one (or two) pion(s). The event occupancy in the liquid argon sensitive volume depends on the neutrino energy and on the final-state signature. A

fiducial volume ensuring the full event containment, inside the sensitive volume, has to be defined on a statistical basis from a Monte Carlo simulation. From a preliminary study we obtained an overall acceptance $\alpha = 72\%$, for fully contained events, to be applied to the sensitive volume of 540 tons. For the oscillation sensitivity study, we used the fully contained events data sample.

We performed separately the study of the sensitivity to oscillations in the $\nu_\mu \rightarrow \nu_\tau$ sector and in the $\nu_\mu \leftrightarrow \nu_e$ sector where upward-going neutrinos are subject to matter effects while crossing the Earth. For downward-going neutrinos crossing the Earth's atmosphere we assume vacuum oscillations.

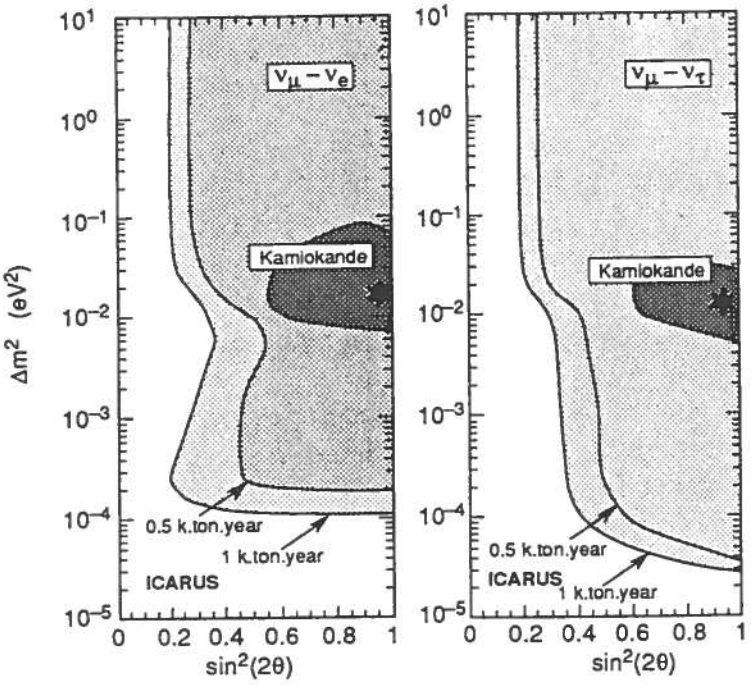

Figure 3: *ICARUS sensitivity (90% C.L.) to atmospheric neutrino oscillations. Allowed regions from the Kamiokande study are also shown.*

We considered the double ratio R defined as:

$$R = \frac{\rho_{\rm obs}}{\rho_{\rm exp}} \tag{1}$$

where $\rho_{\rm exp}$ is the ratio of the total number of $(\nu_\mu + \bar{\nu}_\mu)$ to $(\nu_e + \bar{\nu}_e)$ charged-current events (from neutrinos with energy larger than 200 MeV) expected in the case of no oscillations, integrating over both energy and zenith angle. The $\rho_{\rm obs}$ variable refers to the same quantity, observable in the detector.

The accessible region, in the $(\Delta m^2, \sin^2 2\theta)$ plane, is limited by the total error (σ_R) on the double ratio R. In this case, the main contribution to σ_R is from the statistical error (for one year of running, i.e. an exposure of about 0.5 kton $\times$ yr, $\sigma_R^{\rm stat}/R \sim 25\%$). The systematic

error ($\sigma_R^{\rm syst}/R \sim 5\%$) comes from theoretical uncertainties on fluxes and cross-sections, from the acceptance uncertainty, and from energy and angular resolution of the ICARUS detector. In Fig. 3 we report the results of the sensitivity study for both the $\nu_\mu \to \nu_\tau$ sector and the $\nu_\mu \to \nu_e$ sector.

We note that one year of exposure of the 600-ton ICARUS module to the atmospheric neutrino flux is sufficient to explore the oscillation parameter region indicated by Kamiokande for $\nu_\mu \to \nu_\tau$ and $\nu_\mu \leftrightarrow \nu_e$ oscillations [8].

4 Solar neutrinos

A clear difference from the programme we proposed with the 5000-ton module, is the fact that we put more emphasis on solar neutrinos, because the smaller size of the detector allows for higher resolution (3 mm of wire pitch) and lower background (external shielding). In any case, since the background (mainly from natural radioactivity) increases rapidly at low energy, there is a minimum threshold (about $4 \div 5$ MeV, depending on the shielding) below which electrons produced by solar neutrino interactions cannot be distinguished by other sources. Therefore the ICARUS device is sensitive only to the ^{8}B part of the solar spectrum ($E_\nu^{\rm max} = 14.5$ MeV).

The combined analysis [10] of the present solar neutrino data provides two possible MSW solutions, one 'non-adiabatic' ($\Delta m^2 = 6.2 \times 10^{-6}$ eV^2; $\sin^2(2\theta) = 6.8 \times 10^{-3}$), the other 'adiabatic' or large mixing angle solution ($\Delta m^2 = 9.7 \times 10^{-6}$ eV^2; $\sin^2(2\theta) = 0.62$). If the non-adiabatic MSW solution, which is the most natural one (small mixing) and also the one which best fits the present data, is relevant, then not only is the rate of ^{8}B neutrinos affected but the shape of the neutrino spectrum should be significantly distorted. Therefore, the ICARUS goal in the solar neutrino area is not only to confront the Standard Solar Model [11] (absolute event rate), but also to provide Solar Model independent measurements by observing various independent processes differently affected by possible oscillation.

4.1 *Neutrino scattering on electrons and absorption on argon*

ICARUS can detect solar neutrinos by observing the electron produced in the following two reactions:

(1) $\nu_x + {\rm e} \to \nu_x + {\rm e}$ which occurs with all types of neutrino flavours and for both charged-and neutral-current exchange;

(2) $\nu_{\rm e} + {\rm Ar} \to {\rm K}^* + {\rm e}$ which only occurs with the electron neutrino.

The measurement of the ratio of rates for these two processes provides directly a measurement of the ν_e oscillation probability.

In reaction (1) an isolated electron with energy above the ~ 5 MeV threshold is produced within 25° from the direction of the sun. The efficiency of this selection is 65%. Because 6% of these events also satisfy the selection criteria for the absorption channel, the overall efficiency is reduced to 61%. The angular and isolation cuts reduce the background by a factor 20, and the resulting signal expected in one year, in a fiducial mass of 540 ton, is given in Table 1.

Reaction (2) is expected to proceed through two main channels: (a) superallowed Fermi transition (F) to the 4.38 MeV excited isobaric analogue K* state; (b) Gamow–Teller transitions (GT) to the excited levels below the 4.38 MeV K* state. The two processes are distinguished by the energy and multiplicity of γ-ray emitted in the de-excitation of the K* states and by the energy spectrum of the primary electron. The corresponding rates are also reported in Table 1. In two years, assuming that statistical errors dominate, the experiment

Table 1: Signal, background and contaminations from the other reactions [events/year] in a fiducial mass of 540 ton, for the various channels used in the solar neutrino study. The neutron shield used corresponds to one metre of polythene with thermal neutron absorber.

Reaction	Signal	Background	Contamin.
$\nu_x + e$	290	13	18
$\nu_e + Ar$ (F)	330	3	68
$\nu_e + Ar$ (GT)	430	43	110

will be sensitive to relative variations of the ratio of elastic to Fermi absorption events larger than 12% (90% C.L.). The present two MSW solutions to the solar neutrino apparent deficit [10], correspond to an increase of this ratio of between 10 and 50% for the non-adiabatic solution and between 50 and 70% for the adiabatic solution. Therefore, in two years, if the adiabatic solution is the correct one, we will be able to give a definite confirmation of the solar neutrino oscillation hypothesis, or, if no evidence of oscillations is found, we will exclude the adiabatic solution and most of the non-adiabatic one.

4.2 *Neutrino scattering on deuterium*

We are evaluating [2] an additional and unique way to provide a Solar Model independent measurement, by measuring the shape of the ^{8}B solar neutrino energy spectrum. Considering the possibility of introducing a fraction (5% in mass) of deuterated methane (CD_4) in the liquid argon, this provides quasi-free neutron targets for neutrino interactions resulting in a scattering kinematics which does not suffer from important Fermi motion smearing:

(3) $\nu_e + D \rightarrow e^- + p + p$ ($Q_D = -1.44$ MeV). This reaction has an unambiguous signature, an isolated electron and two protons producing an intense ionization spot around the vertex. The cross-section is well known and increases approximately as E_ν^2.

We note that in the sun ^{8}B neutrinos are produced in the β-decay reaction: $^8B \rightarrow {}^8Be^* + e^+ + \nu_e$ ($Q_B \sim 14.5$ MeV) whose properties are also well known in terms of ordinary nuclear physics. In particular, the ν_e energy spectrum exhibits a linear behaviour in a standard Kurie plot representation.

We intend to reconstruct this Kurie plot by making use of the $\nu_e + D$ cross-section dependence on the neutrino energy. The interesting feature is that the neutrino energy can be

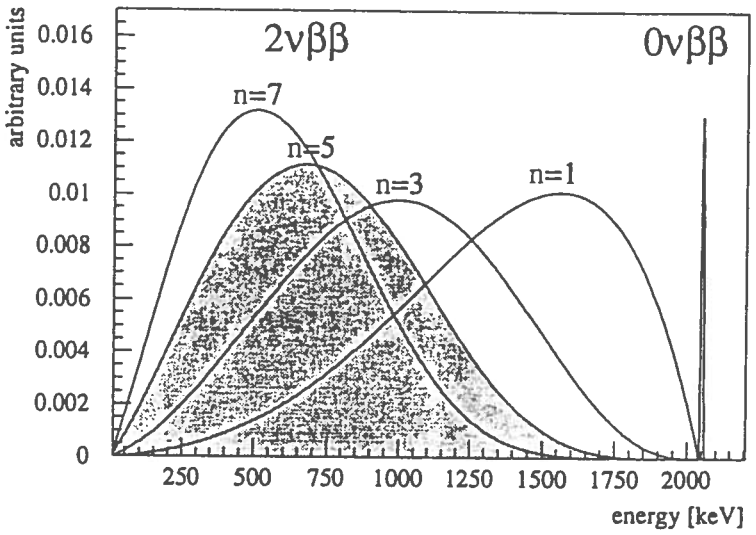

Figure 1: *Spectral shapes of the different investigated Double Beta Decay modes, the continuous spectra are classified by their spectral index n*

stringent limits on a non zero Majorana neutrino mass and right–handed weak currents (RHC). In $\beta\beta$–decay usually four decay modes are discussed[2]:

$$2\nu\beta\beta \;:\; {}^{Z}_{A}X \;\rightarrow\; {}^{Z+2}_{A}X + 2e^- + 2\bar{\nu}_e \qquad (1)$$

$$0\nu\beta\beta \;:\; {}^{Z}_{A}X \;\rightarrow\; {}^{Z+2}_{A}X + 2e^- \qquad (2)$$

$$0\nu\chi\beta\beta \;:\; {}^{Z}_{A}X \;\rightarrow\; {}^{Z+2}_{A}X + 2e^- + \chi \qquad (3)$$

$$0\nu 2\chi\beta\beta \;:\; {}^{Z}_{A}X \;\rightarrow\; {}^{Z+2}_{A}X + 2e^- + 2\chi \qquad (4)$$

Decay mode (1) can be understood as a process of second order Fermi theory, while the observation of the processes (2)–(4) would require physics beyond the standard model. In Fig.1 the experimental signatures of the different decay modes are shown for the isotope ^{76}Ge. In the case of the neutrinoless double beta decay (2) only the two electrons are present in the final state of the decay, resulting in a peak at the Q–value as the expected signal for detection. Since in all other decay modes additional particles are emitted, the expected continuous spectral shape of these decay modes is given by the phase space. To classify the different spectral shapes the spectral index n is used, which corresponds to the power in which the energy is included in the phase space integral. The spectral index of the $2\nu\beta\beta$ decay is n=5.

The observation of the neutrinoless double beta $0\nu\beta\beta$ decay (2) would require massive Majorana neutrinos or a contribution of RHCs or SUSY particles, leptoquarks etc., to the $0\nu\beta\beta$ amplitude. Up to now this decay mode was not

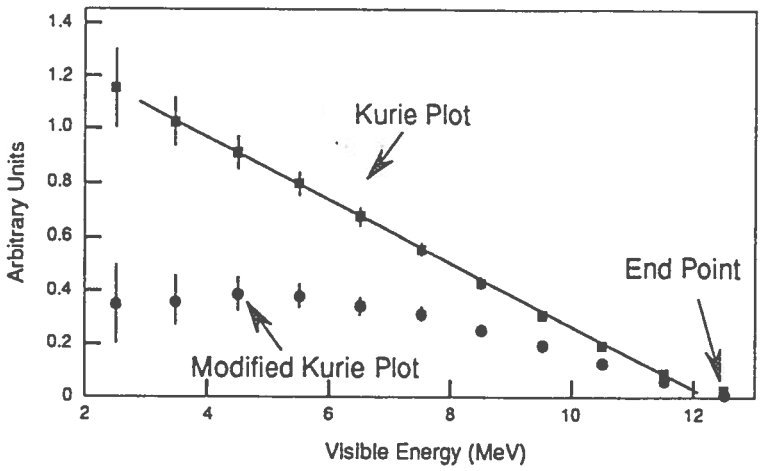

Figure 4: *Kurie plot (no oscillations) and modified Kurie plot with non-adiabatic hypothesis. Error bars correspond to statistical errors from one year of data.*

obtained from the total visible energy through $E_\nu = E_{\rm vis} - Q_D$ and that by measuring the end point of the visible energy spectrum in the Kurie plot ($\sim$ 12.5 MeV), evidence will be provided that the reaction producing these neutrinos is actually ^{8}B decay in the sun.

A rate of 590 events per year is expected for a CD_4 concentration of 5% in mass and for an electron kinetic energy threshold of 4.5 MeV. One can see that, applying this threshold, one collects more than 80% of all ^{8}B neutrino events.

If there is no neutrino oscillation the Kurie plot should follow the expected linear behaviour, while evident departure from the straight line could be found in case of MSW effect, as shown in Fig. 4. In particular for the non-adiabatic solution, it will take two to three years of data to distinguish the two shapes in an unambiguous way.

The deuterated methane experiment seems to be extremely promising, but it certainly represents a second phase application of the 600-ton detector and a detailed feasibility study of such a technique has first to be performed.

5 Proton decay

Even with a relatively low mass, the ICARUS 600-ton experiment can provide important contributions to the proton decay search, in particular for those decay modes (referred to as exotic decay modes) with high multiplicities (three or four particles in the final state) or, more generally, with signatures particularly difficult to identify with previously used detector techniques.

One example of such decay modes is $p \rightarrow e^+ n\ n$ which has been often emphasised because it can be interpreted [12] as the source of the excess electron-like events in the Kamiokande and IMB experiments. This type of event belongs to a class of decay modes with $\Delta B = -\Delta L$ which is one of the distinguishing features of SU(4)$^{\rm colour}$ Grand Unification Theories. This model was first proposed by J. Pati and A.Salam in 1973 [13]. Table 2 reports signal and

Table 2: List of a number of nucleon exotic decay modes with corresponding detection efficiency [%] (including the fiducial volume cut), present limits [$\times 10^{31}$yr] and expected rates [events/yr] in the 600-ton module corresponding to the present limits.

Decay Mode	Efficiency	Pres. Lim.	Events
$p \to e^- k^+ \pi^+$	0.36 (.9)	2.0	2.6
$p \to \mu^- k^+ \pi^+$	0.36 (.9)	0.5	10.5
$p \to \mu^+ k^0_S$	0.72 (.8)	6.4	1.7
$p \to \mu^+ k^0_L$	0.29 (.7)	4.4	1.0
$p \to e^- \pi^+ \pi^+$	0.12 (.9)	3.0	0.59
$p \to \bar{\nu} \pi^+$	0.36 (.85)	2.5	2.0
$p \to e^+ \nu\nu$	0.72 (.85)	1.1	9.6
$p \to \mu^+ \nu\nu$	0.68 (.8)	2.1	4.7
$n \to e^+ e^- \nu$	0.72 (.8)	7.4	1.8
$n \to e^- \pi^+$	0.30 (.75)	6.5	0.83
$n \to \mu^- \pi^+$	0.26 (.7)	4.9	0.91
$n \to \mu^- e^+ \nu$	0.54 (.6)	4.7	2.1
$n \to e^- k^+$	0.68 (.8)	3.2	3.8
$n \to \mu^- k^+$	0.64 (.75)	5.7	2.0
$n \to e^- e^+ e^- \pi^+$	0.36 (.9)	0.1	12
$n \to e^- e^+ e^- k^+$	0.81 (.9)	0.1	27
$n \to \mu^- e^+ e^- \pi^+$	0.36 (.9)	0.1	12
$n \to \mu^- e^+ e^- k^+$	0.81 (.9)	0.1	27

background rates expected for the 600-ton detector for some of the characteristic channels of the Pati–Salam model, assuming that the nucleon lifetime is at the current experimental limit.

The ICARUS technique is particularly well suited to identifying these decay modes, or any decay mode involving several charged particles in the final state. The detector techniques used so far, especially water Cherenkov detectors, do not allow the study of these decay modes in an exclusive mode, as can be argued from the relatively modest present limits. For most of these decays the background in ICARUS is expected to be negligible, hence one single event could be sufficient for discovery.

With the 600-ton module, in a few years, it will be possible to explore a lifetime region exceeding 10^{32} years for most of the channels reported in the above table, with a considerable improvement (a factor 5 to 100) of the present limits for the exotic channels. It is evident that with one single module we cannot reach the lifetime limit of 10^{34} years needed to test fully the minimal SUSY Grand Unification Theory. This is the final goal for the 5000-ton detector. Nevertheless, we will satisfy completely the requirement for the first phase of our programme,

namely to extend the present knowledge of nucleon stability over the widest possible range of decay modes to the same level as the currently best studied channels.

6 Long-baseline neutrinos

As part of the work for the CERN LHC project, injection transfer lines are being designed to bring fast extracted proton beams from the SPS to the LHC. With the planned SPS–LHC proton transfer line TL87, feasibility studies [14], [15], [16] have shown that it is technically possible to derive a neutrino beam pointing to Gran Sasso (GS) 732 km away in Italy, which happens to be in a favourable azimuthal direction with respect to this line. Proton accelerators provide essentially ν_μ beams from the decay of π's and K's produced when the extracted proton beam hits a target. These 'parent' particles are focused towards the detector and left to decay in a tunnel to produce muons and ν_μ's. The muons and all remaining hadrons are dumped at the end of the decay tunnel leaving only the neutrinos travelling towards the detector target. Recently, two independent studies [17], [18], based on detailed Monte Carlo simulations, have been performed to define possible geometries for a CERN neutrino beam set-up and to calculate the corresponding beam fluxes, beam contaminations, and the resulting event rates at Gran Sasso.

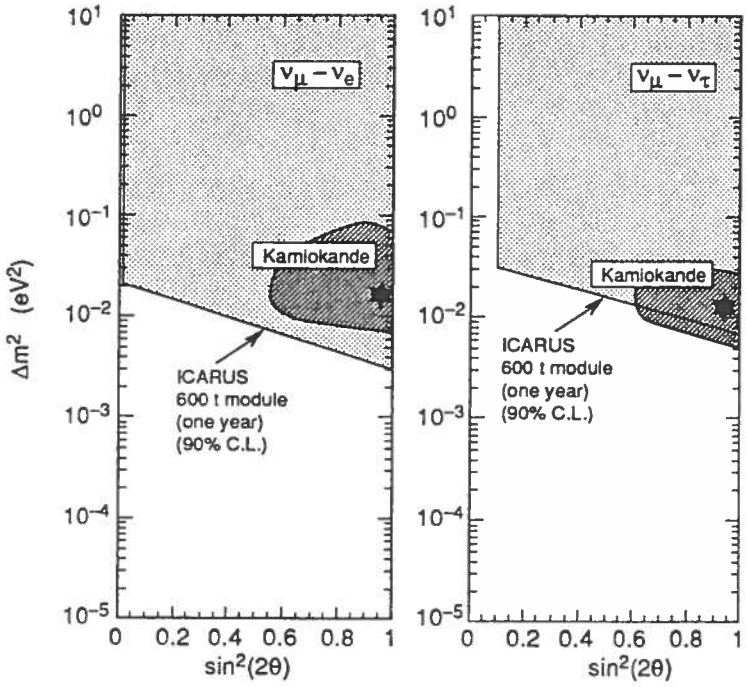

Figure 5: *ICARUS sensitivity (90% C.L.) to long-baseline neutrino oscillations. Allowed regions from the Kamiokande atmospheric neutrino study are also shown.*

The beam simulation studies have shown that the highest proton energy is preferable if one wants to maximize the number of events in the detector. According to Ref. [17] and

assuming that the beam can produce in one year 2×10^{19} 450 GeV protons from the CERN SPS, with a realistic focusing scheme for the secondary particles (very similar to the one currently working at CERN), we expect about 200 ν_μ charged-current events and 1.35 ν_e charged-current events in one year per 100 ton. The corresponding number of neutral-current events is 65. Since the mean energy of the charged-current events is around 25 GeV, then in order to allow for the complete containment of the hadronic component of the event within the detector sensitive volume, we have defined a mean fiducial volume of 350 ton for long-baseline neutrino interactions. It follows that the corresponding total rate is about 790 events per year.

Limits at 90% C.L. in the sensitivity to oscillations for one year (fiducial volume of 350 ton), and for two oscillation hypotheses are reported in Fig. 5.

These limits are based on statistical methods only. For $\nu_\mu \rightarrow \nu_e$, in one year, the sensitivity is sufficient to cover entirely the Kamiokande allowed region of the Δm^2 vs $\sin^2(2\theta)$ plane, see Fig. 5. For $\nu_\mu \rightarrow \nu_\tau$, in one year a good fraction of the region of interest is covered, in particular the best fit value, and in two to three years the region of interest would be entirely covered, Fig.5.

If it turns out that ICARUS confirms the existence of oscillations as indicated from the present studies of atmospheric neutrinos [8], it would be of great interest to use the long-baseline neutrino beam, which gives sensitivity to the same region in the oscillation parameter plane, but with a reduced systematic error since the main source of systematics is the ν_e contamination of the beam. In this case we could eventually tune the neutrino energy spectrum of the beam in order to enhance the sensitivity in the desired oscillation parameter region.

Conclusions

The construction of a first 600-ton ICARUS detector at the Gran Sasso Laboratory has recently been approved and funded.

With this module we aim to assess the technology of using ultrapure argon and the readout technique of ionization data on a large sensitive-mass detector scale.

This detector has a mass close to the Kamiokande detector mass, but the higher efficiency and the much more detailed information which can be collected for each event should rapidly allow us to address several of the fundamental issues of modern underground physics: the study of neutrino physics, with atmospheric neutrinos, solar neutrinos, and long-baseline neutrino beams from CERN can provide definite answers to the neutrino oscillation problem; the study of nucleon decay can allow us to access unexplored lifetime regions for some exotic channels considered in GUT's, with a considerable improvement on the present limits.

Finally, this experiment opens the possibility of exploring a new route towards larger detector volumes, as foreseen in the original ICARUS design: the construction of a number of identical 600-ton detectors installed next to one another.

References

[1] ICARUS Collaboration, "ICARUS II, a second-generation proton decay experiment and neutrino observatory at the Gran Sasso Laboratory," Proposal by the ICARUS Collaboration, *LNGS*-**94/99** Vol. I & II, (1994).

[2] ICARUS Collaboration, "A first 600-ton ICARUS detector installed at the Gran Sasso Laboratory," Addendum to Proposal, *LNGS*-**95/10**, (1995).

[3] C. Rubbia, *CERN-EP/***77-8**, (1977).

[4] ICARUS Collaboration, *NIM* **A332** (1993) 395. *NIM* **A345** (1994) 230.

[5] ICARUS Collaboration, *NIM* **A333** (1993) 567.

[6] ICARUS Collaboration, *NIM* **A355** (1995) 660.

[7] ICARUS Collaboration, *NIM* **A346** (1994) 550.

[8] Y. Fukuda et al., *Phys. Lett.* **B335** (1994) 237.

[9] O. Ryazhskaya, "Is there an excess of electron neutrinos in the flux in the atmosphere?," *JETP Lett.* **60** (1994) 617.

[10] N. Hata, "Solar Neutrinos: Hint for Neutrino Mass," *UPR 0612* **T/9420**, Proc. Solar Modeling Workshop, Institute of Nuclear Theory, U. of Washington, Seattle, March 24, 1994.

[11] J. N. Bahcall and M. H. Pinsonneault, *Rev. Mod. Phys.* **64** (1992) 885.

[12] W.A. Mann, T. Kafka and W. Leeson, *Phys. Lett.* **B291** (1992) 200.

[13] J.C. Pati and A. Salam, *Phys. Rev. Lett.* **31** (1973) 661.

[14] A.E. Ball et al., "CERN Beams for Long Baseline Neutrino Oscillation Experiments," *CERN-SL/***92-75** (BT), (1992).

[15] H. Wenninger et al., "Present and Future Neutrino Beams at CERN," *Nucl. Phys.* **B38** (Proc. Suppl.) (1995) 241.

[16] F. Cavanna, "The CERN–Gran Sasso long-baseline neutrino project," *CERN-PPE/***95–133** (1995).

[17] F. Pietropaolo, presented at the *"Gran Sasso Meeting on Long Baseline Neutrino Experiments,"* Gran Sasso, Dec. 1994.

[18] A.E. Ball, S. Katsanevas and N. Vassilopoulos, "Design Study for a Long Baseline Neutrino Beam," *CERN-ECP/***95–13** (1995).

A CRYOGENIC EXPERIMENT ON DOUBLE BETA DECAY AND SEARCH FOR RARE EVENTS

MEMBERS OF THE GROUP

A.Alessandrello, C.Brofferio, C.Cattadori, D.V.Camin, P.Caspani, O.Cremonesi, E.Fiorini, A.Giuliani, A. Nucciotti, P. Colling+, M.Pavan, G.Pessina, E.Previtali and L.Zanotti

Dipartimento di Fisica dell'Universita' di Milano e INFN, Sezione di Milano

C. Bucci
Laboratori Nazionali del Gran Sasso dell' INFN

+CEE fellowship at the University of Milano under Contract CHRX-CT93-0341,

Abstract

Further measurement on rare events have been performed with the two dilution refrigerators specially made with low radioactivity materials presently running in Hall A and C of the Laboratori Nazionali del Gran Sasso. New results on neutrinoless double beta decay of ^{130}Te have been obtained with an array of 4 TeO_2 crystals of 340 grams each. New and somewhat unexpected results have also been obtained on coherent interactions of WIMPS and on the very rare electron capture of ^{123}Te, perhaps the longest living isotope in nature apart the two neutrino double beta decay isotopes.

Measurements on the contaminations of various crystals of $CdWO_4$ and of TeO_2 from different producers and different producing methods have been performed in the dilution refrigerator of Hall C.

Improved measurements on the internal radioactivity of various samples of lead have been performed and a special shield has been constructed made with ancient Roman lead. It has already been installed in one of the Ge γ-rays spectrometers operating in the low background laboratory.

An array of 20 TeO_2 bolometers of which four with isotopically enriched tellurium , shielded with Roman lead, is in construction

1. Introduction

In the last year the Milano group , in collaboration with the Laboratori Nazionali del Gran Sasso, has continued its searches on rare decays using mainly the thermal detectors described in the previous report. An important improvement of our set-up in 1995 was the installation of a helium liquefier connected with the dilution refrigerator operating in hall A, in addition to the one already operating in Hall C. These liquefiers are essential to reduce the consume of liquid helium and to avoid that helium gas could produce damages in the photomultipliers of the nearby experiments. In addition a liquefier directly connected to each dilution refrigerator unables a much better stabilization of the operating temperature of the bolometer.

2. Present results

An important step in our experiment has been the construction of an array of four detectors of natural TeO_2 of approximately 340 grams each which is presently in operation in Hall A. In more than 3000 hours of effective running time we were able to improve by a factor of two our previous limit on neutrinoless double beta decay of ^{130}Te which has now reached 3×10^{22} years. We would like to add that this experiment , due to the particularly good performance of one of our detectors, has enabled to reach results on different subjects which we consider of interest:

a. we have investigated the low energy region of the spectrum obtained in about 1600 hours of effective running time of one of the detectors with a particularly good resolution and low energy threshold. In a detailed analysis we were able to find experimentally that the quenching factor , namely the ability to record the energy of a nuclear recoil induced by interactions of WIMPS (weakly interacting massive particles) is more that 0.93 in our detector. We could therefore set a limit on coherent interactions on dark matter which is the most stringent obtained so far with a thermal detector.

b. we have searched in the low energy region of the same spectrum for the peak corresponding to electron capture of ^{123}Te, one of the naturally occurring radioactive isotopes . We have found this decay , but with a rate of about 10^{19} years, about six orders of magnitude larger than reported in the literature. This is the longest living nucleus detected so far

apart the two neutrino double beta decaying isotopes. The rate for the decay of this second forbidden unique transition is being calculated by the Milan nuclear theory group.

c. a series of test measurements have been performed in the dilution refrigerator operating in Hall C in view of the future experiments with an enlarged array and with isotopically enriched TeO_2 crystals. We have first operated crystals surrounded by Teflon to investigate the possible alpha emitting contaminations coming from this material and found them to be negligible. We have then tested various crystals produced by our russian collegues, and crystals made as usual by the Shanghai Institute of Ceramics, but with different orientation of crystallization. While the former were not satisfatory , the second gave excellent results thus allowing us to study arrays with crystals with different orientations, which, for the same thermal performances, can be produced more easily and at a lower cost.

d. of extreme importance for our bolometric experiments, even if not performed with the thermal technique, is a series of measurements carried out with Ge γ-ray spectrometers operating in the Gran Sasso Low Radioactivity laboratory of various samples of lead to be chosen for the external shields and expecially of Roman lead. We were able to demonstrate that the radioactive contaminations of a large sample (26 kg) of Roman lead were the lowest ones ever found in lead and in fact in any shielding material (less than one hundred microbequerel/kilograms both for uranium and thorium). Using Roman lead we were then able to construct a Ge spectrometer with very low intrinsic radioactivity to be used for very sensitive measurements of contaminations.

3. The future

The future activity of our group in Gran Sasso will be mainly oriented toward four scientific aims:

a. **determination of the lifetime of two neutrino double beta decay of ^{130}Te.** This measurement is very important because this decay was never been found with direct methods and there are large disagreements in the results obtained with geochemical techniques.To this aim we had ordered to the Shanghai Institute of Ceramics two 340 gram crystals of $^{128}TeO_2$ and two similar crystals of $^{130}TeO_2$. These crystals should be provided to us in a few months and

operated contemporarily in our crystal array. The half lifetime for two neutrino double beta decay will be evaluated from the difference in the corresponding spectra. It will be in addition possible to determine directly the effect of crystalization in the reduction of radioactive contaminants and to perform a definite choice between arrays of natural or isotopic enriched crystals.

b. **improvement of the sensitivity in the measurement of neutrinoless double beta decay.** In order to achieve a better sensitiviy we are attempting to reduce the background by considerably inproving the external shielding adding ten tons of low radioactivity lead. In addition we have already constructed an internal shield made by very low radioactivity Roman placed inside the dilution refrigerator and immediately surrounding our detector array. We are presently constructing an array of 20 crystals to be shielded with Roman lead. The results will enable us to choose between a large array (100) of isotopically enriched crystals of an even larger (up to 1000) array of natural ones.

c. **Dark Matter.** Our experiment was admittedly optimized to search for the peak due to neutrinoless double beta decay in the upper part of the energy spectrum and not for enhancements of in the low energy region induced by interactions of WIMPS. The reduction of background and construction of a larger array will however allow us to considerably improve our present limit on coherent interaction of WIMPS. In addition the very large planned array of hundred crystals would allow a search for WIMPS based on the seasonal effect on the rate of interactions.

d. **Other double beta decay experiments.** Other candidates will be considered and tested for bolometric experiments on double beta decay. We are presently testing in Hall C for the first time in the literature a crystal of NdF_3, since ^{150}Nd could be the best candidate for a double beta decay experiment. The Kurchatov Institute has recently informed us that they were able to isotopically enrich Cadmium in ^{106}Cd and ^{116}Cd. These isotopes would be very promising to search for double beta capture and for double beta decay with crystals of $CdWO_4$ which we have already proved to work as bolometers.

REFERENCES

1. A. Alessandrello, E. Bellotti, C. Brofferio, D.V. Camin, C. Cattadori, O. Cremonesi, N. Ferrari, E. Fiorini, A. Giuliani, M. Pavan, G. Pessina, E. Previtali, and L. Zanotti, "A bromine cryogenic detector for solar and non solar neutrino spectroscopy", Astroparticle Physics 3 (1995) 239.

2. A. Alessandrello, C. Brofferio, O. Cremonesi, E. Garcia, A. Giuliani, A. Nucciotti, S. Parmeggiano, M. Pavan, G. Pessina, E. Previtali et al., "First tests on a large mass, low temperature array detector", Nucl. Instr. and Methods A360 (1995) 363.

3. A. Alessandrello, C. Brofferio, D.V. Camin, C. Cattadori, O. Cremonesi, E. Fiorini, A. Giuliani, A. Nucciotti, M. Pavan, G. Pessina, E. Previtali, L. Zanotti et al., "Thermal detectors for neutrino physics: results and developments", IV Int. Symp. on Weak and Electrom. Inter. in Nuclei, Japan 1995.

4. E. Fiorini, "Thermal detectors for neutrinos, dark matter and rare events", to be published on Nucl. Phys. B.

5. A. Alessandrello, C. Brofferio, O. Cremonesi, E. Garcia, A. Giuliani, A. Nucciotti, S. Parmeggiano, M. Pavan, G. Pessina, E. Previtali et al., "First tests on a large mass, low temperature array detector", Nucl. Instr. and Methods A360 (1995) 363.

Figure captions

Fig.1 The low energy spectrum . The peaks due to Te X-rays (27.4 keV). to ^{123}Te electron capture (30.5 keV) and to ^{210}Pb (46.6 keV) can be seen

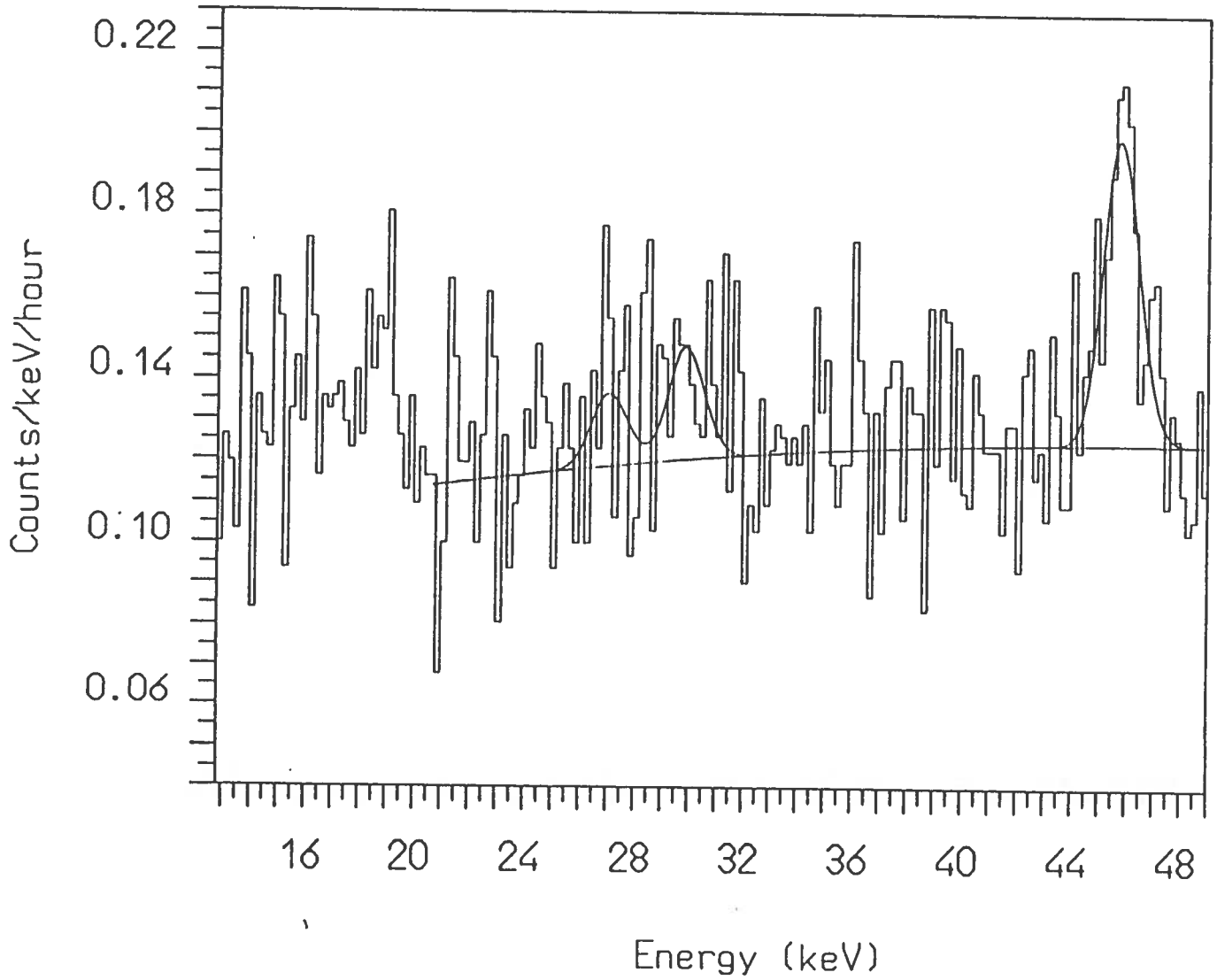
0.22
0.18
0.14
0.10
0.06
Counts/keV/hour
16
20
24
28
32
36
40
44
48
Energy (keV)

Fig. 1

The HEIDELBERG-MOSCOW $\beta\beta$ Experiment with ^{76}Ge: Full Setup

M. Günter, J. Hellmig, G. Heusser, M. Hirsch, C. Hoffmann, H.V. Klapdor -Kleingrothaus †, *B. Maier, H. Päs, F. Petry, Y. Ramachers, H. Strecker, M. Völlinger*
Max-Planck-Institut für Kernphysik, Heidelberg
A. Balysh, S.T. Belyaev †, *A. Gurov, D. Kotel'nikov, V.I. Lebedev*
Russian Science Center Kurchatov Institute, 123 182 Moscow, Russia
A. Müller
Istituto Nazionale di Fisica Nucleare, I-67010 Assergi, Italy
† *spokesmen of the collaboration*

Abstract

The final setup of the HEIDELBERG-MOSCOW double beta decay experiment went into operation this year. Out of 16.9 kg of 86% enriched ^{76}Ge five crystals were grown with a total mass of 11.51 kg. Since February 1995 all five detectors, corresponding to 10.96 kg active mass, are in regular operation in a common shielding in the Gran Sasso underground laboratory. Since no signal is seen for the neutrinoless double beta decay ($0\nu\beta\beta$), the measured data with a statistical significance of 15.05 kg·y results in a new half life limit of $T_{1/2}(0^+ \rightarrow 0^+) > 9.1 \cdot 10^{24}$y. This is the highest limit measured for any $\beta\beta$ decay so far. With this limit a Majorana mass of the neutrinos larger than 0.51 eV (90% C.L.) is excluded.
From the data taken in the previously operated setup with three enriched detectors in a common shielding and with a statistical significance of 10.58 kg·y new results are extracted for the two neutrino double beta decay ($2\nu\beta\beta$) of ^{76}Ge. After a quantitative description of the background the combined result is $T^{2\nu}_{1/2} = (1.77^{+0.01}_{-0.01}(stat)\,^{+0.13}_{-0.11}(syst)) \cdot 10^{21}\ y$.

Introduction

The interest in neutrino physics is constantly increasing, because of the fact that physics beyond the Standard Model of particle physics can be probed. Several indications like the solar ^7Be-neutrino problem and mixed dark matter models give hints on non-vanishing ν-masses like predicted in grand unification theories (GUT). All the indications could be for example explained in a SO(10) scenario with a S_4 horizontal symmetry implying a degenerate neutrino mass of 1–2 eV[1].
The mass region assumed in these models can be tested in second generation $\beta\beta$–experiments like the HEIDELBERG–MOSCOW experiment using large amounts of enriched $\beta\beta$-emitter material. These experiments investigate the nature of the neutrino (Majorana or Dirac particle) and give at present the most

observed. Therefore an upper limit for the effective Majorana neutrino mass can be deduced from the measured half life limit and calculated matrix elements [3]. The Majoron–accompanied neutrinoless double beta decays (3) and (4) as proposed in [4] will be discussed elsewhere in this yearbook [5], just like the impact of double beta decay on the restriction on SUSY parameters and left–right symmetric models [2].

Experiment

Overall there are 16.9 kg enriched Ge in the HEIDELBERG–MOSCOW experiment [7, 8, 9] available with an ^{76}Ge isotopic abundance of 86% compared to 7.8% in natural Ge. The experiment has three main advantages: the excellent energy resolution of the detectors, which favours the search for the expected $0\nu\beta\beta$ peak at 2038.56 ± 0.32 keV [10], the large size of the detectors, concentrating the background in the peaks, and the fact, that the source is equal to the detector, allowing large source strengths. The enrichment was measured for each crystal separately by accelerator mass spectroscopy at the MPI using residues from the crystal fabrication. Out of this raw material five p–type high–purity Ge semiconductor detectors have been built with a total mass of 11.51 kg. All five detectors are now in regular operation in the Gran Sasso underground laboratory, which provides a shielding of 3500 m.w.e. The sensitivity of this setup corresponds to an experiment with natural Ge of more than 1.2 t. The active mass of 10.96 kg is aquivalent to a source strength of 125.5 mol ^{76}Ge–nuclei, which is at present the biggest source strength of all double beta experiments.

Fig. 2 shows the combined sum spectrum of the HEIDELBERG–MOSCOW experiment with a statistical significance of 15.05 kg·y. Due to the large Peak–to–Compton ratio of the big detectors, external γ– activities are easily identified, shifting their background from the Compton–continuum into the peaks. The background identified immediately by the measured γ–lines in the background spectrum consists of:

1. primordial activities of the natural decay chains ^{238}U, ^{232}Th and ^{40}K
2. anthropogenic radio–nuclei, like ^{137}Cs
3. cosmogenic isotopes, produced by activation due to cosmic–rays

The activity of these sources in the setup is measured directly and can be located due to the measured and simulated relative peak intensities. Hidden in the continuous background are the contributions of:

4. the bremsstrahlungs–spectrum of ^{210}Bi (daughter of ^{210}Pb)
5. elastic and inelastic neutron scattering

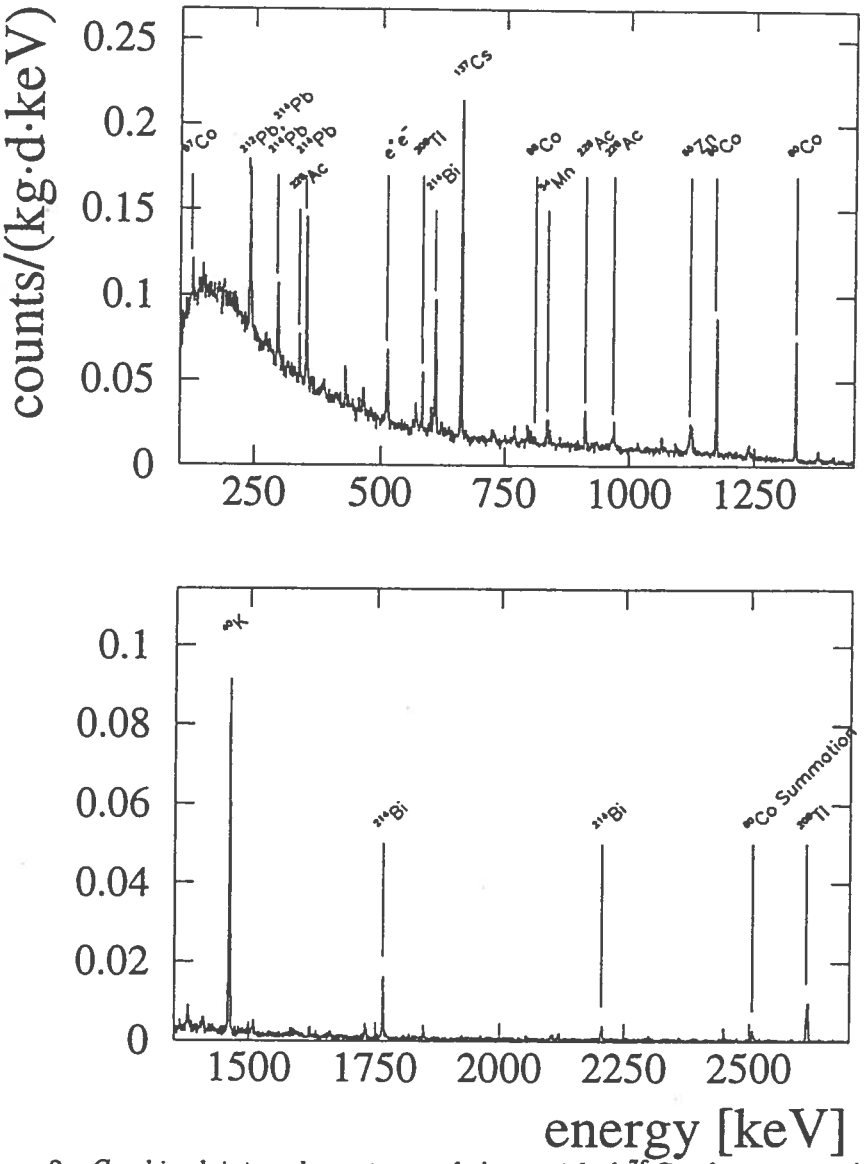

Figure 2: *Combined integral spectrum of the enriched ^{76}Ge-detectors with a statistical significance of 15.05 kg·y*

6. the primary reactions due to myons

Their impact on the background spectrum is determined indirectly in separate activity measurements and integral data evaluation. External α- and

β–activities are shielded by the inactive zone of the Ge–detectors on the outer layer of the crystal. Interpolation from the 10 strongest γ–lines in the background spectrum yields an energy resolution at the ground state transition of the $0\nu\beta\beta$ decay at 2038.56 keV of 3.54 $\pm$ 0.29 keV.

Since the $2\nu\beta\beta$ spectrum is superimposed to all the background components mentioned above, it is very important to understand the exact composition of the measured background in detail. Furtheron the signal–to–background ratio must be in the order of 1:1 for a clear and reliable signal detection. Fulfilling these requirements the background can be unfolded from the measured spectrum and the result will not be effected by the large uncertainties of unknown and unsure background components as in previous experiments[11].

Results

Neutrinoless $\beta\beta$ decay

The combined spectrum in Fig. 2 contains all the data taken, except the first 200 days of measurement with each detector. This initial data of each detector was removed [12], to avoid the implications of any short–lived radioactive impurities. No further cuts were applied. The effect of the first 200 days of data taking is clearly shown in Fig. 3.

The 3σ interval of a hypothetical $0\nu\beta\beta$ peak, determined with the extrapolated resolution stated before, contains 24 events in the combined spectrum with 15.05 kg·y. With the evaluated background left and right of this interval in a 30 keV range we expect in the peak region 27.3 $\pm$ 1.7 events. The achieved background between 2000 keV and 2080 keV is 0.209 $\pm$ 0.013 [counts/keV·y·kg]. Additionally the same region of the spectrum is shown for all data taken with 18.54 kg·y and the difference between these data with 3.49 kg·y.

The effect of the higher initial background activities results in a slightly higher background index and a structure at the decay energy [12]. This structure is dominating in the spectrum with 3.49 kg·y, where only the first 200 days of each detector were summed up, note the different scale of the background index. This shows that the former 'indication' of a $0\nu\beta\beta$ peak on a 2σ level in this experiment could be identified as short–lived background activities, since the real signal must be constant in time. At present we find no positive evidence for a signal of the $0\nu\beta\beta$–decay ($0^+ \rightarrow 0^+$–transition) at 2038.56 keV.

Since there is no signal present we extract a half life limit for the $0\nu\beta\beta$ decay using the method recommended by the Particle Data Group [13]. With the measured resolution and the measured background we can exclude 7.31 (4.03) events with 90% (68%) C.L., resulting in a half life limit with 90%C.L. (68%C.L.) of:

$$T_{1/2}^{0\nu} > 9.1(16) \cdot 10^{24}\, y \qquad (5)$$

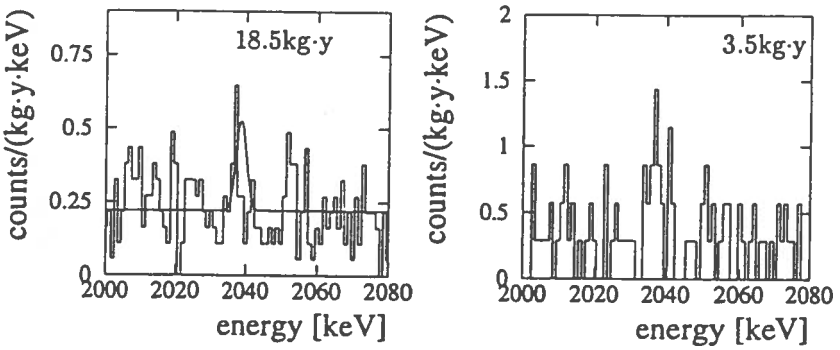

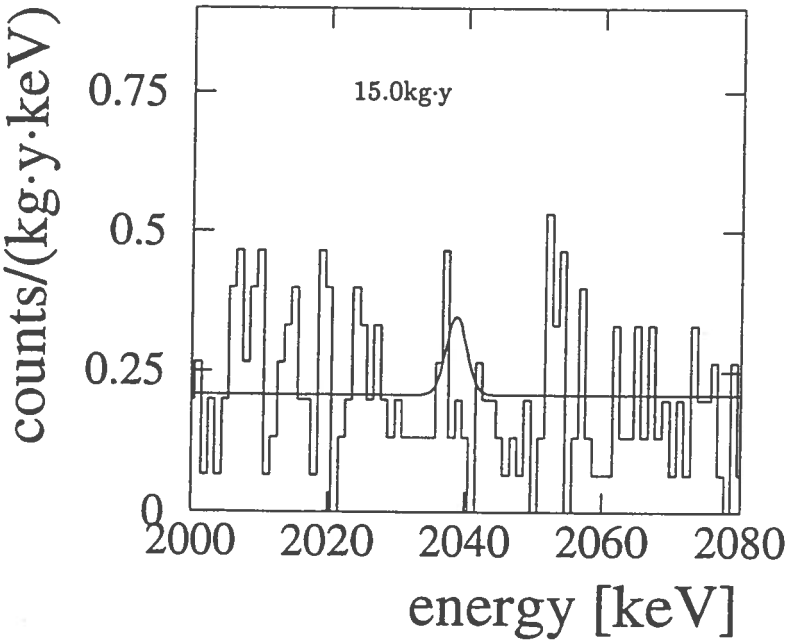

Figure 3: *Region of interest in the combined spectrum for a hypothetical $0\nu\beta\beta$ peak, the inserted curve corresponds to the excluded signal with $T^{0\nu}_{1/2} > 4.1 \cdot 10^{24}$ y (90% C.L.) for all 18.54 kg·y data taken and $T^{0\nu}_{1/2} > 9.1 \cdot 10^{24}$ y (90% C.L.) for 15.05 kg·y, respectively. The difference spectrum with 3.49 kg·y consists of the first 200 days of measurement of each detector.*

This lower half life limit is converted with the matrix elements [3] into an upper limit for the Majorana mass of the neutrinos, neglecting RHC's with 90%C.L. (68%C.L.):

$$\langle m_\nu \rangle < 0.51(0.38)\, eV \tag{6}$$

If RHC's are included in the evaluation we determine the following upper limits with 90%C.L. (68%C.L.):

$$\langle m_\nu \rangle < 0.60(0.45)\, eV \tag{7}$$
$$\langle \eta \rangle < 6.9(4.4) \cdot 10^{-9}\, eV \tag{8}$$
$$\langle \lambda \rangle < 0.9(0.70) \cdot 10^{-6}\, eV \tag{9}$$

$2\nu\beta\beta$ decay

For the evaluation of the $2\nu\beta\beta$ decay and various Majoron emitting decay modes a detailed knowledge of the composition of the experimental background is required. All measured continuous background sources have to be taken into account in the background model, which leaves after subtraction from the originally measured spectra the residual spectra with the spectral shapes searched for. The measured data of the setup with three enriched detectors in a common Pb–shielding between 9/1992 and 11/1994 is used to determine the background in detail and to achieve a more sophisticated understanding of the various background sources. The overall statistical significance of the detectors enr#1, enr#2 and enr#3 in this data acquisition period is 10.576 $kg \cdot y$.

To unfold the background a Monte–Carlo background model based on the CERN code GEANT3 was developed. The background model consists only of measured and clearly identified background activities. The measured activities in the setup are based on 47 identified γ–lines in the spectra of the three enriched detectors and two separate activity measurements of ^{40}K and ^{210}Pb in the LC2–Pb. A uniform distribution of the activities inside a certain volume/material is assumed in the Monte–Carlo–simulation. In principle the setup provides five major possible locations: LC2–Pb shielding, detector chamber, copper parts of the cryostats, plastic parts of the cryostats and the Ge-crystals itself. The interaction and influence between each of the detectors activities with the neighboring detectors is fully included in the background model. The simulated coincidence spectra in comparison to measured coincidence spectra show the good agreement of this approach to build a uniform background model for three detectors simultaneously.

The implemented geometry of the setups and detectors was intensively tested by comparing the results with measured spectra of calibrated sources in defined locations. Each detector was scanned with a collimated ^{133}Ba–source in axial

and radial direction. The deviation between simulation and measurement represents the error of the simulated detector response and is with 7.1% for enr#1, 5.1% for enr#2 and 7.1% for enr#3 valid for energies between 200 keV and 2700 keV.

The dominant background activity at energies below 500 keV is caused by ^{210}Pb contained in the inner LC2–Pb shielding, which contributes through the bremsstrahlung of its daughter ^{210}Bi (Q–value = 1.16 MeV). In this region almost half of the measured events are due to this contamination. The absolute activity with $0.36 \pm 0.03 Bq/kg$ was determined separately by low–level α–spectroscopy of the decay of the ^{210}Bi daughter ^{210}Po.

To include the natural decay chains of ^{238}U (14 γ–lines) and ^{232}Th (9 γ–lines) in the background model the peak intensities of the measured γ–lines are used. Under the assumption of radioactive equilibrium, checked by the constant peak counting rate in time, and a uniform distribution the location was determined by comparing the simulated and measured relative peak intensities. In the case of the ^{238}U decay–chain the detector chamber showed the best agreement, while for the ^{232}Th decay–chain it is more convenient to locate the activity in the copper cryostat of each detector. The possible error of the misplacement is included in the systematical error of the background model. A placement in the Ge–crystal could be ruled out by the absence of any α–lines in the high energy spectra.

During the minimized exposal to the cosmic radiation when the materials were above ground, the copper of the cryostat and the Ge–crystals were activated. In the measuring period the cosmogenic activities of ^{54}Mn, ^{57}Co, ^{58}Co, ^{60}Co and ^{65}Zn are identified through their characteristic γ–lines. Since most of the isotopes decay totally or partly by EC it is possible to distinguish between inner activities in the Ge-crystal (due to the shifted γ–lines with the energy of the deexcitation X–Ray) and outer activities in the copper (unshifted γ–lines). The measured peak intensities were used to normalize the simulated contributions to the background model.

The primordial ^{40}K–content in the LC2-Pb was determined by neutron activation and is in good agreement with the measured data of enr#1 and enr#2. A second ^{40}K-contamination is present in the copper of enr#3.

The anthropogenic activities of ^{137}Cs, ^{207}Bi, ^{125}Sb and ^{134}Cs as surface contaminations are located in the copper parts of the individual detectors. Due to their spectral shape the deviation of a closer or more distant placement affects the simulated detector response not very much.

The main contributions are ^{210}Pb at energies below 500 keV, the natural decay–chains, ^{40}K and ^{60}Co in the copper. To avoid statistical fluctuations in the low energy part the evaluation interval for the $2\nu\beta\beta$ decay was chosen to be 500–2040 keV covering 73.9% of the signal. In this way the subtraction of the background model from the original spectrum with rather large errors at energies below 500 keV does not effect the results on the $2\nu\beta\beta$ decay.

To account for the residual background due to neutrons, myons and not

directly identified background activities a phenomenological straight line is introduced. The slope and intercept is determined between 2.1 MeV and 2.8 MeV for each detector separately and is extended to lower energies. Overall the contribution of this background line is 2.8% of the measured events.

The bin–width of the spectra was chosen to be 20 keV per channel in order to avoid statistical fluctuations when subtracting simulated γ–lines from the measured spectra. The resulting spectra as the difference of measured and background spectra contain only the $2\nu\beta\beta$ signal with a signal–to–background ratio in the evaluation interval of 1:1.7 for enr#1, 1:1.4 for enr#2 and 1:1.8 for enr#3. These ratios are slightly lower than in [8], because the peaks with a significant fraction of counts are included in this former evaluation.

The result of a Maximum–Likelihood–Fit of the data and the theoretically expected $2\nu\beta\beta$ spectrum results in the following half lives for the three enriched detectors with 68% C.L.:

$$T^{2\nu}_{1/2} = (1.62^{+0.03}_{-0.03}(stat)\,^{+0.18}_{-0.14}(norm)$$

$$^{+0.07}_{-0.06}(syst)\,^{+0.13}_{-0.11}(sim)\,) \cdot 10^{21}\,y \qquad (10)$$

$$T^{2\nu}_{1/2} = (1.91^{+0.02}_{-0.02}(stat)\,^{+0.12}_{-0.10}(norm)$$

$$^{+0.12}_{-0.10}(syst)\,^{+0.12}_{-0.10}(sim)\,) \cdot 10^{21}\,y \qquad (11)$$

$$T^{2\nu}_{1/2} = (1.69^{+0.02}_{-0.02}(stat)\,^{+0.17}_{-0.14}(norm)$$

$$^{+0.10}_{-0.08}(syst)\,^{+0.13}_{-0.10}(sim)\,) \cdot 10^{21}\,y \qquad (12)$$

The result for enr#2 is shown in Fig.4.

The presence of isotopes like ^{60}Co in the crystals, ^{68}Ge,^{77}Ge,^{90}Sr and ^{234m}Pa, which could in principle influence or even simulate the $2\nu\beta\beta$ signal [8], are excluded by the spectral shape and endpoint of their continuous spectra [14]. The expected constant integral counting rate in the evaluation interval for the resulting spectra after background subtraction was tested and confirmed for 20 time points during the simulated measuring period, too [14]. The overall result for three detectors with the uniform background model, with 68% C.L. is:

$$T^{2\nu}_{1/2} = (1.77^{+0.01}_{-0.01}(stat)\,^{+0.13}_{-0.11}(syst)\,) \cdot 10^{21}\,y \qquad (13)$$

For comparison two former results for the $2\nu\beta\beta$ decay are shown in Fig. 4, too. The obtained result is slightly higher than in [8] with $(1.42^{+0.13}_{-0.13}) \cdot 10^{21}y$, because the interaction of the detectors between each other was not taken into account in this earlier result of the HEIDELBERG–MOSCOW experiment. The

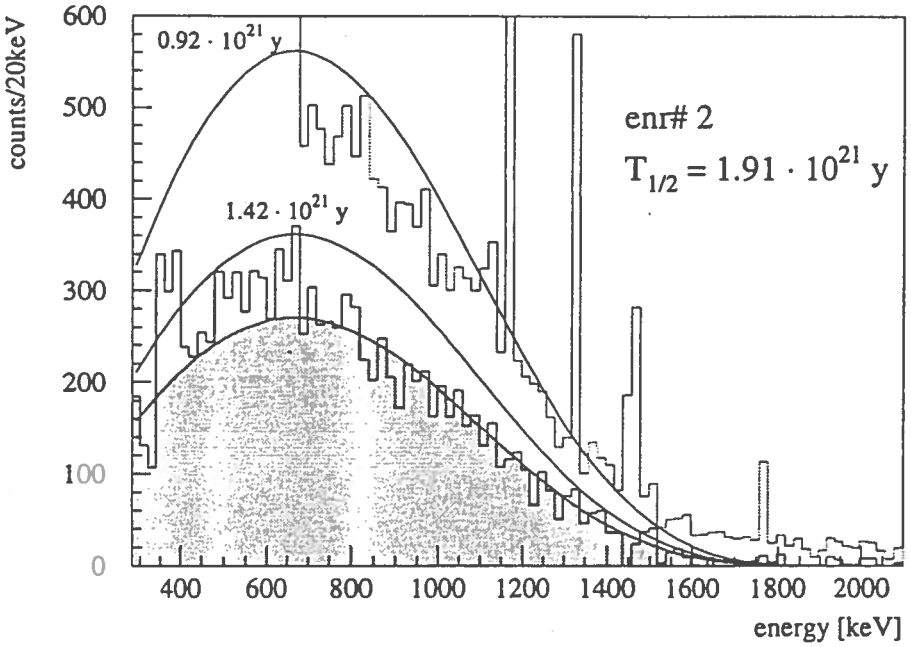

Figure 4: *Result for the evaluation of the $2\nu\beta\beta$ decay of ^{76}Ge in enr#2: original spectrum (dotted line), residual spectrum after subtraction of background model (solid line) and fitted $2\nu\beta\beta$ spectrum (shaded area and for comparison two former $2\nu\beta\beta$ results)*

curve with $0.92^{+0.07}_{-0.04} \cdot 10^{21}y$ from [11], which was corrected to $(1.2^{+0.2}_{-0.1}) \cdot 10^{21}y$ in [15] is still deviating significantly from the result presented here, because the background assumptions made in this experiment were incomplete.

The experiment reached with 21115 $2\nu\beta\beta$–events in the evaluation interval 500–2040 keV the highest statistics of all all $\beta\beta$–experiments for the direct detection of the $2\nu\beta\beta$ decay mode. With a detailed understanding of all major background components the evaluation is not dependent on any cuts applied to the measured data, like it is done in other experiments. Actually the raw data is used for a full background consideration.

Future

The HEIDELBERG-MOSCOW experiment is now exploring the sub-eV range for the mass of the neutrinos. With five enriched detectors with a total mass of 11.51 kg operated in the GRAN SASSO underground laboratory the experiment has reached its full setup. The experiment will probe within five years the neutrino mass down to $\sim$ 0.2 eV. It is obvious that the HEIDELBERG-MOSCOW

experiment will give the sharpest limit for the electron neutrino mass at least till the end of the decade. For further improvements beyond the region of < 0.1 eV one has to think of *very large* experiments with *much bigger* source strength.

References

[1] D.G. Lee, R.N. Mohapatra, Phys. Lett. **B 329** (1994) 463

[2] H.V. Klapdor–Kleingrothaus, Prog. Part. Nucl. Phys. **32** (1994) 261

[3] A. Staudt, K. Muto, and H.V. Klapdor-Kleingrothaus, Europhys. Lett. **13** (1990) 31.

[4] C.P. Burgess and J.M. Cline, Phys. Rev. **D 49** (1994) 5925 and these proceedings

[5] H. Päs in this yearbook

[6] M. Hirsch in this yearbook

[7] M. Beck et al. (HEIDELBERG–MOSCOW Collaboration), Phys. Rev. Lett. **70** (1993) 2853

[8] A. Balysh et al. (HEIDELBERG–MOSCOW Collaboration), Phys. Lett. B **322** (1994) 176–181

[9] M. Beck et al. (HEIDELBERG–MOSCOW Collaboration), Phys. Lett. B **336** (1994) 141–146

[10] J.G. Hykawy et al., Phys. Rev. Lett. **67** (1991) 1708

[11] F.T. Avignone et al., J. Phys. **G 17** (1991) 181

[12] J. Hellmig, Master thesis, University of Heidelberg, 1994

[13] PDG (Particle data group), J.J. Hernández et al., Phys. Lett. **B 239** (1990)

[14] B. Maier, Ph.D. thesis, University of Heidelberg, 1995

[15] F.T. Avignone et al., Prog. Part. Nucl. Phys. **32** (1994) 223

[16] F. Petry, Ph.D. thesis, University of Heidelberg, 1995

Background identification by digital pulse shape analysis

Abstract

Our work concerning digital pulse shape analysis consisted of two steps. A setup of two customary HP-germanium detectors was used to collect samples of pulses with different energies and well defined specifications. Those libraries were the basis for the development of a new approach to distinguish between pointlike and multiple scattered events inside germanium detectors. The new method was tested first in the low-level laboratory in Heidelberg. Than it was applied to one detector of the HEIDELBERG–MOSCOW $\beta\beta$ experiment. It was found that by identifying the multiple scattered events the background in the $0\nu\beta\beta$ region can be reduced by a factor of 5–7.

Introduction

Pulse shapes of particle interaction inside germanium detectors depend on the particle type and its energy. γ–rays from a radioactive source deposit their energy by Compton scattering and photo–absorption. The energy dependence of the fraction of multiple to single interaction is known very well [1]. Although the interactions take place in a very short time distance the different interactions can be seen because of the drift velocities of $8.5{\cdot}10^7 mm/s$ of the electrons and holes in germanium.

For a γ–line with an energy in the range from 300 keV to 3 MeV multiple Compton scattering is the dominating process. On the other hand the scattering length of electrons inside a germanium detector is about 0.8mm [3]. So electrons appear with a pointlike pulse shape.

Generation of single and multiple site events

Events with a single interaction at a defined radius and horizontal position inside a germanium detector were generated [4] by collimating the γ–rays of a source (see Fig. 5). An additional ring collimator between the pulse shape detector which is connected to a LeCroy transient recorder and the coincidence detector is used to select those events which are Compton scattered inside the pulse shape detector at the radius of the collimator ring. By setting energy windows according to the compton scattering formula with the scattering angle between the direction from the source to the pulse shape detector and the direction from the pulse shape detector to the coincidence detector single scattered events at a given horizontal position and radius can be recorded. Multiple site events are recorded by setting the energy window of the pulse shape detector to the energy of a line of a γ source.

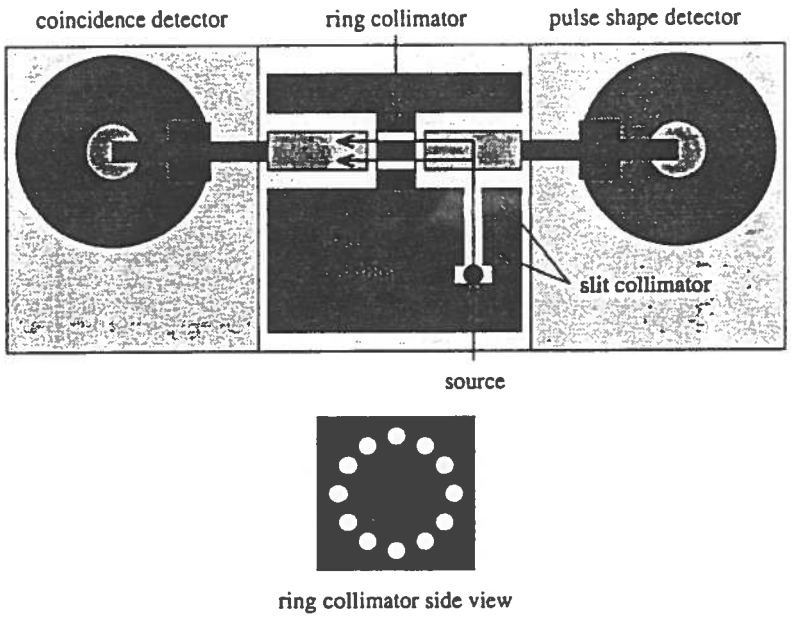

Figure 5: Setup used for generation of single and multiple site events

The pulses were collected into librarys to study the dependencies on the energy, horizontal and radial position for single and multiple site events. From this a phenomenological method was developed to distinguish between pointlike and other events. This method is based on criteria working on parameter mainly calculated from the second derivative of the pulses. For details see [5].

Pulse shape analysis with large crystals

The method was tested with one enriched detector ENR#5 of 2.666 kg active mass. This detector was built in end of 1994 in Heidelberg with an optimized electronic for pulse shape analysis. It could be shown by [5] that pulse shape analysis can be done very efficiently with such detector. In Fig. 6 a spectrum of the background radioactivity inside the low–level laboratory measured with this detector is shown. The filled spectrum is the residual SSE spectrum after the pulse shape discrimination.

Application to double beta experiments

The HEIDELBERG–MOSCOW experiment [6] uses five HP-Ge detectors enriched to 86% with the double beta emitter ^{76}Ge. The double beta decays are traced by the two emitted electrons. The pulse shape of such an event would

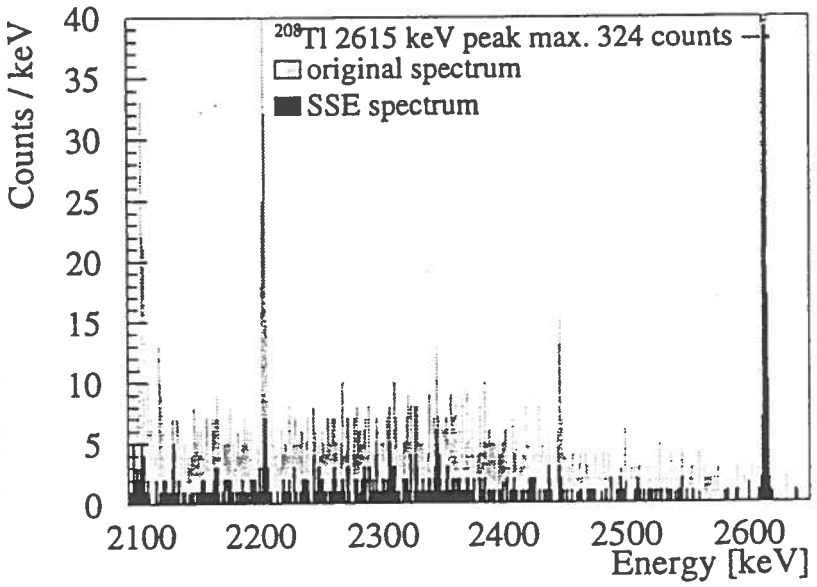

Figure 6: SSE and original spectrum of a background measurement in the low–level laboratory with ENR#5.

be a single site event. Identification of multiple site events among the data can be used to reduce the background of the double beta decay measurement.

In spectra measured in the low level laboratory at Heidelberg the background was reduced by a factor of 4.6 in the energy interval from 2000 keV to 2080 keV see Fig. 6.

The detector was installed later inside the low level shielding in the Gran Sasso laboratory and pulse shapes were recorded since February 1995. After 155.98 kg·days of measurement the background in the energy region from 2000 keV to 2080 keV is 0.4 counts/keV·kg·y for all data and 0.06 counts/keV·kg·y for the single site events (see Fig. 7). This reduction factor of 7.5 is preliminary because of the poor statistics. One single site event remains in the lower part of Fig. 7 right at the decay energy of 2038.58 keV.

In November 1995 the data acquisition system of the HEIDELBERG–MOSCOW experiment was replaced by a VME based system with eight 250 MHz FADC's [7]. With this system pulse shape recording of four detectors now has been started.

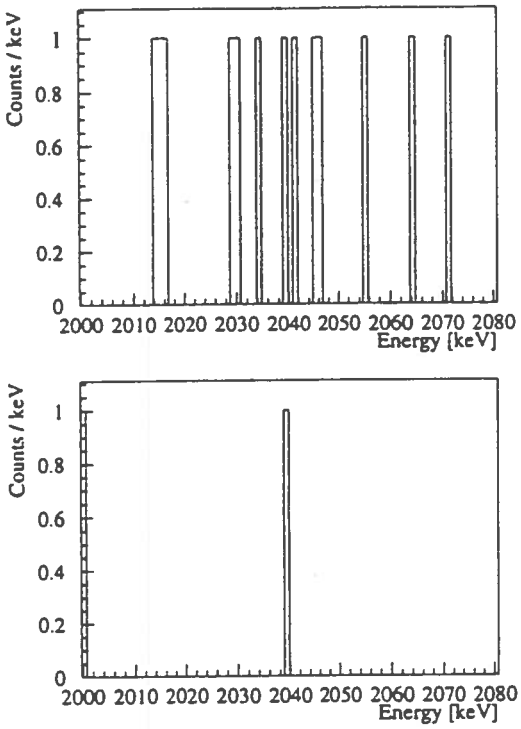

Figure 7: Spectrum with 155.98 kg·days measured at the Gran Sasso laboratory; top: multiple site events; bottom: single site events

Summary

Digital pulse shape analysis has been used for the first time in analysis of the enriched germanium detectors of the HEIDELBERG–MOSCOW $\beta\beta$ experiment. Pulse shape recording has been successfully started in the end of 1995 with for alltogether four detectors of the experiment.

References

[1] J. Roth, et al. IEEE Trans. Nucl. Sci **NS-31** (1984) no. 1 367

[2] G. Ottaviani, C. Canali and A. Alberigi Quaranta, IEEE Trans. on Nucl. Sci. **22** (1975) 192-204

[3] Mukoyama et al., NIM **134** (1976) 125

[4] F. Petry et al., NIM A **332** (1993) 107-112

[5] F. Petry, Ph. D. Thesis, Heidelberg 1995

[6] HEIDELBERG–MOSCOW Collaboration, Phys. Lett. **B 356** (1995) 450

[7] J. Hellmig, Ph. D. Thesis, Heidelberg 1996

Search on $\beta^+\beta+$ and β^+/EC decay of ^{106}Cd

F.A. Danevich, A.Sh. Georgadze, J. Hellmig, M. Hirsch, H.V. Klapdor-Kleingrothaus, V.V. Kobychev, B.N. Kropivyansky, V.N. Kuts, B. Maier, A. Müller, A.S. Nikolaiko, F. Petry, O.A. Ponkratenko, H. Strecker, V.I. Tretyak, M. Völlinger and Yu.G. Zdesenko

During 1995 in the frame of the MPI (Heidelberg)-INR (Kiev) collaboration the joint experiment on double beta decay of ^{106}Cd was continued in the Gran Sasso Underground Laboratory. The background measurements (6700 h) were performed with a large (6.4 cm long, 5.1 cm in diameter) $CdWO_4$ crystal scintillator with mass of 1.064 kg. Such large volume $CdWO_4$ crystals with improved energy resolution have been developed as a result of advances in crystal growth, optimization of light collection and design of a special electronic unit for amplification and shaping of the $CdWO_4$ signal [1]. The number of ^{106}Cd nuclei in this crystal is 2.22 (0.07) 10^{22}. The energy resolution with the Philips XP2412 photomultiplier was 13.2, 11.4 and 9.3% at energy 570, 662 and 1064 keV, respectively (Fig. 1). In the low background set up installed in the Gran Sasso Laboratory the $CdWO_4$ crystal was viewed by a PMT (FEU-167) with a low level of radioactive contaminations. The PMT was connected to the scintillator through a light guide (58 cm length, 10 cm in diameter) made from quartz. The passive shielding for the $CdWO_4$ detector consists of OFHC copper (10 cm) and Boliden lead (10 cm). During the experiment the energy calibration was carried out with a ^{228}Th source every 2-4 days. Remaining shifts in the gain were corrected by software.

Fig. 2 shows the background spectrum measured during 6701 h. The low energy part of the latter represents the β spectrum of ^{113}Cd with a half-life about 10^{16} y and Q_β = 316 keV, and of ^{113m}Cd ($T_{1/2}$= 13.7 y and Q_β = 580 keV). The continuous background up to the energy of 1.3 MeV can be caused by ^{40}K and ^{238}U family nuclei in a crystal. The upper limits of their activities are < 1.7 mBq/kg for ^{40}K and < 1.3 mBq/kg for ^{238}U. The contaminations of $CdWO_4$ by ^{232}Th and ^{226}Ra were estimated by an off-line analysis of the arrival time of the background events. The results are: < 0.005 mBq/kg for ^{227}Ac and < 0.007 mBq/kg for ^{226}Ra. The background rate of the detector in the energy interval of neutrinoless $\beta^+\beta^+$ decay of ^{106}Cd (2.6 -2.9 MeV) is 2.3 counts/(y kg keV).

To estimate the half-life limits for $\beta^+\beta^+$ decay processes of ^{106}Cd the expected response function and detection efficiency of $CdWO_4$ were calculated using the GEANT3 code. The estimation of the excluded effect was made by means of least-square fit of the background model with a possible signal to the experimental spectrum. The following half-life limits were deduced:

$T_{1/2}(0\nu\,\beta^+\beta^+) > 2.2(3.8)\,10^{19}\,y$

90%(68%) *C.L.*

$T_{1/2}(0\nu\,\beta^+/\mathrm{EC}) > 5.5(8.6)\,10^{19}\,y$

90%(68%) *C.L.*

These limits improve the existing ones for ^{106}Cd [2] by a factor of 5–10. A higher sensitivity for neutrinoless $\beta^+\,\beta^+$ and β^+/EC decay was reached only with ^{78}Kr [3], where an enriched source was used. Based on the developments and results of the present work the plan for the second stage of the joint Heidelberg–Kiev research with ^{116}Cd and ^{106}Cd is to reach in the ^{116}Cd experiment a limit on the neutrino mass of less than 0.9 eV.

References

[1] Burachas S.P. et al., NIM **A** (1996) in press

[2] Georgadze A.Sh. et al., Phys. Atom. Nucl. **58** (1995) 1093

[3] Saenz C. et al., Phys.Rev. **C 50** (1994) 1170

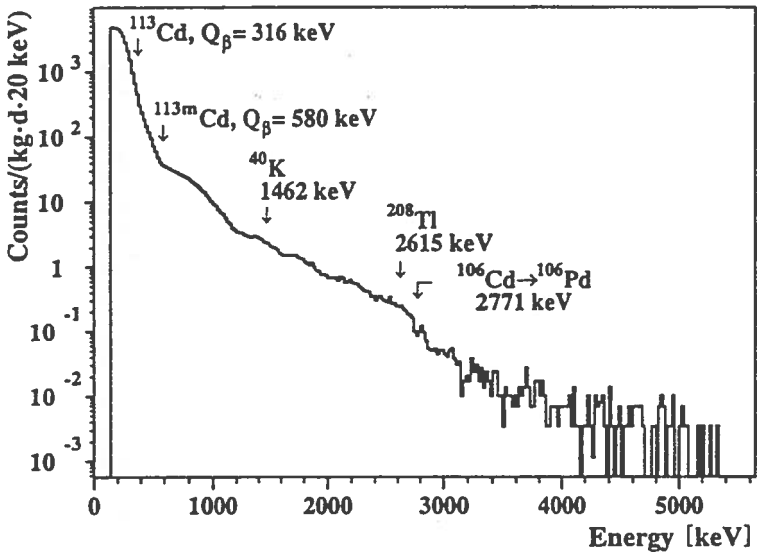

Figure 9: Background spectrum of $CdWO_4$ crystal (1.1 kg) measured in the Gran Sasso Underground Laboratory for 6701 h.

Heidelberg Dark Matter Search

M. Günther, J. Hellmig, G. Heusser, M. Hirsch, H.V. Klapdor–Kleingrothaus, A. Müller, F. Petry, Y. Ramachers, H. Strecker

Abstract

We report about a method for a drastical reduction of background for conventional germanium ionization detectors. It will be possible with this method to set important constraints on the nature of dark matter particles supposed to exist in the halo of our galaxy.

In Heidelberg we concentrate on the direct detection of WIMPs via elastic scattering with detector crystal nuclei. Current efforts by our group aim at a reduction of the background in the low–energy region, *i.e.* for energies smaller say 100keV.

In order to reach the theoretically interesting region of expected neutralino event rates (the neutralino as the lightest supersymmetric particle is the favorite cold dark matter candidate [4]), a background suppression of at least a factor of

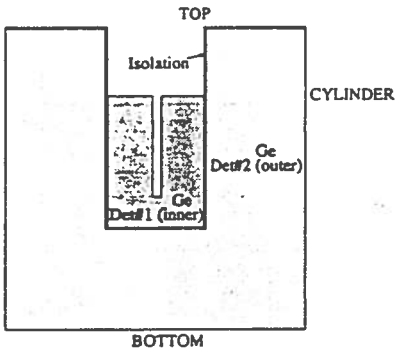

Figure 10: Simulated geometry of the Detindet–configuration (shown as two–dimensional cut). Denoted are the locations of simulated impurities.

ten compared to the background level of the HEIDELBERG–MOSCOW–EXPERIMENT [2, 3] has to be achieved.

Using the knowledge about the background composition of the enriched ^{76}Ge detectors of the HEIDELBERG–MOSCOW–EXPERIMENT [3], we developed a new detector design specialized for WIMP detection. Its background is dominated by radioimpurities of materials very near to the detector crystals, *i.e.* the cryostat system. The purest materials are the crystals themselves. The background in the low–energy region of the measured spectrum is dominated by Compton–scattered photons.

So the idea for the new detector design is schematically the following: In principle we will plug one Ge–crystal into a bigger well–type Ge–crystal and mount these two crystals into one cryostat system. Then the well–type is the active shield for the small measurement–crystal (see fig.). Another idea being worked out at present by a Monte–Carlo simulation is to use segmented planar detector crystals in a multi–layer configuration. This idea uses the same shielding principle, *i.e.* an active shield, but in a full 4π configuration and without an isolation material.

Technologically the idea is not that easy. For the first step of research, *i.e.* a Monte–Carlo–simulation of a simplified geometry, we introduced an electrical isolation between the two crystals because of the leakage currents on the surface of the crystals. As a second step we varied the geometry by introducing a third detector crystal as a cover in order to achieve a (nearly) $4\,\pi$–shield configuration. The results of the simulation are more qualitative than quantitative and can be expressed as: a) The suppression factor, defined as the ratio of unsuppressed to suppressed counts in the interesting low–energy spectrum, can reach values of order 20. Even higher values have been obtained depending on the energy of the photons and the localization of the simulated impurities. The effect of the cover detector can be seen in direct comparison to the design without it in fig. .

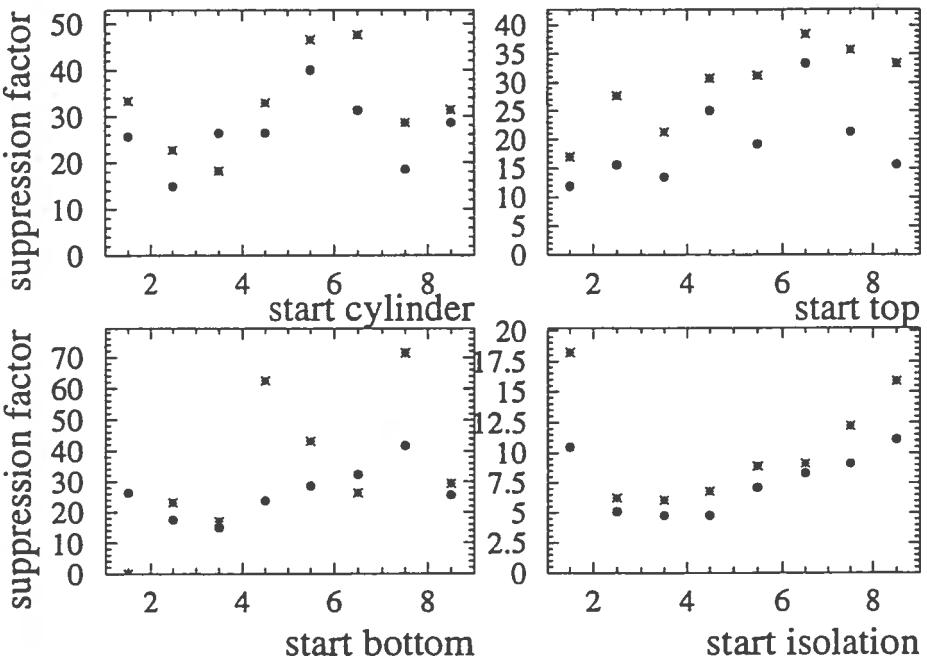

Figure 11: Comparison of designs with (denoted by stars) and without (dots) the cover detector crystal. The x-axis values code the simulated energies (1:238keV; 2:511keV; 3:911keV; 4:1461keV; 5:2204keV; 6:2614keV), the decay chain of Ac228 (7) and a Co60 impurity (8) respectively.

Our expectation based on the background suppression of a factor of twenty is shown in fig. . The conclusion is that we will be able to compete with the aims of so called 'next–generation' experiments, namely of the cryogenic type, by the well understood ionization detector technology.

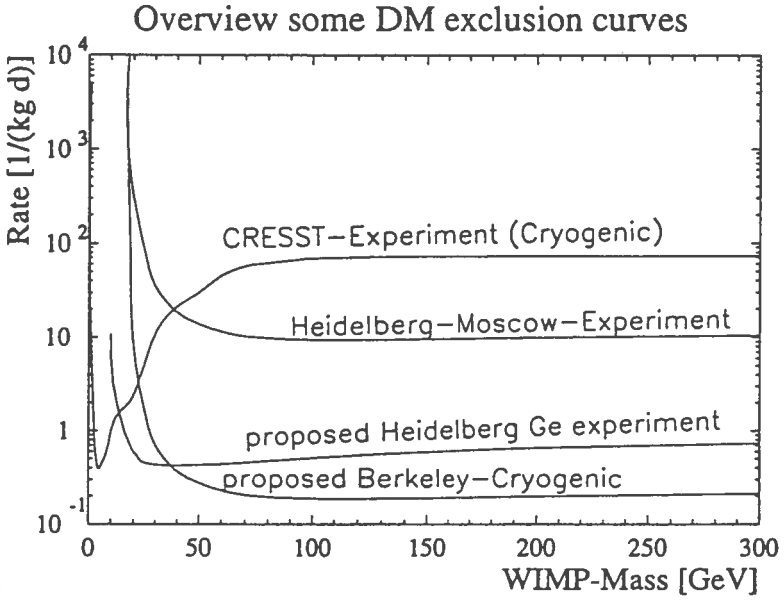

Figure 12: Exclusion plot for WIMP rates as function of the WIMP–mass in detectors of some proposed experiments [4] including the HEIDELBERG–MOSCOW–EXPERIMENT result [5] and an expectation for our Detindet-detector. The region above the curves is excluded at 90% C.L.

References

[1] V. Bednyakov, H.V. Klapdor–Kleingrothaus and S. Kovalenko, Phys. Rev. **D 50** (1994) 7128

[2] HEIDELBERG–MOSCOW–COLLABORATION, Phys. Lett. **B 356** (1995) 450

[3] HEIDELBERG–MOSCOW–COLLABORATION, in press in Phys. Rev. D

[4] W. Seidel *et.al.*, J. Low Temp. Phys. **93** (1993) 797; Phys. Lett. **B 323** (1994) 95; P.D. Barnes *et.al.*, J. Low Temp. Phys. **93** (1993) 791; D. Reusser *et.al.*, Phys. Lett. **B 255** (1991) 143

[5] M. Beck *et.al.*, Phys. Lett. **B 336** (1994) 141

On the observability of Majoron emitting double beta decays

M. Hirsch, H.V. Klapdor-Kleingrothaus, S.G. Kovalenko [1], *H. Päs*

Abstract

Due to claims of unidentified excess events in ongoing double beta experiments and the fine–tuning problem in classical Majoron models in the recent years several new Majoron models were invented. We point out that double beta decays with new Majoron emission depend on new matrix elements, which have not been considered in the literature. A calculation of these matrix elements and phase space integrals was performed. We found that for new Majoron models extremly small decay rates are expected.

In many theories of physics beyond the standard model neutrinoless double beta decays can occur with the emission of new bosons, so–called Majorons:

$$2n \to 2p + 2e^- + \phi \tag{14}$$

$$2n \to 2p + 2e^- + 2\phi \tag{15}$$

In the classical Majoron model invented by Gelmini and Roncadelli in '81 [1], the Majoron is the Nambu–Goldstone boson associated with the spontaneous breaking of the global lepton number symmetry and so generates Majorana masses of neutrinos. However, in this model the Majoron is an electroweak isospin triplet and therefore should contribute the equivalent of two neutrino species to the width of the Z^0, which was ruled out by LEP.

On the other hand, Majoron models in which the Majoron is an electroweak isospin singlet are still viable [2]. The drawback of the singlet Majoron model is that in these models the Majoron couples to the neutrino at tree level with a coupling strength of roughly $g \simeq (m_{\nu_L}/v_{BL})$, where v_{BL} is the symmetry breaking scale. In order to preserve existing bounds on neutrino masses and at the same time get an observable rate for Majoron emitting double beta decays the singlet Majoron model requires severe finetuning.

To avoid such an unnatural fine–tuning in recent years several new Majoron models have been constructed [3, 4, 5], where the terminus Majoron means in a more general sense light or massless bosons with couplings to neutrinos. These models yield different spectral shapes for the sum energy of the outgoing electrons, which can be used to distinghuish these modes from each other and the standard model $2\nu\beta\beta$ decay (see fig. 1). The main novel features of the "New Majorons" are that they can carry units of leptonic charge, that there can be Majorons which are no Goldstone bosons [3] and that decays with the

[1] Joint Institute for Nuclear Research, Dubna, Russia

emission of two Majorons [4] can occur (fig. 13 – 15). The latter can be scalar–mediated or fermion–mediated. In vector Majoron models the Majoron becomes the longitudinal component of a massive gauge boson [5] emitted in double beta processes. For simplicity it is called Majoron, too.

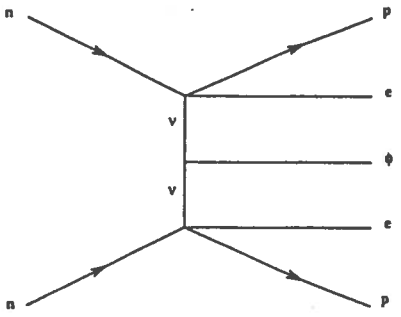

Figure 13: Feynman graph for $\beta\beta\phi$– decays

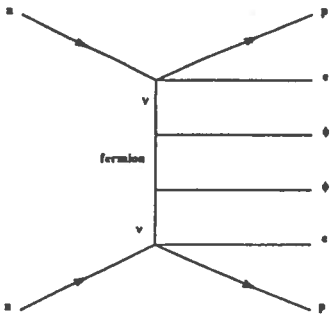

Figure 14: Feynman graph for fermion–mediated $\beta\beta\phi\phi$–decays

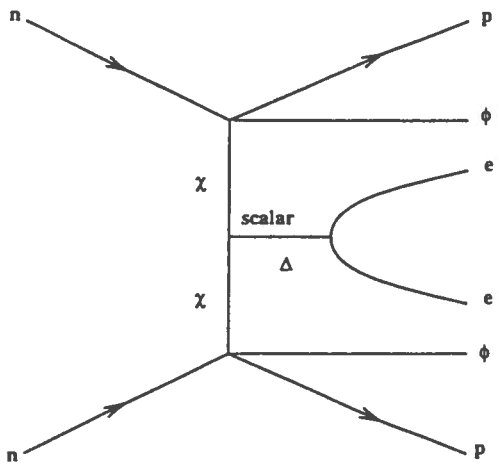

Figure 15: Feynman graph for scalar–mediated $\beta\beta\phi\phi$–decays

All these models were invented with the same intention of giving observable contributions to double beta decays to explain the claims of unidentified excess events near but below the endpoint of the double beta energy spectrum. Thus we felt motivated to analyze the corresponding nuclear matrix elements and phase space integrals. Nuclear matrix elements M_α and phase space integrals G_{BB_α} are necessary to convert experimental half lives (or limits thereof) into informations on values for the effective Majoron neutrino coupling constant

$< g_\alpha >$ according to

$$[T_{1/2}]^{-1} = | < g_\alpha > |^2 \cdot |M_\alpha|^2 \cdot G_{BB_\alpha} \tag{16}$$

for $\beta\beta\phi$-decays, or

$$[T_{1/2}]^{-1} = | < g_\alpha > |^4 \cdot |M_\alpha|^2 \cdot G_{BB_\alpha} \tag{17}$$

for $\beta\beta\phi\phi$–decays. The index α in eqs. (16)–(17) indicates that these terms differ for the different models.

The QRPA calculation of these matrix elements and phase space integrals presented in [2, 7] yields surprisingly small values and therefore extremly small double beta decay rates for new Majoron models. For example, for a typical coupling constant for ordinary models, $\langle g \rangle \approx 10^{-4}$, the half lives of the new decay modes are 6–16 magnitudes larger than the sensitivity of ongoing double beta experiments. From this consideration it is very unlikely that any of the new Majoron models can produce an observable rate in planned or ongoing double beta decay experiments. Only the charged Majoron model [3] could produce an observable effect if the real coupling constant is of order $\mathcal{O}(1)$.

References

[1] G.B. Gelmini and M. Roncadelli, Phys. Lett. **B 99** (1981) 411

[2] Z.G. Berezhiani, A. Yu. Smirnov, J.W.F. Valle, Phys.Lett. **B 291** (1992) 99

[3] C.P. Burgess, J.M. Cline, Phys. Lett. **B 298** (1993) 141; Phys. Rev. **D 49** (1994) 5925

[4] P. Bamert, C.P. Burgess, R.N. Mohapatra, Nucl. Phys. **B 449** (1995) 25

[5] C.D. Carone, Phys. Lett. **B 308** (1993) 85

[6] M. Hirsch, H.V. Klapdor–Kleingrothaus, S.G. Kovalenko, H. Päs, Phys. Lett. **B**, accepted for publication

[7] H. Päs, diploma thesis, Universität Heidelberg, unpublished

Supersymmetric neutrinoless double beta decay

M. Hirsch, H.V. Klapdor-Kleingrothaus, S.G. Kovalenko

Abstract

We have continued our investigations of the supersymmetric contributions to $0\nu\beta\beta$ decay within R-parity violating SUSY models. Besides the purely supersymmetric diagrams it is possible to construct diagrams contributing to $0\nu\beta\beta$ decay which do involve both, a neutrino and supersymmetric partner particles. These new contributions are essentially different from those previously discussed, since they do allow to probe R-parity violating Yukawa couplings of higher generations. Currently absence of $0\nu\beta\beta$ decay of ^{76}Ge from the mixed SUSY-neutrino diagrams implies the following limits on the strengths of the R-parity violation (for masses of superparticles of 100 GeV): $\lambda'_{113}\lambda'_{131} \leq 1.1 \times 10^{-7}$, $\lambda'_{112}\lambda'_{121} \leq 3.2 \times 10^{-6}$ and $\lambda'^2_{111} \leq 6.4 \times 10^{-5}$. These are the most stringent limits on these combination of Yukawa couplings known to date. For the limit on λ'_{111} a more stringent bound from the gluino exchange diagram of $0\nu\beta\beta$ decay ($\lambda'_{111} \leq 3.9 \times 10^{-4}$) is obtained. Contrary to previous belief, we have found that $0\nu\beta\beta$ decay can not only occur in R-parity violating SUSY models but also in the R-parity conserving case if the neutrino is a Majorana particle.

As is well-known neutrinoless double beta decay currently gives the most stringent test of the Majorana nature of the neutrino. Besides, $0\nu\beta\beta$ decay can also occur in R-parity violating versions of the minimal supersymmetric extension of the standard model (MSSM) [1].

We have completed [2] the tree level calculations of the 'pure' $\not{R}_p$ MSSM decays. Constraints on the strength of the R-parity violating interaction from the absence of ^{76}Ge $0\nu\beta\beta$ decay [3] and other double beta decay experiments [4] have been derived. The comparison of the different double beta decay experiments [4] has shown that currently ^{76}Ge provides the most stringent constraints on $\not{R}_p$ MSSM parameters. Furthermore, it was shown that $0\nu\beta\beta$ decay is the most sensitive test of the $\not{R}_p$ MSSM of all low-energy experiments [5] and can compete favorably with the best available accelerator data [6, 7].

As the next step of the investigation of supersymmetric $0\nu\beta\beta$ decay, diagrams which do involve neutrinos *and* supersymmetric particles have been constructed from the basic $\not{R}_p$ MSSM Lagrangian [8]. Figures 16 and 17 show the new mixed SUSY-neutrino exchange diagrams, which can contribute to $0\nu\beta\beta$ decay in lowest order perturbation theory.

These new diagrams differ from those discussed previously in the literature [1, 2] in two respects. The more important is that they allow not only to derive limits on the first generation R-parity violating Yukawa coupling, as was the case for all 'pure' supersymmetric diagrams, but also for those of higher generations. The second is, that these diagrams require the neutrino to be a Majorana particle (the old diagrams are independent of this assumption).

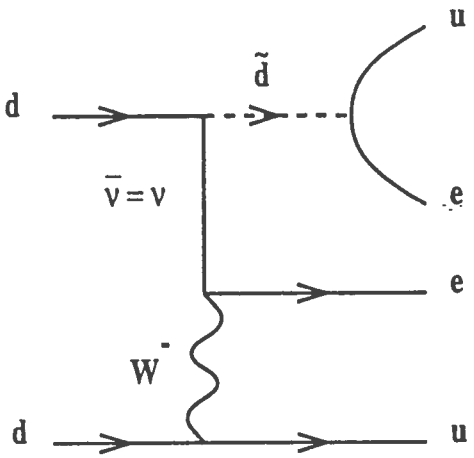

Figure 16: Feynman graph for the mixed SUSY-neutrino exchange mechanism of $0\nu\beta\beta$ decay. R-parity violation occurs through scalar quark exchange.

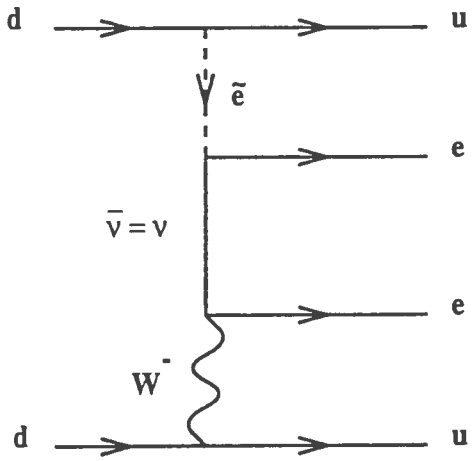

Figure 17: As figure 1, but for scalar lepton exchange.

Following the standard procedure [4], we have calculated the relevant amplitudes of the graphs in figs. 16 and 17. Mixing between scalar superpartners of the left and right-handed fermions has been found to play a crucial role for these diagrams. This can be understood considering that the fermionic propagator for the virtual neutrino involves two terms, one proportional to the neutrino mass and one proportional to the neutrino momentum. In 'usual' neutrinoless double beta decay only terms proportional to the neutrino mass survive, due

to the $(V-A)$ structure of the weak interaction. Mixing between left and right-handed scalar superpartners, on the other hand, gives a contribution proportional to the neutrino momentum. Since the neutrino momentum is of the order of the inverse nuclear radius, $\mathcal{O}(100\ \mathrm{MeV})$, nuclear matrix elements of the new diagrams of fig. 16 and fig 17 are largely enhanced compared to those of the usual neutrino mass mechanism.

These new nuclear matrix elements have then be calculated within the pn-QRPA. These theoretical calculations, together with the experimental limit on the ^{76}Ge decay half life imply stringent limits on the following combinations of R-parity violating Yukawa couplings (for masses of superparticles of 100 GeV) [8]: $\lambda'_{113}\lambda'_{131} \leq 1.1 \times 10^{-7}$, $\lambda'_{112}\lambda'_{121} \leq 3.2 \times 10^{-6}$ and $\lambda'^2_{111} \leq 6.4 \times 10^{-5}$. The limit on λ'_{111} can be compared with the one derived from gluino exchange, $\lambda'_{111} \leq 3.9 \times 10^{-4}$ [3], which is more stringent. For the combinations of Yukawa couplings involving higher generations, on the other hand, the limits quoted are the strongest bounds which have been found so far.

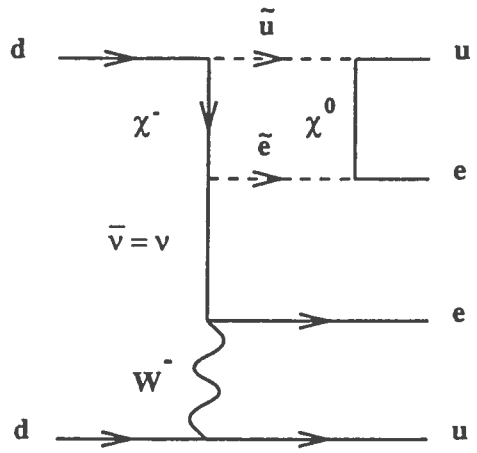

Figure 18: Feynmangraph for $0\nu\beta\beta$ decay in supersymmetric models without R-parity violation.

Up to now, all diagrams of $0\nu\beta\beta$ decay within supersymmetric models required some degree of R-parity violation. However, R-parity violation is *contrary to previous belief* not a necessary ingredient to the theory for $0\nu\beta\beta$ decay to occur.

This is demonstrated in figure 18, which shows an example of a box graph, contributing to $0\nu\beta\beta$ decay, even if all R-parity violating terms of the superpotential are zero. It is relatively easy to see that this graph is R-parity conserving, since all vertices within the box connect pairs of supersymmetric particles. χ^- is the so-called chargino, χ^0 the neutralino, and quarks and leptons with 'tilde' are the superpartners of the quarks and the electron. Lepton number violation

in this graph is induced by the Majorana nature of the neutrino. Fig. 18 is just one example of a completely new class of $0\nu\beta\beta$ decay diagrams. One can easily construct other diagrams of the same order by a crossing of the chargino and neutralino lines and/or by the replacement of the selectron with a sneutrino.

Fig. 18 is - in terms of perturbation theory - a higher order graph and thus involves higher powers of coupling constants. However, if the chargino has a sizeable higgsino component it may still give an important contribution to $0\nu\beta\beta$ decay. We plan therefore to investigate this new class of $0\nu\beta\beta$ decay graphs in detail in the near future.

In summary, it can be stated that neutrinoless double beta decay allows to stringently test R-parity violating (and maybe also R-parity conserving!) supersymmetric models. Due to the surprising results obtained during the last year it seems necessary to do a more detailed analysis of *all* theoretical models, which do allow for lepton number violation. The theory of $0\nu\beta\beta$ decay is even today far from being completely understood!

References

[1] R.N. Mohapatra, Phys. Rev. D 34 (1986) 3457

[2] M. Hirsch, H.V. Klapdor-Kleingrothaus und S.G. Kovalenko, Phys. Lett. B 352 (1995) 1

[3] M. Hirsch, H.V. Klapdor-Kleingrothaus und S.G. Kovalenko, Phys. Rev. Lett. 75 (1995) 17

[4] M. Hirsch, H.V. Klapdor-Kleingrothaus und S.G. Kovalenko, Phys. Rev. D, in the press

[5] V. Barger et al., Phys. Rev. D40 (1989) 2987

[6] J. Butterworth und H. Dreiner, Nucl. Phys. B397 (1993)3

[7] D.P. Roy, Phys. Lett. B 283 (1992) 270

[8] M. Hirsch, H.V. Klapdor-Kleingrothaus und S.G. Kovalenko, Phys. Lett. B in the press

Neutrinoless double beta decay in left-right symmetric models

M. Hirsch, H.V. Klapdor-Kleingrothaus, O. Panella

Abstract

Left-right symmetric models provide a natural framework for neutrinoless double beta decay. In LR models the smallness of the neutrino mass can be quite naturally understood via the famous seesaw mechanism, which requires the existence of a *heavy, right-handed* neutrino. Assuming the existence of at least one right-handed heavy neutrino, absence of $0\nu\beta\beta$ decay of ^{76}Ge currently provides the following limits on the mass and mixing angle of right-handed W-bosons:

$$m_{W_R} \geq 1.1 \text{ TeV} \left(\frac{\langle m_N^{(V)} \rangle}{1TeV}\right)^{(-1/4)},$$

$$tan(\zeta) \leq 4.7 \times 10^{-3} \left(\frac{\langle m_N^{(V)} \rangle}{1TeV}\right)^{(1/2)}.$$

Here $\langle m_N^{(V)} \rangle$ denotes the effective right-handed neutrino mass.

Left-right symmetric models (LR) [1] aim at explaining two of the most puzzling questions of the standard model (SM), both of which are intimately related to neutrinoless double beta decay ($0\nu\beta\beta$): i.) The weak interaction violates parity, and ii.) in the standard model neutrino masses are zero. Especially if current hints on finite neutrino masses are correct, LR models provide a very attractive explanation for their small values - when compared to those of the charged leptons - via the well-known seesaw mechanism [2].

However, the analysis of $0\nu\beta\beta$ decay is usually restricted to the case where all neutrinos are light or simplified by considering only left-handed neutrinos. Motivated by the experimental progress in double beta decay, we [3] therefore reconsidered $0\nu\beta\beta$ decay in LR models, taking into account heavy right-handed neutrinos as well as - for the first time consistently - the effects of the possible Higgs triplet contribution [4].

The inclusion of a Higgs triplet into LR models is a necessary ingredient to preserve the unitarity of the cross section in the *inverse neutrinoless double beta decay*, as pointed out by Rizzo [4]. Moreover, the existence of these additional Higgs fields could naturally explain the Majorana nature of the neutrino and implement a seesaw mechanism into the model.

The extension of the Higgs sector opens up new decay channels for $0\nu\beta\beta$ decay. Besides the usual diagram for heavy Majorana neutrino exchange (see fig. 19), there will exist also a contribution to $0\nu\beta\beta$ decay via the exchange of the doubly-charged component of the triplet, as shown in fig. 20.

Starting from the basic parameterization of the LR charged-current effective Hamiltonian [5], we have derived the decay rate for $0\nu\beta\beta$ decay [6], using only the realistic assumption that there are no neutrinos with mass eigenstates in the

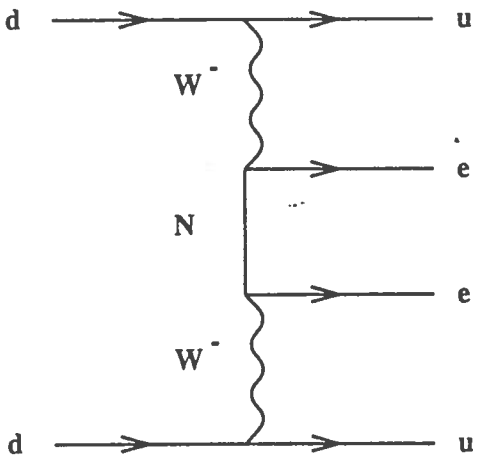

Figure 19: Feynman graph for heavy neutrino exchange in left-right symmetric models contributing to $0\nu\beta\beta$ decay.

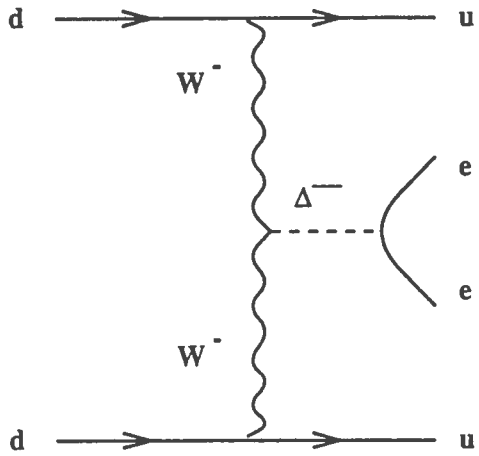

Figure 20: Contribution of the Higgs triplet of LR models to $0\nu\beta\beta$ decay.

mass region between $\mathcal{O}$(10-1000) MeV, but otherwhise keeping both light left-handed and heavy right-handed neutrinos. The formalism was then extended [3] to include consistently the Higgs triplet contribution.

The analyses showed that limits on light neutrinos remain essentially unchanged by this extension of the theory. For the right-handed W-bosons $0\nu\beta\beta$ decay gives the weakest limit in the case when the mass of the doubly-charged higgs goes to infinity. In this case double beta decay bounds mass and mixing

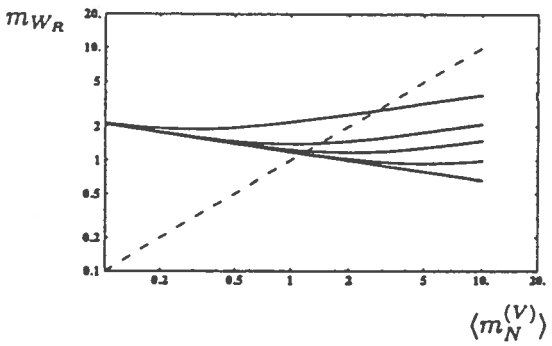

Figure 21: Limits on the mass of the right-handed W-boson from double beta decay and vacuum stability, see text. Axis are in [TeV].

of right-handed W-bosons to be:

$$m_{W_R} \geq 1.1 \text{ TeV } \left(\frac{\langle m_N^{(V)} \rangle}{1TeV}\right)^{(-1/4)},$$
$$tan(\zeta) \leq 4.7 \times 10^{-3} \left(\frac{\langle m_N^{(V)} \rangle}{1TeV}\right)^{(1/2)}.$$

Here $\langle m_N^{(V)} \rangle$ denotes the effective right-handed neutrino mass.

The limit on m_{W_R} is shown in fig. 21. In this figure, the various full curves are limits from $0\nu\beta\beta$ decay as a function of the heavy neutrino mass and for different assumed values of $m_{\Delta^{--}}$ (from top to bottom 0.3, 1.0, 2.0, 5.0 and ∞ TeV). The dashed line is the theoretical limit from vacuum stability [7].

We plan to do a careful comparison of this result with the expectation for an inverse neutrinoless double beta decay experiment at an e^-e^--collider in the future.

References

[1] J.C. Pati and A. Salam, Phys. Rev. D 10 (1974) 275; R.N. Mohapatra and J.C. Pati, Phys. Rev. D 11 (1975) 566,2558; G. Senjanovic and R.N. Mohapatra, Phys. Rev. D 12 (1975) 1502

[2] M. Gell-Mann, P. Ramond and R. Slansky, in: Supergravity, eds. F. van Nieuwenhuizen and D. Freedman, North-Holland, Amsterdam, 1979; R.N. Mohapatra and G. Senjanovic, Phys.Rev. D 23 (1981) 165

[3] M. Hirsch, H.V. Klapdor-Kleingrothaus and O. Panella, subm. to Phys. Lett. B

[4] T.G. Rizzo, Phys. Lett. B116 (1982) 23

[5] M. Doi and T. Kotani, Progr. Theor. Phys. 89 (1993) 139

[6] M. Hirsch and H.V. Klapdor-Kleingrothaus, in: Proc. Int. Workshop on 'Double Beta Decay and related topics', Trento, Italy, April 1995, World Scientific, Singapore, in the press

[7] R.N. Mohapatra, Phys. Rev. D34 (1986) 909

Leptoquarks and neutrinoless double beta decay

M. Hirsch, H.V. Klapdor-Kleingrothaus, S.G. Kovalenko

Abstract

Leptoquarks are hypothetical particles, which can carry both leptonic and baryonic quantum numbers. Such particles can appear in theories, which try to understand charge quantization and the experimental fact that $Q(p) + Q(e^-) = 0$.

Leptoquarks are particles with leptonic and baryonic quantum numbers. Such exotic particles first were discussed in the context of grand unified theories. Masses of these particles should then be of the order of the GUT scale. However, it was later realized that leptoquarks of quite low mass might exist, if certain couplings are forbidden by symmetry arguments. In recent years there has therefore been quite some activity to understand leptoquark phenomenology from the theoretical side [1, 2], as well as experimentally, searching for leptoquarks in *ep*-scattering [3].

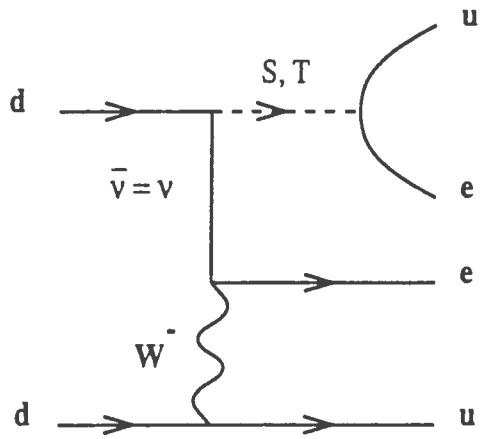

Figure 22: Feynman graph for $0\nu\beta\beta$ decay mediated by a Majorana neutrino and scalar leptoquarks: S (singlet) and T (triplet).

Using the most general effective leptoquark lagrangian consistent with the symmetries of the SM, we have constructed various diagrams contributing to $0\nu\beta\beta$ decay. An example is show in fig. 22. We plan to do a careful examination of the limits on scalar and vector leptoquarks, which can be derived from $0\nu\beta\beta$ decay and other low-energy experiments.

References

[1] M. Leurer, Phys.Rev. D49 (1994) 333

[2] W. Buchmüller, R. Rückl and D. Wyler, Phys. Lett. B191 (1987) 442

[3] H1 Collaboration, Z. Phys. C64 (1994) 545

Neutralino Rates for Cold Dark Matter Detection

V. Bednyakov[a], *M. Hirsch, H.V. Klapdor-Kleingrothaus, S. Kovalenko* [2], *H. Päs, Y. Ramachers*

Abstract

We consider the neutralino as a dominant dark matter particle in the galactic halo and investigate some general issues of direct DM searches via elastic neutralino–nucleus scattering. On the basis of conventional assumptions about the nuclear and nucleon structure we analyse constraints on the SUSY model parameter space accessible by the direct DM searches.

Our activities in dark matter phenomenology concentrate on calculations for dark matter particle candidates within the MSSM (minimal supersymmetric standard model). The problem of direct detection of the favorite DM particle candidate, *i.e.* the neutralino, via elastic scattering off nuclei has attracted considerable efforts during the last decade and remains a field of great experimental and theoretical activity[1, 2, 3, 4, 5, 6].

The SUSY model neutralino (χ) is a Majorana ($\chi^c = \chi$) particle with spin 1/2. There are four neutralinos in the MSSM [7]. They are a mixture of gauginos ($\tilde{W}_3, \tilde{B}$) and Higgsinos ($\tilde{H}_{1,2}$) being SUSY partners of gauge (W_3, B) and Higgs ($H_{1,2}$) bosons. The DM neutralino χ is assumed to be the lightest supersymmetric particle (LSP) and therefore is stable in SUSY models with R–parity conservation.

In the galactic halo neutralinos are assumed to be Maxwellian distributed in velocities with a mean velocity in the earth frame $v \approx 300\,km/s$[8]. Their mass density in the solar system is expected to be about $\rho \approx 0.3 GeV/cm^3$. Therefore, at the earth surface neutralinos might produce a substantial flux ($\Phi = \rho v/M$) of $\Phi > 10^7 cm^{-2} sec^{-1}$ for a particle with mass of $M \approx 1\,GeV$. In view of this one may hope to detect DM particles directly, for instance through elastic scattering from nuclei inside terrestrial detectors.

Currently we undertake a systematic exploration of a broad domain of the MSSM parameter space restricted by well known accelerator constraints and by the cosmological bounds on neutralino relic abundance in the universe (for preliminary results, see fig. 1).

We improved the calculations [4] by the following new ingredients:

- updated accelerator constraints,
- rare b–quark decay constraints, namely experimental constraints on the branching ratio for the $b \to s\,\gamma$ decay,
- next leading order renormalization group equations: now with thresholds for the sfermions,

[2] Joint Institute for Nuclear Research, Dubna, Russia

- threshold effects for rates, spectrum as well as different form factors,
- relaxations of unification assumptions at the SUSY–GUT scale: leading to preliminary investigations for light neutralinos up to 3 GeV.

In result we calculate with the up to now most complete set of equations and updated constraints. Therefore we will first check preliminary results of other groups [2, 5] obtained by more approximate methods.

One result already obtained by our investigation is connected with the role of nuclear spin in DM direct detection experiments. We found that two different DM detectors with ($J = 0,\ A_1$) and ($J \neq 0,\ A_2$) nuclei as target material have equal chances to discover DM events if $A_1, A_2 > 50$.

In conclusion we would like to stress that the efforts to improve existing and to construct new DM detectors are justified by the expectation that these detectors will be able to tackle supersymmetry from a side unreachable for the accelerator experiments.

References

[1] M.W. Goodman and E. Witten, Phys Rev. **D31** (1985) 3059

[2] G. Jungman, M. Kamionkowski and K. Griest to appear in Phys. Rep.

[3] M. Drees and M.M. Nojiri, Phys. Rev. D **48** (1993) 3483

[4] V. Bednyakov, H.V. Klapdor–Kleingrothaus and S. Kovalenko, Phys. Rev. D **50** (1994) 7128

[5] V. Berezinsky, A. Bottino, J. Ellis, N. Fornengo, G. Mignola and S. Scopel, Preprint HEP–PH–9508249

[6] V. Bednyakov, H.V. Klapdor–Kleingrothaus and S. Kovalenko, Preprint HEP–PH–9510292

[7] H.E. Haber, G.L. Kane, Phys. Rep. **117** (1985) 75; H.E. Haber, in Proceedings of the Theoretical Advanced Study Institute, Colorado 1992 (to be published)

[8] K. Freese, J. Frieman and A. Gould, Phys. Rev. **D37** (1988) 3388

1995 STATUS REPORT ON DOUBLE BETA DECAY EXPERIMENT AT GRAN SASSO WITH GERMANIUM DETECTORS (DBGS)

Double beta decay is extensively investigated both from the point of view of theory and experimentally. Neutrinoless decay has intrigued theoreticians and experimentalists in elementary particle physics towards searches beyond the standard model, because of its implications on the lepton number conservation and neutrino properties [1]. Neutrinoless decay, which would violate the lepton number conservation, can be the consequence of a finite neutrino mass and/or of the presence of right-handed weak currents.

The detection of $\beta\beta$ decay to the 0^+_1 excited state gives similar informations about $\beta\beta$ decay as the observation of the decays to the ground 0^+_{gs} state. The energy released in $\beta\beta$ decay to the excited levels is less than for the ground state transition, so the phase space is substantially less. It has been recently shown [2] that the suppression factor respect to the transition to 0^+_{gs} may be not so large, at least for the one-phonon excited states within the framework of the QRPA. In ref.[3] half lives for $(2\nu)\beta\beta$ transitions in ^{96}Zr, ^{100}Mo and ^{150}Nd to the first 0^+_1 excited states of the daughter nuclei were estimated to be of the order of 10^{20} - 10^{21} years, thanks to their large transition energies (2202, 1903 and 2627 keV respectively), assuming that the nuclear matrix elements of the transition to the g.s. and excited 0^+ are the same. Such predictions show that this type of decay can be detected by present low-background detectors. In ref [4] results of a positive signal for ^{100}Mo are reported.

We remind that the half life for $(0^+_{gs} \dashrightarrow 0^+_{gs})$ $(2\nu)\beta\beta$ decay of ^{150}Nd to ^{150}Sm has been recently measured to be $T_{1/2} = (1.88^{+0.69}_{-0.39} \pm 0.19) \times 10^{19}$ y [5]. On the basis of the expected dependence on the phase space, it appears that the present lower limits on the half life for the decay to the first 0^+_1 excited state are very close to the expected one.

However, a model performed within the pseudo SU(3) formalism [6] shows strong suppression of the $(2\nu)\beta\beta$ transitions in ^{150}Nd to the excited states of ^{150}Sm, and inhibition to the first 0^+_1 excited state. Measurements to investigate the half-life region of 10^{20} - 10^{21} years are feasible and become necessary. In addition, if lower limits are obtained, they could be used to limit possible values of the nuclear matrix element.

A possible signature for $\beta\beta$ decay to excited levels is the emission of de-excitation gamma rays from the daughter nuclide. Since the energy of the gamma rays is well defined, a good background rejection can be achieved if the detector has a high energy resolution, as , for instance, germanium diodes have.

2. Experimental setup and results for ^{150}Nd

In fig. 1 the decay scheme for triplet ^{150}Nd-^{150}Pm-^{150}Sm is shown. In this case single β decay is energetically forbidden and the transition energies available for the decay to the first excited levels of ^{150}Sm are particularly high ($Q_{\beta\beta}$ = 2627 kev for the transition to the 0^+_1 excited level of ^{150}Sm). ^{150}Nd is present in natural neodymium with 5.64 % atomic percentual abundance, which makes an experiment using natural neodymium, meaningful.

The detector used is a High Purity Ge diode, 518 cm^3 volume, 113% relative efficiency, installed in the low background facility at Laboratori Nazionali del Gran Sasso [7]. A shielding of OFHC copper and low activity lead with 7 and 25 cm minimum thickness, respectively, was mounted all around the detector to minimize background radiation. To avoid radon contamination, a plastic cover, into which nitrogen vapours were flushed, surrounded the shielding. This protection was changed during the experiment; in the final version of the set up a sealed acrilic box surrounded the lead shielding and a slight overpressure of argon or nitrogen was kept. Radon concentration in the shielding was reduced by a factor 4 respect to the initial situation.
The measurement, with 6500 hour of effective running time, was carried out using eighteen rods of natural metallic neodymium, 2.5 cm diameter and 10 cm height, 6185 g of total mass, each sealed in a very thin paraffin foil to avoid oxidation and placed in a purposely designed plastic marinelli around the detector. The sample was provided by Johnson & Matthey p.l.c.
The detection efficiency of gamma rays has been computed usign a code based on EGS [8] for the ingots. In order to check for the presemce of errors in the use of the code (e.g. mistakes in the description of the geometrical parameteres), many checks have been performed between data and computed values, on sum lines of full energy peaks, with comparison of single and double escape peaks to the full energy peak at 2615 keV, and by checking the shape of the efficiency curve as a function of energy, using different lines from the same element or elements in equilibrium: the agreement between data and calculated values was fairly good [9].
By analysing the spectra, gamma lines from natural radioactive series and other radionuclides have been observed in the samples and contaminations have been computed from their intensities.

2.1 Contaminations from ^{40}K

^{40}K decays via E.C. (10.7%) to ^{40}Ar with the emission of a γ ray at 1460.75 keV. A small contamination has been found, corresponding to $4 \cdot 10^{-6}$ Bq/g (10^{-11} g/g) and a concentration of 10^{-7} g/g of natural potassium.

2.2 Rare Earths

Due to the difficulty in purifing rare earths, the presence of radioactive lantanium and lutetium is expected. ^{138}La decays via E.C. (67.9% of the cases) to ^{138}Ba with the emission of a 1435.9 γ ray or beta decays to ^{138}Ce (32.1%) followed by a 789 keV γ ray. These two lines have been observed: the activity has been calculated from their mean value, thus giving a contamination of $3.6 \cdot 10^{-6}$ Bq/g ($4.15 \cdot 10^{-9}$ g/g) and a concentration of $4.66 \cdot 10^{-6}$ g/g of natural La.
^{176}Lu beta decays of ^{176}Hf, with the emission of four g rays. A strong and well identified signal has been observed at 201.8 keV (84.4%) and 306.9 (93%) and the contamination results to be $2.7 \cdot 10^{-5}$ Bq/g ($1.3 \cdot 10^{-8}$ g/g), and a concentration of $5 \cdot 10^{-7}$ g/g of natural Lu.

2.3 Thorium and Uranium

The secular equilibrium is broken: the ^{228}Ac activity is about one order of magnitude lower than that of ^{212}Pb and its daughters. Such a situation could be the consequence of a quite complete removal of radium from the sample during its preparation. The concentration of ^{228}Ac results to be $2.9 \cdot 10^{-6}$ Bq/g, while the one of ^{212}Pb is $2.8 \cdot 10^{-5}$ Bq/g. The ^{232}Th contamination has been estimated to be $3 \cdot 10^{-5}$Bq/g .

Gamma lines from ^{234m}Pa and ^{234}Pa have been detected and correspond to an activity of $1.85 \cdot 10^{-3}$ Bq/g of ^{238}U. Again the secular equilibrium is broken: the radium concentration has been calculated to be $8 \cdot 10^{-4}$ Bq/g. The activity of the radionuclides descending from ^{226}Ra is dominated by radon and radon daughters in the air and inside the shielding. In the final shielding version, the radon rate has been reduced by a factor 4.

2.4 Double beta search

No evidence is found for any of the de-excitation gamma-lines expected for ββ decay of ^{150}Nd to excited states of ^{150}Sm. The lower limits on the half lives of ^{150}Nd established are summarized in table 1 and compared with the previous published results[9]. In the energy region around 333.9 keV, gamma lines from ^{227}Th (334.5 keV) and ^{228}Ac (332.9 keV) have been found and their contribution has been subtracted, by knowing ^{227}Th and ^{228}Ac contamination independently from other gamma lines. In the energy region around 406.5 keV, the contribution of ^{211}Pb with a gamma line at 404.8 keV has been subtracted.

ββ transition	efficiency	$t_{1/2}$ (90%C.L.) (this work)	$t_{1/2}$ (90%C.L.) (previous work [10])
$0^+ \rightarrow 2^+_1$	2.34 %	$\geq 6.6 \times 10^{19}$ y	$\geq 1.0 \times 10^{3}$ y
$0^+ \rightarrow 0^+_1$	2.66%	$\geq 1.0 \times 10^{20}$ y	$\geq 1.5 \times 10^{18}$ y
$0^+ \rightarrow 2^+_2$	2.84%	$\geq 1.4 \times 10^{20}$ y	$\geq 1.7 \times 10^{18}$ y

Table 1: lower limits on the half lives for ββ decay of ^{150}Nd to ^{150}Sm established in the present study, compared with previous direct measurements [9] of the same decay.

Further measurements have been performed in order to select samples of Nd_2O_3 from which a new sample of metallic neodymium has been produced by J&M. The sample of these new 18 rods has been measured as the previous one. After ~400 hours, a contamination of the following elements has been found: $\sim 7 \cdot 10^{-5}$ Bq/g of ^{238}U, $\sim 10^{-5}$ Bq/g of ^{232}Th, $\sim 8 \cdot 10^{-7}$ Bq/g of ^{176}Lu, $\sim 4 \cdot 10^{-6}$ Bq/g of ^{138}La.
A good improvement (a factor 20) has been obtained for uranium contamination, while for thorium the improvement (a factor 3) is not satisfactory.

3. Conclusions

The results reported here constitute the best lower limits up to date for ββ decay of ^{150}Nd to the excited levels in the daughter nucleus.
The result obtained on natural neodymium has convinced us to improve the measurement by studing further reduction of the background level. In order to obtain a better sensitivity and to investigate in the half-life region for the decay of 10^{20} years, studies on purification of neodymium continue. In addition, coincidence techniques, with low activity germanium and NaI(Tl) detectors are foreseen.

References

1. See for instance T.Tomoda. Rep.Prog.Phys., 54 (1991) 53, A.Morales, Nucl.Phys.B S28a (1992) 181, M.K.Moe and P.Vogel: Double beta decay, UCI-Neutrino 94-5, February 1994- to be published in Ann. Rev. of Nucl. and Part. Science
2. J.Suhonen and O. Civitarese, Phys.Lett. B308 (1993) 212
3. A.S.Barabash, Soviet Phys.JETP 51 (1990) 207
4. A.S.Barabash et al., Phys. Lett. B 345 (1995) 408
5. V. Artemiev et al., Proc. of XXVII Int. Conf. on High Energy Physics, Glasgow, UK, 20-27 July 1994, Vol II, 947, Bussey and Knowles ed.
6. J.G. Hirsch et al., Nucl. Phys. A589 (1995) 445
7. C. Arpesella et al., "A low background counting facility at LNGS", INFN/LNGS note 92/35, 1992
8. W.R. Nelson, H. Hirayama and D.W. Rogers "The EGS4 code system"- SLAC- Rep. 265, Dec 1985
9. C. Arpesella et al., "Gamma ray activity of Neodymium samples", to be published in NIM A
10. E. Bellotti et al., Lett. Nuovo Cimento, 33 (1982) 273

DARK MATTER SEARCHES
WITH LOW ACTIVITY SCINTILLATORS
DAMA activities

1. The experiment with the liquid Xenon target-detector.

Between december 1994 and summer 1995 the ~ 6.5 kg liquid xenon target-detector (filled with Kr-free Xenon enriched at 99.5 % in ^{129}Xe) took data for 97.5 days. The detector was calibrated by a ^{109}Cd source (22 and 88 keV lines) and the achieved energy resolution was $\sigma/E = 0.056+1.19/\mathrm{sqrt}(E[keV])$. The experimental rate in the very low energy region is shown in fig. 1a. Measurements, filling the detector with 2.5 bar of xenon in gaseous phase, have been also performed to study a possible cautelative electromagnetic background subtraction, fig. 1b, (see Nucl. Phys. B35 (1994) 165 for a detailed description of the method).

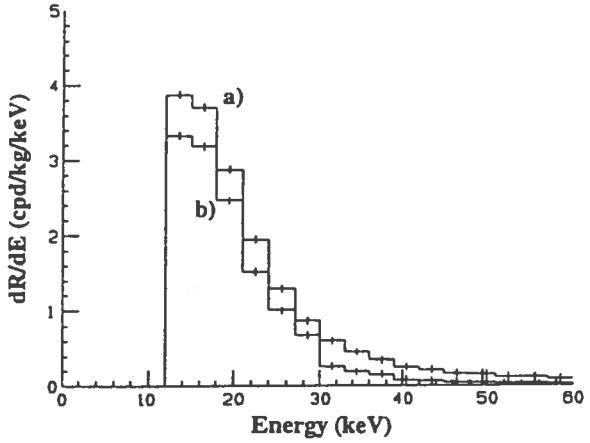

Fig. 1: a) Experimental energy distribution for (6.5 x 97.5) kgxday, considering together the winter and summer data (a). Same data after the subtraction of the contribution estimated by gaseous Xenon measurements (b). The quoted errors are statistical only.

The limit cross-section on proton versus WIMP mass contours from the data considered as a single sample of (6.5 x 97.5) kgxday are shown in fig. 2. In fig. 2A), line (a), the exclusion plot in the spin dependent case is plotted; in that calculation the spin factors calculated in the odd group model and a form factor according to a pure Bessel function have been considered. In fig. 2B), line (a), the case for coherent interaction is shown. From the measurements with the gaseous detector, the contribution from environmental radiations - whose rate does not depend on the detector mass - has been performed; in fig. 2 A and B lines (b) we report the exclusion plots obtained in that case. Notice that due to the higher energy threshold on gaseous detector the contribution from background is assumed cautelatively to be constant from the gaseous to the liquid xenon detector energy threshold.

Because the data were collected for 31.4 days during the winter time (around 2 december; minimal rate due to the annual modulation) and for 66.1 days during the

summer period (around 2 june, maximal rate due to the annual modulation), they can be analyzed also looking for the possible presence of an annual modulation of the rate as a distinctive signature for Dark Matter presence.

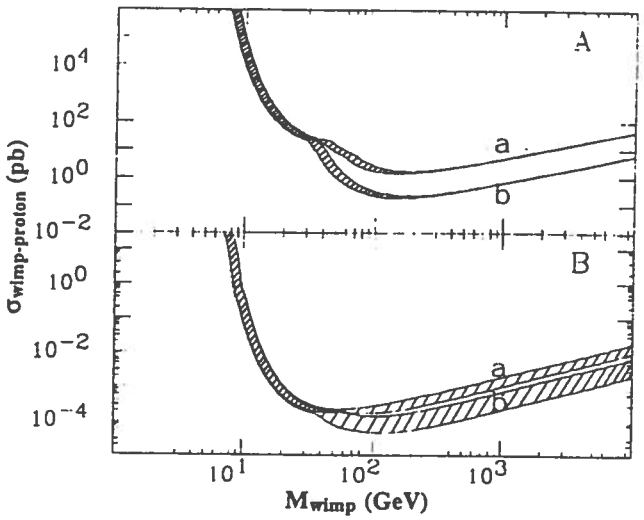

Fig. 2: Limit elastic cross-sections that axially coupled WIMPS would have on proton as a function of WIMP mass (95% C.L.) in the experimental situation of fig. 1. A) spin dependent interaction: unsubtracted data (a), subtracted data (b); B) coherent interaction: unsubtracted data (a), subtracted data (b). The shaded areas show the uncertainties in the quenching factor (0.6-0.8).

For this purpose, temperature, pressure and insulation vacuum have been monitored to have a maximal variation of = 3 % in the whole running periods. The PMT high voltages and electronic line stability have been also daily controlled. Due to the velocity modulation, the Dark Matter rate in the detector will be consequently modulated according to: $S(t)=S_0+S_m \cos(\omega(t-t_0))$, at the first order in the Taylor serie. We analysed only data taken in paired days (opposite in cosine), considering $r=x/\sigma(x)$ where $x = \Sigma_i 2\cos(\omega(t_i-t_0))(N(t_i))$ with N experimental rate (in cpd) at t_i time and $\sigma(x) = \mathrm{sqrt}(4\alpha\Sigma_i N(t_i))$, with $\alpha = \Sigma_i\cos^2(\omega(t_i-t_0))/T = 0.959$ and T the total considered time in days. This analysis can be performed in different energy bins. In case the annual modulation would be absent, the method will provide also the upper limit on S_m at the given C.L.; in fact, $\langle x\rangle = 2T\alpha S_m$. Note that S_m is not positive defined. We derived the confidence level for the presence of a signal modulation in case a r_0 value has been obtained: $\mathrm{C.L.} = 1/\mathrm{sqrt}(2\pi) \int_{-|r_0|}^{+|r_0|} \exp(-x^2/2)\,dx = \mathrm{erf}(r_0/\mathrm{sqrt}(2))$; in case of 90% C.L. we can derive $r_0=1.29$ and $|S_m| < S_{m_{lim}}(90\%\ \mathrm{C.L.}) = 1.29\,\sigma(x)/(2T\alpha)$ cpd.

In table 1 we summarize our analysis considering 8 energy bins between 12 and 36 keV. As one can see, C.L. values higher than 0.90 appear rejecting the hypothesis of no

modulation in the data in those energy bins. Therefore, the presence of annual modulation - in order to exclude or to ascribe this effect to lack of statistics or to systematics - needs to be further investigated. We will remark that in this kind of analysis obviously no role is played by the quenching factor.

Table 1

Statistical analysis for annual modulation of the signal according to K. Freese et al., Phys. Rev. D37 (1988),3388, considering 8 energy bins between 12 and 36 keV.

Energy bin (keV)	r	C.L. (to reject modulation)	$S_{m_{lim}}/M/\Delta E$ (cpd/kg/keV @90% C.L.)
12-15	-3.77	0.998	0.086
15-18	1.85	0.936	0.069
18-21	2.05	0.960	0.060
21-24	0.717	0.526	0.050
24-27	0.663	0.492	0.041
27-30	0.076	0.060	0.034
30-33	2.11	0.966	0.028
33-36	0.915	0.64	0.024

Only for template purpose, we recall that in case the C.L. in table 1 could allow us to claim (as it is not here the case) a clear absence of modulation, exclusion plots would be derived considering the $S_{m_{lim}}$ in table 1 and - as it will be easy to verify - a certain improvement in the low mass region of the exclusion plots will be obtained.

As a by-product of this data taking we obtained experimental limits on the lifetime of electron for the decay into non ionizing particles; a finite value would imply a violation of the law of charge conservation. The present experimental technique consists both of a search for internally absorbed X-ray and Auger electron cascade, which could follow the decay of a K-shell electron in one of the Xenon atoms of the detector: e^- -> anything invisible (e.g. e^- -> majoron + neutrino or e^- -> 3 neutrinos) and of a search for monochromatic γ rays with energy $m_e/2$ to investigate the process e^- -> $\nu_e\gamma$. Considering that in the unsubtracted data no peak evidence was present in one σ around 34.566 keV, we obtained as upper limit for the first decay channel: $\tau_e > 1.5 \times 10^{23}$ years at 68% C.L, reaching at present same sensitivity than the one obtained by Reusser et al. with Ge detector. Regarding the eventual decay e^- -> $\nu_e\gamma$, we collected data for 257 hours in the energy region around 255 keV and in one σ around this value 2 events have been detected; then, considering the relation: $\tau_e > (\varepsilon_{Cu}N_{Cu}+\varepsilon_{Xe}N_{Xe})x(T/N_{excl})$, with $N_{Cu,Xe}$ numbers of e^- in the copper vessel and in the liquid Xenon (4.67×10^{27} and 1.64×10^{27},

respectively), T running time and $\varepsilon_{Cu,Xe}$ detection efficiencies - within 1σ - for the 255 keV photons (ε_{Cu} = 8% and ε_{Xe}= 63%, calculated by EGS4 MonteCarlo program). Assuming the two measured events as background, we derive N_{excl} equal to 2.16 at 68% C.L., to 3.88 counts at 90% C.L. and 9.7 at 99.9% C.L.. Therefore, the upper limits on the electron mean lifetime for the $e^- \rightarrow \nu_e\gamma$ process result: $\tau_e > 2\times10^{25}$ years at 68% C.L., $\tau_e > 1\times10^{25}$ years at 90% C.L. and $\tau_e > 4\times10^{24}$ years at 99.9% C.L.. These limits are similar to those quoted by Balish et al., where however the quoted events have been obtained evaluating the background rate in the interesting energy region larger than the measured ones.

After some upgrading, we have restarted the measurements in november 95 and the data taking is in progress.

2. The experiment to detect delayed coincidences in two planes of low activity NaI(Tl).

Improved results on the search for neutral Strongly Interacting Massive Particles (SIMPs) - i.e. neutral particles with masses from the GeV range up to the GUT scale, interaction cross sections on protons, σ_p, up to $\approx10^{-22}$ cm^2 and $\beta\approx10^{-3}$ - have been achieved.

In 1995 we analyzed the data collected with the final set-up in Gran Sasso adding also the data from some previous prototypes. The final setup was realized by two planes, each one of 2 large high radiopurity NaI(Tl) crystals (132980 cm^2 sr days exposure). In order to reduce the external background, the detectors were placed inside a 4-component shield: 10 cm of low activity copper surrounded by 10-15 cm of Boliden lead, 1 mm thick cadmium foil and 10 to 20 cm of paraffin. The radon around the detector was removed by flushing nitrogen in closed area. In our analysis we considered for recoils two electron equivalent energy regions: i) the first one (from threshold up to 60 keV) is used to analyze mainly single scattering events; 2) the second one (above 60 keV with saturation value around 350 keV) is used to look for multi-bumps time structure or saturated events (i.e. candidates giving multiple scatterings inside the crystals) produced by slow moving SIMPs. No events were registered in the multiple scattering region while the measured "upward" and "downward" delayed coincidences in the mainly single scattering region were fully comparable with the expected random coincidences that dominate also possible delayed coincidences from correlated processes. The total experimental rate was estimated - in each energy region - considering a Poissonian distribution with background. To interpret the data we evaluated the effect of the surrounding rock in case of "downward" delayed coincidences and of the whole Earth in case of "upward" ones. The derived exclusion plots at 90 % C. L. are shown in fig.3 for both type of couplings, coherent and spin dependent. These results allowed us to exclude new regions in the plot cross section versus SIMP mass up to $M_S \approx 10^{16}$ GeV. In addition, considering the present data in terms of neutral nuclearites, a model independent upper limit on their flux can be derived by considering

that in the multiple scattering region the rate depends only on geometrical factors. We obtain at 90% C.L. $\Phi < 8.0 \times 10^{-11}$ $s^{-1}cm^{-2}sr^{-1}$.

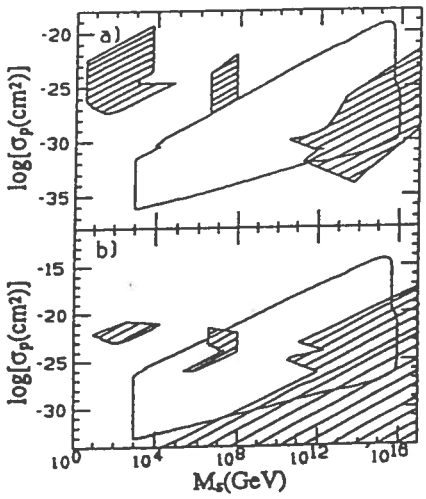

Fig. 3 - Exclusion plots in the plane of SIMP cross section on proton versus SIMP mass: a) coherent interactions; b) spin dependent interactions. The shaded areas refer to the regions not excluded by other authors.

Our investigation of the SIMP hypothesis for Dark Matter allowed us to enter in the GUT mass scale region and to severely constrain the region of geometrical nuclear cross sections that was the interest of our proposal. Its goal has been reached.

3. The 100 kg experimental set-up

The ~ 100 kg very low activity NaI(Tl) experimental apparatus has been installed in Gran Sasso at end of 1995. In this apparatus the shield from environmental gamma and neutron radiation has been strongly improved. A low activity copper housing is now used to contain the PMTs and to connect them to the crystals; they are now also shielded one from the other by using very low activity Copper bricks. The substitution of the plexiglass box with a low activity copper box to contain the crystals assures a good shield both from the light and from the electromagnetic disturbs. These 9 detectors have residual U/Th contaminations ranging from 10^{-12} to 10^{-14} g/g.

List of publications in 1995

1. R.Bernabei, Riv. Nuovo Cim. 18 n.5 (1995).
2. R.Bernabei et al., Astrop.Phys. 4 (1995) 45.
3. P. Belli et al.,Proc. ICRC95 vol.I (1995), 865.
4. P. Belli et al., Nucl. Instr. & Meth. A357 (1995), 329.
4. C. Bacci et al., LNGS-95/50, in press on Astrop.Phys.
5. C. Bacci et al., LNGS-95/57, in press on Astrop.Phys.
6. P. Belli et al., ROM2F-96/08 submitted to Nuovo Cim C.

CRESST Dark Matter Search

S. Cooper[1,3] (speaker), W. Seidel[1] (deputy speaker), N.E. Booth[3], C. Bucci[4], M. Bühler[2], F.v.Feilitzsch[2], P. Ferger[1], A. Gabutti[1], J. Höhne[2], E. Kellner[2], M. Koch[2], M. Loidl[1], O. Meier[1], U. Nagel[2,*], F. Pröbst[1], M.J.J.v.d.Putte[3], A. Rulofs[1], G.L. Salmon[3], M. Sisti[1], L. Stodolsky[1], A. Stolovich[1,†], L. Zerle[1]

[1] *Max-Planck-Institut für Physik, Föhringer Ring 6, D-80805 Munich, Germany*

[2] *Technische Universität München, Physik Department, D-85747 Munich, Germany*

[3] *Univeristy of Oxford, Physics Department, Oxford OX1 3RH, UK*

[4] *Laboratori Nazionali del Gran Sasso, I-67010 Assergi, Italy*

Abstract

We are preparing the CRESST experiment in LNGS to search for dark matter WIMPs using cryogenic detectors with superconducting phase transition thermometers. In the first stage of the experiment we plan to use four 250 g sapphire detectors with thresholds of 0.5 keV and resolutions of 0.2 keV at 1 keV. This will provide sensitivity to WIMP masses below 10 GeV, making our experiment complementary to other dark matter searches. In 1995 the construction of the main cryogenic components was completed and successfully tested. The installation of our equipment in LNGS has begun.

1 Introduction - The Dark Matter Problem

The nature of the missing mass of our Universe is one of the most intriguing open questions of our time. Our theoretical understanding of the evolution of the Universe indicates that its density should be equal to the critical density ($\Omega = 1$) giving us a "closed" Universe, whereas the mass that we can observe in the form of stars, dust, and gas corresponds to only about $\Omega \sim 0.01$, leaving the other 99% as "'missing" or "dark matter". Independent of these theoretical considerations, various astronomical observations indicate that at most $\sim 10\%$ of the mass of spiral galaxies like our own is visible, with the rest then being attributed to dark matter.

The theoretical study of elementary particle physics offers several hypothetical particles as candidates to make up the dark matter: axions, light but not massless neutrinos, and WIMPs (Weakly Interacting Massive Particles). However theory cannot tell us enough

*Permanent Address: Institute of Chemical Physics and Biophysics, EE-0026 Tallinn, Estonia
†Permanent Address: Institute of Physics, EE-2400 Tartu, Estonia

about any of these hypothetical particles to decide which, if any, are the dark matter. For example the WIMP is usually discussed in the framework of the minimal supersymmetric model (MSSM), but this model has not yet been proven to be the correct description of nature, and even within the model there are various free parameters. Together with theoretical colleagues, we have performed a study of the parameter space of the MSSM which indicates that the lightest neutralino could be the dark matter for a range of neutralino masses extending down to 2 GeV [3].

Given the significance of the dark matter problem, we feel it is important that experiments are performed to search for the various candidates for the dark matter. The emphasis of our experiment is on low-mass WIMPs ($2 - 10$ GeV), which are inaccessible to other experiments due to their higher threshold.

2 Technique for Detection of Low-Mass WIMPs

Although we don't know what the dark matter is, we do have fairly definite ideas on some of the properties of the dark matter of our Galaxy. If it is in the form of particles, they can have no interaction stronger than the Weak Interaction. They can thus pass through the Earth (and in particular into the Gran Sasso Underground Laboratory). The particles should be gravitationally bound to our Galaxy, as is our Sun, giving the particles in our vicinity an average velocity of about 300 km/s. In order to provide enough mass to explain the observed rotation velocities of the Sun and other stars about the Galactic center, the local dark matter density should be about 0.3 GeV/cm^3.

WIMPs could be detected via their elastic scattering on nuclei, giving nuclear recoil energies of about a keV for WIMP masses of a few GeV. We already know from previous experimental limits that WIMP scattering rates are low, less than about 1 event per day in a 1 keV bin in a 1 kg detector. This is a very challenging experimental problem, requiring very sensitive detectors with masses in the kg range, as well as a very high purity and good shielding to reduce backgrounds from local radioactivity, with the cosmic ray background being eliminated by performing the experiment in an underground laboratory such as Gran Sasso.

Since low energy nuclei are very inefficient at producing ionization or scintillation, a low-threshold detector needs to act as a calorimeter, detecting the full nuclear energy. At the Max Planck Institute of Physics and the Technical University of Munich we have developed cryogenic calorimeters using superconducting phase transition thermometers. The thermometer is a small thin film of a superconducting material (tungsten) evaporated onto the surface of a sapphire crystal. The detector is run at a temperature (~ 15 mK) where the thermometer is in the middle of its transition between the normal and superconducting phases. Here its resistance is very sensitive to the small rise in temperature caused by a recoiling nucleus.

We have been able to detect 1.5 keV X-rays in a 32 g sapphire crystal with a resolution of 100 eV FWHM [1] in an above-ground laboratory. The local radioactivity already makes the background rate quite high in a detector of this size, so that the development of more massive detectors with this sensitivity requires a shielded underground site. However the model [2] which we have developed to describe the behaviour of our detectors leads us to

expect that we can increase the detector mass by about an order of magnitude without loosing much resolution. For the first phase of our dark matter experiment in Gran Sasso we are making 4 detectors of 250 g each, and hope to achieve a resolution of 200 eV at 1 keV and a threshold of 500 eV. The first such detector has been tested above-ground in Munich. While the detector can be seen to work, the high rate and resulting instability of the baseline prevent any determination of the resolution. We are looking forward to being able to test this detector in a shielded environment in Gran Sasso.

3 CRESST Setup in Gran Sasso

The CRESST (Cryogenic **R**are **E**vent **S**earch with **S**uperconducting **T**hermometers) experiment is designed to look for low-mass WIMPs as the dark matter of our Galaxy, using the cryogenic calorimeters developed in Munich. For this we need to combine the requirements of our detector (an operating temperature of $\sim$ 15 mK, provided by a dilution refrigerator) with the requirements of a low-background experiment (elimination of radioactivity). Since a standard dilution refrigerator is made with various materials (stainless steel, indium vacuum seals) which are much too radioactive, we decided to separate the dilution refrigerator from the detector, as shown in Fig. 1. The dilution refrigerator is based on a standard design from Oxford Instruments, with some modification to increase its mechanical strength. The detector will be placed in the "cold box", which hangs from the dilution refrigerator. This cold box is large enough to accommodate 100 kg of sapphire detectors.

The cold box is made of high-purity copper, with high-purity lead used for the vacuum seals. These materials are known to be among the best available for low radioactivity. As shown in the figure, the cold box will be surrounded by room-temperature shielding comprised of a 14 cm layer of high-purity copper and a 20 cm layer of lead. Special consideration needed to be given to the space between the dilution refrigerator and the cold box. The separation was chosen large enough so that the "neck" of the external shielding, together with the internal shields, eliminates any direct line of sight from the outside world into the cold box. The low temperature is transmitted into the cold box by the 3 cm thick 1 m long copper rod (cold finger). A 20 cm thick lead shield inside a copper can is placed between the mixing chamber and the cold finger, with the low temperature transmitted here by the copper can. This internal shield, combined with another one surrounding the cold finger, serves to block any line of sight for radiation coming from the dilution refrigerator into the experimental volume.

A prototype cold box was designed and constructed in Munich, as was the gas handling system for the dilution refrigerator. The system was set up and its cryogenic properties tested at MPI in the fall of 1995. The temperature as measured in the cold box with ^{60}Co nuclear orientation thermometry reached 6.8 mK, safely below that needed for the operation of our detectors. With this, a major milestone of the experiment has been reached. In December we started disassembling the system and packing it for shipment to Gran Sasso.

The copper for the shielding has undergone special handling [5 in 1995 to assure its purity and to protect it from exposure to cosmic rays (which can transform copper into radioactive elements such as ^{60}Co). The copper was produced electrolytically by the

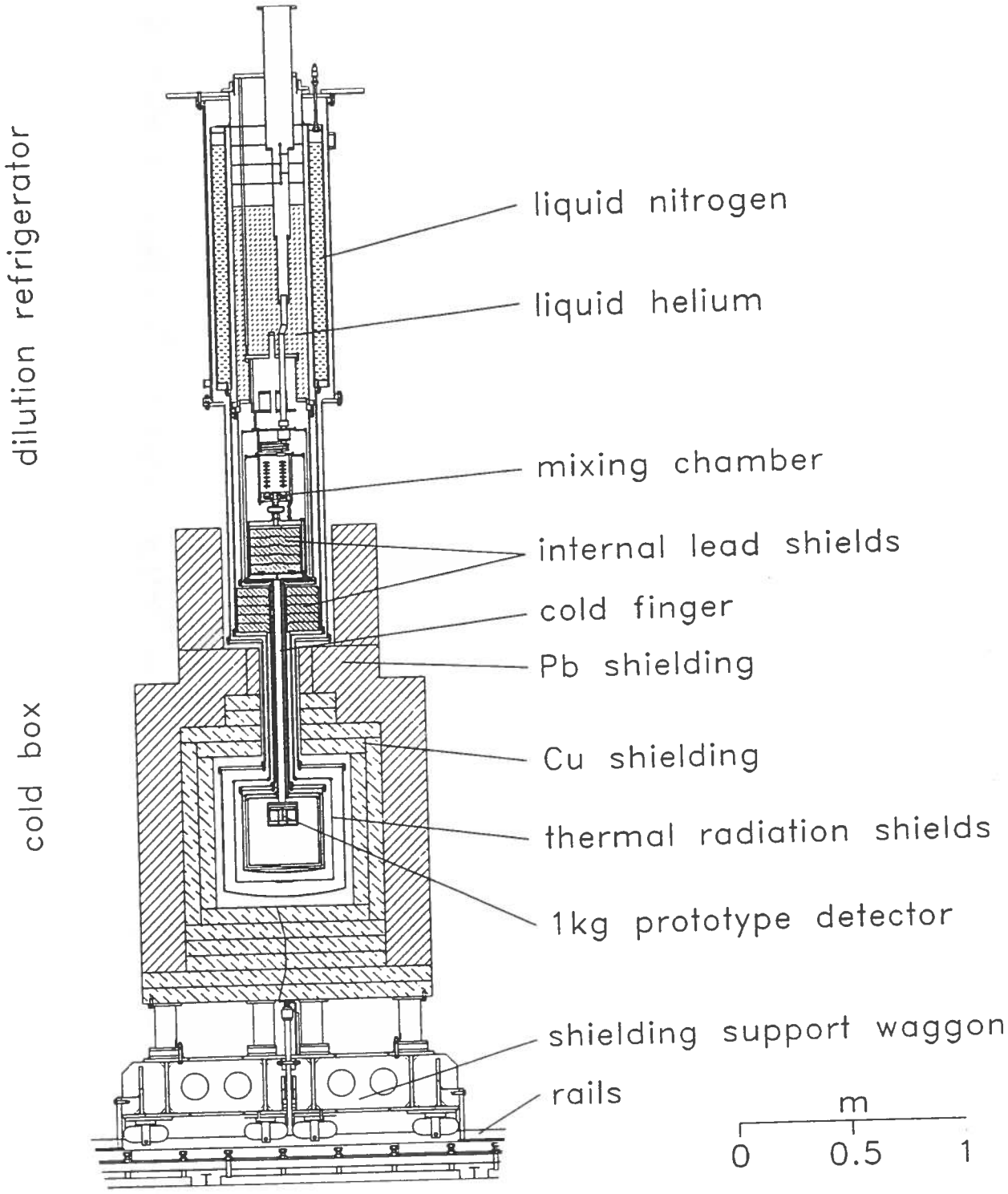

Figure 1: Layout of dilution refrigerator and cold box.

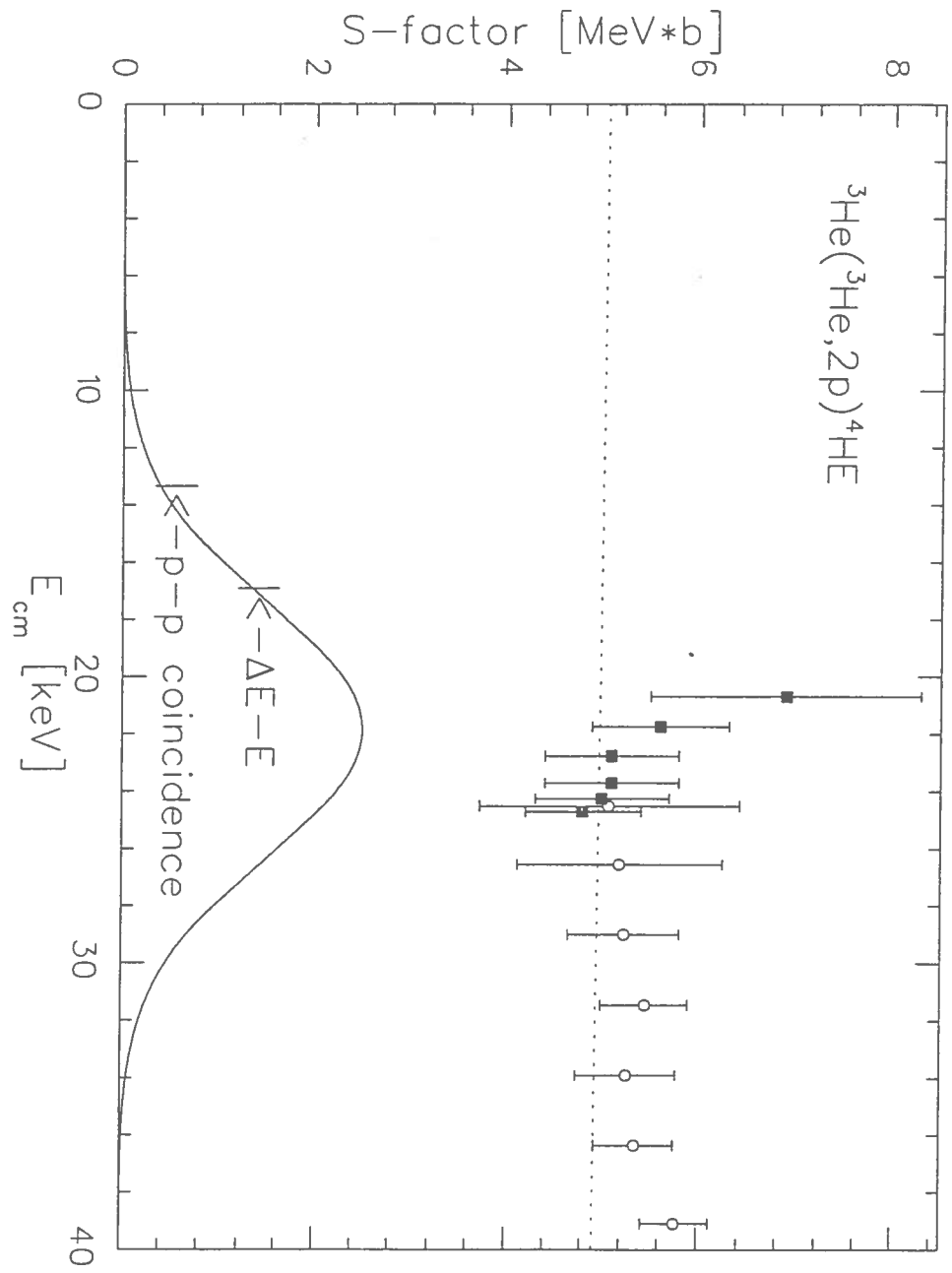

Fig.1 Preliminary results of this experiment (filled squares) compared to previous results shown in the region of the Gamow-peak of our sun. The ordinate of the Gamow-peak is depicted in arbitrary units. Shown are also the low-energy experimental limits that can be achieved with the current ΔE-E detector setup and the new p-p-coincidence setup.

THE INTERFEROMETRIC STATION AT LNGS

Luca Crescentini and Antonella Amoruso

Dipartimento di Fisica, Università dell'Aquila, and I.N.F.N. Gruppo Collegato dell'Aquila, L'Aquila, Italy

The interferometric station was planned to measure relative displacements of three end points located in A, B and C (see Fig. 1). Until last autumn the instrument has been operated as an unequal-arm Michelson interferometer, but since a few months it is operating in an equal-arm configuration. The mechanical and optical set-up of the interferometer, unchanged from unequal-arm to equal-arm configuration, has already been described in previous reports and can be summarized as follows.

The end points of the interferometer constitute of three 1 m^3 concrete blocks, each sitting on a 8 m^3 underground cubic platform. The platforms are embedded in the rock and separated from the gallery floor by means of a 20 cm wide track. As usual, the interferometer works in an evacuated environment. Optical components are firmly attached to the concrete blocks but to some extend uncoupled from the vacuum chambers by means of bellows (see Fig. 2). A temperature controlled building has been built around monument B, where the laser source and all the electronics are kept. Temperature inside the building is maintained at 291 $\pm$ 0.1 K. Room temperature in the galleries is naturally fixed at about 280 $\pm$ 0.4 K. Continuos monitoring of air temperature and pressure inside the building and of air temperature in the galleries is carried out by four solid state thermometers and a capacitive pressure transducer.

As regards the optical apparatus, the retroreflectors of the two arms are "cat's-eyes", which causes the reflected beams to overlap the incident beams, so that an extremely good isolation of the laser itself from the returning light is needed. In order to solve this problem, two Faraday rotators, a Rochon prism and two polarizers are used. One of the two arms of the interferometer (the reference arm in the unequal-arm configuration) contains a phase modulator capable to change its optical lenght. Voltage applied to the phase modulator is sampled by a 12-bit digital-to-analog converter, able to transfer data to a PC through direct memory access (DMA). Unfortunately, wide strain oscillations around 100 Hz, maybe due to mechanical resonances of supporting structures, are present. Since their amplitude can be as large as 2 nϵ, and hence larger than the hysteresis of the reset ciruit, a 6 kHz sampling rate is used. Two memory buffers are alternatively used in input. While one of the two buffers is acquiring, data stored in the latter are digititally filtered using a linear nonrecursive filter, decimated at 20 Hz, and preanalyzed. Depending on how fast strain changes in time, data are more and more filtered, and recorded at a rate variable from 0.5 to 20 Hz.

Figure 3 shows a typical set of raw data, recorded at a variable rate in the unequal-arm configuration, as previously discussed. Both periodical, e.g. earth tides and teleseism, and aperiodical signals are evident. A forty-day stretch of data has been analysed to obtain the noise level of the interferometer, after removing the best fitting tide. The results are plotted in Fig. 4 together with the best data available from the literature (GS-present work; PFO-Pinon Flat Observatory; PM-Poorman Mine; QT-Queensbury Tunnel). At lower frequencies our results are comparable with the previous measurements, while at frequencies higher than 10^{-4} Hz the noise level recorded at Gran Sasso is slightly worse. A preliminary study of environmental effects have shown a strong correlation between pressure and signal (around 0.003 nϵ/Pa) probably caused by unbalancing (0.08 N/Pa) air thrust on terminal supporting structures and their linking to the gallery floor too nearly to the concrete blocks. As regards temperature, a frequency-dependent correlation has been observed between signal and temperature inside the building (around 0.2 nϵ/K), but its effects are relevant only when personnel enters the building. Moreover, the power spectral density of laser frequency fluctuations, when converted to equivalent strain, has proven comparable with the noise level of the interferometer at frequencies higher than 10^{-4} Hz.

In order to test laser effects on strain measurements, a second arm from B to A (see Fig. 1) has been constructed, and, as previously mentioned, the interferometer is now running in an equal-arm configuration. The analysis of the preliminary results have confirmed the influence of pressure fluctuations on the recorded signal and we are presently attempting to solve this problem by using bellows with independent supporting structures, each 1 m far from the concrete blocks, at the ends of the vacuum chambers.

As regards geophysical results, a recent crash of the computer hard disk used to store manipulated data and processing software prevents us from showing graphs. However, a swift strain transient reaching a peak of at least 1 $\mu\epsilon$ has been odserved in about one month from late May 1994, followed by a four month long stable period, a slower decay, and successive increases and decreases of accumulated strain. The physical origin of the course of the recorded strain is not known, but surely it is neither a periodical seasonal effect nor an instrumental one (e.g. laser frequency instabilities). Moreover, on June 2nd 1994, in coincidence with two local earthquakes, permanent offsets of about 10 nanostrain have been recorded, having the same sign as the strain accumulation. About 90 minutes after the last local event, a further aseismic slip of the same order of magnitude and sign has been observed. At the same time, no local seismic activity occurred, while the arrival of surface waves from a distant earthquake has been recorded by the interferometer. No more similar signal behaviour has been observed since then.

Further analysis is in progress about free oscillations and variations of earth tides amplitudes and phases.

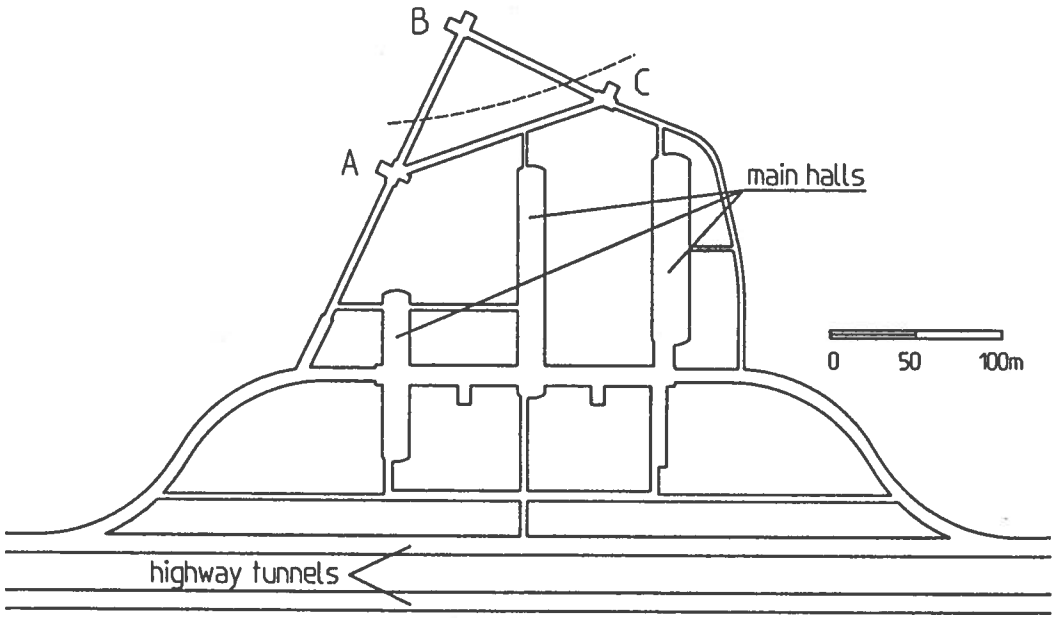

Fig. 1

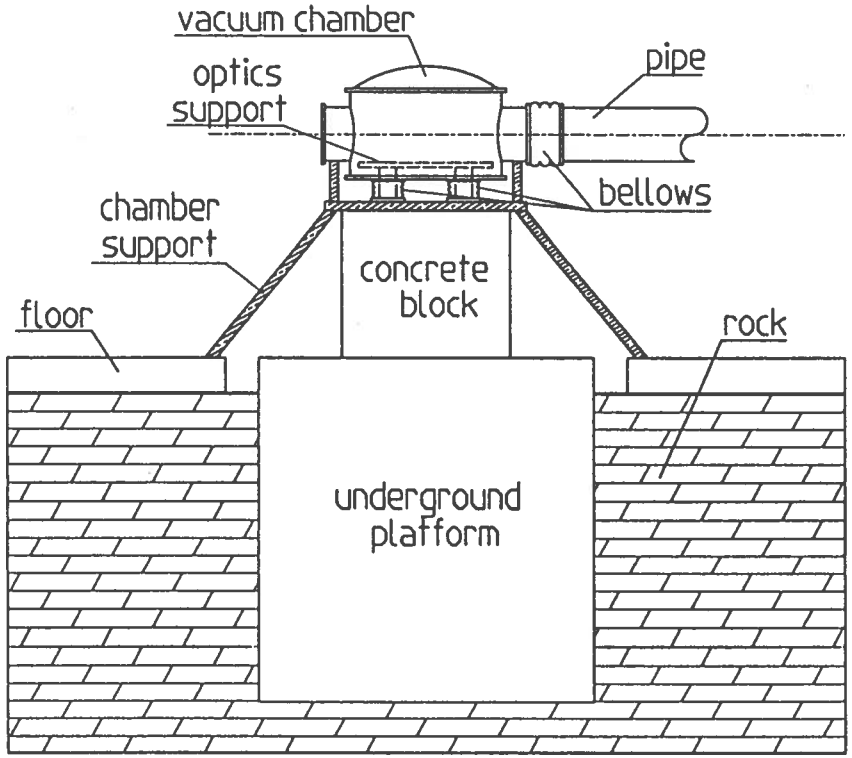
vacuum chamber
optics support
pipe
bellows
chamber support
concrete block
floor
rock
underground platform

Fig. 2

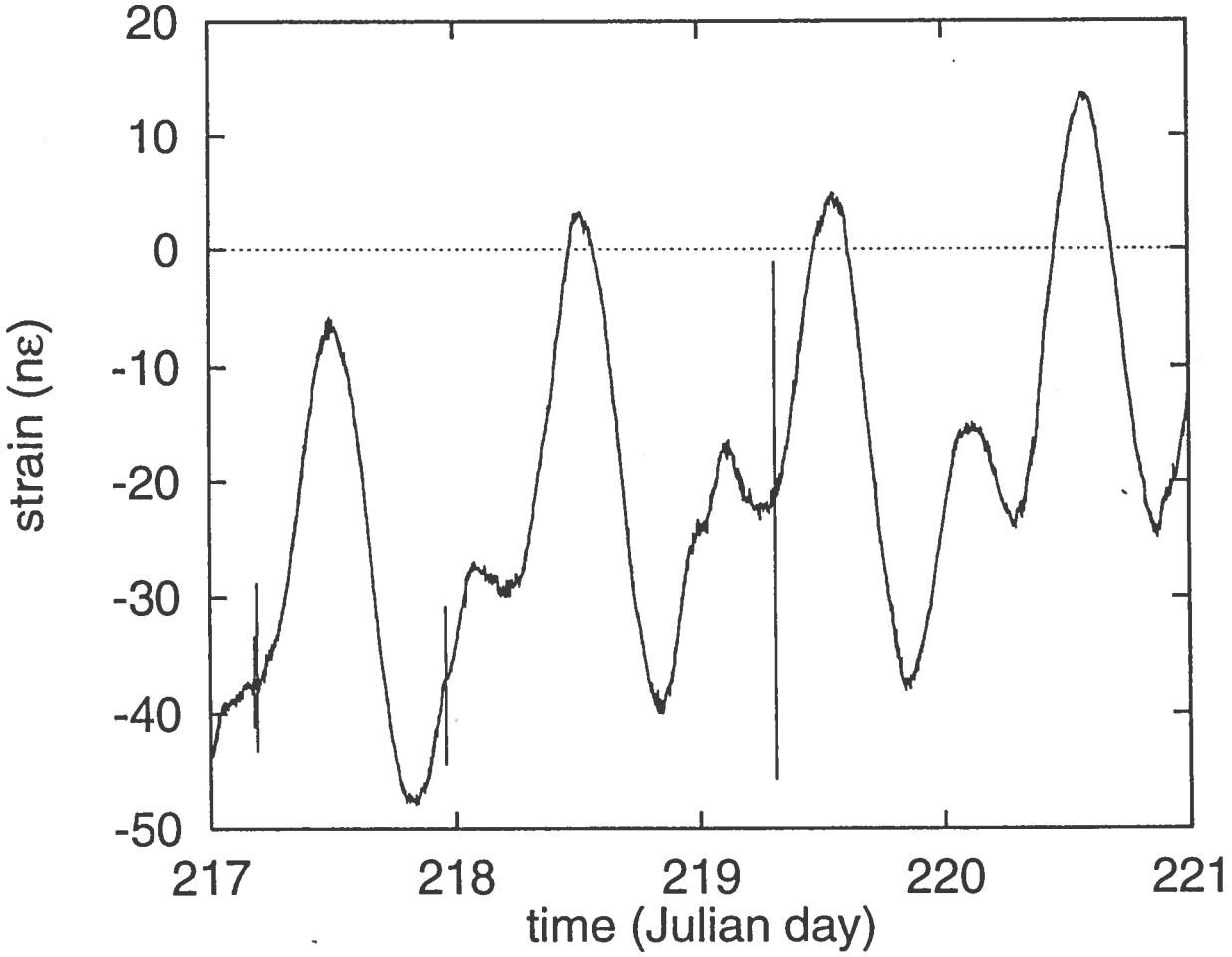
20
10
0
-10
-20
-30
-40
-50
strain (nε)
217
218
219
220
221
time (Julian day)

Fig. 3

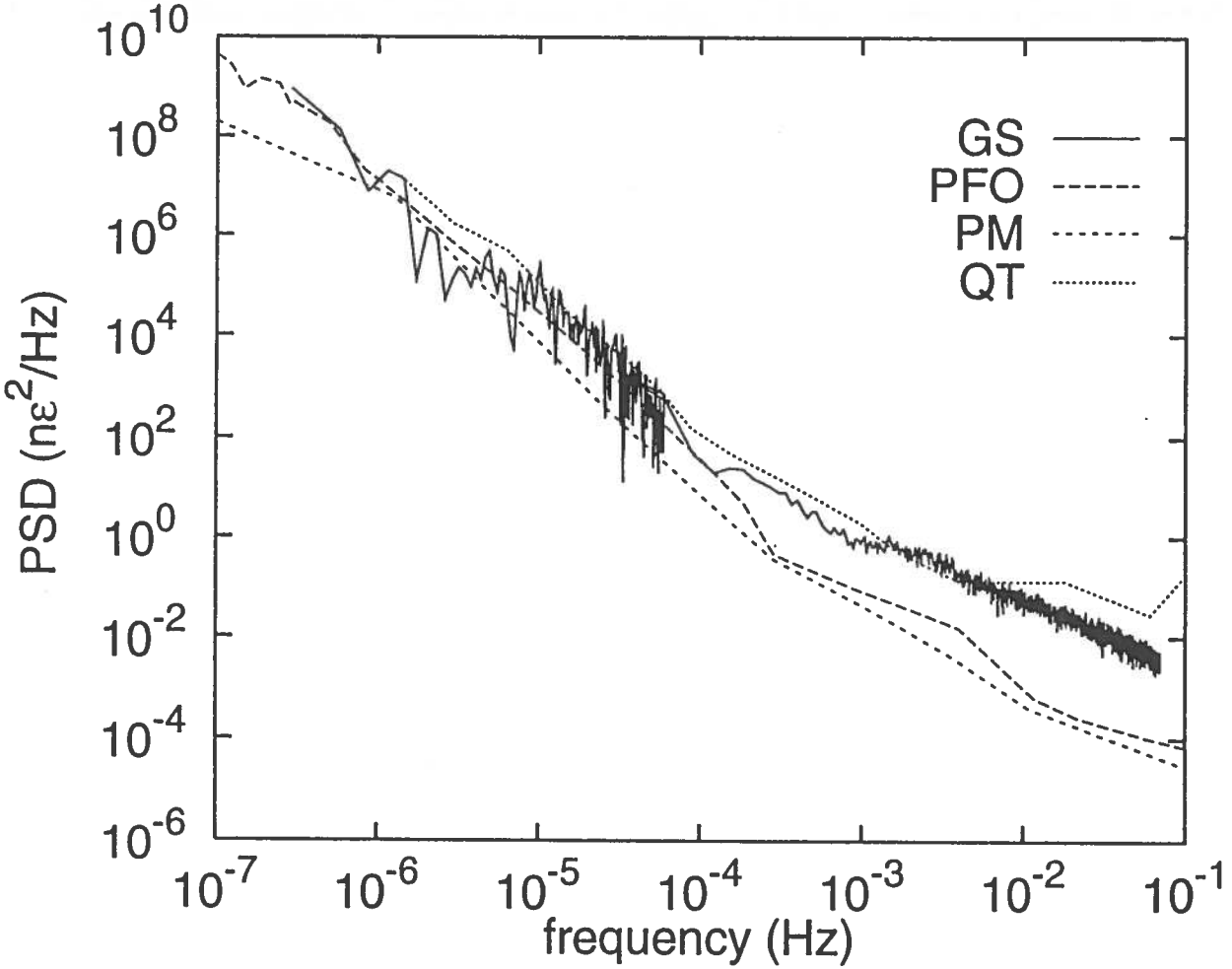
PSD (nε²/Hz)
frequency (Hz)
GS
PFO
PM
QT
10^10
10^8
10^6
10^4
10^2
10^0
10^-2
10^-4
10^-6
10^-7
10^-6
10^-5
10^-4
10^-3
10^-2
10^-1

Fig. 4

THEORETICAL GROUP

Astroparticle Physics

The Astroparticle Theory group of LNGS in 1995 included V.Berezinsky, P.Blasi (PhD student), P.DiBari (student) and M.Kachelriess (PhD student from Bochum University, Germany). The group worked in close collaboration with A.Dolgov (Valencia University, Spain), B.Hnatyk (Lviv University, Ukraine), and with the European Network TAN.

Scientific work

The main field of the work is astroparticle physics, including solar neutrinos, high-energy neutrino astrophysics, relativistic astrophysics and cosmology.

From several works in progress, the following results can be singled out.

V.Berezinsky, A.Dolgov and M.Kachelriess suggested the new type of semiclassical radiation: the curvature radiation of pions by a proton moving along a curved trajectory. A method of calculations is developed and applications are considered. The paper is published in Phys. Lett.B.

V.Berezinsky, P.Blasi and B.Hnatyk developed a new model for gamma-ray bursts in SNI explosion. The shock strips the outer layer of the star and accelerates the particles hydrodynamically. These particles interact with accreting gas, producing the gamma-burst. The paper is accepted for publication in Astrophys. Journal.

V.Berezinsky in collaboration with Torino group (A.Bottino et al) and J.Ellis (CERN) studied the Minimal Supersymmetric Model with soft breaking terms and radiatively induced EW symmetry breaking. The set of basic restrictions, including no-fine-tuning and scalar mass non-universality, is suggested. The applications for neutralino as Dark Matter Particle are obtained.

Theoretical Activity in LNGS and Conferences

By the efforts of the Astroparticle Theory group there was organized the International Discussion Workshop in LNGS "Beryllium Neutrino Problem".

The members of the theoretical group gave the following review talks at the International Conferences:

V. Berezinsky, "Solar Neutrino Problem 1995", 30th Recontres de Moriond, 12-18 March, 1995

V.Berezinsky, "Highlights of Astroparticle Physics", Europhysics Conference on High Energy Physics, Brussels, July 27 - August 2, 1995

V.Berezinsky, "Neutrino Astronomy", Cosmic Ray, Particle and AsTroparticle Physics, Florence, 11- 13 September 1995

V.Berezinsky, "Non-Baryonic Dark Matter", TAUP 95, Toledo, 17 - 21 September, 1995.

PUBLICATIONS IN JOURNALS AND PROCEEDINDGS IN 1995

1. V.Berezinsky, A.Dolgov and M.Kachelriess
Curvature Radiation by Ultrarelativistic Protons
Phys. Lett. B 351 (1995) 261

2. V.Berezinsky
High Energy Neutrinos from AGN Nucl. Phys. B (Proc. Suppl.) 38 (1995) 363

3. V.Berezinsky
The Solar Neutrino Problem
Nuovo. Cim. 18C (1995) 671

4. R. Protheroe, T. Stanev and V. Berezinsky
Electromagnetic Cascades and Cascade Nucleosynthesis in the Early Universe
Phys. Rev. D 51 (1995) 4134

5. V. Berezinsky
Neutrino Astronomy from eV to PeV
Proc. of Int. Workshop "Astroparticle Physics" (ed's A. Weiss et al),
Max-Planck Institute fur Astrophysics, p.59, 1995

6. V.Berezinsky and A.Z.Gazizov
High Energy Neutrinos from "Bright Phase"
Proc of Int. Workshop "Quantum Systems" (ed's A.Barut et al) , 23 -29 May 1994,
Minsk, World Scientific, p.345, 1995

7. V. Berezinsky
High Energy Neutrino Astronomy
Proc. of the Third Gleb Wataghin School (ed's C.D.Chinellato et al), July 11-16, 1994,
DRCC-IFGW, p. 105, 1995

Lattice gauge theories.

Another theoretical activity in the LNGS concerns Lattice Gauge Theories. The group involved consists of A. F. Grillo (LNGS), G. Di Carlo (LNF), A. Galante (LNF and University of L' Aquila), K. Colanero (LNGS and University of L' Aquila) and R. Aloisio (LNGS and University of l' Aquila). The group has collaborations with V. Azcoiti and V. Laliena of the Zaragoza University (Spain).

The activity of the group during 1995 has concerned the study of gauge theories on the lattice, with the inclusion of dynamical degrees of freedom, using a method developed by our group (MFA, for Microcanonical Fermionic Average), which we mainly used for simulations of Abelian models.

Two-dimensional QED with fermions (Schwinger Model) has been fully studied, both in the Kogut-Susskind and Wilson realizations for lattice fermions. In the last case we have determined the phase structure of the theory in the $\beta - \kappa$ plane.

In the four-dimensional model we have continued our analysis of the properties of the continuum limit of the theory. Our method, unlike more traditional ones, allows the study of the theory directly in the fermions zero mass (chiral) limit. We have exploited this possibility for a high precision determination of the critical coupling.

We have also studied a more general model, with the addition of a four-fermion coupling (*a la* Nambu Jona-Lasinio); the results indicate non trivial critical exponents.

Finally, we started a program of simulations of QCD at finite temperature and density with the use of the MFA method.

The main part of the numerical analysis has been performed using semi-dedicated transputer netwrks in LNF, LNGS and Zaragoza.

PUBLICATIONS IN JOURNALS IN 1995

1. " Lee-Yang zeros and the chiral phase transition in compact lattice QED." V. Azcoiti, I.M. Barbour, R. Burioni, G. Di Carlo, A.F. Grillo and G. Salina. Phys. Rev. D51 (1995) 5199.

2. " Chiral susceptibilities in noncompact QED: a new determination of the *gamma* exponent and the critical couplings." V. Azcoiti, G. Di Carlo, A. Galante ,A.F. Grillo, V. Laliena and C. Piedrafita. Phys. Lett. B353 (1995) 279.

3. " The Gauged Nambu-Jona Lasinio model: a mean field calculation with non mean field exponents." V. Azcoiti, G. Di Carlo, A. Galante ,A.F. Grillo, V. Laliena and C. Piedrafita. Phys. Lett. B355 (1995) 270.

MINUTES OF THE FOURTH MEETING OF THE GRAN SASSO SCIENTIFIC COMMITTEE

(GRAN SASSO, MARCH 23-25 1995)

The fourth meeting of the Gran Sasso Scientific Committee has been held on March 23-25, in connection with the workshop on "Future Experiments at Gran Sasso".

On the 23th and 24th, in the workshop on "Future experiments at Gran Sasso", many talks have been presented on the following topics:

- solar neutrinos
- double beta decay, dark matter and nuclear physics
- high energy cosmic ray physics, search for rare events in cosmic radiation and gravitational collapse
- neutrino physics with long baseline experiments

On the 25th, C. Rubbia presented the status report on the Icarus project.

Later in the morning, a conference has been held with the participation of the Minister of Science, G. Salvini, with the presence of scientific and political authorities. L. Maiani, President of INFN, E. Bellotti and P. Monacelli presented the activities at LNGS.

Closed sessions of the Scientific Committee

23/3/95
7 p.m.
Present: E. Bellotti (president), R. Barbieri, B. Borgia, L. Di Lella, R. Turlay, G. Wolf, P. Monacelli

During the meeting the following subjects have been pointed out to require special attention:

The future of Gallex beyond 1996 (Gallium Neutrino Observatory?)
Approval of Borexino
The problem of space in hall C and additions of new halls.

24/3/95
9 p.m.
Present: E. Bellotti, R. Barbieri, B. Borgia, L. Di Lella, A. Menzione, R. Turlay, G. Wolf, P. Monacelli

In the first part of the session G. Bellini, F. Calaprice, G. Ranucci, members of the Borexino collaboration, presented further details on the results obtained with the Counting Test Facility (CTF) at LNGS during the first months of the year. The Committee was impressed by the high quality of the data obtained with the CTF.

Final recommendations of the Scientific Committee

The Committee considers the recent achievements at the Gran Sasso Laboratory a great success and notes the growing attractiveness of its experimental program. Gran Sasso has become an international laboratory.

Based on the success of current experiments running at Gran Sasso and the prospects for further fundamental experiments, the Committee is of the opinion that the current limitation of underground hall space is becoming serious and recommends that ways be found for the construction of additional underground halls already foreseen.

Given the importance of the pp component of the solar ν spectrum, the Committee is of the opinion that the Gallex experiment should continue taking data until the solar neutrino deficit is understood.

The Scientific Committee congratulates the Borexino collaboration for the data presented and the high purity levels achieved, fulfilling the requirements to perform the experiment proposed.

The Committee believes that the physics is exciting and that the experiment can reach the performance claimed by the proponents.

The Committee recommends the experiment to be approved. In view of other second generation experiments under construction and addressing similar physics questions, the experiment should be constructed and installed with high priority.

During the workshop, very interesting and novel technical solutions have been presented for the detection of solar neutrinos covering the entire spectrum, with high rate and in real time. From the point of view of solar neutrino spectroscopy third generation detectors with such capabilities will be essential for a complete understanding of the problem. The Committee recommends to the Director of the laboratory to support this line of research.

The members of the Hellaz collaboration should be encouraged to present a formal letter of intent to LNGS.

The Committee is convinced that long baseline neutrino experiments capable of reaching $\sin^2(2\theta)<0.01$ and Δm^2 as low as 10^{-3} cover an important part of the parameter space of neutrino oscillations that cannot be explored otherwise.

The Committee suggests a call for letters of intent for such experiments.

A "Baby Icarus" of 370 tons of fiducial mass, presented for the first time at this meeting, is considered a viable step towards the originally planned total mass of 5000 tons.

The Committee is looking forward to receive a written document from the ICARUS collaboration of the Baby Icarus, giving a short description of :

- physics potential
- engineering solutions
- time schedule
- cost evaluation

The Scientific Committee expects this report within a short time.

The Committee was pleased about the ongoing activities and the progress made in the fields of double decay and dark matter searches.

The Committee recognizes the strong interest in measuring low cross section reactions of importance for astrophysics in a low background environment. The Committee recommends that a careful study should be made on the compatibility of a heavy ion accelerator installation with the other low background activities in the underground laboratory of Gran Sasso.

The Committee appreciated the results from EAS-TOP both as a stand-alone experiment and in coincidence with the underground experiments LVD and MACRO.

The Committee took note of preliminary ideas for possible detector modification and upgrades which were also presented at the Workshop. In the opinion of the Committee, the EAS-TOP experiment would profit if one or more international groups would join the efforts for the upgrade program.

The Committee heard a progress report by the LVD collaboration which has now two towers almost fully equipped and in operation.

In line with the recommendations made at the Third Meeting on 20-21 May 1994, the Committee hopes that the liquid scintillator necessary to equip a third tower will be found before the end of this year.

The Committee is pleased with the results of the MACRO collaboration on monopole search and on the study of underground muons.

The Committee was interested to hear that the MACRO experiment can also address the problem of atmospheric neutrinos by observing upward going muons. First successful operation of a TRD module as a way to measure the muon energy was also reported.

The Committee considers very low background radio purity measurements to be of great importance for many experiments looking for low energy and rare events at Gran Sasso.

The Committee was pleased to hear of the good progress by the group searching for a deviation from black body radiation in cosmic background radiation (TRIS).

The Committee believes that in view of the growing experimental program and of the increasing number of users the staff of the Laboratory should be increased accordingly.